

INFORMATION TO USERS

This manuscript has been reproduced from the microfilm master. UMI films the text directly from the original or copy submitted. Thus, some thesis and dissertation copies are in typewriter face, while others may be from any type of computer printer.

The quality of this reproduction is dependent upon the quality of the copy submitted. Broken or indistinct print, colored or poor quality illustrations and photographs, print bleedthrough, substandard margins, and improper alignment can adversely affect reproduction.

In the unlikely event that the author did not send UMI a complete manuscript and there are missing pages, these will be noted. Also, if unauthorized copyright material had to be removed, a note will indicate the deletion.

Oversize materials (e.g., maps, drawings, charts) are reproduced by sectioning the original, beginning at the upper left-hand corner and continuing from left to right in equal sections with small overlaps.

Photographs included in the original manuscript have been reproduced xerographically in this copy. Higher quality 6" x 9" black and white photographic prints are available for any photographs or illustrations appearing in this copy for an additional charge. Contact UMI directly to order.

Bell & Howell Information and Learning
300 North Zeeb Road, Ann Arbor, MI 48106-1346 USA
800-521-0600

UMI[®]

UNIVERSITY OF OKLAHOMA

GRADUATE COLLEGE

MULTIDISCIPLINARY DESIGN OPTIMIZATION OF A FIGHTER AIRCRAFT
WITH DAMAGE TOLERANCE CONSTRAINTS AND A PROBABILISTIC MODEL
OF THE FATIGUE ENVIRONMENT

A Dissertation

SUBMITTED TO THE GRADUATE FACULTY

in partial fulfillment of the requirements for the

degree of

Doctor of Philosophy

By

ALBERT J. ARRIETA
Norman, Oklahoma
2001

UMI Number: 3004874



UMI Microform 3004874

Copyright 2001 by Bell & Howell Information and Learning Company.

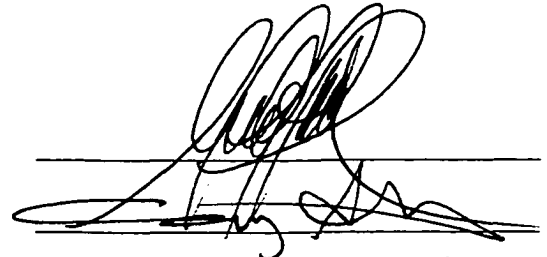
All rights reserved. This microform edition is protected against
unauthorized copying under Title 17, United States Code.

Bell & Howell Information and Learning Company
300 North Zeeb Road
P.O. Box 1346
Ann Arbor, MI 48106-1346

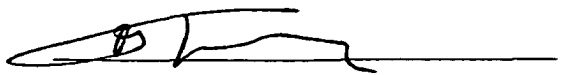
DESIGN OPTIMIZATION OF A FIGHTER AIRCRAFT WITH DAMAGE
TOLERANCE CONSTRAINTS AND A PROBABILISTIC MODEL OF THE
FATIGUE ENVIRONMENT

A Dissertation APPROVED FOR THE
SCHOOL OF AEROSPACE AND MECHANICAL ENGINEERING

BY



D. Baroni



C.W. Bert

ACKNOWLEDGMENTS

I would like to thank my major professor, Dr. Alfred G. Striz, for his support and suggestions. His letters of recommendation were key to obtaining the Gates Millennium Scholarship and the American Institute of Aeronautics and Astronautics Foundation Award Scholarship. I would also like to thank the other members of my Doctoral Committee: Dr. Bert, Dr. Baldwin, Dr. Altan, and Dr. Trafalis. Acknowledgement goes to Dr. Venkayya, AFRL/VASD, Wright-Patterson AFB, for providing the topic of my Ph.D. dissertation. Spending three summers working in his office and having access to the ASTROS program was crucial to completing my research. I also want to acknowledge James Harter's contribution in the use of AFGROW and Bob Gerami's instrumental role in my research on fatigue load spectra development. My research in those areas would have taken considerably more time without their help.

Finally, I want to thank my parents, Manual and Cata Arrieta, for their support and encouragement.

TABLE OF CONTENTS

ACKNOWLEDGMENTS.....	IV
LIST OF TABLES	VIII
LIST OF ILLUSTRATIONS.....	X
ABSTRACT.....	XIII
CHAPTER	
I. INTRODUCTION TO FATIGUE IN AIRCRAFT STRUCTURAL DESIGN	1
1.1 BACKGROUND	1
1.2 OBJECTIVES.....	5
1.3 DISSERTATION ORGANIZATION	6
II. ELEMENTS OF FRACTURE MECHANICS.....	8
2.1 STRESS INTENSITY FACTOR.....	9
2.1.1 <i>Superposition</i>	11
2.1.2 <i>Compounding</i>	12
2.1.3 <i>Similarity Ratio Method</i>	12
2.1.4 <i>Finite Element Method</i>	13
2.2 PLANE STRESS VERSUS PLANE STRAIN IN FRACTURE MECHANICS	14
2.3 CRACK TIP PLASTIC ZONE	16
2.4 FRACTURE TOUGHNESS	18
2.5 FATIGUE CRACK GROWTH	24
2.6 NUMERICAL INTEGRATION.....	29
2.6.1 <i>Constant Amplitude/Block Loading</i>	29
2.6.2 <i>Cycle-By-Cycle</i>	30
2.7 MEAN STRESSES.....	30
2.8 WALKER CRACK GROWTH RATE EQUATION.....	32
2.9 FORMAN CRACK GROWTH RATE EQUATION.....	32
2.10 SPECTRUM LOADING AND LOAD HISTORY EFFECTS	33
2.10.1 <i>Introduction</i>	33
2.10.2 <i>Wheeler Model</i>	38
2.10.3 <i>Generalized Willenborg Model</i>	42
2.10.4 <i>Elber Crack Closure Model</i>	45
III. FATIGUE LOAD SPECTRA DEVELOPMENT IN MILITARY AIRCRAFT.....	49
3.1 INTRODUCTION	49
3.2 SOURCES OF REPEATED LOADS	50
3.2.1 <i>Ground Loads</i>	51
3.2.2 <i>Flight Maneuver Loads</i>	53
3.2.3 <i>Gust Loads</i>	59

3.2.4 Pressurization Loads	64
3.2.5 Landing Loads	65
3.2.6 Miscellaneous Loads	68
3.3 DESIGN SERVICE LIFE AND MISSION PROFILES	69
IV. A NEW MODEL OF THE FATIGUE ENVIRONMENT	73
4.1 INTRODUCTION	73
4.2 NORMAL LOAD FACTOR EXCEEDANCES	74
4.3 CUMULATIVE DISTRIBUTION FUNCTIONS	74
4.4 APPROACH	80
4.5 LOAD FACTOR REGRESSION ANALYSES	82
4.6 LOAD FACTOR PROBABILITY FUNCTIONS	87
4.7 AIR-TO-AIR SEGMENT PROBABILITY CORRECTION	89
4.8 ROLL RATE AND ROLL ACCELERATION PROBABILITY FUNCTIONS	93
4.8.1 Roll Rate Probability Function	93
4.8.2 Roll Acceleration Probability Function	96
4.9 CONCLUSION	99
V. FLIGHT-BY-FLIGHT LOAD HISTORY DEVELOPMENT	101
5.1 INTRODUCTION	101
5.2 ORDERING THE MISSION MIX	101
5.3 MISSION SEGMENT IDENTIFICATION	103
5.4 NUMBER OF MANEUVER LOAD CYCLES COMPUTATION	110
VI. AEROELASTICITY ANALYSIS OF A FIGHTER AIRCRAFT	118
6.1 INTRODUCTION	118
6.2 STRUCTURAL AND AERODYNAMIC MODELS	118
6.3 BOUNDARY CONDITIONS	123
6.4 AEROELASTIC MODEL VERIFICATION	124
6.5 AERODYNAMIC PRESSURES	125
6.6 TRIM RESULTS FROM MSC ASTROS AND ZONA ASTROS	126
6.7 SEGMENT STRESS/LOAD RATIO ANALYSES	128
VII. FATIGUE STRESS HISTORY DEVELOPMENT	131
7.1 INTRODUCTION	131
7.2 STRESS FUNCTIONS FOR SYMMETRIC MANEUVERS	131
7.3 STRESS FUNCTIONS FOR ASYMMETRIC MANEUVERS	134
7.4 STRESS HISTORY POST-PROCESSING	136
7.4.1 Clipping the Stress History	136
7.4.2 Normalizing the Stress History	138
VIII. THE DEVELOPMENT OF DTA CONSTRAINTS	139
8.1 INTRODUCTION	139
8.2 THROUGH-THE-THICKNESS CRACK	140
8.3 SEMI-ELLIPTICAL SURFACE CRACK	142
8.4 CORNER CRACK IN A HOLE	145
8.5 CONCLUSIONS	147

IX. OPTIMIZATION RESULTS.....	149
9.1 INTRODUCTION.....	149
9.2 OPTIMIZATION WITH DTA CONSTRAINTS.....	153
9.5 MULTIDISCIPLINARY DESIGN OPTIMIZATION.....	158
9.6 CONCLUSIONS.....	165
X. CONCLUSIONS AND RECOMMENDATIONS.....	167
10.1 CONCLUSIONS.....	167
10.2 RECOMMENDATIONS.....	169
10.3 FINAL WORDS.....	171
REFERENCES.....	172
Appendix A: Load_occurrence.exe.....	178
Appendix B: Mission Segment Regression Analyses.....	193
Appendix C: Mission Segment Probability Analyses.....	200
Appendix D: Load_history.exe.....	209
Appendix E: Global_local.exe.....	214
Appendix F: Spectrum_clipping.exe.....	221

LIST OF TABLES

Table 2-1 Shutoff Overload Ratios for Aluminum, Steel, and Titanium.....	45
Table 3-1 Typical Gust Response Factors \bar{A} and N_o for a Fighter/Attack Aircraft	62
Table 3-2 Determining the Number of Landings Per Mission	67
Table 4-1 Typical Normal Load Factor Exceedance Distributions per Mission	
Segment for Fighter/Attack Aircraft per 1,000 Flight Hours	75
Table 4-2 Median Ranks for the Advanced Transition Segment Load Factor	
Exceedance Data	76
Table 4-3 Comparison of Median and Mean Ranks	78
Table 4-4 Comparison of Median Rank and Normalized Load Factor Exceedance	
Plotting Positions for the Advanced Transition Segment.....	79
Table 4-5 Exceedance Curve Fit for Positive Load Factors: Advanced	
Transition Segment.....	83
Table 4-6 Exceedance Curve Fit Results for Negative Load Factors: Advanced	
Transition Segment.....	84
Table 4-7 Probability of Occurrences for Positive Load Factors: Advanced	
Transition Segment.....	88
Table 4-8 Probability of Occurrences for Negative Load Factors: Advanced	
Transition Segment.....	89
Table 4-9 Original Probability of Occurrences for Positive Load Factors:	
Air-To-Air Segment (partially reproduced from Appendix C).....	90
Table 4-10 Corrected Probabilities of Normal Load Factor Occurrences for the	
Air-to-Air Segment.....	92
Table 4-11 Roll Rate and Roll Acceleration Exceedance Data from the	
Composite Mission of a Fighter Aircraft.....	93
Table 4-12 Probability of Roll Rate Occurrences for the Composite Mission.....	95
Table 4-13 Original Probability of Roll Acceleration Occurrences	97
Table 4-14 Corrected Probabilities of Roll Acceleration Occurrences.....	99
Table 5-1 Mission Type Distribution.....	102
Table 5-2 Mission Distribution Variation and Duration	102
Table 5-3 Mission Utilization Rates, Total Flight Hours, and Number of Flights	103
Table 5-4 Block Definition for 500 Flight Hours	103
Table 5-5 Segment Identification for the Air-to-Air, Air-to-Ground, and	
Training Missions.....	104
Table 5-6 Air-To-Air Mission Payload Inventory	105
Table 5-7 Air-To-Air Mission Gross Weight and Configuration History.....	105
Table 5-8 Air-To-Ground Mission Payload Inventory	105
Table 5-9 Air-To-Ground Mission Gross Weight and Configuration History	105
Table 5-10 Training Mission Payload Inventory	106
Table 5-11 Training Mission Gross Weight and Configuration History.....	106
Table 5-12 Air-To-Air Mission I Flight Conditions	107
Table 5-13 Air-To-Air Mission II Flight Conditions.....	108
Table 5-14 Air-To-Air Mission III Flight Conditions.....	108

Table 5-15 Air-To-Ground Mission I Flight Conditions.....:	109
Table 5-16 Air-To-Ground Mission II Flight Conditions	109
Table 5-17 Training Mission Flight Conditions	110
Table 5-18 Maneuver Type Prorate Factors by Mission Segments	111
Table 5-19 Lifetime Load Factor Occurrence Summary:	112
Table 5-20 Air-To-Air Segment Load Factor History in the Air-To-Air Mission I.....	114
Table 6-1 Aerodynamic Stability Derivatives from Original Finite Element Model	125
Table 6-2 Aerodynamic Stability Derivatives from Improved Finite Element Model ...	125
Table 6-3 Net Aerodynamic Pressures for Select Aerodynamic Panels	126
Table 6-4 Trim Results for MSC-ASTROS and ZONA ASTROS	127
Table 7-1 Maximum Principal Stresses for Symmetric Positive Load Factor Maneuvers in the Air-To-Air Mission: Ascent Segment.....	132
Table 7-2 Principal Stresses for Symmetric Negative Load Factor Maneuvers in the Air-To-Air Mission: Ascent Segment.....	133
Table 7-3 Maximum Principal Stresses for Antisymmetric (Roll) Maneuvers in the Air-To-Air Mission: Ascent Segment.....	135
Table 7-4 Stress Function Parameters for All Mission Types and Segments	137
Table 7-5 Selecting the Clipping Stress Level.....	138
Table 8-1 SMF Iterations for the Through-the-Thickness Crack	141
Table 8-2 SMF Iterations for the Semi-Elliptical Surface Crack	143
Table 8-3 SMF Iterations for a Corner Crack in a Hole.....	145
Table 8-4 Fatigue Stress Allowable Summary for Three Crack Configurations.....	148
Table 9-1 ASTROS Load Cases for Optimization.....	151
Table 9-2 Optimization Weight Histories with DTA Constraints	153
Table 9-3 Number of Active Constraints by Load Case: Stores.....	155
Table 9-4 Number of Active Constraints by Load Case: No Stores.....	155
Table 9-5 Final Thicknesses of the Master Elements with DTA Constraints	156
Table 9-6 Principal Stresses for Element 2549.....	157
Table 9-7 Principal Stresses for Element 2598.....	158
Table 9-8 Aileron Effectiveness Constraints.....	160
Table 9-9 Lift Effectiveness Constraints.....	161
Table 9-10 Optimization History with Multidisciplinary Constraints	161
Table 9-11 Maximum Constraint Values with Underwing Stores, Run 1	163
Table 9-12 Maximum Constraint Values without Underwing Stores, Run 2	163
Table 9-13 Final Design Variable Values with Multidisciplinary Constraints	165

LIST OF ILLUSTRATIONS

Figure 1-1 Typical Stress-Strain Diagram.....	2
Figure 1-2 Flow Chart of Approach.....	6
Figure 2-1 The Three Fracture Modes of Loading	10
Figure 2-2 Plane Stress and Plane Strain in Fracture Mechanics	15
Figure 2-3 Crack Tip Stress Field.....	16
Figure 2-4 Crack Tip Plastic Zone Size	17
Figure 2-5 Fracture Toughness and Fatigue	18
Figure 2-6 Effect of Thickness on Fracture Toughness	19
Figure 2-7 Plane Strain Fracture Toughness Versus Yield Strength	21
Figure 2-8 Variation of Fracture Toughness with Temperature	21
Figure 2-9 Crack Plane Orientation Code for Rectangular Sections	22
Figure 2-10 Crack Plane Orientation Code for Tilted Specimens	23
Figure 2-11 Crack Plane Orientation Code for Cylinders.....	23
Figure 2-12 Fracture Toughness Versus Thickness at Room Temperature for Various Aluminum Alloys: L-T Direction	24
Figure 2-13 Three Regions of Fatigue Crack Growth Response.....	26
Figure 2-14 Paris Model of Region II in the $da/dN-\Delta K$ Curve	28
Figure 2-15 Effect of Stress Ratio on Crack Growth Rate.....	31
Figure 2-16 Retardation Caused by a Tensile Overload	34
Figure 2-17 Crack Tip Residual Compressive Stresses Caused by an Overload	35
Figure 2-18 Four Different Overload Patterns.....	36
Figure 2-19 Crack Growth Following Different Overload Patterns in 7075-T6	36
Figure 2-20 Random Loading in a Bracket	37
Figure 2-21 Wheeler Model for Crack Growth Retardation	39
Figure 2-22 Overload Plastic Zone 2 is Chosen to Minimize Φ_R	40
Figure 2-23 Calibration of Wheeler Model for Flight-By-Flight Loading.....	41
Figure 2-24 Wheeler Prediction of Crack Growth Using Block Loading.....	41
Figure 2-25 Predicted Crack Growth and Test Data for Titanium Specimens Using an Aircraft Spectrum with Four Stress Levels.....	42
Figure 2-26 Flow Chart for Spectrum Loading Fatigue Analysis with the Wheeler Model.....	43
Figure 2-27 The Willenborg, Engle, and Wood Retardation Model	44
Figure 2-28 Elber Plasticity-Induced Closure Model	46
Figure 2-29 Effective Stress Intensity Factor Range for the Elber Model.....	46
Figure 2-30 Variation in Crack Closure Stress Intensity Factor Caused by Changing Load Level	48
Figure 3-1 Power Spectral Density of Airfield Surface Roughness	51
Figure 3-2 Symmetric Steady State Maneuvers	55
Figure 3-3 Symmetric Abrupt Maneuver	55
Figure 3-4 a) Roll Initiation from a Balanced Turn b) Followed by a Steady State Roll ..	57
Figure 3-5 Computing Occurrences from an Exceedance Plot	58
Figure 3-6 Exceedance Plot for a Lifetime of Gust Loads.....	63

Figure 3-7 Determining the Number of Δn_z Occurrences Caused by Gusts	63
Figure 3-8 Determining the Number of $ \Delta M $ Occurrences Caused by Gusts.....	64
Figure 3-9 Frequency Distribution of Sink Speeds in 1,000 Landings.....	66
Figure 3-10 Selection of Airspeed and Altitude Combinations.....	71
Figure 4-1 Median Rank R and Complementary Values F for Positive Load Factor Exceedances for the Advanced Transition Segment	77
Figure 4-2 Median Rank for Positive Load Factor Exceedances for the Advanced Transition Segment in Semi-Log Scale.....	78
Figure 4-3 Comparison of Median Rank and Normalized Exceedance for Advanced Transition Segment Load Factor	79
Figure 4-4 Advanced Transition Segment: Positive Load Factor Exceedance Regression Analysis	83
Figure 4-5 Advanced Transition Segment: Negative Load Factor Exceedance Regression Analysis with the 5th Order Exponential-Polynomial Model.....	85
Figure 4-6 Advanced Transition Segment: Negative Load Factor Exceedance Regression Analysis with the 4th Order Exponential-Polynomial Model.....	85
Figure 4-7 Regression Analysis of Normal Load Factor Data with a Seven-Point Parabola	90
Figure 4-8 Air-To-Air Segment Normal Load Factor Exceedance Data with Corrected Extrapolation to 1.25g	91
Figure 4-9 Roll Rate Exceedance Regression Analysis	94
Figure 4-10 Roll Acceleration Exceedance Regression Analysis.....	96
Figure 4-11 Regression Analysis of Roll Acceleration Data with a Five-Point Parabola	98
Figure 4-12 Corrected Roll Acceleration Exceedance Data with Extrapolation to 0.0 rad/s ²	98
Figure 5-1 Wing Station Identification	106
Figure 5-2 Air-To-Air Mission General Profile	107
Figure 5-3 Air-To-Ground Mission General Profile.....	108
Figure 5-4 Training Mission Profile	109
Figure 5-5 Load Factor History for the First Air-To-Air Mission I.....	116
Figure 5-6 Load Factor History for the First Training Mission.....	117
Figure 5-7 Load Factor History for the First Air-To-Ground Mission I.....	117
Figure 6-1 Left-Hand Side Aerodynamic Model with Sidewinder Missile	119
Figure 6-2 Finite Element Model of a Fighter Aircraft Structure.....	120
Figure 6-3 Aerodynamic Panel Model of a Fighter Aircraft.....	120
Figure 6-4 Wing Structure Finite Element Model	121
Figure 6-5 Lower Wing Skin Finite Element Model	122
Figure 6-6 Aerodynamic Model Superimposed on the Finite Element Structural Model.....	122
Figure 6-7 ZONA ASTROS Aerodynamic Panel Model.....	127
Figure 6-8 Wing Deflection for a 9g Pull-up at Mach 0.95 and 10,000 ft.....	127
Figure 6-9 Air-to-Air Mission Stress/Load Ratios	129
Figure 6-10 Air-to-Ground Mission Stress/Load Ratios.....	129
Figure 6-11 Training Mission Stress/Load Ratios	130

Figure 7-1 Maximum Principal Stresses for Symmetric Positive Load Factor Maneuvers in the Air-To-Air Mission: Ascent Segment.....	132
Figure 7-2 Clipped Cycle	137
Figure 8-1 Through-the-Thickness Crack in an Infinitely Wide Panel.....	140
Figure 8-2 SMF Iterations for a Through-the-Thickness Crack.....	141
Figure 8-3 Crack Growth History for the Through-the-Thickness Crack.....	142
Figure 8-4 Semi-Elliptical Surface Crack in an Infinitely Wide Panel.....	143
Figure 8-5 SMF Iterations for the Semi-Elliptical Surface Crack.....	143
Figure 8-6 Crack Growth History for the Semi-Elliptical Surface Crack.....	144
Figure 8-7 Corner Crack in a Hole in an Infinitely Wide Panel.....	145
Figure 8-8 SMF Iterations for a Corner Crack in a Hole	146
Figure 8-9 Crack Growth History for the Corner Crack in a Hole	147
Figure 9-1 Master Element Location in the Right Lower Wing Skin.....	150
Figure 9-2 Optimization Weight Histories with DTA Constraints.....	154
Figure 9-3 Design Variables (1-8) Versus Optimization Run	156
Figure 9-4 Design Variables (9-17) Versus Optimization Run	157
Figure 9-5 Weight History with Multidisciplinary Constraints.....	162
Figure 9-6 Maximum Constraint Values: Underwing Stores, Run 1	164
Figure 9-7 Maximum Constraint Values: No Underwing Stores, Run 2	164

ABSTRACT

Damage tolerance analysis (DTA) was considered in the global design optimization of an aircraft wing structure. Residual strength and fatigue life requirements, based on the damage tolerance philosophy, were investigated as new design constraints. In general, accurate fatigue prediction is difficult if the load environment is not known with a high degree of certainty. To address this issue, a probabilistic approach was used to describe the uncertain load environment. Probabilistic load spectra models were developed from flight recorder data. The global/local finite element approach allowed local fatigue requirements to be considered in the global design optimization. AFGROW fatigue crack growth analysis provided a new strength criterion for satisfying damage tolerance requirements within a global optimization environment. Initial research with the ASTROS program used the probabilistic load model and this damage tolerance constraint to optimize cracked skin panels on the lower wing of a fighter/attack aircraft. For an aerodynamic and structural model of an F-16, ASTROS simulated symmetric and asymmetric maneuvers during the optimization. Symmetric maneuvers, without underwing stores, produced the highest stresses and drove the optimization of the inboard lower wing skin. Asymmetric maneuvers, with underwing stores, affected the optimum thickness of the outboard hard points. Subsequent design optimizations included von Mises stress, aileron effectiveness, and lift effectiveness constraints simultaneously. This optimization was driven by the DTA and von Mises stress constraints and, therefore, DTA requirements can have an active role to play in preliminary aircraft design.

CHAPTER I

INTRODUCTION TO FATIGUE IN AIRCRAFT STRUCTURAL DESIGN

1.1 Background

The primary purpose of any structure is to resist and transmit applied loads. The aerodynamic loads of an aircraft wing and empennage are transmitted into their spars and make their way into the fuselage substructure of bulkheads and stringers, eventually ending up in the fuselage skin. Because an aircraft must operate in many different conditions, a variety of loads, some of which are time varying, are applied to the structure. An aircraft must be designed to fly in turbulent weather, withstand hard landings, and perform certain maneuvers. Some aircraft fuselage structures will experience numerous cycles of expansion and contraction, similar to a toy balloon, caused by internal pressurization. Unfortunately, the nature of weather is chaotic and the loads of known flight maneuvers cannot be predicted exactly. However, with past experience, the magnitude and frequency of these loads can be determined using statistics and probability. These results will not insure that an aircraft will never experience more severe loads. It is the pilot who ensures that the aircraft remains within the stress limits or "design envelope". The pilot must prevent the penetration into severe weather, bad landings, and must fly within the design gross weight limit. Poor piloting will impose loads on the structure that it was not designed to carry. Military aircraft experience higher loads compared to the civilian fleet. They perform gut wrenching g-pulling turns

and fly high speeds at lower altitudes where gust intensities are greater. Some even perform “controlled crash landings” on a pitching aircraft carrier.

Early criteria for determining the magnitude of loads were often conservative and arbitrary. As knowledge of the loading environment increased, the loading development criteria required a more meaningful approach, and predicted loads came closer to those experienced in flight. Through experience, a safety factor such as 1.5 was used in the design to provide reserve strength. The safety factor was multiplied by the limit loads to obtain the design loads, otherwise known as ultimate loads, as shown in Figure 1-1. The

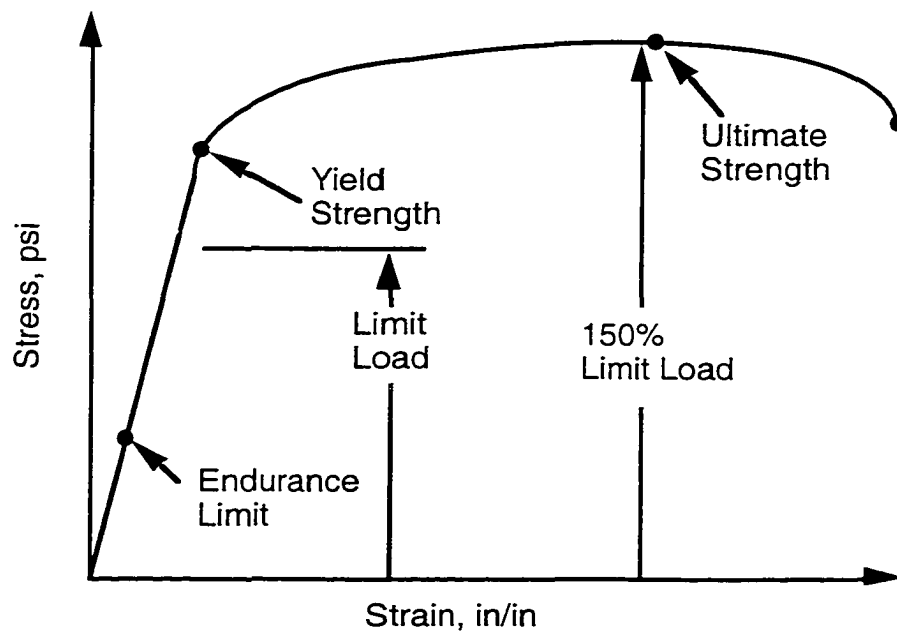


Figure 1-1 Typical Stress-Strain Diagram

safety factor was intended to address unknown variations in loads, stresses, material properties, and manufacturing tolerances. Unfortunately, the historical development of aircraft coincided with the use of high strength metal alloys which were fatigue notch

sensitive. This meant that designing to ultimate loads was no longer sufficient to provide structural integrity. A fatigue crack could grow with loads well below the limit loads.

In 1970, the United States Air Force (USAF) implemented a damage tolerance philosophy to eliminate fatigue cracking problems found on various aircraft¹. This resulted in several USAF military specifications such as MIL-STD-1530² and MIL-A-83444³. Because of these specifications, aircraft manufacturers were required to incorporate damage tolerance requirements into aircraft design. The objective of damage tolerance requirements is “to protect the safety of flight structures from potentially deleterious effects of material, manufacturing and processing defects through proper material selection and control, control of stress levels, use of fracture resistant design concepts, manufacturing and process controls and the use of careful inspection procedures.”² The damage tolerant design process will use fail-safety concepts or slow fatigue crack growth analysis to meet these requirements. Such analysis is called damage tolerance analysis (DTA).

Fracture mechanics is the mathematical tool used in damage tolerance analysis. Fracture mechanics provides the concepts and equations used to determine how cracks grow and affect the strength of a structure⁴. Fracture mechanics has matured over the last 40 years into a practical engineering tool.

Fatigue crack growth rate is primarily dominated by material properties and the stress history. The stress history must be relatively benign in magnitude and frequency to produce a long crack growth life. Since the stress history is determined by the intended usage of the aircraft, reducing the stress magnitudes through redesign of the local structure has been used to meet the design life requirements. Chaperon, Sawyer, and

Jones⁵ optimized the shape of a structural cutout in their research to reduce local stresses and maximize fatigue life.

If the fatigue life of a fracture critical location (FCL) is too short, then redesign of the structure will be needed, or an inspection program will be required during service. The USAF DTA policy requires the crack growth life of a noninspectable FCL to be double the design life. The assumed initial crack size for noninspectable structures is 0.05 inch at holes and cutouts or 0.25 inch for other locations. If the crack is inspectable at a base or depot, then an inspection is required at one-half the crack growth life. The assumed initial crack size for inspectable structures is 0.25 inch at holes and cutouts or 0.5 inch for other locations. If the fatigue life of an inspectable area is twice the design life, then no inspection is needed during service. Accounting for fatigue early in the design process can remove or reduce inspection requirements, thereby reducing operational costs. This requires a methodology for linking DTA within the global design optimization environment.

Structural optimization typically considers global issues such as flutter, dynamics, internal load paths, and gross stress calculations. Detailed local structural analyses are impractical in a global design optimization of an aircraft. Fatigue is a localized phenomenon requiring detailed structural analysis; however, local issues such as fatigue are generally not considered in a global analysis. Including DTA criteria in the global analysis would distort the optimization. But if local fatigue design requirements are not met, costly global redesigns may be needed. Therefore, providing local fatigue requirements in the global aircraft design optimization would be beneficial. The solution is to perform a global analysis of the structure first, subject to global behavior and

manufacturing constraints, and then use the local load path, load spectra, and stiffness results as input for a local structural analysis. Results of the local DTA analysis are then used to define constraints and sensitivities in a subsequent global optimization loop.

1.2 Objectives

The first objective of this research focused on modeling the fatigue load environment with only a few parameters using the Axum[®] program⁶. The data in this research consisted of maneuver normal load factors. Load factor data due to gusts were excluded. The probabilistic loads program “Load_occurrence.exe”, in Appendix A, developed probability distribution functions from the fatigue load models and generated a normal load factor history. The load factor history defines a fighter aircraft’s usage throughout its lifetime.

The second objective of this research linked damage tolerance analysis with aircraft design optimization by using the Automated STRuctural Optimization System⁷ (ASTROS) multidisciplinary analysis and design program. ASTROS’s existing modeling capabilities were utilized to develop a structural finite element model and aerodynamic model of a fighter aircraft. The program “Global_local.exe”, in Appendix E, took local stress data from ASTROS flight maneuver analyses and the aircraft load factor history, and built a fatigue stress history. This stress history was used to perform iterative fatigue crack growth analyses of an inboard lower wing skin panel which ultimately produced a fatigue stress allowable. This fatigue stress allowable was used as a maximum principal stress constraint in the global design optimization of the wing structure. This approach is illustrated in Figure 1-2.

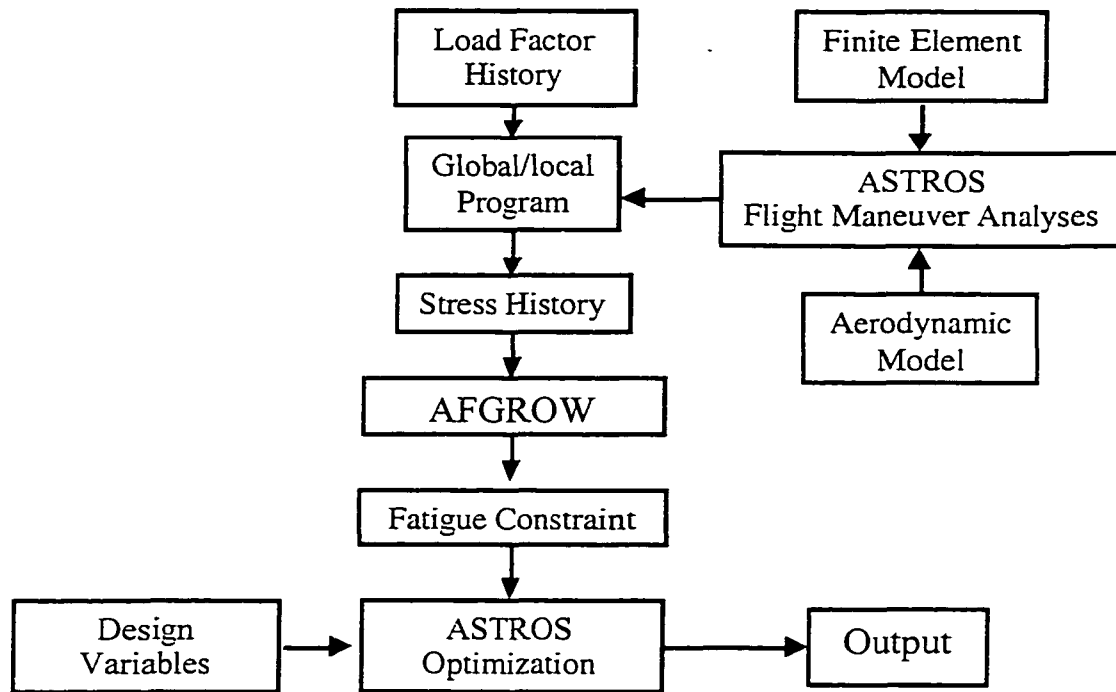


Figure 1-2 Flow Chart of Approach

1.3 Dissertation Organization

This dissertation is organized into ten chapters. The first chapter provides some background into aircraft design with metal fatigue, and describes the motivation and objective of this research. The second chapter gives a thorough background on the theory of linear elastic fracture mechanics adapted from a course I developed and taught at Tinker Air Force Base, Oklahoma. The third chapter discusses sources of fatigue loads and traditional load spectra development methods in USAF aircraft. Chapter four presents research results that replace traditional fatigue environment data with probability models. Chapter five describes the construction of a fighter flight-by-flight load history from the probability models of the previous chapter. Chapter six contains the ASTROS aeroelasticity results of a fighter aircraft needed to transform the load history from Chapter five into the stress history described in Chapter seven. Chapter eight explains

how a damage tolerance constraint for a fighter aircraft lower wing skin was developed using AFGROW⁸ and the stress history developed in Chapter seven. The results of the lower wing skin optimization are presented in Chapter nine. The last chapter consist of a brief summary of the most important findings, conclusions, and recommendations.

CHAPTER II.

ELEMENTS OF FRACTURE MECHANICS

Fatigue is a process which causes premature failure of a structure subjected to repeated loads. It is characterized as a progressive failure phenomenon that proceeds by the initiation and propagation of cracks to an unstable size. Fatigue is controlled by four factors: stress history, material properties, chemical environment, and manufacturing quality. The frequency of application, magnitude, sequence, and algebraic sign of the loads affects fatigue onset and the rate of crack growth. Certain materials are prone to fatigue while others are highly resistant. The chemical (corrosion), temperature, and loading rate environment can also interact with the fatigue process. The manufacturing quality of the structure includes details such as local stress concentrations, existing flaws, surface finish irregularities, and residual stresses.

During the growth of a crack, the structural strength decreases until it becomes too low to support the maximum loads experienced during operational service and fracture occurs[†]. Thus, cracks must be prevented from growing to a size at which the remaining strength (residual strength) would be inadequate to sustain the loads. This requires knowledge of how strength is reduced by crack length. To determine safe operational life, one must be able to calculate the time at which a crack becomes too long and produces fracture. Therefore, damage tolerance analysis is performed to provide information on structural strength reduction as a function of crack size and to determine crack growth life. The accuracy of the respective DTA depends on the accuracy of the material properties, predicted loads, and stresses.

Fracture mechanics is the mathematical tool employed in DTA. The fracture mechanics analysis starts with an initial crack length a_i . The initial crack length is often assumed. This assumption is based on experience with similar components and typical flaws created by the manufacturing process, dictated by the nondestructive inspection method and inspector skill, or defined by a regulatory authority. A fracture critical location (FCL) is a safety-of-flight structural detail susceptible to fatigue, and its location is determined through experience stress analysis, and/or full scale fatigue testing. In the USAF DTA philosophy, cracks are assumed to exist in fracture critical locations and to grow in the worst orientation even in the newest structures.

A crack in a solid can be loaded in three different ways as shown in Figure 2-1: mode I, mode II, or mode III. Mode I, or "opening mode", is caused by normal stresses (σ_x , σ_y , σ_z). Mode I is the most common mode because cracks prefer to grow perpendicular to the maximum principal stress direction (pure Mode I). The maximum principal stress direction is the orientation of stress flow that creates the largest algebraic normal stress and zero shear stress simultaneously. Mode II, or "sliding mode", is caused by in-plane shear stresses (σ_{xy}). Mode III, or "tearing mode", is caused by out-of-plane shear stresses (σ_{xz} , σ_{yz}).

2.1 Stress Intensity Factor

The stress intensity factor K is the single parameter used to characterize the severity of a crack. This parameter is based on the crack tip stress field and is related to load, crack size, and geometry. The stress intensity factor is defined in Eq. (2.1) where σ

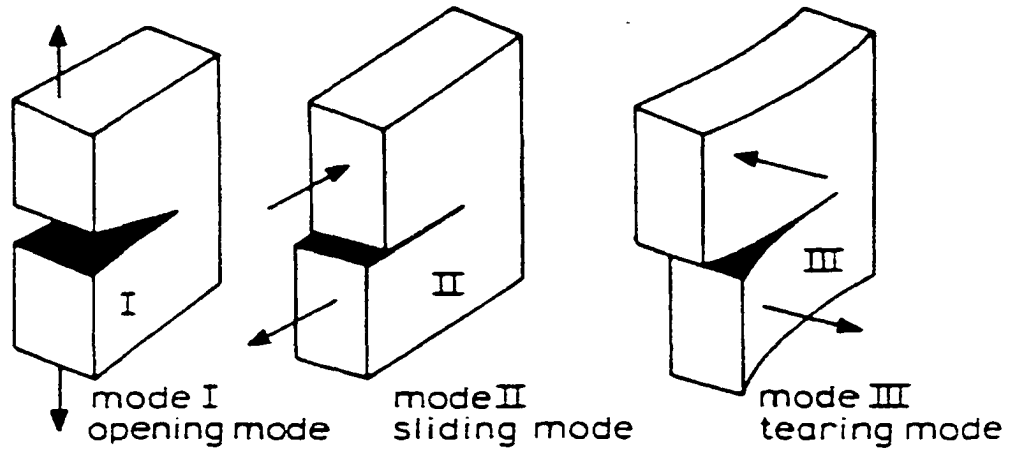


Figure 2-1 The Three Fracture Modes of Loading⁹

is the gross stress and a is the crack length. The variable β depends on the specimen and crack geometry. The dimensionless function β is highly affected by the component geometry or structural configuration. That is, β will change with the geometry of the problem. Change the component or configuration and β will change. Sometimes the letter F is used in the literature instead of β . The remaining terms in the stress intensity factor equation, $\sigma\sqrt{\pi a}$, typically will remain the same regardless of the structural configuration.

$$K = \sigma\sqrt{\pi a} \cdot \beta \quad (2.1)$$

Every fracture mechanics problem requires knowledge of the stress intensity factor for the crack of interest. Handbooks of stress intensity factors such as *The Stress Analysis of Cracks Handbook*¹⁰ by Tada, Paris, and Irwin, contain a large collection of stress intensity factor solutions. Unfortunately, a real structural problem can be so unique that an existing handbook stress intensity factor solution is not available. The engineer

will need to approximate the stress intensity factor solution using one or more of the following methods: superposition of known handbook stress intensity factor solutions, compounding of known handbook β solutions, the similarity ratio method, the boundary element method, or the finite element method. Crack growth prediction programs such as AFGROW do not require the whole stress intensity factor that was computed from these methods. These programs only need the geometry factor β for a range of crack sizes. To compute β in Eq. (2.2), the estimated stress intensity factor is divided by the remote applied stress and the square root of pi times the crack length.

$$\beta = \frac{K}{\sigma \sqrt{\pi a}} \quad (2.2)$$

Values for β in many engineering problems range from 1 to 1.4. Errors in β are small compared to the uncertainties in a damage tolerance analysis. The accuracy of a damage tolerance analysis is determined primarily by material properties, load levels, load history, service environment, and assumptions. A 5 to 10% error in β is usually acceptable.

2.1.1 Superposition⁴

Stress intensity factor solutions for a given loading mode (i.e., modes I, II, or III) can be added because of their basis in linear elasticity. Therefore, the stress intensity factors for complex loading conditions of the same mode can be computed from the superposition of simpler stress intensity factor solutions readily found in handbooks. The simpler stress intensity factor solutions must have the same geometry. If different modes of loading are present in the problem, then superposition cannot be used. One cannot add

K_I to K_{II} or K_{III} . The goal in superposition is to reduce the complicated real structure to a number of simpler configurations with known stress intensity factor solutions. In Eq. (2.3), adding the stress intensity factor solutions of these simpler configurations will give the stress intensity factor solution of the complicated structure. This method is useful when there is more than one force (or moment) acting to grow the crack in a given mode.

$$\text{Mode I: } K_{\text{complicated}} = K_1 + K_2 + K_3 + \dots \quad (2.3)$$

2.1.2 Compounding⁴

The goal in compounding is to reduce the complicated structure to a number of simpler configurations with known handbook β factors. In the literature, β factors are sometimes called “correction factors” because they correct the stress intensity factor for geometry effects. The compounding method simply multiplies the individual β factors together in Eq. (2.4) to create an effective β factor that accounts for all the geometric effects. Individual β factors are used to account for finite width effects, front wall effects, back wall effects, holes, and crack shape (i.e., elliptical flaws).

$$K = \beta_1 \cdot \beta_2 \cdot \beta_3 \cdot \dots \cdot \sigma \sqrt{\pi a} \quad (2.4)$$

2.1.3 Similarity Ratio Method¹¹

This method of calculating complex stress intensity factors is similar to compounding. Instead of using β , this method multiplies and divides whole stress intensity factor solutions together to account for the effects of different geometries and loads. The goal in the similarity ratio method is to reduce the complicated real structure

into a number of simpler configurations with known stress intensity factor solutions. This method is an approximation. It does not provide exact values of stress intensity factor solutions. Simple approximations such as this method are acceptable in engineering when alternative methods such as finite element analyses are too time consuming.

2.1.4 Finite Element Method⁴

The finite element method has been used in two ways to determine stress intensity factors as a function of crack length; the indirect method and the direct method.

The indirect finite element method is used to model an uncracked structure for stress in the proposed region of crack growth. The resulting stress is "corrected" for the presence of a hypothetical crack using Green's functions, weight functions, or the finite element alternating method (FEAM). Some programs compute stress intensity factors automatically, others require additional manipulation of the results to calculate stress intensity factors. The advantage of the indirect method is that the crack does not have to be modeled explicitly in the finite element mesh or manually incremented after each stress intensity factor calculation. Accordingly, the indirect method does not require special "singular" crack tip elements that model the square root singularity of the crack tip.

The direct finite element method requires the engineer to model the crack in the finite element mesh. Easy results are produced if special "singular" crack tip elements are used around the crack tip. Many commercially and publicly available finite element computer programs include subroutines to calculate stress intensity factor. Programs such as MSC NASTRAN, MECHANICA, FRANC2D/L, and FRANC3D have singular

crack tip elements and compute stress intensity factors automatically; others require additional manipulation of the results to calculate stress intensity factors. Most fracture problems require a stress intensity factor at several crack lengths; therefore the modeled crack has to be manually incremented. This requires the finite element model to be regenerated and is very time consuming. FRANC2D/L and FRANC3D automatically increment the crack length and calculate the stress intensity factors without requiring the engineer to regenerate the finite element model.

2.2 Plane Stress Versus Plane Strain in Fracture Mechanics

In two-dimensional stress analysis, there exist two families of problems or states of stress: plane stress or plane strain. Typically, one can classify a stress analysis problem as either “plane stress” or “plane strain,” depending on the values of stress (σ_Z) and strain (ϵ_Z) in the out-of-plane direction (along the Z axis).

If a thin plate is subjected to in-plane loads or stresses along its edges the thickness of the thin plate will decrease because of the Poisson effect. The thin plate provides no resistance to thinning in the Z direction; therefore, $\sigma_Z = \sigma_{XZ} = \sigma_{YZ} = 0$, and $\epsilon_Z \neq 0$. This is a plane stress problem.

If a thick plate is subjected to in-plane loads or stresses along its edges the thickness of the thick plate will not decrease significantly. The thick plate provides a large resistance to Poisson thinning in the Z direction; therefore, $\epsilon_Z = 0$. Because the plate resists thinning in the Z direction, tensile stresses are developed internally in the Z direction as a "counter-reaction". We therefore find that $\sigma_Z \neq 0$. This is a plane strain

problem.

The concepts of plane stress and plane strain apply to fracture mechanics. These are important concepts to understand. One needs to know what state of stress the fracture mechanics problem is in before attempting to solve it. The state of stress, plane strain, plane stress, or something in-between, will affect the final fracture event. This will be discussed further in the section “2.4 Fracture Toughness.” Figure 2-2 below shows how the roll of material at the crack tip wants to contract in the thickness direction due to the large stresses that are present. In the thick plate with a crack and a low remote stress; however, the roll of material is thin and no contraction takes place. This condition is plane strain. In the thin plate with a crack and low remote stress, the roll of material is free to contract. This condition is plane stress.

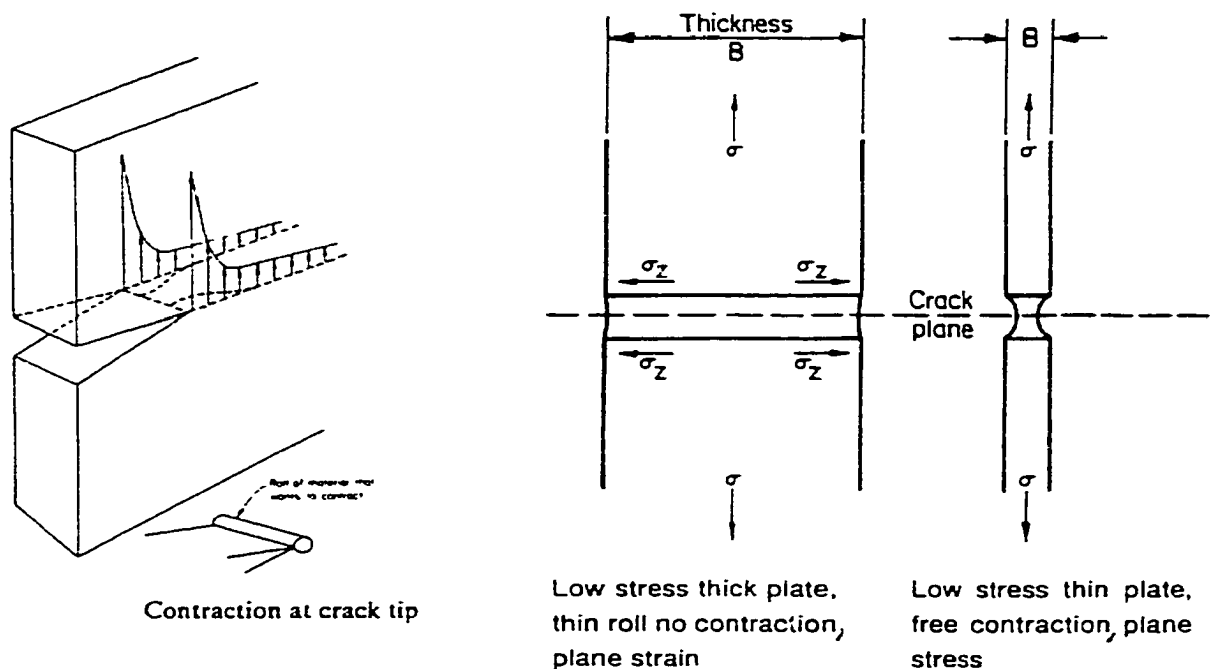


Figure 2-2 Plane Stress and Plane Strain in Fracture Mechanics⁴

2.3 Crack Tip Plastic Zone

According to the elastic theories of fracture mechanics, the stresses near the tip of a crack approach infinity as one approaches closer and closer to the tip. Infinite stresses cannot exist in real materials; instead, the material yields ($\sigma \geq \sigma_{YS}$) in front of the crack tip. This region of yielding in Figure 2-3 is called the “crack tip plastic zone.” This crack tip plasticity controls crack growth and fracture. If the plastic zone size r_p is small relative to the local geometry (r_p/t and $r_p/a < 0.1$ where t = thickness), then the stress intensity factor, K , is valid. The special field of fracture mechanics that meets the above conditions is called Linear Elastic Fracture Mechanics (LEFM). Linear Elastic Fracture Mechanics also requires that the local nominal stresses in the crack plane be less than the yield strength. Typically, 0.8 times yield strength is used as the limit.

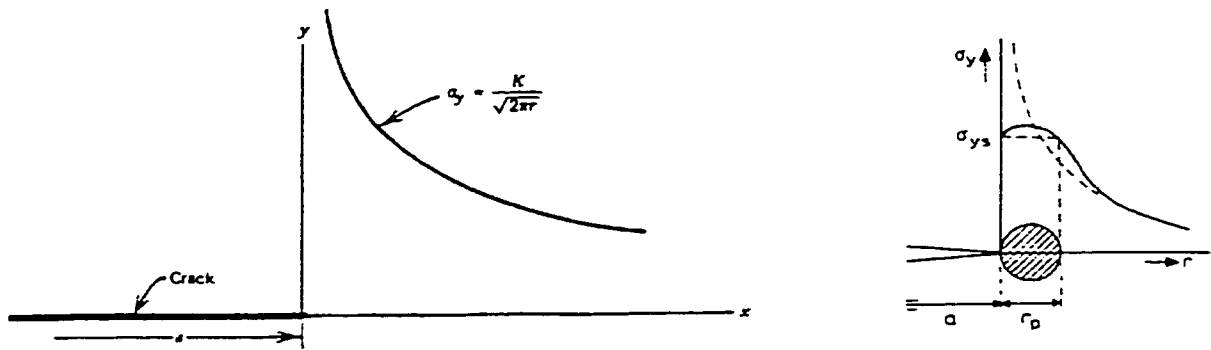


Figure 2-3 Crack Tip Stress Field¹²

The plastic zone size at the crack tip r_p can be calculated as a function of stress intensity factor and yield strength for plane stress in Eq. (2.5) and for plane strain in Eq. (2.6).

In plane stress:

$$r_p = \frac{1}{2\pi} \left(\frac{K}{\sigma_{YS}} \right)^2 \quad (2.5)$$

In plane strain:

$$r_p = \frac{1}{6\pi} \left(\frac{K}{\sigma_{ys}} \right)^2 \quad (2.6)$$

The plane stress plastic zone size is three times larger than the plane strain plastic zone size. This may seem trivial now but will become important when discussing fracture toughness. The circular plastic zone shape shown above is just one model. There are other plastic zone shape models.

Even in thick parts under plane strain, the surfaces perpendicular to the crack tip will be in plane stress as shown in the three dimensional drawing of the plastic zone in Figure 2-4. But because the majority of the plastic zone is under plane strain, the crack behaves as a plane strain fracture mechanics problem.

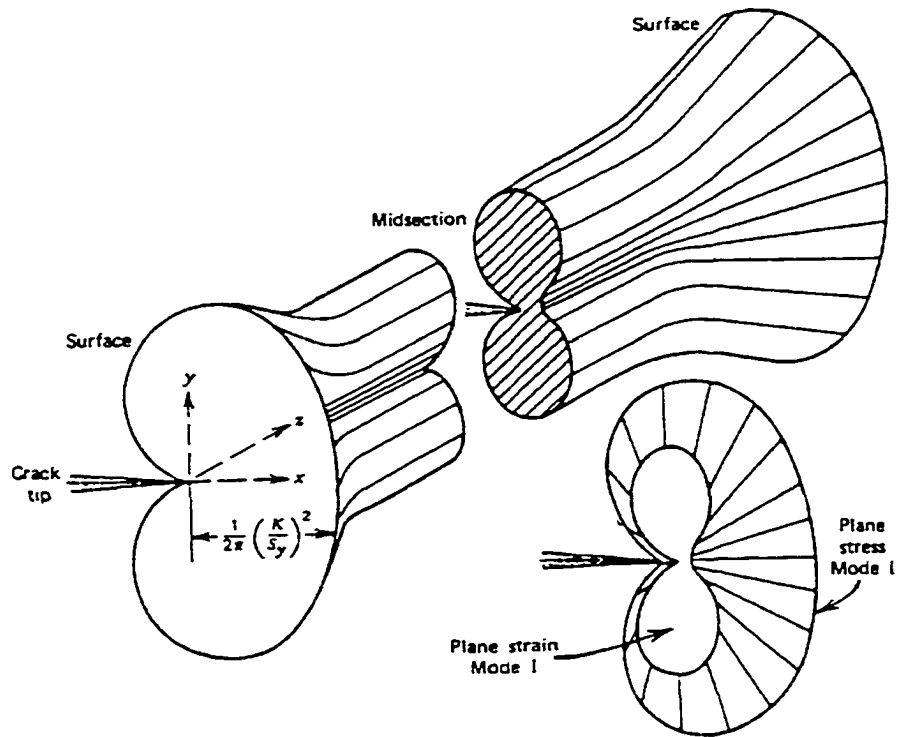


Figure 2-4 Crack Tip Plastic Zone Size¹²

2.4 Fracture Toughness

Fracture toughness is a cracked material's ability to resist fracture. Fracture toughness can be measured for brittle materials from tests using specimens with fatigue cracks and known stress intensity factor expressions. Fracture toughness is not the same as strength. Fracture toughness is the critical (maximum) value of stress intensity factor for which a crack extends in a rapid, unstable manner without an increase in load. These critical values of stress intensity factors are denoted with a subscript c . In general, fracture toughness depends on the material, temperature, strain rate, environment, thickness, and to a lesser extent, on crack length. If fracture toughness, crack length, and stress intensity factor are known for a particular crack problem undergoing monotonic loading, the fracture stress or residual strength can be determined. Also, fracture toughness represents the maximum stress intensity factor at the last cycle of fatigue fracture in Figure 2-5 and can be used to obtain the critical crack size a_f for fracture under cyclic loading.

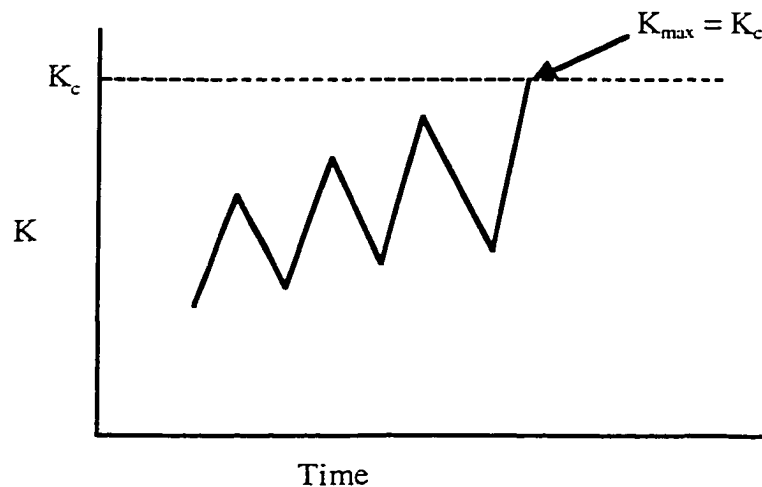


Figure 2-5 Fracture Toughness and Fatigue

Fracture toughness is not a true material property like Young's modulus or Poisson's ratio. It varies with thickness as depicted in Figure 2-6. For the same material, thin components have higher fracture toughness and slant fracture morphology. The highest value of fracture toughness occurs in thin components and is called the "plane stress fracture toughness."

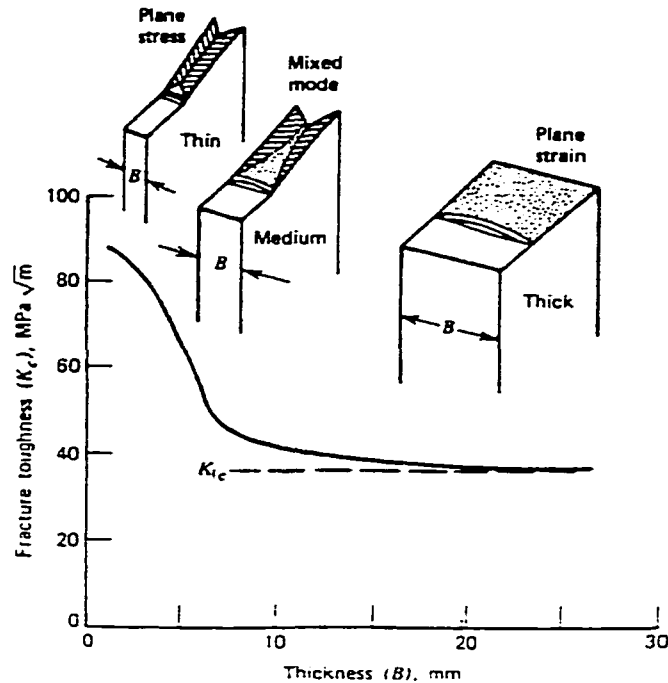


Figure 2-6 Effect of Thickness on Fracture Toughness¹²

Because of plane stress conditions, thin components have a large crack tip plastic zone which dissipates large amounts of energy in the process of yielding. The more energy dissipates through yielding, the tougher the component. As thickness is increased, fracture toughness decreases. For thick components experiencing the plane strain stress state, the fracture surface is flat and the fracture toughness approaches an asymptotic minimum value. Any additional increase in thickness does not change fracture toughness. This minimum value of fracture toughness is called the "plane strain fracture

toughness” K_{Ic} . This is pronounced “kay one cee.” The subscript I refers to mode one loading.

Plane strain fracture toughness values are determined by the standardized test procedure, *The American Society for Testing and Materials E-399*, “Standard Test Method for Plane-Strain Fracture Toughness of Metallic Materials.”¹³ The values of fracture toughness between plane stress and plane strain fracture toughness are called “transitional fracture toughness” or “mixed mode fracture toughness.”

Plane strain fracture toughness K_{Ic} is considered a true material property because it is independent of thickness. Published values of plane strain fracture toughness K_{Ic} and transitional fracture toughness K_C are available in the USAF *Damage Tolerant Design Handbook*¹⁴. From laboratory data, Eq. (2.7) has been developed to determine the thickness B^* required for plane strain fracture toughness¹³.

$$B^* \geq 2.5 \cdot \left(\frac{K_c}{\sigma_{ys}} \right) \quad (2.7)$$

Low strength, ductile materials are subject to plane strain fracture toughness at room temperatures only if they are very thick. Therefore, most plane strain fracture toughness data have been obtained for the medium and higher strength materials.

A general trend for plane strain fracture toughness at room temperature, as a function of yield strength is given in Figure 2-7. It shows that a wide range of plane strain fracture toughness exists for a given metal. A high yield material produces a decrease in plane strain fracture toughness and, thus, an increased chance of fracture¹². Even for a given yield strength, a wide variability exists for plane strain fracture toughness depending on the material quality. Low impurity materials produce higher

fracture toughness values.

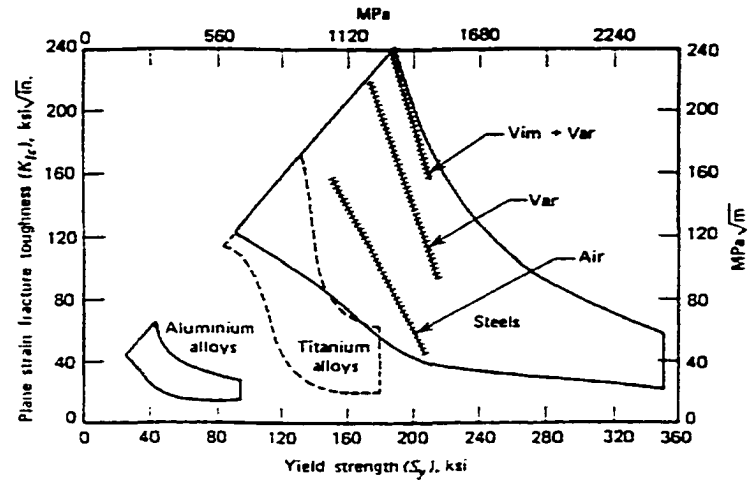


Figure 2-7 Plane Strain Fracture Toughness Versus Yield Strength¹²

Fracture toughness is also dependent on temperature and strain rate. The fracture toughness decreases as the temperature decreases as shown in Figure 2-8. Increased strain rate has the same effect on fracture toughness as decreasing temperature. Higher strain rates produce lower fracture toughness.

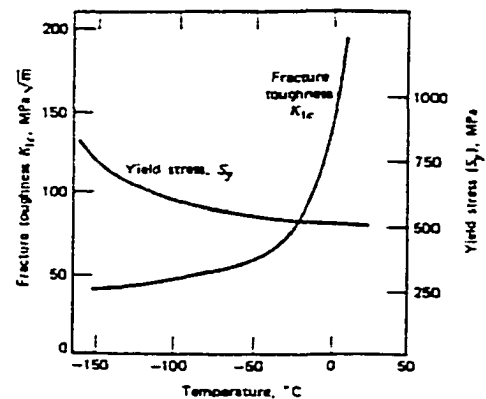


Figure 2-8 Variation of Fracture Toughness with Temperature¹²

The metals used on aircraft are not truly isotropic. The manufacturing processes used to give a component its shape instill some anisotropy to the metal. Ultimate strength, Young's modulus, and Poisson's ratio of a plate in the longitudinal (L) or rolling direction may be different from those in the width or transverse (T) direction. This is also true for crack growth and fracture toughness data. Fracture toughness is dependent

on orientation of the crack plane relative to the grain direction in a test specimen or structural component. It is very important that the correct fracture data are selected for the grain direction that matches the structure. Of course, this requires knowledge of the grain direction in the structure. The grain direction must not be assumed or guessed. Production drawings can provide information on grain direction.

The orientation of the crack relative to the grain direction is specified by a pair of grain direction symbols. The first digit specifies the grain direction perpendicular to the crack plane. The second digit specifies the grain direction parallel to the fracture direction. The six basic grain direction pairs are: T-L, T-S, L-T, L-S, S-L, and S-T. The direction of maximum grain flow is L, T is the direction of least deformation, and S is the third orthogonal direction. The crack plane orientation codes for rectangular sections, tilted specimens, and for cylinders are depicted in Figure 2-9 through Figure 2-11.

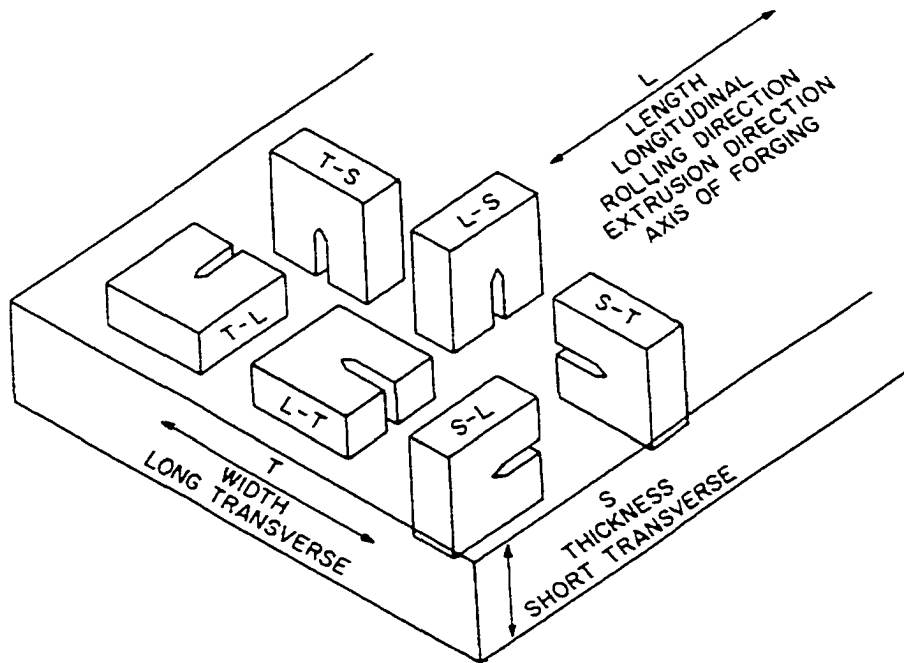


Figure 2-9 Crack Plane Orientation Code for Rectangular Sections^{13,14}

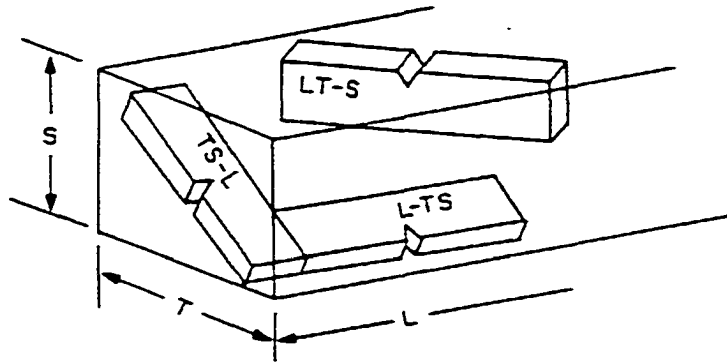


Figure 2-10 Crack Plane Orientation Code for Tilted Specimens^{13,14}

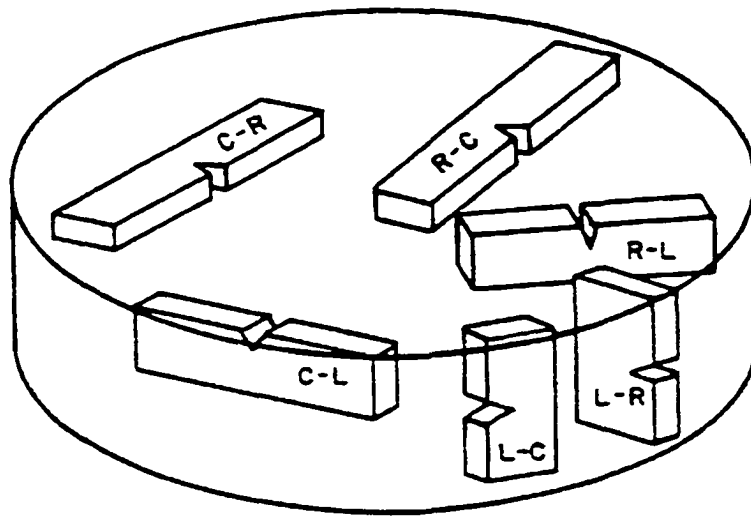


Figure 2-11 Crack Plane Orientation Code for Cylinders^{13,14}

Figure 2-12 displays the room temperature fracture toughness versus thickness for several aluminum alloys in the L-T direction. The plane stress fracture toughness is easily visible at the smaller thickness values. From inspection of this figure, it appears that the 7000 series aluminum alloys typically have lower fracture toughness than the 2000 series aluminum alloys. For this reason, 7000 series aluminum alloys should be avoided in structures where tensile loads are predominant.

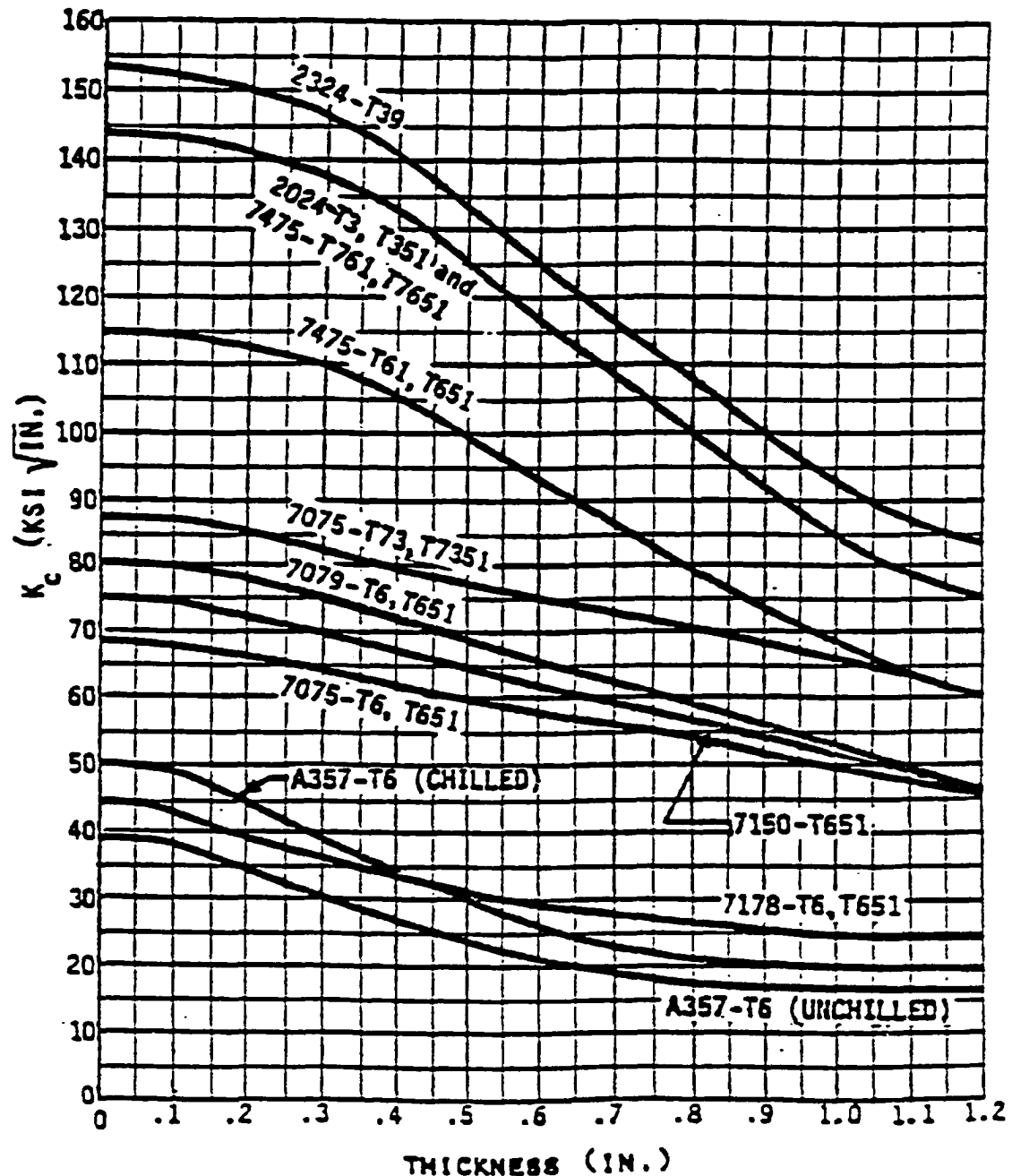


Figure 2-12 Fracture Toughness Versus Thickness at Room Temperature for Various Aluminum Alloys: L-T Direction¹⁵

2.5 Fatigue Crack Growth

Fatigue cracks grow at speeds inherent to the material. Some materials historically chosen for their high yield strengths are now known to be notorious for fast

growing fatigue cracks (i.e., 7075-T6, 7178-T6) when exposed to cyclic loads. These materials should be avoided in the design of damage tolerant structures. The fatigue crack growth rate is measured by the calculus differential da/dN or incremental change in crack length a with respect to change in cycle count N . Typical units are inches per cycle. The speed of a fatigue crack is not constant, but changes with crack length, stress level, and environment. To account for this, the fatigue crack growth rate for a given material is given by a da/dN - ΔK relationship in Eq. (2.8). This da/dN - ΔK relationship can be found in the literature as graphs of da/dN versus ΔK data for various materials¹⁴.

$$da/dN = f(\Delta K) \quad (2.8)$$

The ΔK parameter in Eq. (2.9) is called the cyclic stress intensity factor range. It is the difference in stress intensity factors calculated between the peak and valley of a load cycle. The peak load produces the maximum stress in a cycle which provides the maximum stress intensity factor K_{\max} . The adjacent valley (minimum) load produces the minimum stress in the same cycle, which provides the minimum stress intensity factor, K_{\min} . When repeated loads are present, the cyclic stress intensity factor ΔK controls the fatigue crack growth rate da/dN .

$$\Delta K = K_{\max} - K_{\min} = \Delta \sigma \sqrt{\pi a} \cdot \beta \quad (2.9)$$

$$K_{\max} = \sigma_{\max} \sqrt{\pi a} \cdot \beta \quad (2.10)$$

$$K_{\min} = \sigma_{\min} \sqrt{\pi a} \cdot \beta \quad (2.11)$$

The da/dN - ΔK curve is developed from laboratory test specimens using the *American Society for Testing and Materials Standard E 647*¹⁶. The da/dN - ΔK curve can be divided into three regions as depicted in Figure 2-13. The threshold value of ΔK_{th} ,

below which no crack growth is indicated, defines Region I. In Region II, stable crack growth is indicated where the crack growth rate function $da/dN-\Delta K$ is typically modeled as a power law equation. The power law equation is a straight line in log-log coordinates. Region III is the accelerated crack growth region where the Region II relationship is no longer valid. In Region III, as K_{\max} approaches K_c , the crack growth accelerates to fracture.

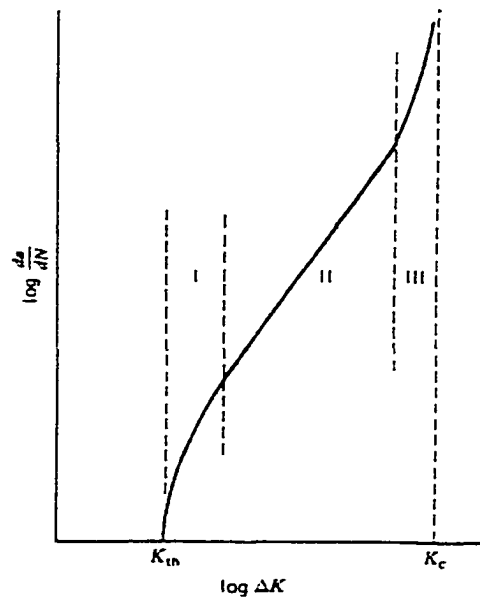


Figure 2-13 Three Regions of Fatigue Crack Growth Response¹²

The $da/dN-\Delta K$ curve is a material property curve and is geometry independent. The $da/dN-\Delta K$ curve removes dependence on initial crack length, stress range $\Delta\sigma$, or load range ΔP . Stress intensity factor is the common denominator. As stress intensity factor can consider the effects of different crack configurations, similitude is provided. Because of similitude, we can use these data developed from test specimens for actual aircraft structures. Similitude only works when the load spectrum is of constant amplitude.

Similitude is not valid when the loading spectrum is of variable amplitude. The solution to this problem will be discussed in “2.10 Spectrum Loading and Load History Effects.”

In DTA, the goal is to compute crack growth life N in terms of cycles, flight hours, or the number of flights. A mathematical model of the da/dN - ΔK curve in Region II is normally developed. Region II is a straight line which makes curve fitting easier and most of the cracking takes place there¹². This mathematical model, or curve fit, is called the crack growth rate equation. The Paris¹⁷, Walker¹⁸, and Forman¹⁹ equations are examples of popular crack growth rate equations. Once a crack growth rate equation has been modeled to the da/dN - ΔK curve, crack growth life N can be found by numerical integration of Eq. (2.12). The fracture toughness, K_{IC} , controls the point of fracture thereby defining final fatigue crack length a_f .

$$N = \int_{a_i}^{a_f} \frac{da}{f(\Delta K)} \quad (2.12)$$

The Paris crack growth rate equation will be discussed first. The Paris Equation is used to model the straight-line portion in Region II of Figure 2-14 on the following page. The parameters C and m are empirical constants computed by fitting a straight line through the data on a da/dN - ΔK curve. Substituting the Paris Eq. (2.13) into Eq. (2.12), for crack growth life for an edge crack in a semi-infinite sheet ($\beta = 1.122$), produces Eq. (2.14).

$$\frac{da}{dN} = C\Delta K^m \quad (2.13)$$

$$N = \int_{a_i}^{a_f} \frac{da}{C\Delta K^m} = \int_{a_i}^{a_f} \frac{da}{C[1.122\Delta\sigma\sqrt{\pi a}]^m} \quad (2.14a)$$

$$N = \frac{1}{C[1.122\Delta\sigma\sqrt{\pi}]^m} \int_{a_i}^{a_f} \frac{da}{a^{m/2}} \quad (2.14b)$$

$$N = \frac{1}{C[1.122\Delta\sigma\sqrt{\pi}]^m} \frac{2}{m-2} \left[\frac{1}{a_i^{\frac{m-2}{2}}} - \frac{1}{a_f^{\frac{m-2}{2}}} \right] \quad (2.14c)$$

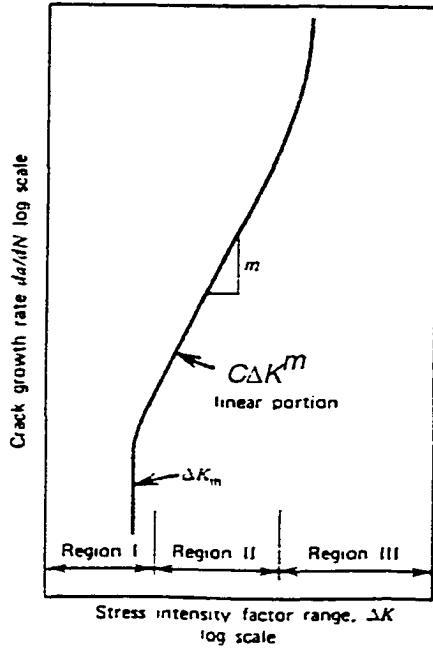


Figure 2-14 Paris Model of Region II in the da/dN - ΔK Curve¹²

Typical values of m fall in the range $2 < m \leq 8$. An exact closed form solution for this simple problem exists because β is independent of crack length a . In most cases, β varies with crack length a , and the problem is numerically integrated as discussed in section “2.6 Numerical Integration.” From inspection of the solution for N , the following observations can be made. The material is specified by constants C and m and by selection of a crack growth rate equation. The geometry of the problem is specified through β .

The issue of mixed mode fatigue crack growth in a multi-axial loading environment can be addressed by using the maximum principal stress, as fatigue cracks grow perpendicular to the maximum principal stress direction. The maximum principal stress is used as the remote stress in the pure mode I fracture mechanics equations.

2.6 Numerical Integration

In most real damage tolerance analysis problems, β is a function of crack length and a closed form solution to the integral is not available. Instead, da/dN is approximated with $\Delta a/\Delta N$ and the integral is solved numerically. Below are outlines of two procedures used in some crack growth prediction computer codes. The first outline presents the steps for constant amplitude and block loading problems. The second outline presents the steps for cycle-by-cycle problems used in spectrum loading. The Paris equation is used here but other crack growth rate equations may be used as well.

2.6.1 Constant Amplitude/Block Loading

Step 1: Compute the critical crack length using the stress intensity factor, limit load stress, and fracture toughness or from a residual strength curve.

Step 2: Assuming a crack length increment Δa , such as $\Delta a = 5\% \times a_{OLD}$, compute a new crack length, a_{NEW} , and then a_{AVG} .

$$a_{NEW} = a_{OLD} + \Delta a \quad (2.15)$$

$$a_{AVG} = 1/2(a_{NEW} + a_{OLD}) \quad (2.16)$$

Step 3: Compute ΔK :
$$\Delta K = K_{\max} - K_{\min} = \Delta \sigma \sqrt{\pi a} \beta(a) \quad (2.17)$$

Step 4: Compute cycle increment ΔN using the approximation ...

$$\frac{\Delta a}{\Delta N} = C \Delta K^m \quad (2.18)$$

$$\Delta N = \frac{\Delta a}{C \Delta K^m} \quad (2.19)$$

Step 5: Go to Step 2. Repeat calculations incrementing crack length until the critical crack length is reached or the net section yields, whichever comes first. Then, sum all ΔN 's for a life estimate.

2.6.2 Cycle-By-Cycle

Step 1: Compute the critical crack length using the same method as above.

Step 2: Determine stress range $\Delta\sigma_i$ and corresponding crack length a_i for one cycle N_i .

Step 3: Compute crack length increment Δa_i over the next cycle ($\Delta N=1$).

$$\Delta a_i = \frac{da}{dN_i} = C\Delta K_i^m = C\left[\Delta\sigma_i\sqrt{\pi a_i}\beta(a_i)\right]^m \quad (2.20)$$

Step 4: Compute new crack length produced by this one cycle.

$$a_{i+1} = a_i + \Delta a_i \quad (2.21)$$

Step 5: Increment cycle count by one.

$$N_{i+1} = N_i + 1 \quad (2.22)$$

Step 6: Go to Step 2. Repeat calculations incrementing crack length until the critical crack length is reached or the net section yields, whichever comes first. The last value of N_{i+1} will be a life estimate.

2.7 Mean Stresses

The Paris Equation, $da/dN = C\Delta K^m$, does not account for mean stresses. Consider two problems containing equal length cracks in a plate made from the same material. Problem 1 is loaded in constant amplitude from 0 to 10 psi and problem 2 is loaded in constant amplitude from 10 to 20 psi. Both problems produce the same stress range $\Delta\sigma$

and, thus, ΔK , but different crack growth rates. Problem 2 has higher crack growth rate values because of its higher mean stresses compared to problem 1. Instead of differentiating these problems with mean stress, their stress ratios are used. The stress ratio R is the ratio of minimum stress to maximum stress. As Figure 2-15 indicates, crack growth rate increases with stress ratio for a given ΔK . Therefore, the stress ratio will be used to model the mean stress effect.

It is not surprising that the Paris equation doesn't completely describe crack growth. It only has one load term, ΔK . A more sophisticated crack growth rate equation that includes the stress ratio is needed. Two crack growth rate equations containing stress ratio will be discussed next.

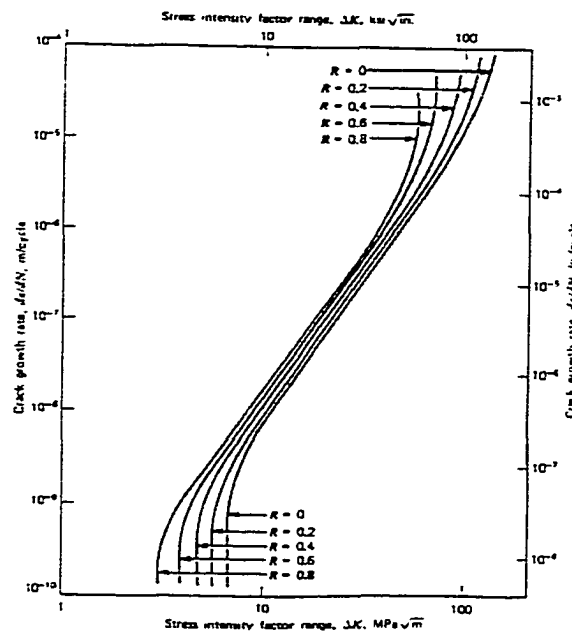


Figure 2-15 Effect of Stress Ratio on Crack Growth Rate¹²

2.8 Walker Crack Growth Rate Equation

The Walker crack growth rate equation is an improvement over the Paris equation because it accounts for mean stresses by including the stress ratio¹⁸. The Walker equation has three empirical constants, C , m , and n , obtained through curve fitting da/dN - ΔK data. The constant C is the value of da/dN when $R = 0$ and $\Delta K = 1$. The constant n is the slope of the linear portion of the da/dN - ΔK curve just as in the Paris equation. The constant m is the Walker exponent that controls the shift in crack growth rate data as R changes. The Walker equation is sometimes used in an alternate form where ΔK is replaced with K_{MAX} , but both rate equations produce the same answers.

$$\frac{da}{dN} = C[\Delta K(1-R)^{m-1}]^n \quad (2.23)$$

$$\text{Alternate form:} \quad \frac{da}{dN} = C[K_{MAX}(1-R)^m]^n \quad (2.24)$$

2.9 Forman Crack Growth Rate Equation

The Forman crack growth rate equation is an improvement over the Walker equation¹⁹. The Forman equation models the upper portion of the da/dN - ΔK curve (Region III) where the growth rate becomes asymptotic to the value of ΔK at fracture, i.e., fracture toughness. The Forman equation has three constants that need to be determined. The constants C and n are found from curve fitting the da/dN - ΔK curve. The constant C is the value of $da/dN(K_c-1)$ when $R = 0$ and $\Delta K = 1$. The constant n is again the slope of the linear portion of the da/dN - ΔK curve in Region II as with the Paris equation. The constants C and n are not equal to the Paris constants C and n . The constant K_c is the

fracture toughness limit for the material in use as ΔK increases. In other words, K_c is the asymptotic limit for the crack growth curve at $R = 0$.

$$\frac{da}{dN} = \frac{C\Delta K^n}{[(1-R)K_c - \Delta K]} \quad (2.25)$$

2.10 Spectrum Loading and Load History Effects

2.10.1 Introduction

None of the crack growth rate equations discussed earlier can properly predict the effects of load sequencing in variable amplitude or “spectrum” loading. If a laboratory crack growth specimen was tested at 10,000 cycles at 20 ksi stress range followed by 10,000 cycles at 10 ksi stress range its fatigue life would be different compared to a second specimen tested at 10,000 cycles at 10 ksi followed by 10,000 cycles at 20 ksi. The order or sequence of the 20 ksi block versus the 10 ksi block makes a difference in fatigue life N . Application of the 20 ksi block first will produce a phenomenon called crack retardation which temporarily slows crack growth and, thus, provides an increase in life. The crack growth rate equations discussed so far (i.e., Paris, Forman, Walker) would predict the same life for both test specimens.

This should not be surprising. The da/dN - ΔK curves are developed under constant amplitude loading. Because of this discrepancy between laboratory constant amplitude loading and spectrum loading, similitude is lost. The da/dN - ΔK curves need to be modified to account for spectrum loading on structures. In practice, the crack growth rate equations are modified by a retardation model and the da/dN - ΔK curves are used in their original state. Three common crack growth retardation models are the Wheeler

Model, the Generalized Willenborg Model, and the Elber Closure Model. Before these retardation models are discussed in detail, a general explanation of retardation will be described.

Given a precracked test specimen in constant amplitude loading, a single tensile overload is introduced as shown in Figure 2-16. Obviously this tensile overload must be less than the fracture load for the current crack length. Crack growth slows, sometimes stopping, and then returns to its normal speed. This delay or retardation in crack growth rate increases the fatigue life of the specimen.

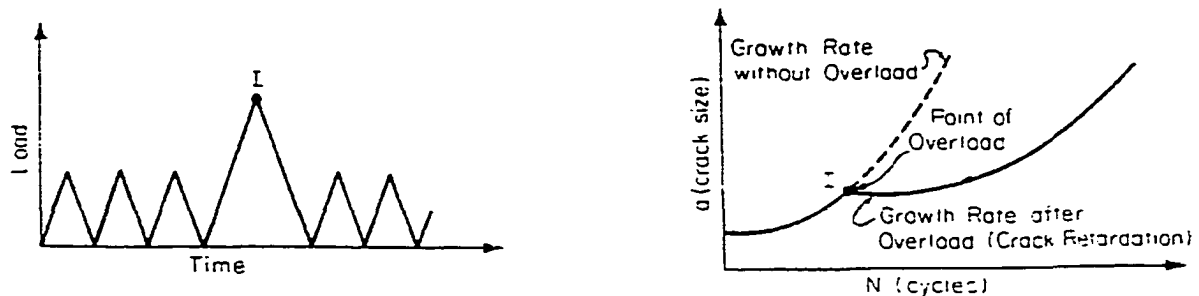


Figure 2-16 Retardation Caused by a Tensile Overload²⁰

The observed load interaction is caused by the residual stresses in the crack tip plastic zone. The tensile overload produces a tensile plastic zone larger than in previous cycles. When the load is relaxed during the load cycle, the surrounding elastic (unyielded) material places the crack tip plastic zone into compression. The surrounding elastic material wants to return the crack tip plastic zone to a zero strain state at the end of the load cycle but the crack tip plastic zone has permanently deformed (yielded) and can never return to zero strain by itself. The result of load equilibrium is that the plastic zone in Figure 2-17 experiences compressive residual stresses and the surrounding elastic material experiences tensile residual stresses. Any subsequent applied remote tensile

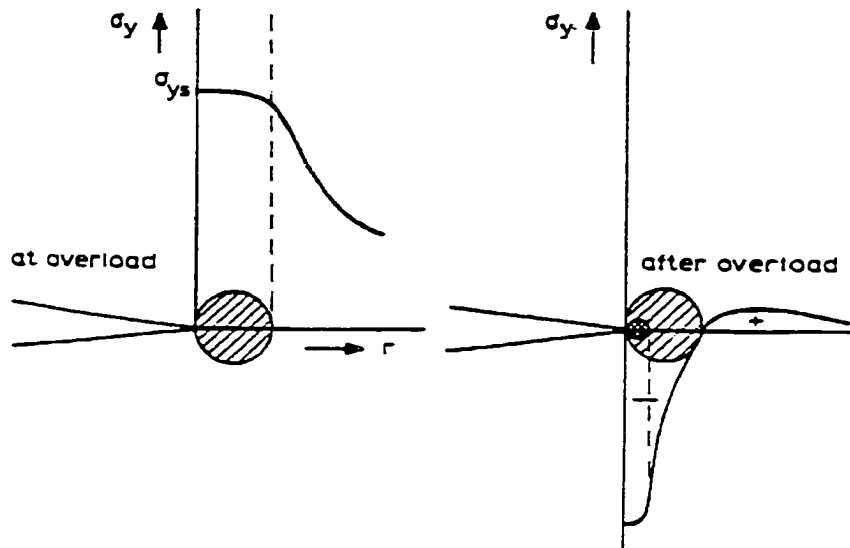


Figure 2-17 Crack Tip Residual Compressive Stresses Caused by an Overload¹²

stress must first overcome the compressive residual stresses at the crack tip; therefore, the effective tensile stress range $\Delta\sigma$ is smaller and the crack grows slower. If an underload (compressive overload) is sufficiently large to cause yielding in compression, then any retardation effects from a previous tensile overload can be reduced or eliminated. Conversely, after an underload cycle, crack growth is accelerated.

Sequence effects of overloads and underloads can play a very important role in crack growth retardation and acceleration. In these cases, knowledge of the exact details of the load history is crucial in performing an accurate life prediction. The crack growth results of four overload patterns in Figure 2-18 are presented in Figure 2-19 for 7075-T6 aluminum²¹.

In some load histories, the sequence effects cancel each other and knowledge of the exact history is not important. According to Fuchs and Stephens¹², a few qualitative rules have been developed, through experience, to tell when sequence effects must be

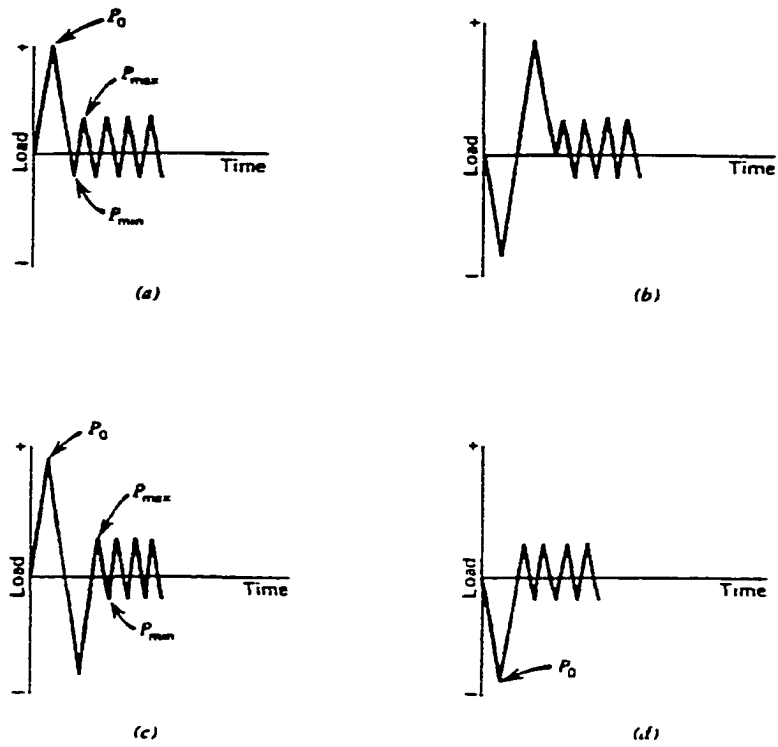


Figure 2-18 Four Different Overload Patterns¹²

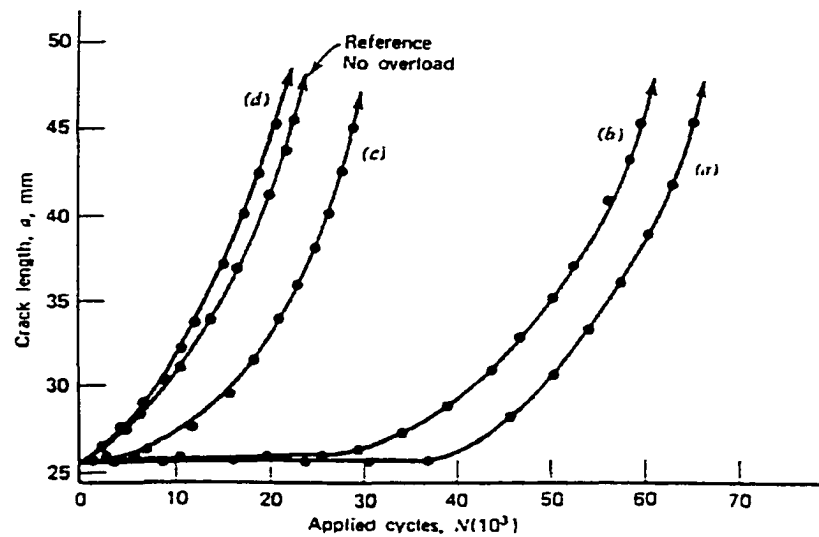


Figure 2-19 Crack Growth Following Different Overload Patterns in 7075-T6¹²

considered in predicting life. If the sequence of service load is completely unknown, one must decide whether to assume significant sequences or not. If the loading is Gaussian random with a narrow frequency band there will be no definable sequence. Figure 2-20 is an example of approximate narrow band Gaussian loading. The negligible effect of sequence is explained by the short intervals between the large amplitudes, which produce the greatest damage. If this load history had fewer large amplitudes

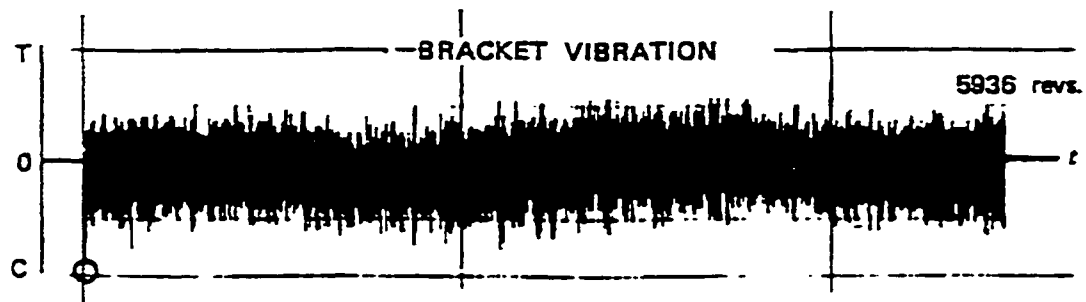


Figure 2-20 Random Loading in a Bracket¹²

(overloads/underloads) and many more small amplitudes (as in commercial aircraft wings), the damage done by the small amplitudes and the sequence effects would be significant. If the loading history shows infrequent one-sided spikes, as for instance in the ground-air-ground (GAG) cycles of aircraft, one should expect sequence effects. Infrequent tensile overloads produce retardation of crack growth or crack arrest. Compressive overloads (underloads) large enough to produce yielding can produce the opposite effect. Currently, the most accurate means of predicting the fatigue life in sequence dependent variable amplitude loading requires cycle-by-cycle integration of a retardation model.

Retardation after an overload is a complicated phenomenon that no one really understands. The three retardation models mentioned here are empirical. They require

one or more curve fitting constants that are material dependent and must be obtained from laboratory testing using similar loading spectrums. Changing the material and/or loading spectrum will change these empirical retardation constants. Some retardation models assume the plastic zone in front of the crack tip to be responsible for retardation while other models assume that crack closure effects cause retardation.

2.10.2 Wheeler Model

The Wheeler model²², which is widely used, assumes that the plastic zone in front of the crack tip due to the overload is responsible for retardation. This model relates the crack growth rate to the overload plastic zone size $r_{y(o)}$ and the current plastic zone size $r_{y(c)}$ depicted in Figure 2-21. Wheeler assumes that retardation remains in effect as long as the current plastic zone remains inside the overload plastic zone (Figure 2-21b). The overload effects disappear when the current plastic zone touches the outer boundary of the overload plastic zone (Figure 2-21c).

For a crack that has grown Δa since the overload, Wheeler defines the retardation factor in Eq. (2.27). The subscript (o) refers to an overload condition. The symbol γ is an empirical parameter. In Eq. (2.28) the current crack growth rate is reduced from the baseline constant amplitude $da/dN-\Delta K$ data by Φ_R . The baseline constant amplitude crack growth rate equation would be one of the three rate equations mentioned earlier: Paris, Forman, or Walker. The retardation factor Φ_R varies from zero to one. When $\Phi_R = 1$, no retardation exists. This temporary reduction in crack growth rate provides the increase in life.

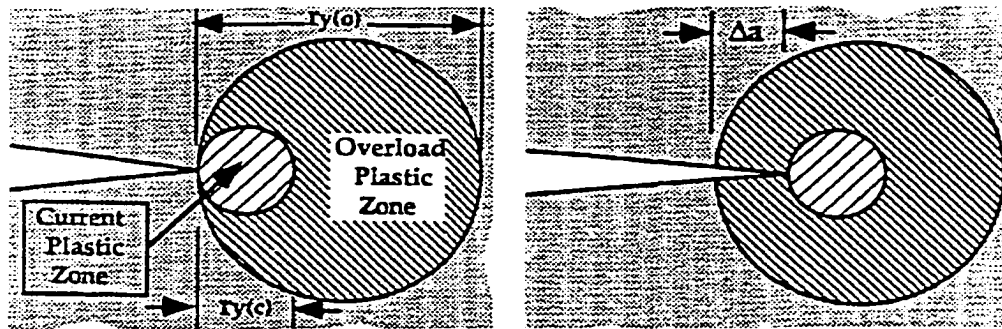
$$r_{y(o)} = \frac{1}{\Psi\pi} \left(\frac{K_o}{\sigma_{YS}} \right)^2 \quad (2.27a)$$

$$r_{y(c)} = \frac{1}{\Psi\pi} \left(\frac{K_{max}}{\sigma_{YS}} \right)^2 \quad (2.27b)$$

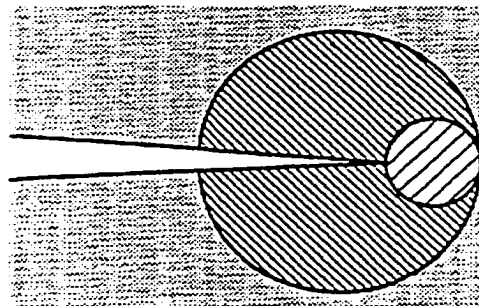
where $\Psi = 2$ (plane stress), or $\Psi = 6$ (plane strain).

$$\Phi_R = \left[\frac{\Delta a + r_{y(c)}}{r_{y(o)}} \right]^2 \quad (2.27c)$$

$$\left(\frac{da}{dN} \right)_R = \Phi_R \cdot \left(\frac{da}{dN} \right)_{baseline} \quad (2.28)$$



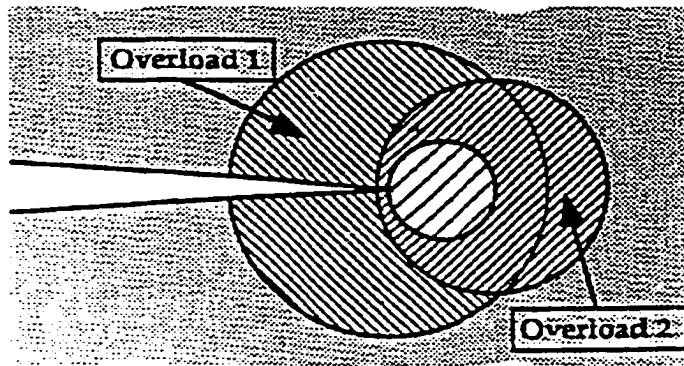
(a) Immediately following the overload. (b) After the crack propagates Δa .



(c) Propagation through the overload plastic zone.

Figure 2-21 Wheeler Model for Crack Growth Retardation⁹

In variable amplitude loading where several overloads can occur separated by smaller amplitude cycles, the Wheeler model will choose the overload plastic zone such that the retardation factor is minimized regardless of which overload occurred first. Minimizing the retardation factor Φ_R will maximize crack growth retardation. In Figure 2-22, the retardation factor produced by overload plastic zone 2 is smaller than that produced by overload plastic zone 1. Therefore, the parameters from overload plastic zone 2 are used to compute Φ_R in Eq. (2.27).



$$\Phi_R = \left[\frac{\Delta a_2 + r_{v(c)}}{r_{v(o)2}} \right]^\gamma$$

Figure 2-22 Overload Plastic Zone 2 is Chosen to Minimize Φ_R ⁹

The Wheeler exponent γ depends on the material and spectrum. It is determined from fatigue testing of a laboratory specimen made of the same material and thickness and loaded with a similar load history as the actual structural component intended for analysis. After the crack growth fatigue test is finished, the Wheeler exponent is arbitrarily changed in a fatigue prediction code until both test and computer results match. The computer model can then be used for structural life predictions of the actual component. Wheeler used $\gamma = 1.43$ for D6AC steel in Figure 2-23 and $\gamma = 3.4$ for Ti-6Al-4V. For the block loading in Figure 2-24, Wheeler uses $\gamma = 1.3$.

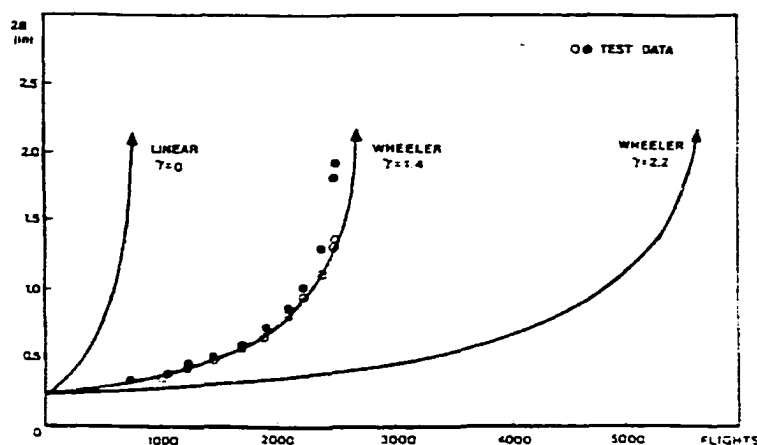


Figure 2-23 Calibration of Wheeler Model for Flight-By-Flight Loading⁴

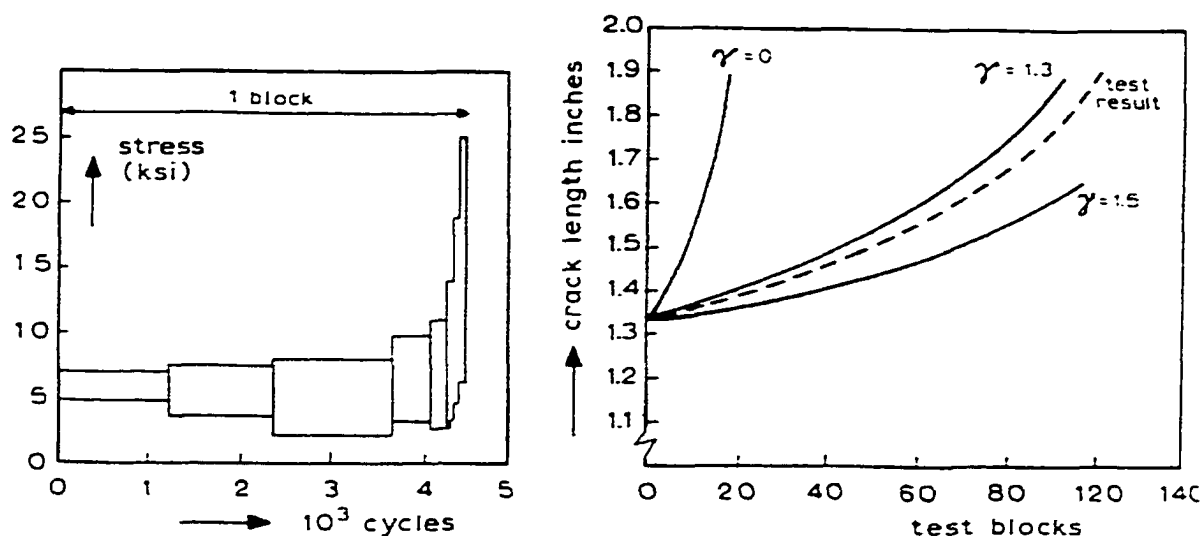


Figure 2-24 Wheeler Prediction of Crack Growth Using Block Loading²²

Most retardation models can be empirically adjusted to improve the correlation between experimental crack size versus life data and predictions. The advantage of the Wheeler model is that it contains only one empirical constant. Figure 2-25 shows predicted crack growth curves and test data for titanium specimens tested with an aircraft service loading history. After empirically adjusting the Wheeler exponent, predictions can be made for the same general spectrum shape for structural parts at different stress

levels and for different crack configurations (i.e., K). The flow diagram in Figure 2-26 is for a numerical crack growth life prediction involving the Wheeler Retardation Model and spectrum loading.

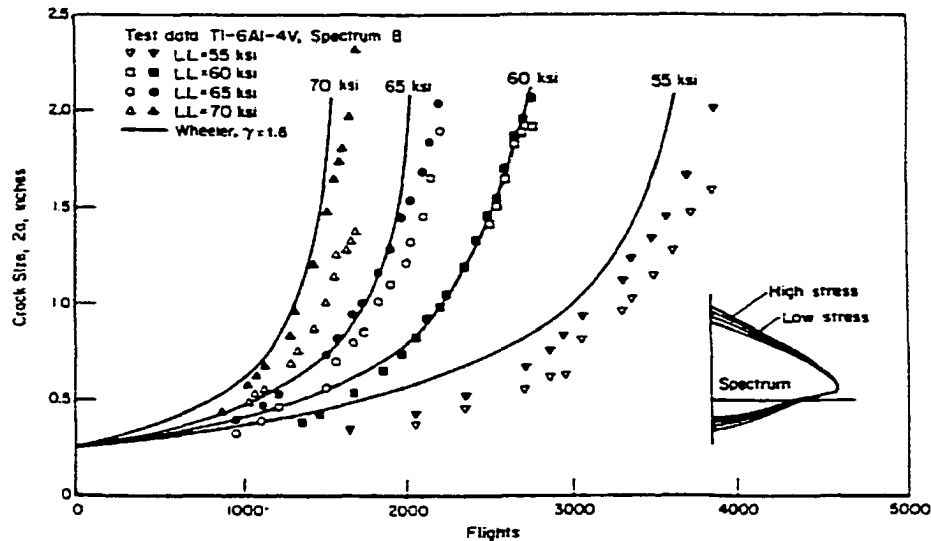


Figure 2-25 Predicted Crack Growth and Test Data for Titanium Specimens Using an Aircraft Spectrum with Four Stress Levels⁴

2.10.3 Generalized Willenborg Model

The Generalized Willenborg retardation model²³ is an improvement over the standard Willenborg retardation model. The Generalized Willenborg retardation model is an empirical yield zone model very similar to the Wheeler model in the sense that it looks at the plastic zone ahead of the crack tip. This retardation model uses an “effective” stress intensity factor K_{eff} based on the size of the yield zone in front of the crack tip shown in Figure 2-27. This effective stress intensity factor in Eq. (2.32) is produced when the original stress intensity factor is reduced by the compressive residual stresses in

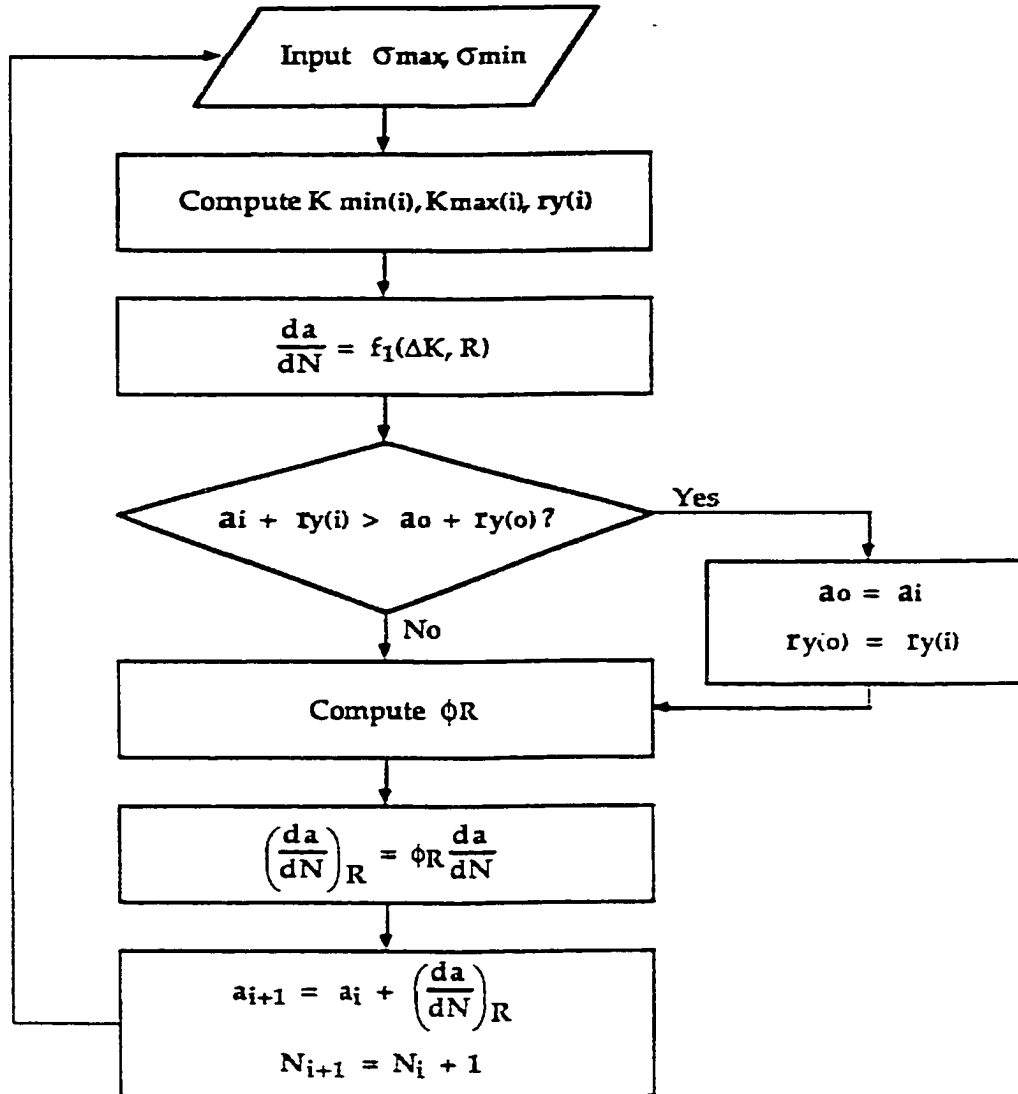


Figure 2-26 Flow Chart for Spectrum Loading Fatigue Analysis with the Wheeler Model⁹

the plastic zone due to an overload from a previous fatigue cycle. The end result is a stress intensity factor range, ΔK_{eff} and a new lower than normal stress ratio R_{eff} in Eq (2.33). This effective stress intensity factor range and lower stress ratio are used in a crack growth rate equation containing stress ratio, such as Forman or Walker, to produce retardation. Note that ΔK_{eff} is equal to ΔK without retardation.

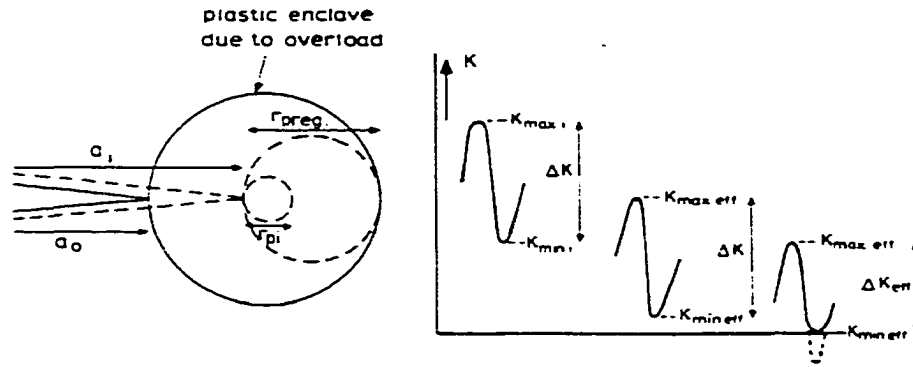


Figure 2-27 The Willenborg, Engle, and Wood Retardation Model²³

$$r_o = \frac{1}{\Psi \pi} \left(\frac{K_{max,o}}{\sigma_{YS}} \right)^2 \quad (2.29)$$

$$\Phi = \frac{1 - K_{thres}/K_{max}}{SOLR - 1} \quad (2.30)$$

$$K_r = \Phi \cdot \left[K_{max,o} \sqrt{1 - \frac{a_i - a_o}{r_o}} - K_{max} \right] \quad (2.31)$$

$$K_{max(eff)} = K_{max} - K_r \quad \text{and} \quad K_{min(eff)} = K_{min} - K_r \quad (2.32)$$

$$R_{eff} = \frac{K_{min(eff)}}{K_{max(eff)}} \quad (2.33)$$

$$\frac{da}{dN} = \frac{C \Delta K_{eff}^n}{(1 - R_{eff}) K_c - \Delta K_{eff}} \quad (2.34)$$

The subscript (o) refers to an overload condition. It is changed each time a maximum load exceeds a previous maximum, or when the current plastic zone touches the overload yield zone. At this point, K_r is zero because the current crack plastic zone touches the overload yield zone, therefore, no retardation occurs. The parameter K_{thres} is the ΔK threshold for $R = 0$. The variable Ψ specifies the stress state from 2 for plane stress to 6 for plane strain. The ratio of the overload maximum stress to the subsequent

maximum stress required to stop further crack growth is known as the “shutoff overload ratio” (SOLR). The shutoff overload ratio is a material dependent parameter that must be determined from laboratory testing. Typical values of SOLR for aluminum, steel, and titanium are given in Table 2-1.

$$SOLR = \frac{\sigma_{\text{overload}}}{\sigma_{\text{maximum}}} \quad (2.35)$$

Table 2-1 Shutoff Overload Ratios for Aluminum^{24,25}, Steel, and Titanium²⁶

Material	SOLR
Aluminum	2.5 to 3.0
Steel	2.0 to 2.5
Ti-6Al-4V	2.7

2.10.4 Elber Crack Closure Model

This retardation model is an empirically based closure model that uses an effective stress range concept to describe load sequence interaction effects in spectrum fatigue crack growth life predictions^{27,28,29}. Elber discovered that fatigue cracks would not immediately open with the application of a small remote tensile stress. According to linear elastic solid mechanics, one would expect the crack tip to open immediately when the remote tensile stress is greater than zero. Elber also discovered that large compressive residual stresses were present over the crack face at zero load. This phenomenon depicted in Figure 2-28 is caused by the plastic wake behind the crack tip. The plastic wake is the remnant of the previous plastic zones. This plastic zone wake forces the upper and lower crack faces together “closing” the crack.

Elber assumed that crack growth would only occur when the applied remote tensile stress was greater than the compressive residual stress holding the crack closed.

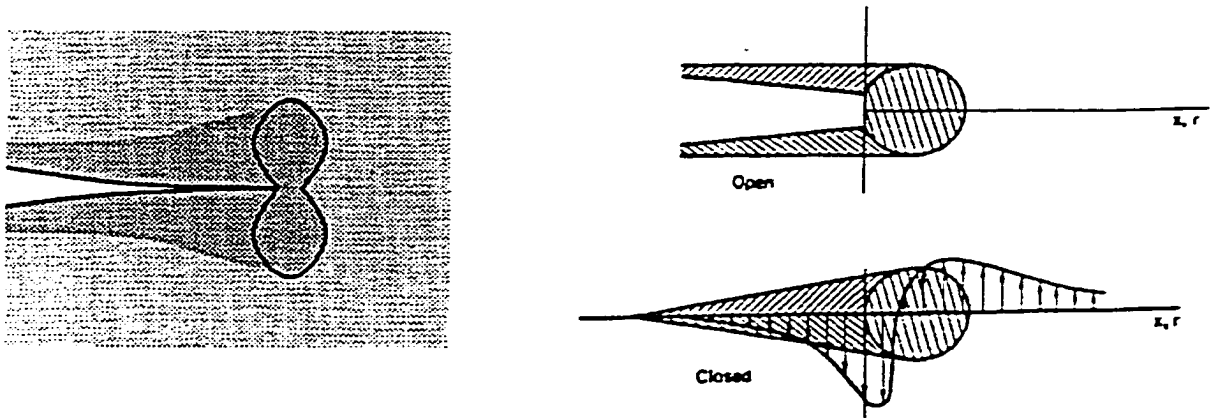


Figure 2-28 Elber Plasticity-Induced Closure Model^{9,4}

This particular stress is called the “crack opening stress.” Therefore, the controlling stresses in the crack growth process should be the maximum stress and the crack opening stress. These stresses are used to calculate the corresponding maximum and crack opening stress intensity factors and, subsequently, the effective stress intensity factor range, ΔK_{eff} , in Figure 2-29. The crack will not grow until the crack tip is opened. This occurs when the remote stress exceeds the crack opening stress. The stress intensity factor at the crack opening stress is K_{op} .

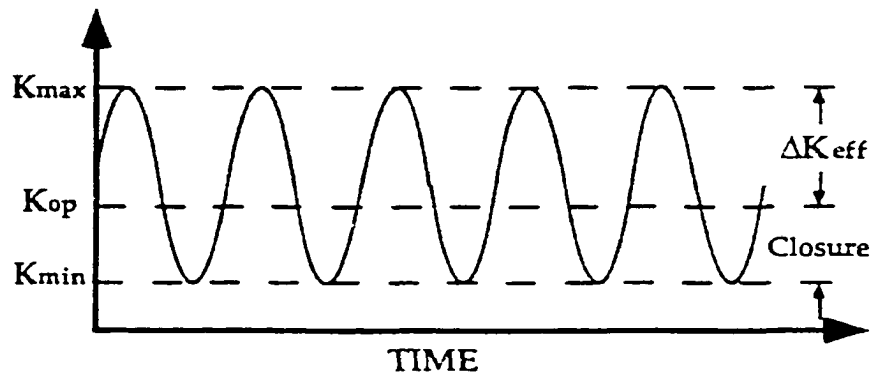


Figure 2-29 Effective Stress Intensity Factor Range for the Elber Model⁹

The effective stress range is defined in Eq. (2.36) where σ_{op} is the crack tip opening stress found through experiments.

$$\Delta\sigma_{eff} = \sigma_{max} - \sigma_{op} \quad (2.36)$$

Elber defined the closure factor C_i in Eq. (2.37).

$$C_i = \sigma_{op}/\sigma_{max} \quad (2.37)$$

Thus, the effective stress range is defined in Eq. (2.38).

$$\Delta\sigma_{eff} = \sigma_{max}(1 - C_i) \quad (2.38)$$

A crack growth rate equation, such as Paris, can now be modified by replacing ΔK with ΔK_{eff} . In Eq. (2.39), the Paris model from Eq. (2.13) is modified to include the Elber retardation model.

$$\frac{da}{dN} = C(\Delta K_{eff})^m = C[\sigma_{max}(1 - C_i)\sqrt{\pi a}\beta]^m \quad (2.39)$$

There have been several crack closure models developed since Elber. Budiansky and Hutchinson³⁰ performed work in this area. Recent models were proposed by Creager and Sunder (see below). In variable amplitude loading, the crack opening stress will vary with load history. Thus, these crack closure models predict crack acceleration in low-to-high loading sequences and crack retardation in high-to-low loading sequences. Displayed below in Figure 2-30, the original crack opening stress intensity factor K_A transitions to K_B , increasing ΔK_{eff} and, therefore, causes crack acceleration. The subsequent high-to-low loading sequence transitions the opening stress level, reduces ΔK_{eff} and, therefore, produces retardation.

This transitional behavior of the crack opening stress level needs to be defined by

equations which account for stress ratio. In AFGROW, the crack opening load ratio (C_{f0}) is defined as the ratio of the stress opening level to the maximum stress at $R = 0$.

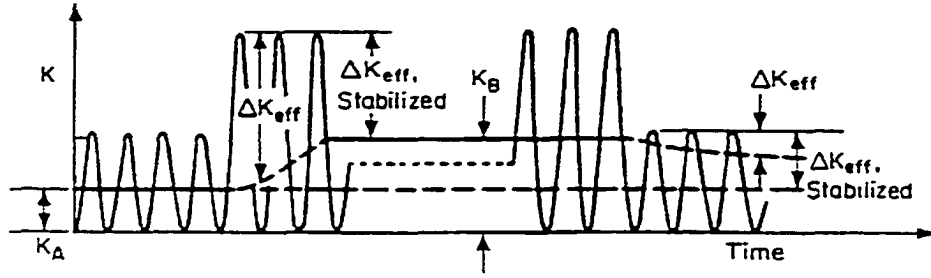


Figure 2-30 Variation in Crack Closure Stress Intensity Factor Caused by Changing Load Level²⁰

$$C_{f0} = \sigma_{op} / \sigma_{max} \quad (2.40)$$

The model used in AFGROW is based on work performed by Creager and Harter on the B-2 bomber damage tolerance analysis in 1982-83. To account for the changing stress ratio R in variable amplitude loading, AFGROW uses Eq. (2.41) in its closure model.

$$C_f = 1.0 - [(1.0 - C_{f0})(1.0 + 0.6R)(1.0 - R)] \quad (2.41)$$

CHAPTER III

FATIGUE LOAD SPECTRA DEVELOPMENT IN MILITARY AIRCRAFT

3.1 Introduction

Load sequences are due to repeated loads. Thus load sequences attempt to duplicate the loads that an aircraft will experience during its lifetime. Before constructing load sequences, it is necessary to estimate the number of load occurrences and to know their severity. This information is obtained from an estimate of the expected usage of a new aircraft or from data of existing aircraft.

Expected usage of new aircraft is defined by the Air Force to meet an operational need and is given as a series of mission profiles. Mission profiles define:

- a. Airspeed, altitude, and gross weight history with time
- b. Number of each mission during the aircraft's life
- c. External stores configuration, cargo distribution, average fuel use, pressurization cycles, number of touch-and-go landings, actuation cycles of movable structures
- d. Any other information, which results in repeated loading.

This information is used to determine the flight conditions that are used to compute load magnitudes and the distributed flight time. Load magnitudes and distributed flight time are used to compute the number of load occurrences.

Usage frequency may be presented as the number of times a given load level (i.e., normal load factor n_z) is exceeded for a reference flight time. A reference flight time of 1,000 hours is often used for convenience. This load level distribution is combined with mission profile information to produce a table of occurrences at each desired load level.

Data on n_z alone are not enough to compute all loads. Additional aircraft response parameters are also needed: lateral and longitudinal accelerations; pitch, roll, and yaw rates; and pitch, roll, and yaw accelerations.

This set of data is called a multivariable set and is typically collected from aircraft structural flight data recorders installed on 10% to 13% of the fleet. These data are collected as part of the USAF Aircraft Structural Integrity Program (ASIP) Load/Environmental Spectra Survey (L/ESS).

It is necessary to know the load time history or sequence of loads at any point on the structure during its design life. After finding the applied loads on a flight-by-flight basis, the resulting stress histories are computed for selected points on the airframe and damage tolerance analyses are performed on the structure.

3.2 Sources of Repeated Loads

The primary repeated loads result from ground handling, flight maneuvers, and atmospheric turbulence or gusts. Cabin pressurization is another source of repeated loads for pressurized aircraft. Pilot induced maneuver loads drive metal fatigue in high g-designed aircraft such as fighters. Loads due to turbulence and ground operations are not significant. Conversely, turbulence and ground loads drive metal fatigue in low g-design aircraft such as bombers and transports. Miscellaneous repeated loads include operation of flaps, speed brakes, and ejection of stores.

3.2.1 Ground Loads³¹

These loading conditions include takeoff, landing rollout, taxiing, braking, turning, pivoting, engine run-up, and testing. Ground loads, including landing impact, are not significant for high-load-factor aircraft such as fighters but are very significant for bomber and cargo type aircraft particularly at high gross weight. The amount of data for ground maneuvers varies from plentiful (i.e., airfield surface roughness) to nonexistent for other ground operations.

Taxi loads are based on a spectrum of vertical loading while the aircraft is operating on prepared or unprepared fields, or from the airfield roughness and aircraft dynamic response. The airfield roughness is determined from profile elevation measurements made at the centerline and some distance on each side. Profile elevations are converted to power spectral density (PSD) by Fourier transforms of the auto-correlation function of the profile elevations. Airfield roughness PSD in Figure 3-1 is specified by $\Phi(\Omega) = A\Omega^{-n}$, where A and n are constants, Ω is the reduced frequency in rad/ft, and $\Phi(\Omega)$ has the dimensions of $\text{in}^2/\text{rad}/\text{ft}$.

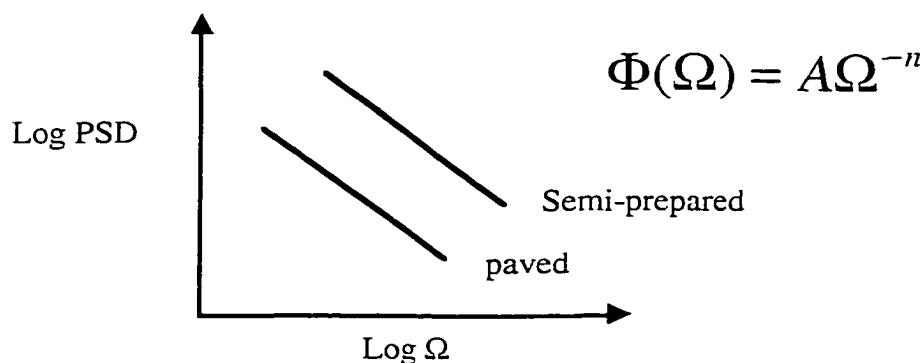


Figure 3-1 Power Spectral Density of Airfield Surface Roughness

The PSD intercept values for matted and assault airfields, which are smoothed by bulldozers and graders, is about ten times greater than paved airfields. Unprepared airfields PSD intercept curves are about 100 times higher than paved airfields³². PSD gives the magnitude and frequency spectrum for a generated set of airfield profile elevations. Elevations for paved airfields can be considered normally distributed for wavelengths less than 100 ft³³.

The number of cycles of loading are determined by performing dynamic analyses of the aircraft at several weights and, then, finding for each weight condition the magnitude and number of peaks for a selected distance (at least 1,000 ft) of taxiing. Several sections of taxiway of different surface roughness are used and the results are combined.

Takeoff loads development is similar to taxi load development except aircraft ground speed is variable, and aircraft aerodynamics and powerplant thrust have a greater effect. The vertical downward tail force applied at rotation increases main gear loads by approximately the same value as the tail force. The number of cycles of loading is determined similarly to the taxi phase.

In the landing rollout all gear is on the ground. The runway surface requirements are the same as those for takeoff and taxi. The difference is caused primarily by braking. Braking produces torque in the main wheels which induces drag and, subsequently, increases the nose gear vertical load. The combined gear forces cause structural shears, torques, and moments. The drag force caused by hard braking is determined by increasing the coefficient of friction, μ , for the surface³⁴. Braking is usually applied as hard ($\mu = 0.8$) for 2 times and medium ($\mu = 0.4$) for 5 times during each mission. The

braking (drag) loads can be broken down by aircraft weight because the landing weight and the number of landings are known.

Turning loads result from steering the nose wheel. These side forces are based on a side load factor and are significant loads. The aircraft usually will make as many left-hand as right-hand turns which is about 5 to 10 turns each for every full-stop landing. The aircraft is typically considered a rigid body in the analysis. No wheel side slipping is considered.

Towing loads are divided between forward and aft directions, and between takeoff and landing weights.

3.2.2 Flight Maneuver Loads³¹

Flight maneuvers and gusts are the most important loading sources in DTA. The type of aircraft affects the relative importance of maneuver and gusts. Small, highly maneuverable aircraft such as fighters, attack aircraft, and trainers, which have relatively rigid structures, are affected more by maneuvers than by gusts. Larger, less maneuverable aircraft such as bombers and transports are affected more by gusts than maneuvers.

Flight maneuver loads are the loads developed on the aircraft structure by pilot induced control deflections during flight. The magnitudes and frequency of the occurrence of maneuver loads are based on tabulations of occurrences from similar type aircraft. The normal load factor n_z is the one basic parameter whose occurrences of peak values have been tabulated for a variety of flight conditions. To determine the type of maneuver which caused a load, additional response parameters are needed: lateral and longitudinal accelerations; roll, pitch, yaw rates and accelerations; and airspeed, altitude,

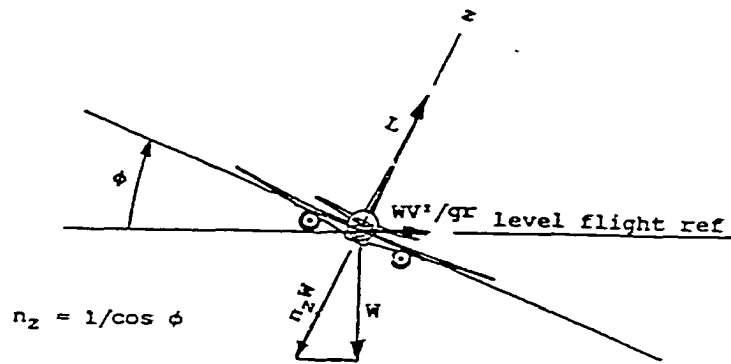
and gross weight. Specific maneuvers chosen for inclusion in the loads sequence development must be defined specifically for each aircraft type.

Under some flight conditions, loads from gusts are superimposed on the flight maneuver loads. A Normal load factor represents the aircraft response to the combination of maneuvers and gust loads. All data used to determine flight maneuver loads include atmospheric turbulence effects which are encountered simultaneously with a maneuver.

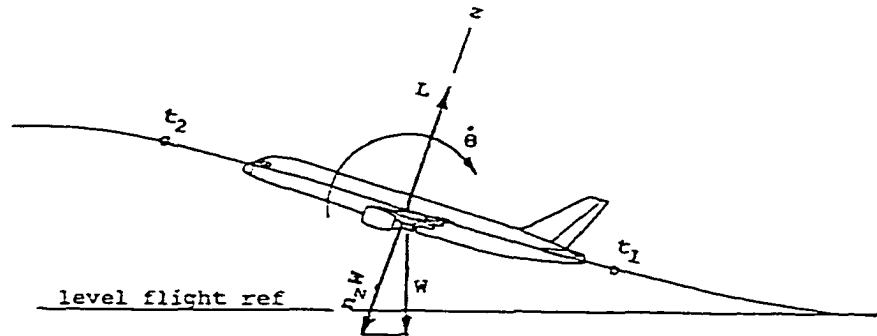
The 1.0g load is the starting and ending value for a maneuver or gust load cycle. The magnitude of the steady level flight 1.0g load depends on altitude, airspeed (Mach number), aircraft weight, center-of-gravity, mass distribution, and deployment of lift or drag devices.

Flight maneuvers can be classified as either symmetrical or unsymmetrical (i.e., roll). Airspeed, Mach number, and altitude are considered constant during the maneuver.

Symmetrical maneuvers induce external loads that are symmetrical about the vertical plane through the aircraft centerline. Symmetrical maneuvers are balanced turning flight, pull-up, or push-over. Aircraft roll and yaw perturbations are neglected or assumed zero. Symmetrical maneuvers can be classified as steady state or abrupt. Symmetric steady state maneuvers produce the maximum design wing loads for symmetrical maneuvers. The balanced turn and pull-up maneuvers are described in Figure 3-2. The pitch rate is constant, therefore, pitch acceleration is zero. A symmetric abrupt maneuver involves a single rapid application of the elevator which produces a pitch acceleration. Symmetric abrupt maneuvers are the unchecked elevator condition shown in Figure 3-3 and the elevator check back condition.



b. Correctly balanced turn



a. Steady pull-up

Figure 3-2 Symmetric Steady State Maneuvers³⁵

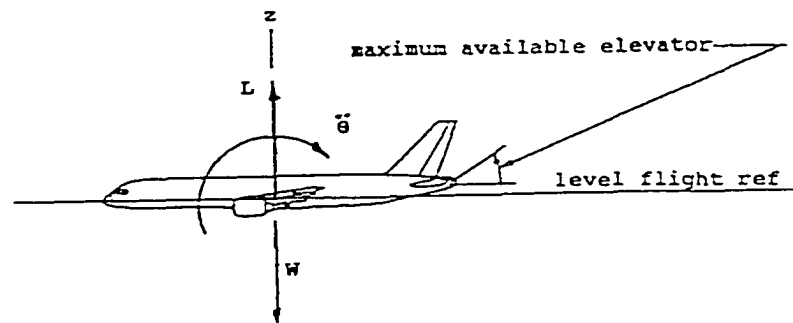


Figure 3-3 Symmetric Abrupt Maneuver³⁵

Wing load calculations for symmetrical maneuvers require the following parameters: normal load factor n_z , pitching acceleration about the center-of-gravity (rad/s^2), pitching velocity (rad/s), wing reference angle of attack α_w (deg), inertia

properties due to operating equipment weight (OEW), fuel, airspeed, and Mach number.

Unsymmetrical loads are primarily the result of rolling maneuvering flight. Rolling maneuvering flight is usually performed in conjunction with a specified symmetrical load factor producing asymmetrical loads. Asymmetrical conditions are defined as incremental loads due to roll and yaw before inclusion of symmetrical flight load increments. Again, airspeed and Mach number, hence altitude, are constant throughout the rolling maneuver. Yaw and roll cross-coupling effects are neglected.

Roll performance is the ability of an aircraft to change the lateral direction of its lift vector. Since the lift force is primarily responsible for turning an aircraft, roll performance predicts the ability of a fighter to change its orientation. Roll performance may be defined as a measure of the aircraft's agility.

The rolling motion of an aircraft is produced by the action of its lateral control system which include ailerons, spoilers, and differential tails. Aerodynamic roll controls operate by increasing lift on one side of the aircraft relative to that on the other, thus, producing a rolling moment. The roll will accelerate to a maximum value as depicted in Figure 3-4a and stabilize at that rate to produce the steady state roll maneuver in Figure 3-4b. Roll acceleration is zero in steady state roll. The stabilized roll rate is achieved when a damping moment is generated which balances the moment produced by the roll controls. The damping moment is produced primarily by lift differences between the upward moving wing and the downward moving wing. The stabilized roll rate is affected by wingspan. Aircraft with shorter wingspans can attain a higher stabilized roll rates for the same speed and control deflection.

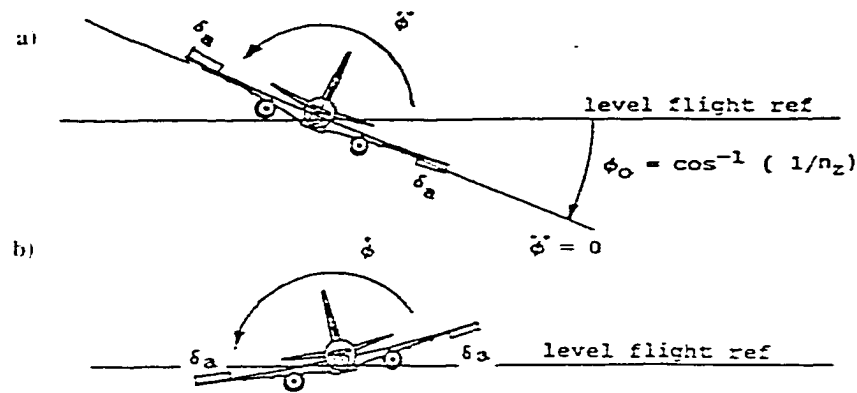


Figure 3-4 a) Roll Initiation from a Balanced Turn b) Followed by a Steady State Roll³⁵

During short periods of roll, the maximum stabilized roll rate may not be reached. A certain length of time is needed to accelerate the roll rate from zero to its maximum value. Therefore, roll acceleration is often the driving factor in fighter aircraft performance. Roll acceleration is a function of the moment of inertia of the aircraft and any available power assisted (hydraulic) control systems.

Dynamic maneuver loads introduce structural deflections caused by the rate of application. These loads cannot be described by rigid body equations of motion. Dynamic maneuver loads are affected by loading rate, airframe flexibility, and airframe size.

The aircraft is considered to be a rigid body maneuvering in space in maneuver load computations. Load equations are developed that relate forces and moments acting on the aircraft to angular rates, angular accelerations, and linear accelerations at the center-of-gravity.

The normal load factor is the preferred indicator for all load peak occurrences. This motion parameter is also a very good indicator for wing load magnitudes. The pitch acceleration is the preferred indicator for horizontal tail loads, and the yaw acceleration is

the preferred indicator for vertical tail loads.

The primary response parameters used for loads determination, when forces produce only translation and acceleration, are n_z and n_y .

$$n_z = 1 + \frac{a_z}{g} \quad , \quad n_y = \frac{a_y}{g} \quad (3.1)$$

The n_z distribution is used to find the magnitude and frequency of occurrence of symmetrical loads. The n_y distribution is used to find the magnitude and frequency of occurrence of lateral loads. The best indicator of load occurrences is the parameter which best predicts the load of interest.

The exceedance plot is a plot of the number of occurrences which equal or exceed particular values in a unit of time. A hypothetical example of a maneuver normal load factor exceedance plot is shown below in Figure 3-5.

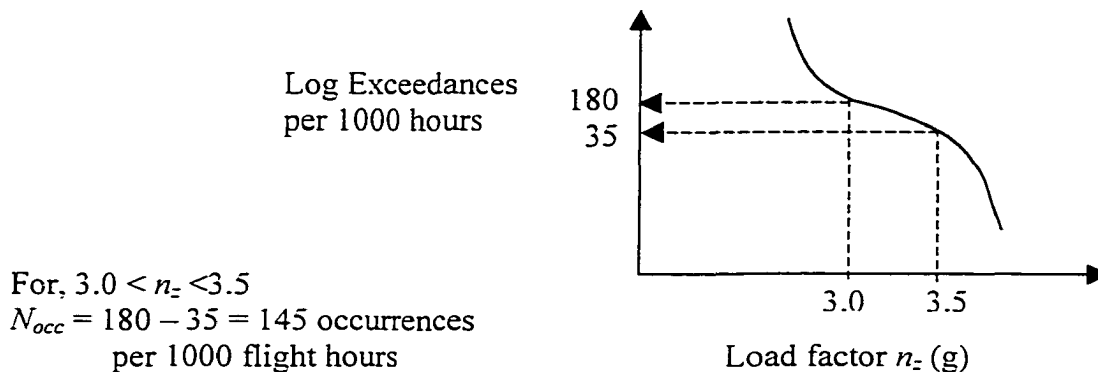


Figure 3-5 Computing Occurrences from an Exceedance Plot³¹

The number of occurrences is assigned to the midpoint of the range. In the above example, 145 occurrences would be assigned to $n_z = 3.25g$. The number and size of parameter ranges depends on the sensitivity of the load to changes in the parameter.

3.2.3 Gust Loads³¹

The aircraft in flight experiences a large number of gust loads. Gust loads are caused by atmospheric turbulence. These loads are represented by a PSD characterization of the turbulent environment. The PSD method describes gust loads as a continuous random process. The influence of flexibility must be considered in the aircraft response analysis, and this analysis must include all significant flexible degrees of freedom. The aircraft response parameters \bar{A} and N_o are needed. The response parameter \bar{A} is the ratio of rms incremental load to rms gust velocity and N_o is the characteristic frequency of response. Both parameters are found from a dynamic analysis of the aircraft. The recorded flight data, with maneuver flight data removed, provide information on gust encounters during flight.

Small, rigid aircraft are designed by considering vertical and lateral gusts independently in a one-dimensional analysis. Large, flexible aircraft require analyses which include the interaction of lateral and vertical gusts.

It is assumed that turbulence is a stationary random process having a Gaussian distribution over small distances and time. The response of aircraft center-of-gravity (CG) vertical accelerations to gusts has been used to develop PSD descriptions of gusts. The total turbulence experienced by an aircraft is the summation of a series of distinct turbulence exposures. A stationary Gaussian process describes each exposure.

The Von Karman spectrum³⁶ uses a vertical gust PSD spectrum expression. The PSD for vertical velocity is given by Eq. (3.2) where, σ_w^2 = rms gust velocity, L = longitudinal scale of turbulence, and Ω = frequency. The parameter L is set equal to altitude up to 2,500 ft and then held constant at 2,500 ft for all higher altitudes.

$$\Phi_w(\Omega) = \sigma_w^2 \frac{L}{\pi} \frac{\left[1 + \frac{8}{3}(1.339L\Omega)^2\right]}{\left[1 + (1.339L\Omega)^2\right]^{1/6}} \quad (3.2)$$

The statistical description³⁷ of gust velocity was developed in the form of a probability density function for σ_w in Eq. (3.3). The parameters P_1 and P_2 are percent of total flight time in each condition, and b_1 and b_2 are values of σ_w for the time spent in each condition. Both sets of data are found from measured data. Two distinct distributions of σ_w are visible in this equation: storm and nonstorm conditions. It should be noted that this is a one-dimensional description. A three-dimensional approach would be more appropriate when the ratio of wing span to scale of turbulence is high³⁸.

$$f(\sigma_w) = P_1 \frac{1}{b_1} \sqrt{\frac{2}{\pi}} \cdot e^{-\left(\frac{\sigma_w^2}{2b_1^2}\right)} + P_2 \frac{1}{b_2} \sqrt{\frac{2}{\pi}} \cdot e^{-\left(\frac{\sigma_w^2}{2b_2^2}\right)} \quad (3.3)$$

Rice's³⁹ derivation of the number of exceedances at a given rms level, based on a stationary Gaussian disturbance, is defined in Eq. (3.4). Here, $N(y)$ is the number of occurrences of y per unit time exceeding the y level, and N_o is the characteristic frequency.

$$N(y) = N_o \int_0^\infty f(\sigma_w) \cdot e^{\left(-\frac{y^2}{2\sigma_w^2 \bar{A}^2}\right)} d\sigma_w \quad (3.4)$$

Substituting $f(\sigma_w)$ into $N(y)$ yields Eq. (3.5) where Δy is any incremental load quantity value such as normal load factor (Δn_z) or wing bending moment (ΔM). This equation can determine the exceedance spectrum for any load quantity caused by gusts.

$$N(y) = N_o \left[P_1 \cdot e^{-\frac{\Delta y}{b_1 \bar{A}}} + P_2 \cdot e^{-\frac{\Delta y}{b_2 \bar{A}}} \right] \quad (3.5)$$

To find \bar{A} , the PSD function Φ_w in Eq. (3.2) is normalized with σ_w as shown below.

$$\Phi_N(\Omega) = \frac{L}{\pi} \frac{\left[1 + \frac{8}{3}(1.339L\Omega)^2\right]}{\left[1 + (1.339L\Omega)^2\right]^{11/6}} \quad (3.6)$$

The function \bar{A} is now represented by Eq. (3.7) where $|T_y(\Omega)|$ is the aircraft transfer function for load quantity y as a response to a unit sinusoidal gust input.

$$\bar{A} = \frac{\sigma_y}{\sigma_w} = \left[\int_0^\infty \Phi_N(\Omega) \cdot |T_y(\Omega)|^2 d\Omega \right]^{1/2} \quad (3.7)$$

The characteristic frequency, N_o , is the number of times per second that the response quantity crosses the zero axis with a positive slope.

$$N_o = \frac{V}{2\pi} \left[\frac{\int_0^\infty \Omega^2 \Phi_w(\Omega) \cdot |T_y(\Omega)|^2 d\Omega}{\int_0^\infty \Phi_w(\Omega) \cdot |T_y(\Omega)|^2 d\Omega} \right]^{1/2} \quad (3.8)$$

Finally, the number of exceedances of a given load increment, Δy , is given by Eq. (3.9) where t is total time for each Mach-altitude-weight combination associated with the corresponding P_1 , P_2 , b_1 , b_2 , and is specified by the mission profiles.

$$N(\Delta y) = N_o t \left[P_1 \cdot e^{-\frac{\Delta y}{b_1 \bar{A}}} + P_2 \cdot e^{-\frac{\Delta y}{b_2 \bar{A}}} \right] \quad (3.9)$$

Values of $N(\Delta y)$ are computed for the expected range of incremental load, Δy . The exceedance curve for incremental gust load factor should not be extended to less than one occurrence per lifetime. Incremental load factor values midway between the values used to develop the maneuver load spectrum are used. The number of occurrences represented by each range is assigned to the midpoint value of the range. Next, an

exceedance plot is drawn for each load quantity using the above equation. These plots are entered at the same exceedance values for the given normal load factor values. Load quantity values are read at these two points, and the number of occurrences found earlier is assigned to the midpoint of the load quantity. In other words, the number of occurrences of a load quantity is equal to the number of occurrences of the corresponding normal load factor.

Load quantity values are incremental loads from 1.0g flight. Total occurrences include positive and negative gust responses and must be separated into positive and negative loads from 1.0g flight.

Typical gust response factors \bar{A} and N_o at the center-of-gravity n_z and wing root bending moment (BM) for fighter/attack aircraft are given below for various flight conditions.

Table 3-1 Typical Gust Response Factors \bar{A} and N_o for a Fighter/Attack Aircraft³¹

Item	Condition					
	I	II	III	IV	V	VI
Mach Number	0.25	0.50	0.90	0.90	1.8	2.0
Altitude	0	0	0	25,000	35,000	45,000
Gross Weight	25,000	35,000	40,000	32,000	30,000	30,000
Hours per life	500	225	225	2000	200	50
\bar{A} (C.G. n_z)	.015	.021	.032	.012	.008	.009
N_o (C.G. n_z)	1.40	2.20	3.10	2.00	2.50	2.50
\bar{A} (wing root BM)	10,340	22,300	20,000	10,400	7,500	7,250
N_o (wing root BM)	3.5	2.98	4.30	3.50	5.80	5.80

The cumulative occurrences plot (or exceedance plot) for incremental load factor due to a lifetime of gust loads is shown below in Figure 3-6. This plot is used for both positive and negative values of incremental load factor, Δn_z .

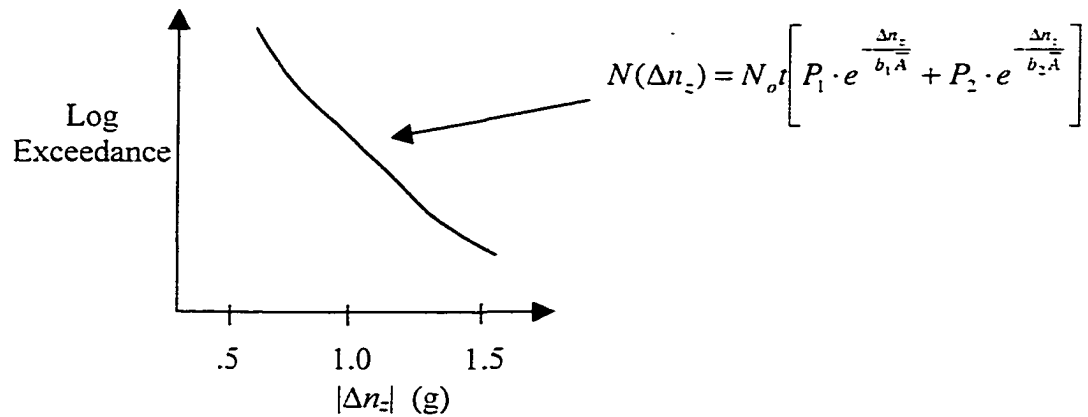


Figure 3-6 Exceedance Plot for a Lifetime of Gust Loads³¹

A hypothetical example follows in Figure 3-7. Given the ranges for incremental load factor Δn_z as (0.25,0.75), (0.75,1.25), (1.25,1.75), find the number of occurrences for $\Delta n_z = 1.0$.

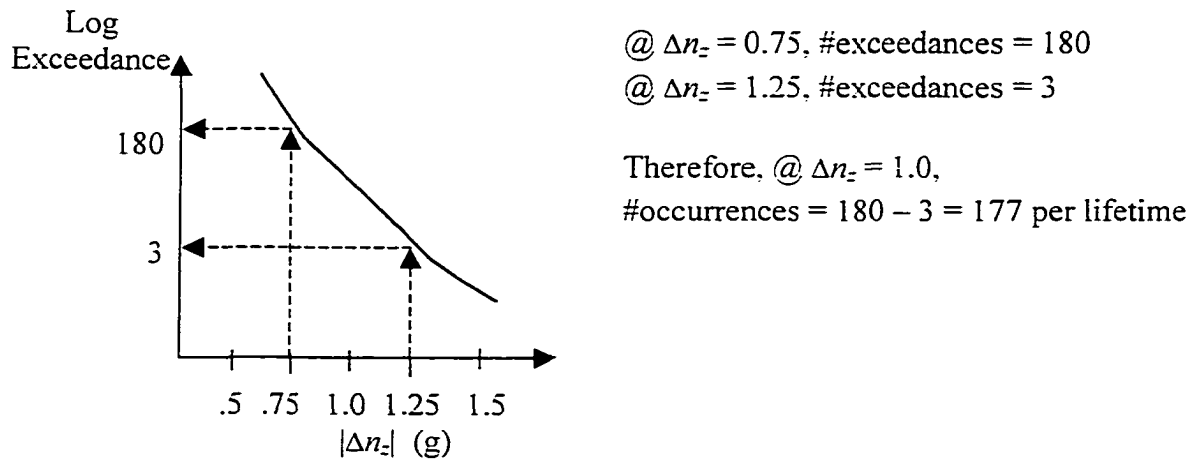


Figure 3-7 Determining the Number of Δn_z Occurrences Caused by Gusts³¹

The wing bending moment is now determined from the wing bending moment exceedance plot, Figure 3-8 on the next page, using the same (180,3) exceedance range.

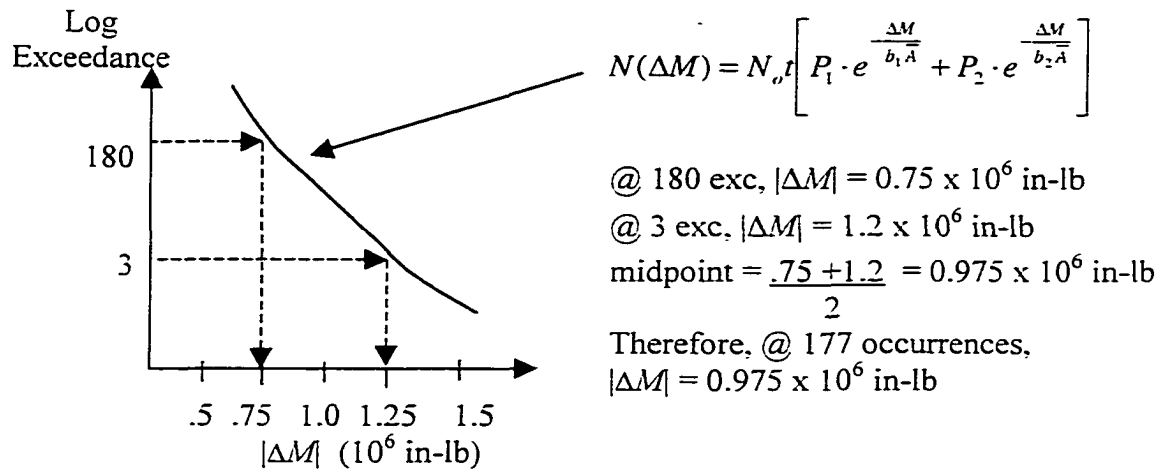


Figure 3-8 Determining the Number of $|\Delta M|$ Occurrences Caused by Gusts³¹

The positive and negative moments at the wing root are found by adding and subtracting the midpoint incremental moment, 0.975×10^6 in-lb, to the 1g moment at this location. This process is performed for any needed load quantity.

An alternative approach could have determined the number of occurrences for each of the flight conditions. After the number of occurrences per hour is determined, computation of occurrences per flight based upon the number of hours, during which each condition occurs per flight, can be done.

For most flight conditions, gust and maneuver loads are considered to occur independently and are assigned in the load sequence as separate discrete events.

3.2.4 Pressurization Loads

The load spectrum for aircraft pressurization is determined from the flight mission segments. A relief valve controls cabin pressure. The relief valve's maximum setting is usually considered as the pressurization loading. Pressurization loads are caused by air being forced inside the cabin in order to maintain a pressure altitude schedule on the

aircraft interior. The pressure differential causes static loads on the aircraft structure. Body shape and flight dynamic pressure can cause additional loading. Differential pressure increases with altitude until a specified altitude is met. At this point, differential pressure is held constant up to the service ceiling in some aircraft designs. The number of occurrences of pressure cycles depends on the number of times the aircraft reaches the mission design altitudes.

More than one pressurization cycle per flight can be expected for cargo aircraft performing air drops or resupply missions. Fighter aircraft may have at least two pressurization cycles per flight during combat. Cockpit differential pressure is relieved prior to air combat to minimize ballistic damage to the pressurized structure. After combat, the cockpit is pressurized again during the return leg of the mission.

The pressurization loads are added to the gust and maneuver loads in computing the stress sequences.

3.2.5 Landing Loads³¹

The effect of landing loads on structural damage tolerance analysis can be important. The cyclic landing loads are affected by the dynamic response of the landing gear and the aircraft structure flexibility. Vertical sink speed, aircraft weight, and forward speed at landing must be considered simultaneously.

Landing loads are not significant on fighter or high load factor aircraft unless sink speeds are unusually high. The landing impact loads are usually included in the airframe loading spectrum for cargo and bomber aircraft. Landing impact loads are always used in the landing gear structure and landing gear backup structure fatigue load spectrum. The significant parameters in determining landing impact loads are:

- a. Main gear sink speed, aircraft forward ground speed, and weight
- b. Rigid body inertia characteristics and flexible modes
- c. Surface friction at time of wheel contact to determine spin-up and spring-back loads
- d. Landing gear oleo, tire load, and deflection characteristics.

A distribution of sink speed values is used to find the distribution of landing loads. Sinking speed data are usually portrayed as a frequency distribution of sinking speed in feet per second (fps) versus the number of occurrences per 1,000 landings, as depicted in Figure 3-9.

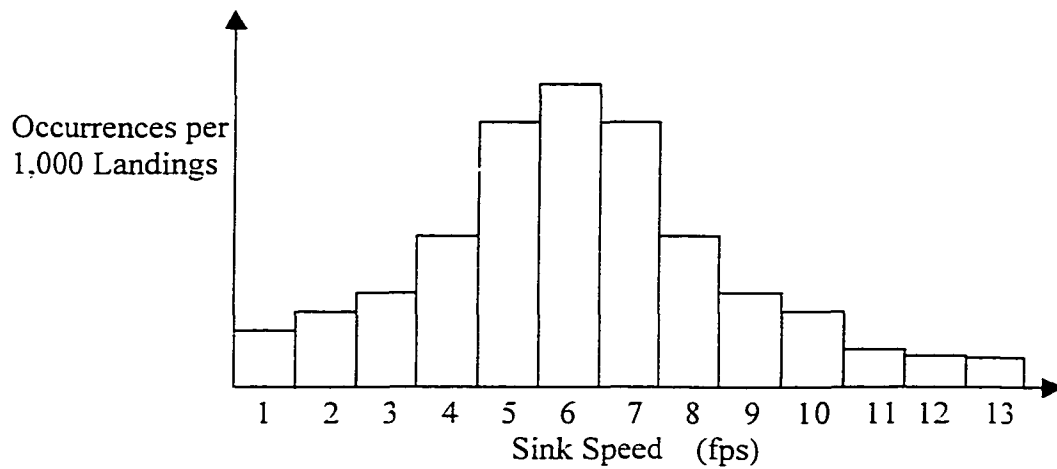


Figure 3-9 Frequency Distribution of Sink Speeds in 1,000 Landings

Drag loads are created between the runway surface and tires during landing. Drag loads are the result of the vertical load and runway surface friction. Spring-back loads are also created during landing as the initial rearward deflection of landing gear causes a subsequent forward rebound. The forward rebound acceleration times the gear mass produces a forward acting load. Vertical loads, drag loads, and moments are produced at

the gear structural attachment points. These loads and moments affect the bending moments, shears, and torques throughout the aircraft structure.

The number of landings per mission can be predicted from the percentage of aircraft life to be used for each mission and the mission time. First, the total mission time for the aircraft life is computed by multiplying the percentage of aircraft life for each mission by the service life. The number of landings can now be found by dividing the total time for each mission by the mission time. An example of the number of landings of a fighter aircraft designed for 5,000 hour service life in the 20,000 lb landing weight configuration is presented in Table 3-2 below.

Table 3-2 Determining the Number of Landings Per Mission³¹

Mission	Usage (% of life)	Total Time (hr)	Landing Weight (lb)	Mission Time(min)	No. of Landings
Training	10	500	20,000	60	500
Air-to-Air	30	1,500	20,000	90	1000
Admin	5	250	20,000	60	250
...
					$\Sigma = 1,750$

With the sink speed distribution information and the number of landings corresponding to aircraft landing weight, the number of landings at each sink speed level can be determined for each landing weight. This is demonstrated in the following example. The total number of landings at 20,000 lb landing weight is 1,750. The number of occurrences of 1 fps sink speed from a sink speed distribution plot is 180 per 1000 landings. The number of occurrences of 1 fps sink speed at 20,000 lb landing weight is determined from Eq. (3.10).

$$\frac{180}{1000} \times 1,750 = 315 \text{ occurrences at 1 fps} \quad (3.10)$$

The number of occurrences of sink speed should be rounded off. Any extra landings should be removed from the low sink speed occurrences to maintain a total sum of sink speeds equal to the total number of landings in the aircraft life.

With the above information, a dynamic analysis is conducted where the rigid body and flexible modes are contained within the vertical plane. The sink speeds are the initial conditions at the main landing gear in the analysis, and the equations of motion determine the ground forces and displacements, velocities, and accelerations at points around the aircraft. The accelerations are used to produce shears and moments at various structural locations. These values are compared to shears and moments produced by gusts, maneuvers, or other sources of loads. If the magnitude of landing shear and moment loads are significant, then they are included in the load spectrum.

Other factors to consider for landing loads are pilot input, wing spoiler activation timing, gusts, crosswinds, multiple main gear, and positive runway grade.

Aircraft designers use a landing approach descent velocity criterion of approximately 200 feet per minute (fpm) or 3 fps mean sink speed. Maximum sink speed is about 600 fpm or 10 fps. These criteria are not adequate for some transport aircraft which perform assault landings into short airfields. These aircraft can have a high descent velocity (1,000 fpm) and a low approach speed of 80 to 100 knots.

3.2.6 Miscellaneous Loads

Other sources of loads, which may be included in the development of the load spectra, are the operation of speed brakes, maneuvering flaps, landing gear, and the

separation of stores during flight. The number of occurrences of these loads can be determined from the mission profiles.

3.3 Design Service Life and Mission Profiles

The load sequences are developed from the definition of the design service life, the mission profiles, and the load frequency spectra to be used for each mission profile or mission segment. The USAF provides this information to the contractor.

The design service life establishes the total flight and ground operational hours for aircraft life. The design life of fighters is usually low, around 4,000 to 5,000 hours. This is the result of high design stresses needed for a high percentage of the aircraft design life. Cargo aircraft are designed for long life around 20,000 to 30,000 hours because of low design stresses. Bombers are typically designed for lives of 10,000 to 15,000 hours. The mission profiles establish time in mission segments such as takeoff, landing, maneuvering, cruise, ascent, and descent with the related flight conditions of airspeed, altitude, and gross weight. The load spectra provide information on the magnitude and occurrence of maneuvering, gust, landing, and ground loads.

Mission profiles for all aircraft can be divided into similar mission segments, such as:

- | | |
|---------------------|--------------------------|
| a. Ground handling | h. Taxi |
| b. Takeoff | i. Ascent |
| c. Cruise | j. Air-to-air |
| d. Air-to-ground | k. Instrument/navigation |
| e. Loiter | l. Advanced transition |
| f. Descent | m. Landing |
| g. Aerial refueling | n. Terrain following. |

The mission profiles of each type of aircraft consist of a sequence of these segments. The time spent in each segment, severity of the maneuvering, and gust encounter probability will be different for each type of aircraft. Mission segments are the mission phases used in the final analysis and development of load spectra. Segments are defined by altitude, airspeed, and maneuvering severity. Segments can be subdivided if basic flight conditions change. A separate load spectrum is used for each segment where load sequences are based on the frequency of occurrences of the normal load factor.

Transport, cargo, and tanker aircraft mission profiles have large variations in gross weight and length of flight. Maneuvering is minimal. If cargo and fuel conditions span a wide range, then, several mission profiles may be used such that the variation in gross weight may be considered in load computations. Mission segments, which cover a wide range of airspeed, altitude, or gross weight, may be subdivided to account for all loading environment factors.

Bomber missions generally contain long flight time, high altitude with high-speed cruise, low altitude with high-speed cruise, and terrain following mission segments. The flexibility of bomber aircraft may vary significantly. The load sequences must be developed to include the loads that cause damage.

Attack aircraft missions consist of uniform two-hour flight times, several altitude and airspeed changes, much maneuvering, and large variations in external stores. Fighter aircraft missions consist of less than two-hour flight times, high-speed flight at high altitude, variations in altitude and airspeed, and variations in external stores.

Trainer aircraft are designed for specific mission training needs. These aircraft often have different flying characteristics. The training aircraft missions are defined by

the particular use desired for each aircraft.

Mission profiles cover a wide range of altitude, airspeed, configuration, and gross weight conditions. The number of flight conditions needs to be limited in order to reduce the load analysis to a manageable problem. Airspeed and altitude combinations are determined by averaging the beginning and ending airspeed and altitude for each mission segment. In Figure 3-10, ranges, or blocks, for both airspeed and altitude are then chosen and tabulated. Altitude blocks are the same as those used to determine turbulence induced loads. Percent of the life for each mission segment is also tabulated. Joint distributions of time at airspeed-altitude combinations are then obtained by summing the lifetime percentage of airspeed and altitude combinations. The combination with the highest percentage of time within a block represents that block.

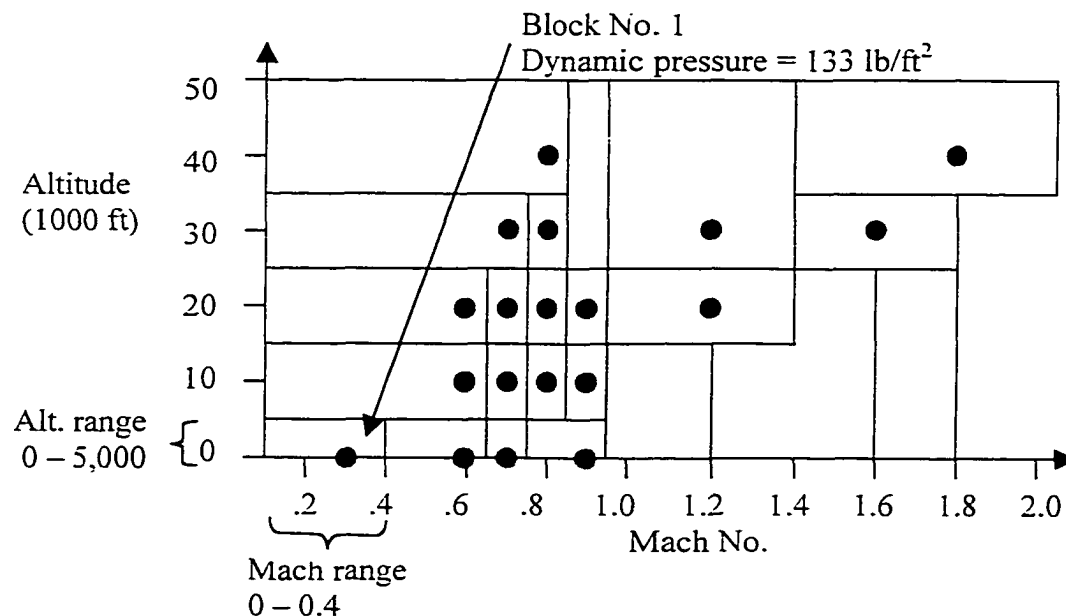


Figure 3-10 Selection of Airspeed and Altitude Combinations³¹

In Figure 3-10, block number 1 has an altitude range of 0 to 5,000 feet and a Mach number range of 0 to 0.4. The representative altitude and Mach number selected for this block is 0 ft and 0.3, respectively. The black circle indicates this data point.

The gross weight ranges used in load computation are based on expected aircraft configurations, fuel, and cargo. For fighter and attack aircraft, there must be several blocks to cover the range of external store weights and their inertial properties. An analysis weight is selected to represent each weight range (i.e., midpoint) which corresponds to a particular configuration. Cargo and transport aircraft require a fine breakdown of fuel weights to account for possible variations. Cargo weights are selected to cover the expected range of cargo capacity. Fuel weights are selected to cover the possible range of values. Loads are computed at each combination of fuel and cargo weights. Loads at other combinations can be found by interpolation.

CHAPTER IV

A NEW MODEL OF THE FATIGUE ENVIRONMENT

4.1 Introduction

The aircraft flight environment consists of time varying fatigue loads, which are externally imposed on the structure and are the primary influence on fatigue prediction. Traditionally, large amounts of data in the form of exceedance curves or tables are needed to develop fatigue load histories for each flight. Therefore, several tables with numerous exceedance values are necessary for the fatigue load spectra development of a new aircraft.

Lincoln⁴⁰ observed a wide variation in velocity, altitude, and weight in the air-to-air and air-to-ground segments of a military aircraft. He computed the probability that a load would occur in a given interval of airspeed, normal load factor, altitude, and weight by taking the VGH histogram (the frequency of airspeed, normal load factor, altitude, and weight) and dividing by the total number of load occurrences. In contrast, the research in this chapter focuses on modeling the fatigue load environment with only a few parameters and probability distribution functions. Regression analysis is used to develop these models. Here, the data consist of maneuver normal load factors, roll rates, and roll accelerations. Load factor data due to gusts are excluded. The results in the following sections focus on the advanced transition segment load factor exceedance data for a fighter aircraft. The approach used on the advanced transition segment is consistently used on the other flight segment load factor, roll rate, and roll acceleration exceedance

data with a few exceptions. These exceptions are discussed in detail.

4.2 Normal Load Factor Exceedances

Load factors are derived from acceleration measurements taken by an accelerometer placed at the aircraft center-of-gravity and recorded on a structural flight data recorder. Straight and level turbulence free flight produces a normal load factor of 1.0g. As an accelerometer can only measure departures from 1.0g, no data are available for this load factor. The cumulative frequency at which a load factor level is met or exceeded is called an exceedance. Thus, exceedance is a cumulative occurrence. Exceedances are computed by adding all the occurrences up to and including the desired load factor level. Load factor exceedances are typically plotted on semi-log scale or tabulated. Normally, exceedances are computed separately for the negative and positive load factors and for different flight segments. The fighter flight segments used in this dissertation are ascent, cruise, formation, descent, air-to-air combat, air-to-ground, loiter, instrument and navigation, and advanced transition. The exceedance values recorded in 1000 hours for these segments are listed in Table 4-1.

4.3 Cumulative Distribution Functions

The plotting position F or ordinate on a cumulative distribution graph is an area of much disagreement. In a cumulative distribution graph, an estimate of F is plotted versus the data set. The quantity F is the percentage of the total population occurring before it. The true values of F are unknown and need to be estimated with a rank or plotting position. Three common plotting positions found in the literature are midpoint, mean, and median ranks where i is the position of a data point listed in ascending order and n is

**Table 4-1 Typical Normal Load Factor Exceedance Distributions per Mission
Segment for Fighter/Attack Aircraft per 1,000 Flight Hours³¹**

n_z	Ascent	Cruise	Descent	Loiter	Air-Ground	Air-Air	Advanced Transition	Formation	Instrument & Navigation
-2.5						2.8	4.9		
-2.0					1.9	21	20	3	0.76
-1.5					4.2	170	60	9.8	1.6
-1.0					4.2	710	170	51	8
-0.5					4.2	2000	910	750	200
0.0					4.2	11000	11000	19000	5100
0.5					4.2	170000	62000	120000	34000
1.5	80010	25000	45000	68000	220000	410000	92000	170000	36000
2.0	12010	13000	27000	24000	200000	330000	50000	50000	12000
2.5	2010	7700	15000	9800	160000	270000	28000	15000	4100
3.0	270	3800	8100	3400	120000	210000	13500	6200	1700
3.5	30	1800	3600	1300	82000	160000	7200	3100	730
4.0	3	700	1000	430	51000	120000	3200	1700	310
4.5		210	210	160	30000	83000	1500	900	120
5.0		13	13	48	13000	52000	620	400	32
5.5				13	6500	33000	210	150	12
6.0				2.8	2700	20000	50	46	4.4
6.5					1000	12000	14	12	1.6
7.0					330	6800	4.6	2.3	
7.5					110	3800	1.7		
8.0					30	1900			
8.5					8.8	1000			
9.0					2.0	480			
9.5						230			
10.0						110			

the total number of data points in Eqs (4.1) through (4.3). Another approach to obtain F , realized in this research, is to normalize the exceedances in the load factor, roll rate, and roll acceleration data. Recall, an exceedance is a cumulative frequency and relative frequency is used to approximate probability. Therefore, a normalized exceedance curve is a cumulative distribution function for negative load factor data. The normalized exceedance values are the plotting positions F . For positive load factor, roll rate, and roll acceleration, normalizing the exceedance curve produces the complementary cumulative distribution function $R(x) = 1 - F(x)$. In this case, the normalized exceedance values are the plotting positions R . This probability distribution function is analogous to the

reliability function. If needed, the corresponding cumulative distribution functions can be found with $F(x) = 1 - R(x)$. Normalized exceedance is used to obtain the plotting positions before the regression analyses are performed. The following discussion in this section determines the validity of using normalized exceedance for plotting positions instead of the formulas listed below.

$$\text{Midpoint rank:} \quad F_i = \frac{(i - 0.5)}{n} \quad (4.1)$$

$$\text{Mean rank}^{41}: \quad F_i = \frac{i}{n + 1} \quad (4.2)$$

$$\text{Median rank (Benard's approximation)}^{42}: \quad F_i = \frac{i - 0.3}{n + 0.4} \quad (4.3)$$

Johnson⁴³ reported that the estimate of the population statistics is the objective in variation research, not the sample statistics. Therefore, the median rank is a more useful population estimate of plotting positions than midpoint rank or mean rank when dealing with small samples of data. Table 4-2 and Figure 4-1 show the application of the median rank, Eq.(4.3), to positive load factor exceedance data for the advanced transition

Table 4-2 Median Ranks for the Advanced Transition Segment Load Factor Exceedance Data

Load Factor	Exceedances	Median Rank, R
1.5	92000	0.99999
2.0	50000	0.54347
2.5	28000	0.30434
3.0	13500	0.14674
3.5	7200	0.07826
4.0	3200	0.03478
4.5	1500	0.01630
5.0	620	0.00674
5.5	210	0.00228
6.0	50	0.00054
6.5	14	0.00015
7.0	5	0.00005
7.5	2	0.00002

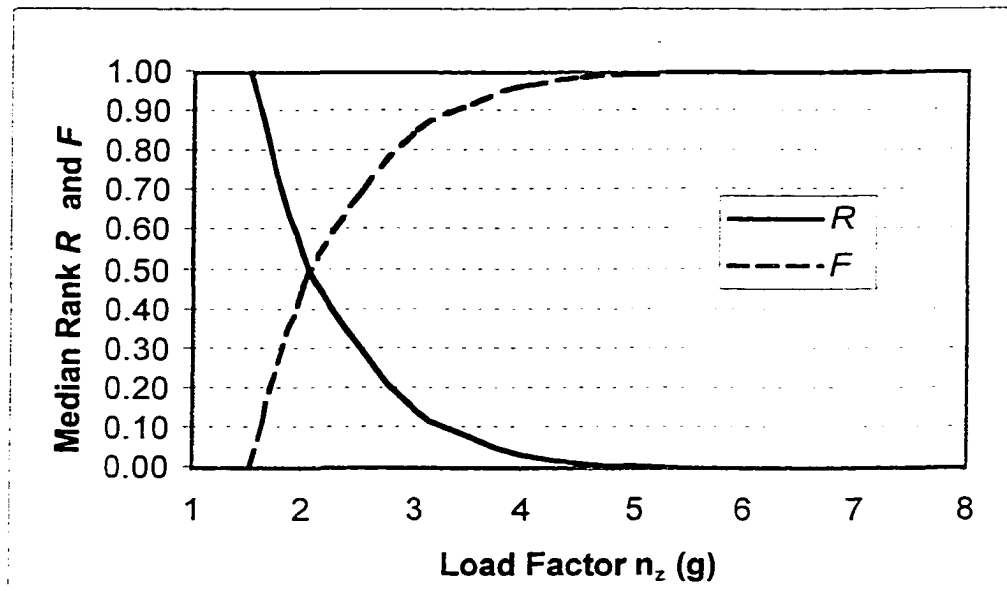


Figure 4-1 Median Rank R and Complementary Values F for Positive Load Factor Exceedances for the Advanced Transition Segment

segment. Johnson also mentioned that, with small samples, it is better to order data according to life and build a cumulative distribution plot. The estimate of the integral of the frequency function is easier than the direct estimation of the frequency function itself. Cumulative frequency (exceedance) is the integral of the load factor frequency of occurrence function. This explains why regression analyses of the normal load factor exceedance data were more successful than those of the load factor frequency of occurrence data in earlier research. Figure 4-2 uses a semi-log scale which is typical of the load factor exceedance spectra format.

Based on the previous discussion, it appears that the use of normalized exceedances for plotting positions is incorrect. But Nelson⁴⁴ reported that with reasonable size samples, there is very little difference in the results with different plotting positions. In practice, plotting positions differ little compared with the randomness of the data. But one should consistently use one kind of plotting position when comparing

samples. Table 4-3 shows the differences between mean and median ranks becoming smaller with larger sample size.

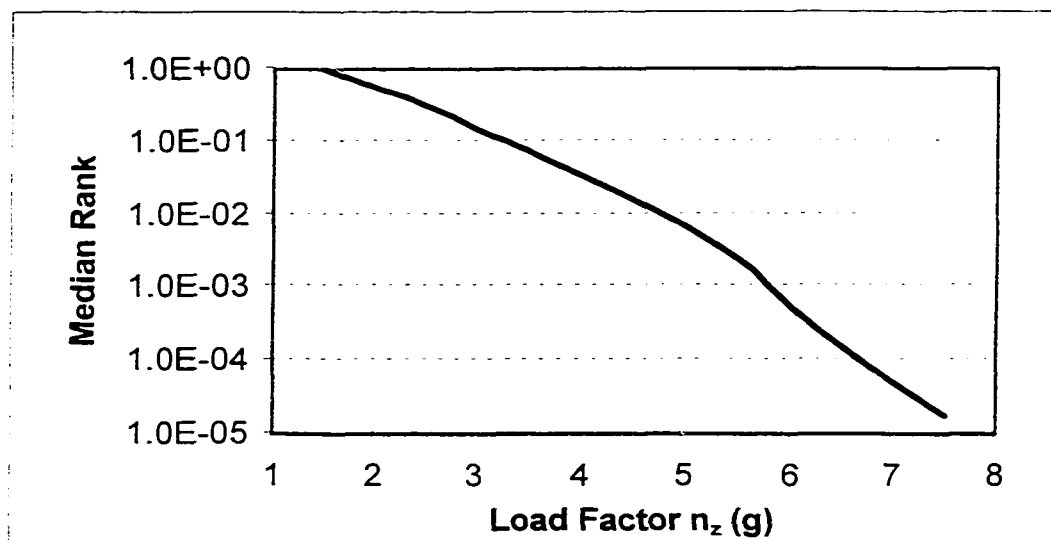


Figure 4-2 Median Rank for Positive Load Factor Exceedances for the Advanced Transition Segment in Semi-Log Scale

Table 4-3 Comparison of Median and Mean Ranks

i	Median Rank	Mean Rank	Percent Difference (%)
1	0.01104	0.01563	41.6
2	0.02681	0.03125	16.6
3	0.04259	0.04688	10.1
4	0.05836	0.06250	7.1
5	0.07413	0.07813	5.4
...
63	0.98896	0.98438	-.46

Table 4-4 indicates little difference between median ranks and normalized exceedances with the advanced transition segment load factors. Both values of median ranks and normalized exceedances are plotted in Figure 4-3 for comparison. From this figure, one can conclude that using normalized exceedance is a valid approach for determining the plotting positions for cumulative distribution functions.

Table 4-4 Comparison of Median Rank and Normalized Load Factor Exceedance Plotting Positions for the Advanced Transition Segment

Load factor (g)	Exceedances	Plotting Positions	
		Median Rank	Normalized Exceedance
1.5	92000	0.99999	1.00000
2.0	50000	0.54347	0.54348
2.5	28000	0.30434	0.30435
3.0	13500	0.14674	0.14674
3.5	7200	0.07826	0.07826
4.0	3200	0.03478	0.03478
4.5	1500	0.01630	0.01630
5.0	620	0.00674	0.00674
5.5	210	0.00228	0.00228
6.0	50	0.00054	0.00054
6.5	14	0.00015	0.00015
7.0	5	0.00005	0.00005
7.5	2	0.00002	0.00002

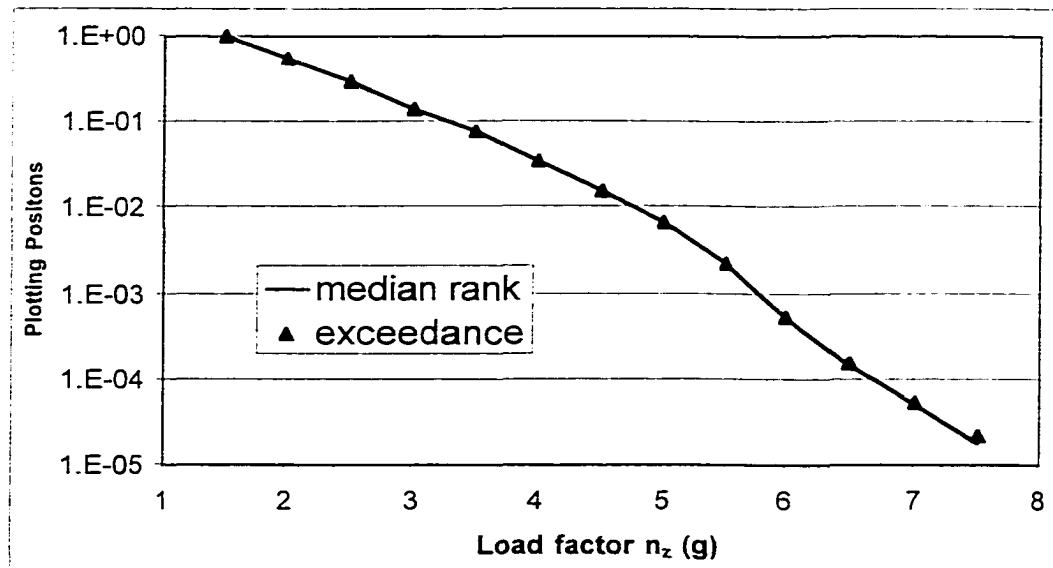


Figure 4-3 Comparison of Median Rank and Normalized Exceedance for Advanced Transition Segment Load Factor

4.4 Approach

Mathematical models of the ascent, loiter, cruise, formation, air-to-air, descent, instrument and navigation, advanced transition, and air-to-ground segment exceedance data in Table 4-1 are created using Axum[®] software⁶. Axum[®] has the capability to combine a polynomial of a specified order with an exponential equation into one regression model. Polynomials of order one through five are combined with the exponential equation to fit the negative and positive load factor exceedance data separately. A regression analysis of exceedance data is difficult because the orders of magnitude vary from 1 to 100,000. The exponential-polynomial model in Eq. (4.4) addresses the nonlinear behavior of the semi-log exceedance plots.

$$Exc = a \cdot e^{(b \cdot n_z + c \cdot n_z^2 + d \cdot n_z^3 + \dots)} \quad (4.4)$$

An adjusted coefficient of determination $_{adj}R^2$ is often used to judge the adequacy of a regression model⁴⁵. It is a measure of the amount of reduction in the variability of the data accounted by the regression model. If $_{adj}R^2$ is near 1.0, the model is supposedly a good representation of the data. However, previous work⁴⁶ indicated that $_{adj}R^2$ is not a reliable or sensitive indicator of the correlation between the actual data and the corresponding fitted values. Instead of relying on the subjective evaluation of graphs, a new method is used to determine correlation performance. The residual is the difference between an observed data point and the corresponding fitted value from the regression model. The percent residual (or percent difference) is first computed for each load factor level by dividing the residual by its observed data value and multiplying by 100%. The absolute values of the percent residuals from each load factor level are then used to compute a mean percent residual for each regression model. A low mean percent

residual indicates a good correlation between the actual data and the regression model.

The next step is to compute cumulative distribution functions from the best regression models and calculate the probability for each load factor. The FORTRAN program “Load_occurrence.exe”, which can be found in Appendix A, is used to perform these computations. When dealing with small samples, the median rank is often used to approximate the population cumulative distribution functions. But as verified in section “4.3 Cumulative Distribution Functions,” median ranks provide no advantage here because of the large number of available data. As discussed in that section, a normalized exceedance curve is a cumulative distribution function for negative load factor data. Cumulative distribution functions $F(n_z)$ such as Eq. (4.5) are computed by normalizing the fitted exceedance curve in Eq. (4.4) with the maximum exceedance used in the probability analysis. The maximum exceedance for negative load factor data is extrapolated at 0.75g. Extrapolation is necessary because load factor is a continuous random variable and therefore probability must be defined over an interval of load factors. For positive load factors, normalizing the fitted exceedance equation with the maximum exceedance used in the probability analysis produces the complementary cumulative distribution function $R(n_z)$ in Eq. (4.6). The maximum exceedance used to normalize positive load factor data is extrapolated to 1.25g.

$$F(n_z) = \frac{a \cdot e^{(b \cdot n_z + c \cdot n_z^2 + d \cdot n_z^3 + \dots)}}{Exc(n_z = 0.75g)} \quad n_z < 1.0g \quad (4.5)$$

$$R(n_z) = \frac{a \cdot e^{(b \cdot n_z + c \cdot n_z^2 + d \cdot n_z^3 + \dots)}}{Exc(n_z = 1.25g)} \quad n_z > 1.0g \quad (4.6)$$

Because normal load factor is a continuous random variable, probability is defined as the difference between the above distribution functions evaluated at load factor

intervals⁴⁷. The load factor data for the USAF fighter segments in Table 4-1 vary by 0.5g increments, therefore, probability is computed over the uniform interval $n_z \pm 0.25$ with Eqs. (4.7) and (4.8). The load factor interval is represented by its mean. This is done for each load factor level in the data set and for each flight segment in Table 4-1.

$$P(n_z - .25 < n_z < n_z + .25) = F(n_z + .25) - F(n_z - .25) \quad n_z < 1.0g \quad (4.7)$$

$$P(n_z - .25 < n_z < n_z + .25) = R(n_z - .25) - R(n_z + .25) \quad n_z > 1.0g \quad (4.8)$$

4.5 Load Factor Regression Analyses

The 5th order exponential-polynomial model in Eq. (4.9) provided excellent correlation with the advanced transition segment positive load factor data in Table 4-1. The results in Table 4-5 on the following page show a trend toward lower mean percent residuals with increasing polynomial order. Unlike $_{adj}R^2$, the mean percent residual displayed a significant reduction with increasing polynomial order and data correlation. It also appeared to be more sensitive to data correlation improvements than $_{adj}R^2$. The final mean percent residual was 4.5% and $_{adj}R^2$ was 0.9996. This correlation with positive load factors was visually confirmed in Figure 4-4 on the next page. The F ratio test was used to evaluate the statistical significance of the regression models. This test is based on the F distribution which is the ratio of two independent chi-square random variables⁴⁵. It is one of the most useful distributions in statistics. The 5th order exponential-polynomial model passed the F ratio test.

$$Exc = 49367.9 \cdot e^{(2.878n_z - 2.548n_z^2 + .7456n_z^3 - .1036n_z^4 + .005256n_z^5)} \quad 1.5 \leq n_z \leq 7.5 \quad (4.9)$$

Table 4-5 Exceedance Curve Fit for Positive Load Factors: Advanced Transition Segment

n_z (g)	Exceedances	Regression Analysis Results				
		Exponential Equation	2nd order	3rd order	4th order	5th order
1.5	92000	198063	86290	83334	97353	91505
2.0	50000	78788	52004	52004	46884	51449
2.5	28000	31341	29061	29619	25474	26798
3.0	13500	12467	15059	15445	14189	13757
3.5	7200	4959	7235	7398	7526	6995
4.0	3200	1973	3223	3265	3610	3412
4.5	1500	785	1332	1332	1519	1519
5.0	620	312	510	504	557	589
5.5	210	124	181	177	180	194
6.0	50	49	60	58	53	55
6.5	14	20	18	18	15	15
7.0	4.6	7.8	5.2	5.2	4.7	4.2
7.5	1.7	3.1	1.4	1.4	1.6	1.7
Mean % residual		45.7	11.6	12.1	7.0	4.5
$adj R^2$		0.9785	0.9980	0.9979	0.9992	0.9996

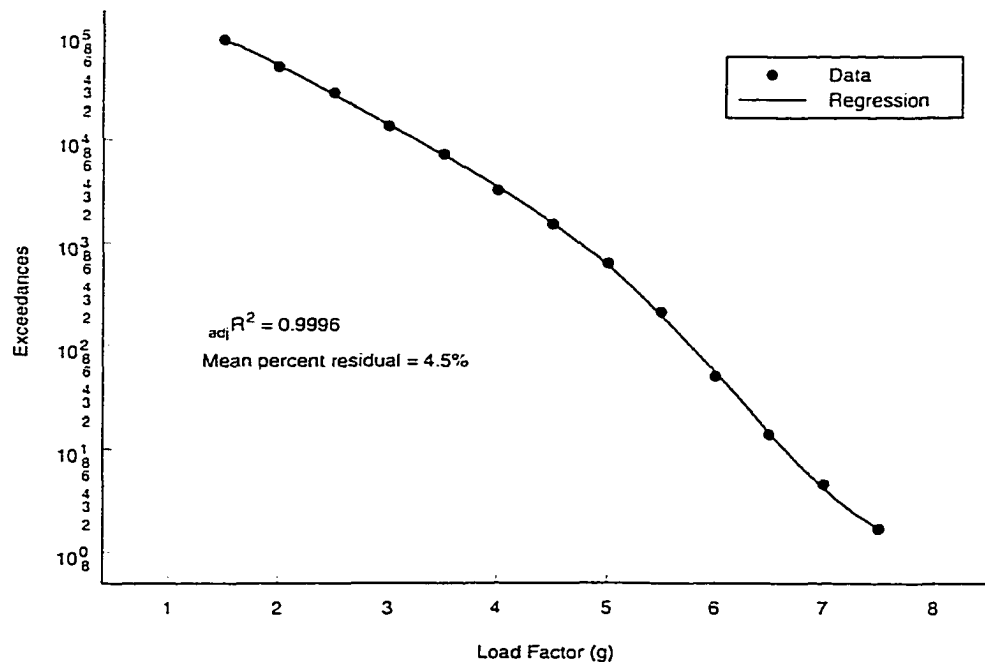


Figure 4-4 Advanced Transition Segment: Positive Load Factor Exceedance Regression Analysis

Five more regression analyses were performed on the advanced transition segment exceedance data in Table 4-1 over the negative load factor range. Table 4-6 indicates that the 5th order exponential-polynomial model in Eq. (4.10) and Figure 4-5 on the following page provided the best curve fit with a mean percent residual of 0.28% and $_{adj}R^2$ of 1.00. Here extrapolation of Eq. (4.10) at 0.75g produced an exceedance less than the exceedance at 0.5g. However, the exceedance at 0.75g should be greater than the exceedance at 0.5g according to historical trends. For this reason, the 4th order exponential-polynomial model in Eq. (4.11) and in Figure 4-6 was chosen as the best curve fit model for the advanced transition segment over the negative load factor range. This curve produced a satisfactory mean percent residual of 7.6%, $_{adj}R^2$ of 0.9975, and passed the F ratio test. Again, the mean percent residual was a better judge of regression model adequacy.

$$Exc = 1.098 \times 10^4 \cdot e^{(5.126n_z - 1.044n_z^2 + 3.563n_z^3 - 1.861n_z^4 - .2931n_z^5)} \quad -2.5 \leq n_z \leq 0.5 \quad (4.10)$$

$$Exc = 9888 \cdot e^{(+.484n_z - 0.6772n_z^2 - 1.487n_z^3 - 0.3948n_z^4)} \quad -2.5 \leq n_z \leq 0.5 \quad (4.11)$$

Table 4-6 Exceedance Curve Fit Results for Negative Load Factors: Advanced Transition Segment

n_z (g)	Exceedances	Regression Analysis Results				
		Exponential Eq.	2nd order	3rd order	4th order	5th order
-2.5	4.9	3.2	5.8	5.4	4.8	4.9
-2.0	20	15	15	16	22	20
-1.5	60	73	51	55	53	60
-1.0	170	348	218	218	169	169
-0.5	910	1657	1165	1087	1042	914
0.0	11000	7883	7883	7354	9588	10980
0.5	62000	37507	67430	72278	63664	62019
Mean % residual		47.7	21.3	19.1	7.6	0.28
$_{adj}R^2$		0.9738	0.9922	0.9904	0.9975	1.0000

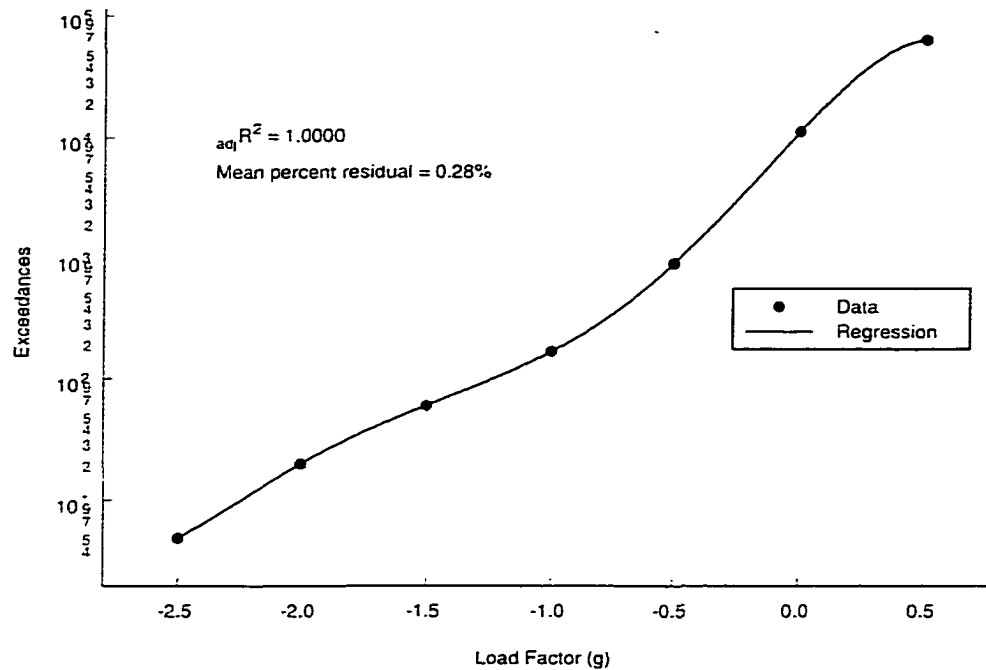


Figure 4-5 Advanced Transition Segment: Negative Load Factor Exceedance Regression Analysis with the 5th Order Exponential-Polynomial Model

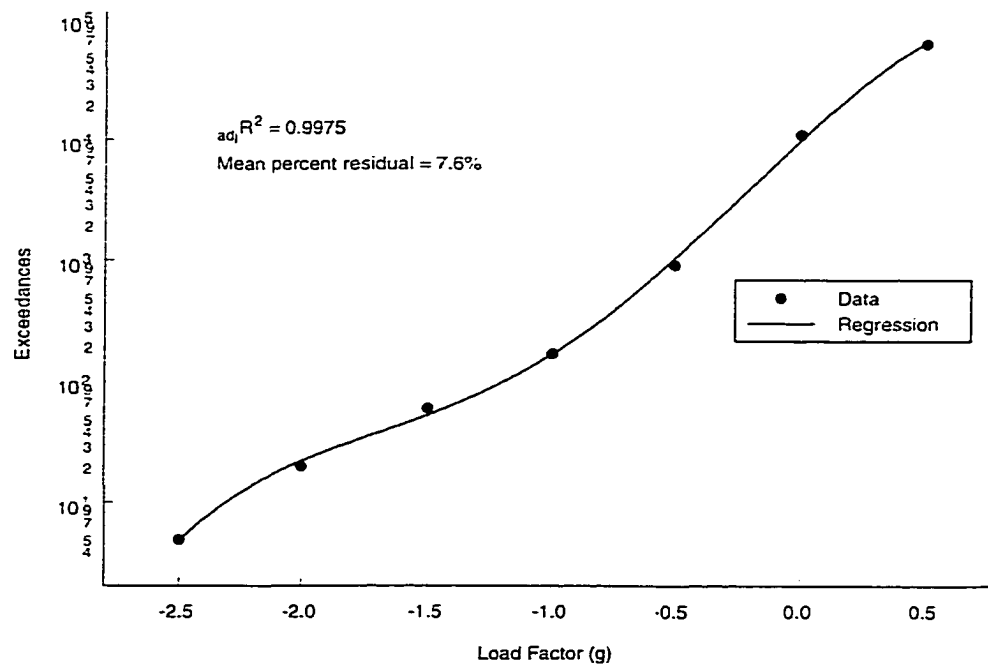


Figure 4-6 Advanced Transition Segment: Negative Load Factor Exceedance Regression Analysis with the 4th Order Exponential-Polynomial Model

Regression analyses were performed on the remaining flight segments, and the results for the cruise, ascent, descent, instrument and navigation, air-to-air, air-to-ground, formation, and loiter segments can be seen in Eqs. (4.12) through (4.23). These segments are plotted in Appendix B to demonstrate the capability of the exponential-polynomial equation to model significantly different exceedance data.

Cruise:

$$Exc = 1.056 \times 10^{13} \cdot e^{(-35.89n_z + 25.49n_z^2 - 9.004n_z^3 + 1.538n_z^4 - 0.1027n_z^5)} \quad 1.5 \leq n_z \leq 5.0 \quad (4.12)$$

Ascent:

$$Exc = 6.954 \times 10^6 \cdot e^{(-2.6112n_z - 0.2621n_z^2)} \quad 1.5 \leq n_z \leq 4.0 \quad (4.13)$$

Descent:

$$Exc = 2.522 \times 10^4 \cdot e^{(2.483n_z - 2.122n_z^2 + 0.5737n_z^3 - 0.06181n_z^4)} \quad 1.5 \leq n_z \leq 5.0 \quad (4.14)$$

Instrument and Navigation:

$$Exc = 2.875 \times 10^7 \cdot e^{(-6.848n_z + 2.105n_z^2 - 0.3661n_z^3 + 0.02209n_z^4)} \quad 1.5 \leq n_z \leq 6.5 \quad (4.15)$$

$$Exc = 5366 \cdot e^{(6.046n_z - 2.935n_z^2 - 3.276n_z^3 - 0.7019n_z^4)} \quad -2.0 \leq n_z \leq 0.5 \quad (4.16)$$

Air-to-Air:

$$Exc = 5.545 \times 10^5 \cdot e^{(-0.08894n_z - 0.07688n_z^2)} \quad 1.5 \leq n_z \leq 10 \quad (4.17)$$

$$Exc = 1.006 \times 10^4 \cdot e^{(3.918n_z + 2.638n_z^2 + 1.695n_z^3 + 0.2968n_z^4)} \quad -2.5 \leq n_z \leq 0.5 \quad (4.18)$$

Air-to-Ground:

$$Exc = 1.784 \times 10^5 \cdot e^{(0.4369n_z - 0.1895n_z^2)} \quad 1.5 \leq n_z \leq 9.0 \quad (4.19)$$

$$Exc = 45.37 \cdot e^{(1.586n_z)} \quad -2.0 \leq n_z \leq -1.5 \quad (4.20)$$

Formation:

$$Exc = 8.561 \times 10^7 \cdot e^{(-5.535n_z + 1.065n_z^2 - 0.09015n_z^3)} \quad 1.5 \leq n_z \leq 7.0 \quad (4.21)$$

$$Exc = 14,419.64 \cdot e^{(5.17n_z - 1.11n_z^2 - 0.80n_z^3)} \quad -2.0 \leq n_z \leq 0.5 \quad (4.22)$$

Loiter:

$$Exc = 2.629 \times 10^6 \cdot e^{(-2.823n_z + 0.3187n_z^2 - 0.03826n_z^3)} \quad 1.5 \leq n_z \leq 6.0 \quad (4.23)$$

4.6 Load Factor Probability Functions

Probability functions for all flight segments were developed from the best regression analyses. Normalizing Eq. (4.9) with 113,963.94, i.e., the number of exceedances at 1.25g, produced the probability distribution function in Eq. (4.24) for the advanced transition segment positive load factor data. The probabilities for the positive load factor levels were computed with Eq. (4.8) and are listed in Table 4-7.

$$R(n_z) = \frac{49367.9 \cdot e^{(2.878n_z - 2.548n_z^2 + 7.456n_z^3 - 1036n_z^4 + 0.05256n_z^5)}}{113963.94} \quad n_z > 1.0g \quad (4.24)$$

The cumulative distribution function in Eq. (4.25) for negative load factor data was derived by normalizing Eq. (4.11) with 91,963.7, i.e., the number of exceedances extrapolated at 0.75g. The probabilities for the negative load factor levels were computed with Eq. (4.7) and are listed in Table 4-8. The probabilities of the load factor level occurrences for the remaining flight segments in Table 4-1 are listed in Appendix C.

$$F(n_z) = \frac{9888 \cdot e^{(4.484n_z - 0.6772n_z^2 - 1.487n_z^3 - 0.3948n_z^4)}}{91963.7} \quad n_z < 1.0g \quad (4.25)$$

**Table 4-7 Probability of Occurrences for Positive Load Factors: Advanced
Transition Segment**

n_z (g)	Predicted	$R(n_z)$	Probability	n_z (g)
1.25	113963.9	1.0000000		
1.50	91505.0	0.8029298	0.38811	1.5
1.75	69733.4	0.6118898		
2.00	51449.0	0.4514501	0.28473	2.0
2.25	37284.8	0.3271634		
2.50	26798.1	0.2351457	0.15862	2.5
2.75	19208.0	0.1685447		
3.00	13756.6	0.1207104	0.08225	3.0
3.25	9834.7	0.0862968		
3.50	6995.1	0.0613800	0.04308	3.5
3.75	4925.3	0.0432178		
4.00	3412.1	0.0299398	0.02294	4.0
4.25	2310.4	0.0202734		
4.50	1519.4	0.0133322	0.01181	4.5
4.75	964.9	0.0084665		
5.00	589.2	0.0051697	0.00544	5.0
5.25	345.1	0.0030282		
5.50	194.0	0.0017021	0.00211	5.5
5.75	105.0	0.0009213		
6.00	55.1	0.0004837	0.00067	6.0
6.25	28.4	0.0002493		
6.50	14.6	0.0001283	0.00018	6.5
6.75	7.7	0.0000674		
7.00	4.2	0.0000372	0.00005	7.0
7.25	2.5	0.0000224		
7.50	1.7	0.0000153	0.00001	7.5
7.75	1.4	0.0000125		

Table 4-8 Probability of Occurrences for Negative Load Factors: Advanced Transition Segment

n_z (g)	Predicted	$F(n_z)$	Probability	n_z (g)
0.75	91963.7	1.000000		
0.50	63663.7	0.692270	0.69152	0.5
0.25	28369.1	0.308482		
0.00	9888.4	0.107525	0.27415	0.0
-0.25	3157.2	0.034331		
-0.50	1042.0	0.011331	0.03013	-0.5
-0.75	386.6	0.004204		
-1.00	169.0	0.001837	0.00325	-1.0
-1.25	87.9	0.000955		
-1.50	52.9	0.000575	0.00058	-1.5
-1.75	34.6	0.000376		
-2.00	22.2	0.000241	0.00024	-2.0
-2.25	12.1	0.000132		
-2.50	4.8	0.000052	0.00012	-2.5
-2.75	1.1	0.000012		

4.7 Air-to-Air Segment Probability Correction

The normal load factor exceedance model for the air-to-air segment produced erroneous results when extrapolated to 1.25g. The probability of occurrence for 1.5g was less than 2.0g. A portion of the air-to-air segment probability of occurrence table from Appendix B is reproduced in Table 4-9. This error was caused by the inability of the exponential-polynomial model to predict values outside its original data range. This problem was solved by fitting a seven-point parabola to the exceedance data over the range of 1.5g to 4.5g in Figure 4-7 on the following page. The parabola in Eq. (4.26) was successfully used to extrapolate the exceedance of 447,919.3 to 1.25g. Figure 4-8 displays the air-to-air segment load factor exceedance data with the corrected extrapolation to 1.25g.

$$Exc = 15952n_z^2 - 203643n_z + 677548 \quad (4.26)$$

Table 4-9 Original Probability of Occurrences for Positive Load Factors: Air-To-Air Segment (partially reproduced from Appendix C)

n_z (g)	Predicted	$R(n_z)$	Probability	n_z (g)
1.25	439966.4	1.0000000		
1.50	408139.1	0.9276597	0.14768	1.5
1.75	374993.2	0.8523222		
2.00	341243.9	0.7756136	0.15326	2.0
2.25	307562.2	0.6990584		
2.50	274553.8	0.6240336	0.14733	2.5
2.75	242744.0	0.5517330		
3.00	212567.0	0.4831438	0.13270	3.0
3.25	184361.3	0.4190350		
3.50	158369.0	0.3599570	0.11278	3.5
3.75	134740.1	0.3062510		
4.00	113540.4	0.2580660	0.09087	4.0
4.25	94761.1	0.2153825		
4.50	78331.5	0.1780396	0.06962	4.5
...		

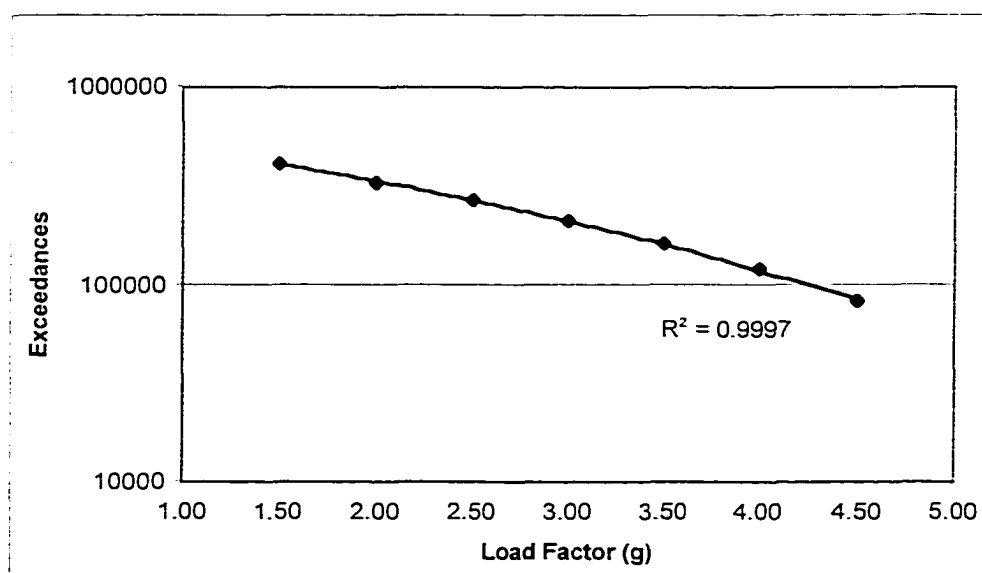


Figure 4-7 Regression Analysis of Normal Load Factor Data with a Seven-Point Parabola

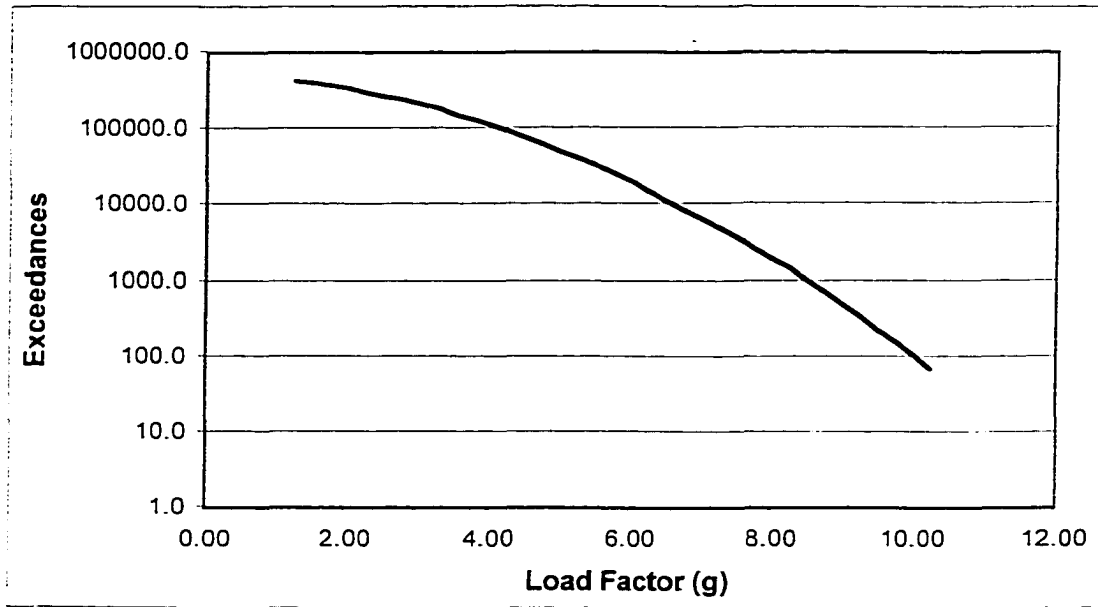


Figure 4-8 Air-To-Air Segment Normal Load Factor Exceedance Data with Corrected Extrapolation to 1.25g

The corrected probabilities of occurrences for the load factor levels are given in Table 4-10 below. The column of exceedances in this table were normalized to 447,919.3 to produce the corresponding distribution function values $R(n_z)$ represented by Eq. (4.27). Probabilities of occurrences for the normal load factor levels were determined, in the same manner as before, from the difference of distribution function $R(n_z)$ values computed over intervals of $\pm 0.25g$. These computations were performed with Eq. (4.8).

$$R(n_z) = \frac{49367.9 \cdot e^{(2.878n_z - 2.548n_z^2 + 7.456n_z^3 - 10.36n_z^4 + 0.005256n_z^5)}}{447,919.3} \quad n_z > 1.0g \quad (4.27)$$

$$P(n_z - .25 < n_z < n_z + .25) = R(n_z - .25) - R(n_z + .25) \quad n_z > 1.0g \quad (4.8)$$

Table 4-10 Corrected Probabilities of Normal Load Factor Occurrences for the Air-to-Air Segment

n_z (g)	Exceedance	$R(n_z)$	Probability	n_z (g)
1.25	447919.3	1.00000000		
1.50	408139.1	0.91118907	0.16281	1.5
1.75	374993.2	0.83718923		
2.00	341243.9	0.76184255	0.15054	2.0
2.25	307562.2	0.68664661		
2.50	274553.8	0.61295388	0.14471	2.5
2.75	242744.0	0.54193697		
3.00	212567.0	0.47456556	0.13034	3.0
3.25	184361.3	0.41159502		
3.50	158369.0	0.35356598	0.11078	3.5
3.75	134740.1	0.30081348		
4.00	113540.4	0.25348402	0.08926	4.0
4.25	94761.1	0.21155843		
4.50	78331.5	0.17487855	0.06838	4.5
4.75	64131.1	0.14317566		
5.00	52003.0	0.11609896	0.04993	5.0
5.25	41765.1	0.09324250		
5.50	33222.0	0.07416961	0.03481	5.5
5.75	26173.6	0.05843385		
6.00	20423.5	0.04559628	0.02320	6.0
6.25	15784.1	0.03523878		
6.50	12082.0	0.02697359	0.01479	6.5
6.75	9159.7	0.02044952		
7.00	6877.9	0.01535515	0.00903	7.0
7.25	5115.1	0.01141961		
7.50	3767.7	0.00841153	0.00528	7.5
7.75	2748.7	0.00613656		
8.00	1986.1	0.00443406	0.00296	8.0
8.25	1421.4	0.00317325		
8.50	1007.5	0.00224923	0.00159	8.5
8.75	707.3	0.00157903		
9.00	491.8	0.00109793	0.00082	9.0
9.25	338.7	0.00075610		
9.50	231.0	0.00051572	0.00041	9.5
9.75	156.1	0.00034840		
10.00	104.4	0.00023311	0.00019	10.0
10.25	69.2	0.00015448		

4.8 Roll Rate and Roll Acceleration Probability Functions

The roll rate and roll acceleration exceedance data are provided here for a complete mission instead of individual mission segments. The data in Table 4-11 were taken from the composite mission of a fighter aircraft and represent 1,000 hours of flight time. The composite mission exceedance data are the averages of exceedance data from all mission types such as air-to-air and air-to-ground. The Axum[®] program was used again to perform regression analysis of the roll rate and roll acceleration exceedance data with the exponential-polynomial model. The mean percent residual was calculated in each regression analysis to find the best model.

Table 4-11 Roll Rate and Roll Acceleration Exceedance Data from the Composite Mission of a Fighter Aircraft

Roll Rate (rad/s)	Exceedances	Roll Acceleration (rad/s ²)	Exceedances
0.25	98,233.5	1.0	119,255.6
0.75	49,053.3	3.0	36,433.5
1.25	18,241.5	5.0	6,183.9
1.75	7,269.1	7.0	786.8
2.25	1,897.1	9.0	45.8
2.75	442.7	11.0	4.7
3.25	112.9	13.0	0.7
3.75	25.0	15.0	0.2
4.25	3.1	-	-
4.75	0.3	-	-

4.8.1 Roll Rate Probability Function

The 4th order exponential-polynomial model in Eq. (4.28) provided excellent correlation with the roll rate p exceedance data in Table 4-11 for the composite mission. The regression results indicate a trend toward lower mean percent residuals with

increasing polynomial order. The final mean percent residual was 5.4% and $_{adj}R^2$ was 0.9995. This correlation is visually confirmed in Figure 4-9.

$$Exc = 1.154 \times 10^5 \cdot e^{(-.4642p - 1.04p^2 + .2567p^3 - .02888p^4)} \quad 0.25 \leq p \leq 4.75 \quad (4.28)$$

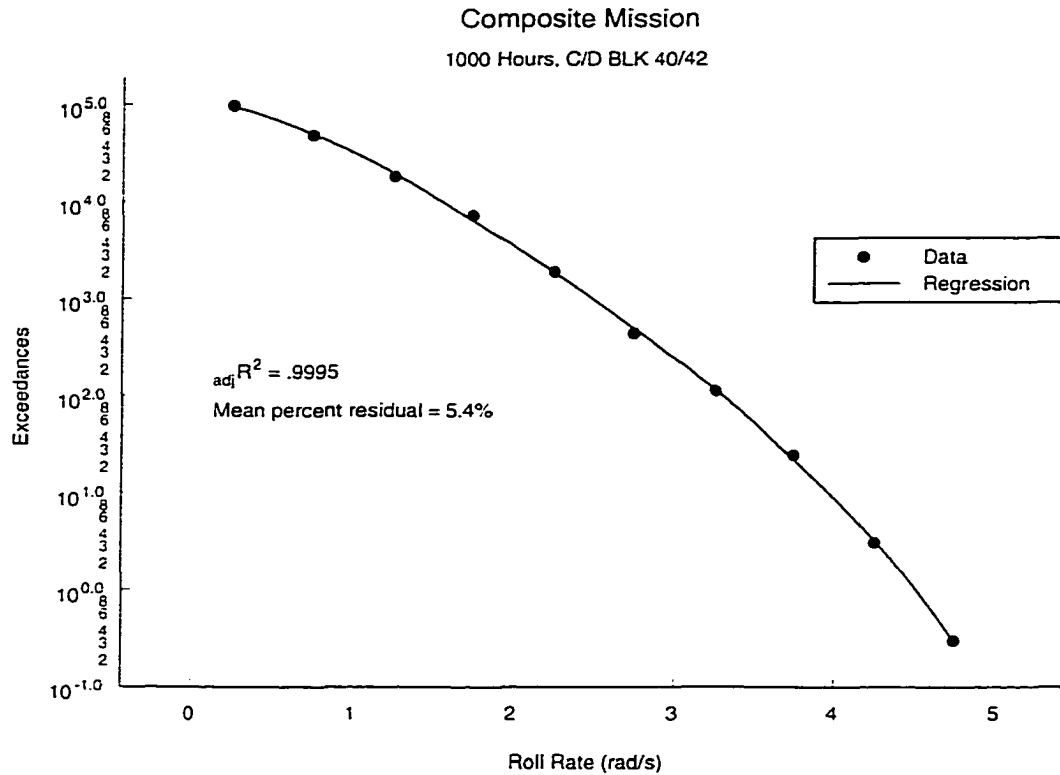


Figure 4-9 Roll Rate Exceedance Regression Analysis

The roll rate probability distribution function was computed from the best regression model represented by Eq. (4.28). Normalizing Eq. (4.28) with the maximum exceedance produced the probability distribution function in Eq. (4.29). The maximum roll rate exceedance was extrapolated to 0.0 rad/s in order to compute the probability of 0.25 rad/s occurring. Extrapolation was necessary because roll rate is a continuous random variable, therefore probability must be defined over an interval of roll rate values encompassing 0.25 rad/s. Probabilities of occurrences for roll rate levels were

determined in Eq. (4.30) from the difference of distribution function values. Eq. (4.29). computed over intervals of $p \pm 0.25$ rad/s. Table 4-12 provides the probabilities of roll rate occurrences between 0.25 rad/s and 4.75 rad/s. These probabilities were computed by the *load_occurrence* program mentioned earlier in the discussion of normal load factor probability development.

$$R(p) = \frac{1.154 \times 10^5 \cdot e^{(-.4642p - 1.04p^2 + .2567p^3 - .02888p^4)}}{115400.0} \quad (4.29)$$

$$P(p - .25 < p < p + .25) = R(p - .25) - R(p + .25) \quad (4.30)$$

Table 4-12 Probability of Roll Rate Occurrences for the Composite Mission

Roll Rate (rad/s)	Predicted	R(p)	Probability	Roll Rate (rad/s)
0.00	115400.0	1.0000000		
0.25	96665.1	0.8376526	0.36986	0.25
0.50	72717.8	0.6301373		
0.75	50119.6	0.4343118	0.35109	0.75
1.00	32201.9	0.2790456		
1.25	19570.3	0.1695868	0.18039	1.25
1.50	11384.6	0.0986534		
1.75	6397.7	0.0554396	0.06836	1.75
2.00	3495.7	0.0302917		
2.25	1864.1	0.0161532	0.02188	2.25
2.50	971.1	0.0084154		
2.75	493.5	0.0042762	0.00631	2.75
3.00	243.5	0.0021102		
3.25	115.9	0.0010041	0.00165	3.25
3.50	52.7	0.0004562		
3.75	22.6	0.0001955	0.00038	3.75
4.00	9.0	0.0000778		
4.25	3.3	0.0000283	0.00007	4.25
4.50	1.1	0.0000092		
4.75	0.3	0.0000026	0.00001	4.75
5.00	0.1	0.0000006		

4.8.2 Roll Acceleration Probability Function

Three more regression analyses were performed on the roll acceleration exceedance data in Table 4-11. The 3rd order exponential-polynomial model in Eq. (4.31) and Figure 4-10 provided a mean percent residual of 7.1% and $\text{adj}R^2$ of 0.9992.

$$Exc = 1.298 \times 10^5 \cdot e^{(0.0185 \dot{p} - 0.1555 \dot{p}^2 + 0.006318 \dot{p}^3)} \quad 1.0 \leq \dot{p} \leq 15.0 \quad (4.31)$$

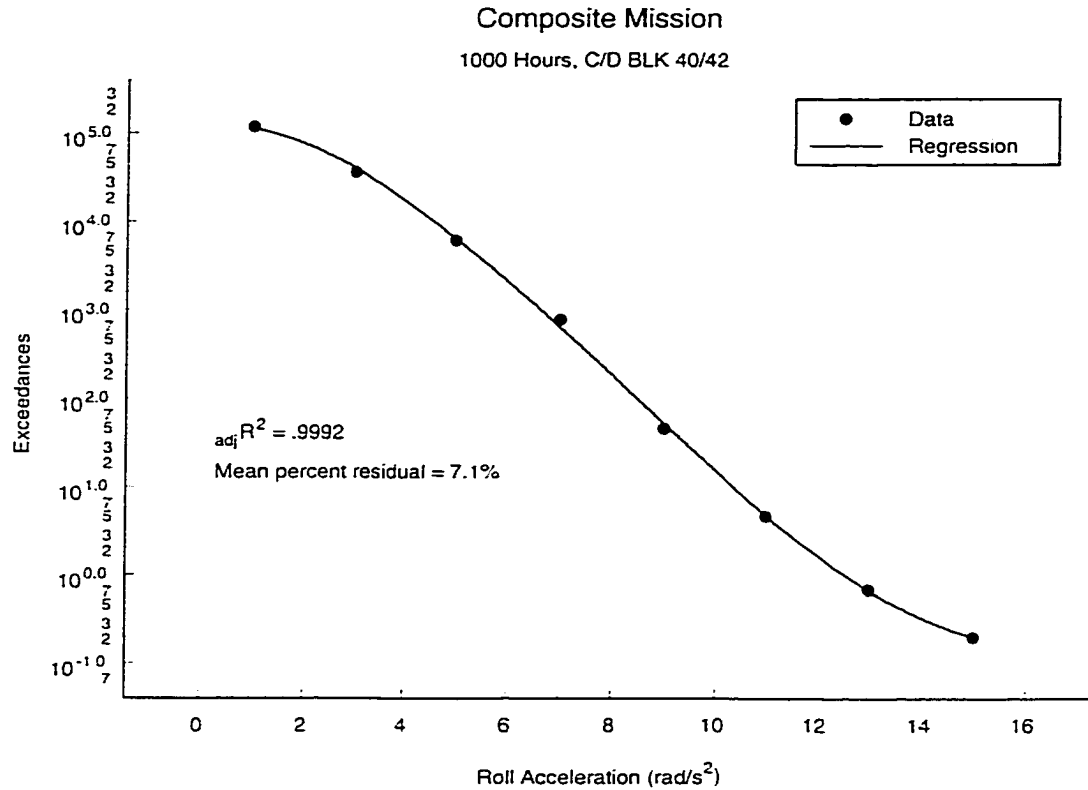


Figure 4-10 Roll Acceleration Exceedance Regression Analysis

Roll acceleration is a continuous random variable and the probability distribution function was constructed in a similar manner as before by normalizing the exceedance regression model above with the maximum exceedance. Probability of occurrence for each roll acceleration level in Table 4-11 was subsequently computed over an interval of $\dot{p} \pm 1.0 \text{ rad/s}^2$ using Eqs. (4.32) and (4.33). Therefore, extrapolation to 0.0 rad/s^2 was

needed to compute probability of occurrence at 1.0 rad/s². Extrapolation of Eq. (4.31) to a roll acceleration of 0.0 rad/s² produced unexpected results as indicated in Table 4-13 below. The probability of occurrence of 1.0 rad/s² was smaller than the probability at 3.0 rad/s². This was caused by the inability of the exponential-polynomial model to predict values outside its original data range.

$$R(\dot{p}) = \frac{1.298 \times 10^5 \cdot e^{(0.0185 \dot{p} - 0.1555 \dot{p}^2 + 0.006318 \dot{p}^3)}}{129,800.0} \quad (4.32)$$

$$P(\dot{p} - 1.0 < \dot{p} < \dot{p} + 1.0) = R(\dot{p} - 1.0) - R(\dot{p} + 1.0) \quad (4.33)$$

Table 4-13 Original Probability of Roll Acceleration Occurrences

Roll Acceleration (rad/s ²)	Predicted	R(\dot{p})	Probability
0.0	129800.0	1.0000000	
1.0	113899.1	0.8774968	0.41401
2.0	76061.2	0.5859880	
3.0	40148.3	0.3093092	0.45195
4.0	17397.9	0.1340358	
5.0	6428.5	0.0495264	0.11783
6.0	2103.7	0.0162070	
7.0	633.2	0.0048785	0.01480
8.0	182.1	0.0014029	
9.0	52.0	0.0004003	0.00129
10.0	15.3	0.0001177	
11.0	4.8	0.0000371	0.00010
12.0	1.7	0.0000130	
13.0	0.68	0.0000052	0.00001
14.0	0.33	0.0000025	
15.0	0.20	0.0000015	0.00000
16.0	0.16	0.0000012	

This problem was solved by fitting a five-point parabola through the exceedance data in Figure 4-11 for roll accelerations of 1.0 to 5.0 rad/s². The resulting model represented by Eq. (4.34) was used to extrapolate the exceedance of 166,318 to 0.0 rad/s² roll acceleration. The roll acceleration exceedance data with extrapolation to 0.0 rad/s²

$$Exc = 4778.5\dot{p}^2 - 56032\dot{p} + 166318 \quad (4.34)$$

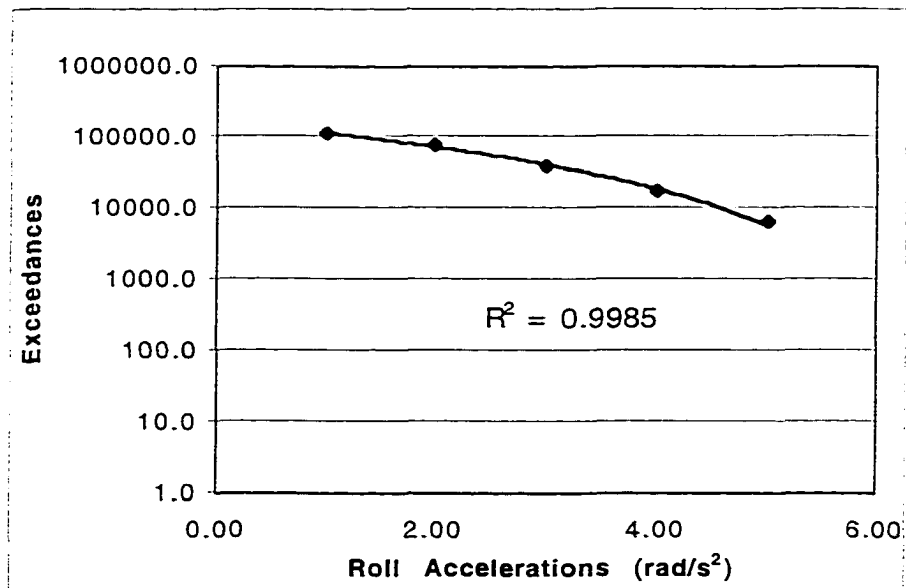


Figure 4-11 Regression Analysis of Roll Acceleration Data with a Five-Point Parabola

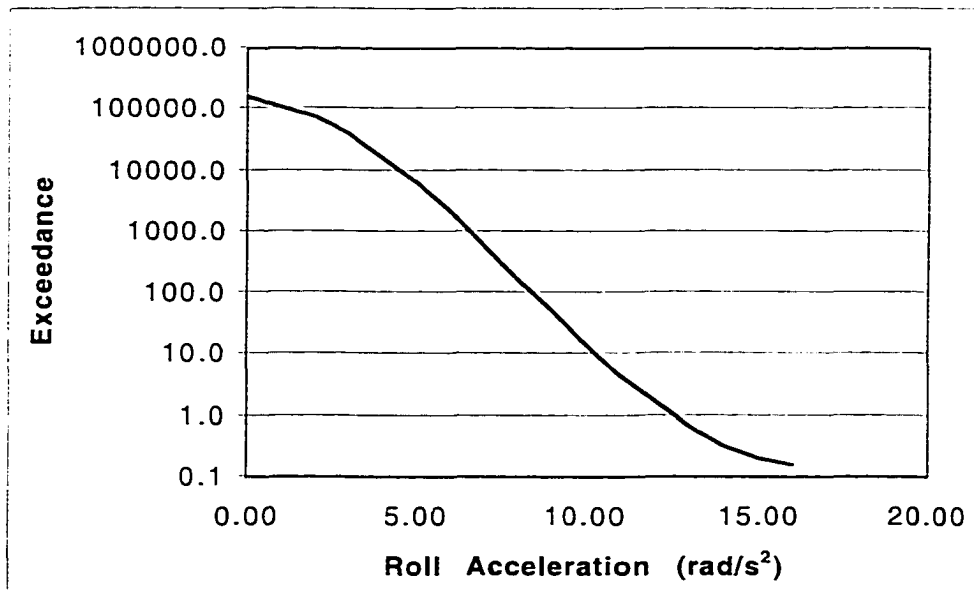


Figure 4-12 Corrected Roll Acceleration Exceedance Data with Extrapolation to 0.0 rad/s²

are shown in Figure 4-12. The exceedance extrapolated to 0.0 rad/s² was used to normalize Eq. (4.31) to produce the new probability distribution function in Eq. (4.35). The probability equation (4.33) was still used to compute the probabilities of occurrences for roll accelerations of 1.0 rad/s² to 16.0 rad/s². The new probabilities of occurrences for the roll acceleration levels are listed in Table 4-14. The probability of occurrence for 1.0 rad/s² was now higher than the probability of occurrence at 3.0 rad/s², as expected.

$$R(\dot{p}) = \frac{1.298 \times 10^5 \cdot e^{(0.0185 \dot{p} - 0.1555 \dot{p}^2 + 0.006318 \dot{p}^3)}}{166,318.0} \quad (4.35)$$

Table 4-14 Corrected Probabilities of Roll Acceleration Occurrences

Roll Acceleration (rad/s ²)	Exceedances	R(\dot{p})	Probability
0.0	166318.0	1.0000000	
1.0	113899.1	0.6848271	0.54268
2.0	76061.2	0.4573242	
3.0	40148.3	0.2413950	0.35272
4.0	17397.9	0.1046060	
5.0	6428.5	0.0386520	0.09196
6.0	2103.7	0.0126485	
7.0	633.2	0.0038073	0.01155
8.0	182.1	0.0010949	
9.0	52.0	0.0003124	0.00100
10.0	15.3	0.0000919	
11.0	4.8	0.0000289	0.00008
12.0	1.7	0.0000101	
13.0	0.68	0.0000041	0.00001
14.0	0.33	0.0000020	
15.0	0.20	0.0000012	0.00000
16.0	0.16	0.0000009	

4.9 Conclusion

The feasibility of generating probabilistic models of fatigue spectra data has been demonstrated using an exponential-polynomial regression analysis of the load factor, roll

rate, and roll acceleration exceedance data. The adjusted coefficient of determination is not always a reliable or sensitive indicator of correlation between a regression model and the exceedance data. A successful approach was found by plotting the nonlinear exceedance data on semi-log scale and decreasing the mean percent residual with higher order polynomials. The exponential-polynomial equation modeled the ascent, cruise, formation, air-to-air, air-to-ground, loiter, instrument and navigation, advanced transition, and descent flight segments despite the significant differences in their behavior. This equation was also used to model the roll rate and acceleration flight data for a fighter aircraft composite mission. A parabolic regression analysis was used in the air-to-air segment load factor model and roll acceleration model development because the exponential-polynomial equations could not properly extrapolate the maximum exceedance values in these two cases. Other than the maximum exceedances, the remaining air-to-air load factor and roll acceleration exceedance data were modeled with exponential-polynomial equations. These exponential-polynomial equations formed the core of probability functions that uniquely characterized the fatigue environment.

CHAPTER V

FLIGHT-BY-FLIGHT LOAD HISTORY DEVELOPMENT

5.1 Introduction

The analyses and tests of the static and dynamic structural loads, which are expected to occur over the life of an aircraft, require that they be ordered in a definite sequence. The sequence describes the peaks and valleys at each load level; from this, the magnitude of each load cycle is determined. The life time sequence of loads is developed on a flight-by-flight basis and is described in five steps:

1. Order the aircraft flights by mission in a representative life history.
2. Identify the mission segments within each mission, and define their flight conditions such as gross weight, airspeed, and altitude.
3. Determine the number of maneuver and gust load cycles at each load level in each mission segment.
4. Order the maneuver and gust load cycles within each mission segment.
5. Place the load cycles from all other sources within each mission segment.

5.2 Ordering the Mission Mix

The mission mix refers to the number of each mission type included in the sequence. The mission mix is defined in the specified design criteria. It usually specifies either the number of flights or the number of flight hours in the service life along with the percent mix by mission type. The example used in this research was a typical fighter aircraft with a 5,000 hour design life and three basic mission types, air-to-air, air-to-

ground, and training, distributed according to Table 5-1. The details of this step follow.

Table 5-1 Mission Type Distribution

Mission Type	Distribution
Air-To-Air (AA)	70%
Air-To-Ground (AG)	20%
Training	10%

Significant variations of air-to-air and air-to-ground missions are possible and, therefore, require a unique mission name to differentiate them. These are designated below by I, II, and III.

Table 5-2 Mission Distribution Variation and Duration

Mission Definition	Distribution	Mission Duration(hours)
Air-to-Air I	40% of AA	1.5
Air-to-Air II	40% of AA	1.0
Air-to-Air III	20% of AA	0.8
Air-to-Ground I	60% of AG	1.2
Air-to-Ground II	40% of AG	1.0
Training	100%	2.0

The next step is the computation of the mission utilization rates, the total mission flight hours, and the total number of flights for each mission type as shown in Table 5-3. The number of flights is determined by dividing the total mission flight hours by the mission duration. The numbers of flights are rounded off or up to a number divisible by 10 to produce whole flights in the reduced hour block described below.

The lifetime mission sequence should be based on an observed sequence of similar missions for the same type of aircraft. This method is based on the observation that aircraft flying assignments usually follow specific groupings of missions as various flying skills are being taught or from combat situations. Because complete life mission sequences are not available for current or new aircraft, a shortened block of missions,

approximating 10% of the original design life, will be used. This 500-hour block of missions in Table 5-4 will be repeated 10 times to complete the 5,000 hour lifetime requirement.

Table 5-3 Mission Utilization Rates, Total Flight Hours, and Number of Flights

Type	Distribution	Utilization Rate	Mission hours	No. of Flights
AA: 70%	AA I 40%	$70 \times .4 = 28\%$	1,400	$933 \approx 930$
	AA II 40%	$70 \times .4 = 28\%$	1,400	1,400
	AA III 20%	$70 \times .2 = 14\%$	700	$875 \approx 880$
AG: 20%	AG I 60%	$20 \times .6 = 12\%$	600	500
	AG II 40%	$20 \times .4 = 8\%$	400	400
Training: 10%	100%	10%	500	250
				Total = 4,360

Table 5-4 Block Definition for 500 Flight Hours

Mission	No. of Flights	Hours	Subtotal (hrs)
T	1	2.0	
AA I	9	13.5	
AA II	10	10.0	
AA III	5	4.0	
(repeat 10 times)			295
T	2	4.0	
AG I	10	12.0	
AG II	8	8.0	
(repeat 5 times)			120
T	2	4.0	
AA I	3	4.5	
AA II	40	40.0	
AA III	38	30.4	
T	3	6.0	84.9
Total = 436 flights			Total = 499.9 hr

5.3 Mission Segment Identification

Each mission is divided into segments to simplify loading analysis. The segment descriptions and the segment sequences are obtained from specified mission profiles.

The same segment sequence is used each time a particular mission occurs in the 500-hour block. The segment sequences for the three basic mission types are given in Table 5-5 below. The segments consist of simultaneously occurring Mach numbers, altitudes, gross weights, configurations, and associated times for each mission. These data sets are called flight conditions or "points-in-the-sky". These flight conditions are chosen to give representative loading conditions for each segment and to limit the number of load calculations to a reasonable number. If any parameter such as Mach number, altitude, or gross weight varies over a large range within a segment, then the segment is divided to provide a better representation of the loading condition.

Table 5-5 Segment Identification for the Air-to-Air, Air-to-Ground, and Training Missions

Air-to-Air	Air-to-Ground	Training
Ascent	Ascent 1	Ascent 1
Formation 1	Cruise 1	Cruise
Air-to-Air	Air-to-Ground	Instrument/navigation 1
Formation 2	Ascent 2	Ascent 2
Cruise	Cruise 2	Loiter
Descent	Descent	Instrument/navigation 2
-	-	Descent

The gross weight time history for each mission type is replaced with discrete weights to simplify calculations. Payload inventory data are provided in Table 5-6, Table 5-8, and Table 5-10 to help define these discrete gross weights. The external stores listed in these tables are placed at wing stations defined in Figure 5-1. Weight values are selected to represent changing configurations and fuel use. The weight and configuration values in Table 5-7, Table 5-9, and Table 5-11 are use to compute the aircraft inertial properties.

Table 5-6 Air-To-Air Mission Payload Inventory

Item	Payload Item	Wing Station	Weight (lb)
A	Two AIM-9 missiles w/launchers	1, 9	513.6
B	Max internal fuel (1,072 gl)	-	6,864.0
C	Centerline fuel (172.7 gl)	5	1,105.4
D	Pilot	-	250.0
		Total	8,733

Table 5-7 Air-To-Air Mission Gross Weight and Configuration History

Gross Weight (lb)	Configuration/Fuel	External Stores
23,300	Dry wing, Fus 100%	A,C
20,000	Dry wing, Fus 59%	A,C
18,000	Dry wing, Fus 33%	A,C
16,000	Dry wing, Fus 8%	A,C

Table 5-8 Air-To-Ground Mission Payload Inventory

Item	Payload Item	Wing Station	Weight (lb)
A	Two AIM-9 missiles w/launchers	1, 9	514.0
B	Max internal fuel (1,072 gl)	-	6,864.0
C	Two under wing tanks (740 gl)	6, 4	4,736.0
D	Six 500 lb MK82 bombs	7, 3	4,869.0
E	AN/ALQ-131 ECM POD	5	2,200.0
F	Two AGM-65 Mavericks	8, 2	1,400.0
G	Pilot	-	250.0
		Total	20,833.0

Table 5-9 Air-To-Ground Mission Gross Weight and Configuration History

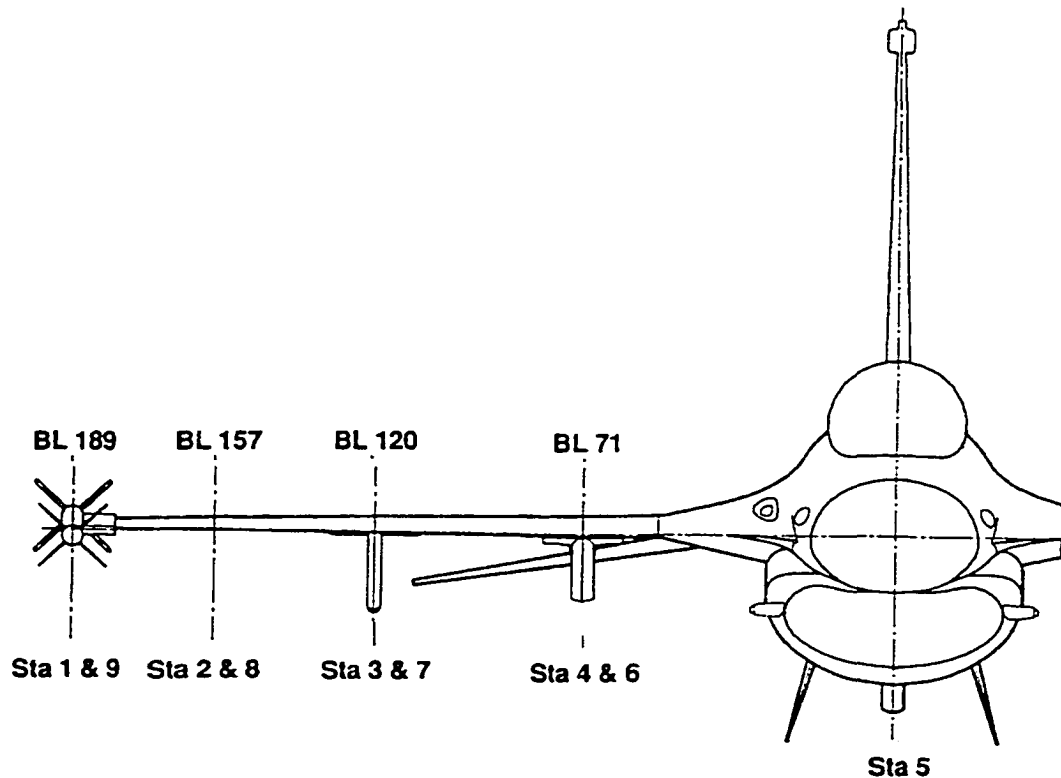
Gross Weight (lb)	Configuration/Fuel	External Stores
35,400	Dry wing, Fus 100%	A,C,D,E,F
32,000	Dry wing, Fus 70%	A,C,D,E,F
20,000	Dry wing, Fus 21%	A,C,E
18,000	Dry wing, Fus 4%	A,C,E

Table 5-10 Training Mission Payload Inventory

Item	Payload Item	Wing Station	Weight (lb)
A	Two AIM-9 missiles w/launchers	1,9	514.0
B	Max internal fuel (1,072 gl)	-	6,864.0
C	Two under wing tanks (740 gl)	6, 4	4,736.0
D	Centerline external fuel (300 gl)	5	1,920.0
E	LANTIRN(FLIR) navigation and targeting pods(two)	3,7	1,149.0
F	Pilot	-	250.0
		Total	15,433.0

Table 5-11 Training Mission Gross Weight and Configuration History

Gross Weight (lb)	Configuration/Fuel	External Stores
30,000	Dry wing, Fus 100%	A,C,D,E
25,000	Dry wing, Fus 63%	A,C,D,E
20,000	Dry wing, Fus 26%	A,C,D,E
18,000	Dry wing, Fus 11%	A,C,D,E

**Figure 5-1 Wing Station Identification**

The mission profiles and flight conditions used in this research follow in Figure 5-2 through Figure 5-4 and Table 5-12 through Table 5-17. The time duration of each segment in a mission is obtained from the mission profile. The total service lifetime (hours/life) for each segment is computed by multiplying the number of flights throughout the 5,000 hour service life with the segment time. This total service lifetime for a segment is used to determine the number of load factor occurrences described in the next section. For example, the total service lifetime for the ascent segment in the air-to-air mission is computed using Eq. (5.1).

$$\text{Hours/life} = 930 \text{ flights} \times 10 \text{ min/mission} \times \frac{1}{60} = 155.0 \text{ hours} \quad (5.1)$$

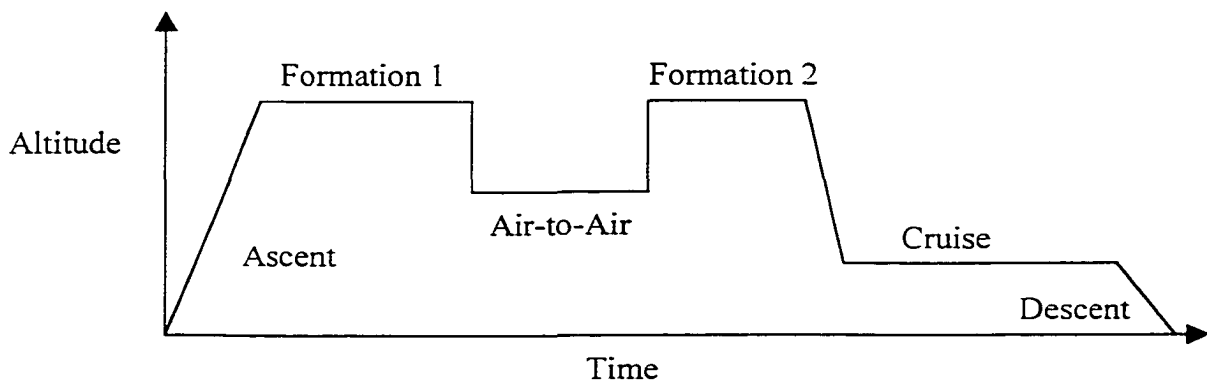


Figure 5-2 Air-To-Air Mission General Profile

Table 5-12 Air-To-Air Mission I Flight Conditions

AA I (1.5hr)					
Segment	GW (lb)	Mach-Alt (kft)	Time(min)	Hours/ Life	No. of Flights
Ascent	30,000	.7 - 10	10	155.0	930
Formation 1	30,000	1.2 - 30	25	387.5	930
Air-to-Air	25,000	.9 - 20	10	155.0	930
Formation 2	25,000	1.2 - 30	10	155.0	930
Cruise	20,000	.7 - 10	25	387.5	930
Descent	20,000	.3 - 0	10	155.0	930
			Total = 90	Total = 1,395	

Table 5-13 Air-To-Air Mission II Flight Conditions

AA II (1.0hr)					
Segment	GW (lb)	Mach-Alt (kft)	Time(min)	Hours/ Life	No. of Flights
Ascent	30,000	.7 - 10	10	233.333	1400
Formation 1	30,000	1.2 - 30	15	350.000	1400
Air-to-Air	25,000	.9 - 20	5	116.667	1400
Formation 2	25,000	1.2 - 30	15	350.000	1400
Cruise	20,000	.7 - 10	10	233.333	1400
Descent	20,000	.3 - 0	5	116.667	1400
			Total = 60	Total = 1.400	

Table 5-14 Air-To-Air Mission III Flight Conditions

AA III (0.8hr)					
Segment	GW (lb)	Mach-Alt (kft)	Time(min)	Hours/Life	No. of Flights
Ascent	30,000	.7 - 10	10	146.667	880
Formation 1	30,000	1.2 - 30	15	220.000	880
Air-to-Air	25,000	.9 - 20	5	73.333	880
Formation 2	25,000	1.2 - 30	8	117.333	880
Cruise	20,000	.7 - 10	5	73.333	880
Descent	20,000	.3 - 0	5	73.333	880
			Total = 48	Total = 704.0	

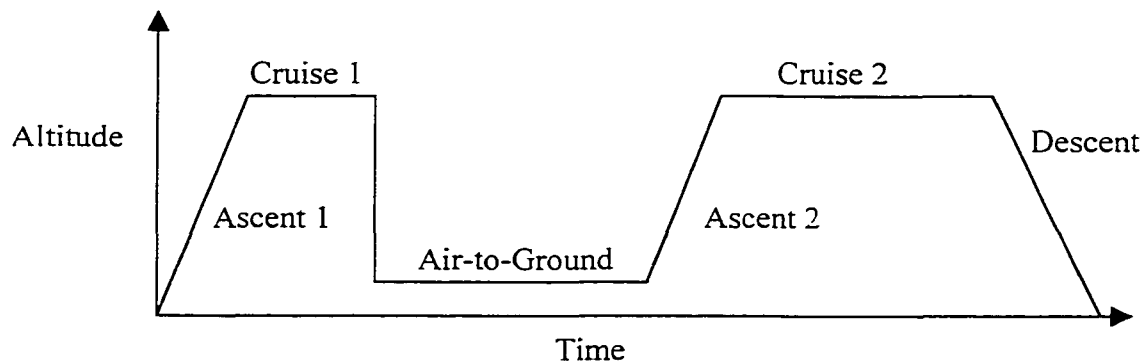
**Figure 5-3 Air-To-Ground Mission General Profile**

Table 5-15 Air-To-Ground Mission I Flight Conditions

AG I (1.2hr)					
Segment	GW (lb)	Mach-Alt (kft)	Time(min)	Hours/Life	No. of Flights
Ascent 1	35,000	.7 - 10	5	41.667	500
Cruise 1	35,000	1.2 - 30	10	83.333	500
Air-Ground	30,000	.8 - 1	25	208.330	500
Ascent 2	20,000	.7 - 20	5	41.667	500
Cruise 2	20,000	1.2 - 20	14	116.667	500
Descent	20,000	.3 - 0	13	108.333	500
			Total = 72	Total = 600.0	

Table 5-16 Air-To-Ground Mission II Flight Conditions

AG II (1.0hr)					
Segment	GW (lb)	Mach-Alt (kft)	Time(min)	Hours/Life	No. of Flights
Ascent 1	35,000	.7 - 10	5	33.333	400
Cruise 1	35,000	1.2 - 30	10	66.667	400
Air-Ground	30,000	.8 - 1	25	166.667	400
Ascent 2	20,000	.7 - 20	5	33.333	400
Cruise 2	20,000	1.2 - 20	10	66.667	400
Descent	20,000	.3 - 0	5	33.333	400
			Total = 60	Total = 600.0	

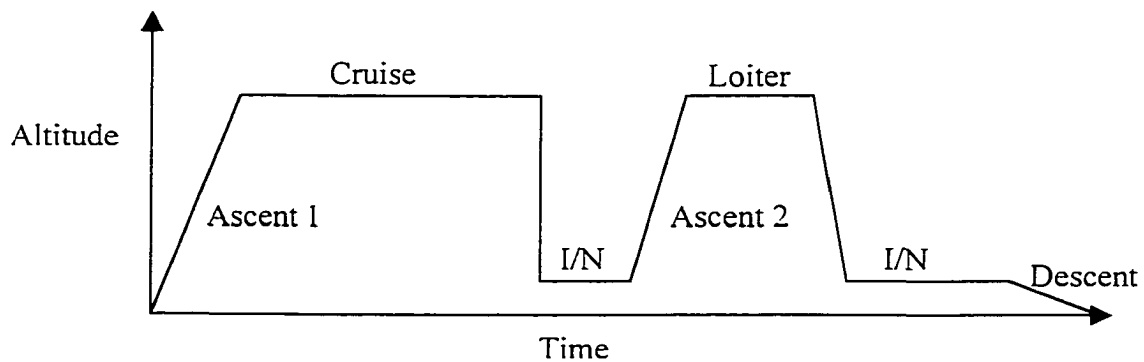
**Figure 5-4 Training Mission Profile**

Table 5-17 Training Mission Flight Conditions

T (2.0 hr)					
Segment	GW (lb)	Mach-Alt (kft)	Time(min)	Hours/Life	No. of Flights
Ascent 1	35,000	.8 - 10	5	20.833	250
Cruise	35,000	.7 - 20	50	208.333	250
Instrument/ Navigation (I/N) 1	30,000	.6 - 2	12	50.000	250
Ascent 2	25,000	.7 - 10	5	20.833	250
Loiter	25,000	.6 - 20	12	50.000	250
Instrument/ Navigation (I/N) 2	20,000	.6 - 2	20	83.333	250
Descent	20,000	.3 - 0	16	66.667	250
			Total = 120	Total = 500.0	

5.4 Number of Maneuver Load Cycles Computation

The calculation of the number of maneuver load cycles in each mission segment is based on the frequency of the occurrence of the normal load factor n_z . The occurrence of load levels was given by a regression analysis curve of the normal load factor exceedance spectrum for each mission segment as determined in Chapter 4.0. The load factor occurrences were prorated among four maneuver types: the steady-symmetric (steady), abrupt-symmetric (abrupt), right or left steady-asymmetric (Rasyms or Lasyms), and right or left abrupt-asymmetric (Rasyms or Lasyms) maneuvers according to Table 5-18. This was performed separately for positive and negative load factors using the FORTRAN program *load_occurrence.exe* developed in Chapter 4.0. No pitch acceleration frequency or exceedance data were available. The parameter range used in flight data recorders for pitch acceleration indicated that the maximum value permissible is 3.0 rad/s^2 . Therefore, all abrupt-symmetric occurrences were conservatively assigned a pitch acceleration of 3.0 rad/s^2 . The steady-asymmetric occurrences were individually

assigned roll rate values varying from 0.25 rad/s to 4.75 rad/s in proportion to their corresponding probabilities in Table 4-12. The abrupt-asymmetric occurrences were individually assigned roll acceleration values varying from 1.0 rad/s² to 15.0 rad/s² in proportion to their corresponding probabilities in Table 4-14. All asymmetric occurrences were divided in half to represent left and right rolling maneuvers. A program output summary for the air-to-air segment in the air-to-air mission I is given in Table 5-19. This program was executed 37 times for the 37 different segments in the 3 basic mission types.

Table 5-18 Maneuver Type Prorate Factors by Mission Segments

Type	Ascent	Cruise	Descent	Loiter	Air-ground	Air-Air	Formation	Inst-nav
Steady Symm	0.50	0.50	0.50	0.50	0.075	0.18	0.50	0.50
Abrupt Symm	0.05	0.05	0.05	0.05	0.675	0.02	0.05	0.05
Steady Asymm	0.40	0.40	0.40	0.40	0.200	0.70	0.40	0.40
Abrupt Asymm	0.05	0.05	0.05	0.05	0.050	0.10	0.05	0.05

The *load_occurrence.exe* program uses a random number generator to select occurrences, without replacement, into a fatigue load history. A randomly selected positive load factor occurrence is paired with a randomly selected negative load factor occurrence. All occurrences are used. The seed of the random number generator is based on the computer system clock. If the number of negative occurrences is less than that of positive occurrences (or vice-versa), 1.0g occurrences are added to the negative (or positive) load factor occurrences. This insures that both pools of positive and negative occurrences are equal prior to the random selection and sequencing process. The 1.0g

load factor occurrence represents constant speed, constant altitude level flight. Therefore, no maneuver type is assigned to 1.0g occurrences.

**Table 5-19 Lifetime Load Factor Occurrence Summary:
Air-To-Air Segment, Air-To-Air Mission I**

Nz	probability	occ	Symmetric Maneuver		Asymmetric Maneuver			
			steady-.180	abrupt-.020	steady-.700		abrupt-.100	
					Left	Right	Left	Right
-2.5	0.3536E-05	0.1	0	0	0	0	0	0
-2.0	0.2910E-04	0.8	0	0	0	0	0	0
-1.5	0.1520E-03	4.1	1	0	1	1	0	0
-1.0	0.4851E-03	13.1	2	0	5	5	1	1
-0.5	0.1637E-02	44.1	8	1	15	15	2	2
0.0	0.1495E-01	402.5	72	8	141	141	20	20
0.5	0.9827E+00	26463.1	4763	529	9262	9262	1323	1323
1.5	0.1628E+00	10299.7	1854	206	3605	3605	515	515
2.0	0.1505E+00	9523.6	1714	190	3333	3333	476	476
2.5	0.1447E+00	9154.6	1648	183	3204	3204	458	458
3.0	0.1303E+00	8245.6	1484	165	2886	2886	412	412
3.5	0.1108E+00	7008.2	1261	140	2453	2453	350	350
4.0	0.8926E-01	5646.4	1016	113	1976	1976	282	282
4.5	0.6838E-01	4326.0	779	87	1514	1514	216	216
5.0	0.4993E-01	3158.9	569	63	1106	1106	158	158
5.5	0.3481E-01	2202.0	396	44	771	771	110	110
6.0	0.2320E-01	1467.4	264	29	514	514	73	73
6.5	0.1479E-01	935.6	168	19	327	327	47	47
7.0	0.9030E-02	571.2	103	11	200	200	29	29
7.5	0.5283E-02	334.2	60	7	117	117	17	17
8.0	0.2963E-02	187.5	34	4	66	66	9	9
8.5	0.1594E-02	100.9	18	2	35	35	5	5
9.0	0.8229E-03	52.1	9	1	18	18	3	3
9.5	0.4077E-03	25.8	5	1	9	9	1	1
10.0	0.1939E-03	12.3	2	0	4	4	1	1
segment type: AAI_air-air								
total segment hours per A/C life = 155.000								
# of missions with segment = 930								
sum segment occurrences per A/C life = 90173								
sum segment cycles per A/C life = 63249								
number of cycles per segment = 68								
number of missions with extra cycle = 9								

The next step is to determine the number of occurrence cycles in each segment for each flight using Eq. (5.2). This equation takes the integer value of the total number of cycles in each segment divided by the number of flights in the life of the aircraft⁴⁸. The integer function is used because a fraction of a cycle cannot exist.

$$cycles_{segment} = \text{int}\left(\frac{cycles}{no. flights}\right) \quad (5.2)$$

However, it is important to account for all occurrence pairs or cycles in the load factor history. A flight segment has one extra cycle every time the accumulation of the fractions (*cycles/no. flights*) becomes one. The number of flights with one extra cycle (f_{1xc}) can be found with Eq. (5.3).

$$f_{1xc} = \text{cycles} - \text{int}\left(\frac{\text{cycles}}{\text{no. flights}}\right) \times \text{no. flights} \quad (5.3)$$

In the fighter example, the number of flights containing the air-to-air segment in air-to-air mission I was 930 and the total number of cycles in this segment was 63,249 according to Table 5-19. Thus, the number of cycles in the first air-to-air segment was 68. The cycles from the first flight involving this air-to-air segment are listed with their maneuver types, roll rates, and roll accelerations in Table 5-20. The number of flights with 69 cycles in the segment was 9. This process was repeated for other flight segments such as ascent, cruise, air-to-ground, instrument and navigation, loiter, and descent. The subsequent segment load factor histories can now be “stitched” together according to Table 5-5, to form a complete flight. This has to be done for every flight to form a flight-by-flight load spectrum.

The FORTRAN program *load_history.exe* read these segment load factor history files in accordance with the 500-hour block definition in Table 5-4 and sequenced the segment load factor cycles into a complete flight. This was done for all segments, and the resulting flights were ordered, according to this 500-hour block definition, into one sequential file written to the hard drive. This final file contained load factor cycles for 500 hours of flight time. The program listing for *load_history.exe* and the 500-hour block definition input file can be found in Appendix D. The load factor histories for the first flights of the air-to-air mission, the air-to-ground mission, and the training mission

are plotted in Figures 5-5 through 5-7, respectively. The next step in this research is to convert these load factors into stresses for a particular location in a structure using the ASTROS software. Once this is done, fatigue crack growth analysis can be performed.

Table 5-20 Air-To-Air Segment Load Factor History in the Air-To-Air Mission I

segment type: AAI_air-air				
Flight 1 No. cycles = 68				
cycle	load factor	maneuver type	p(rad/s)	pdot(rad/s2)
1	3.5	Rasym	0.75	0.00
	1.0	-----	0.00	0.00
2	2.0	Lasym	0.25	0.00
	0.5	Lasym	0.75	0.00
3	5.0	Lasym	0.25	0.00
	0.5	Rasym	0.00	1.00
4	1.5	steady	0.00	0.00
	0.5	Rasym	1.75	0.00
5	1.5	steady	0.00	0.00
	1.0	-----	0.00	0.00
6	4.5	Lasym	0.25	0.00
	1.0	-----	0.00	0.00
7	2.0	Lasym	0.25	0.00
	1.0	-----	0.00	0.00
8	4.0	Lasym	0.75	0.00
	0.5	Rasym	0.00	1.00
9	1.5	steady	0.00	0.00
	1.0	-----	0.00	0.00
10	4.5	Lasym	0.25	0.00
	0.5	Rasym	0.75	0.00
11	4.5	Rasym	0.25	0.00
	1.0	-----	0.00	0.00
12	4.5	Lasym	0.75	0.00
	0.5	Rasym	0.75	0.00
13	1.5	Lasym	0.25	0.00
	0.5	Lasym	2.25	0.00
14	2.5	Rasym	1.25	0.00
	1.0	-----	0.00	0.00
15	3.5	Rasym	0.25	0.00
	0.5	Rasym	1.75	0.00
16	5.0	steady	0.00	0.00
	1.0	-----	0.00	0.00
17	3.5	Lasym	0.75	0.00
	1.0	-----	0.00	0.00
18	2.0	Rasym	1.25	0.00
	1.0	-----	0.00	0.00
19	2.5	Rasym	0.75	0.00
	1.0	-----	0.00	0.00
20	5.0	steady	0.00	0.00
	0.5	Lasym	1.25	0.00
21	2.5	steady	0.00	0.00
	0.5	Rasym	0.75	0.00
22	2.5	steady	0.00	0.00
	1.0	-----	0.00	0.00
23	2.5	steady	0.00	0.00
	1.0	-----	0.00	0.00

24	4.5	Lasyns	1.25	0.00
	0.5	Lasyns	0.25	0.00
25	2.0	Lasyns	0.75	0.00
	1.0	-----	0.00	0.00
26	5.5	steady	0.00	0.00
	1.0	-----	0.00	0.00
27	1.5	Rasyns	1.25	0.00
	1.0	-----	0.00	0.00
28	4.0	Lasyns	0.75	0.00
	1.0	-----	0.00	0.00
29	2.0	Lasyna	0.00	1.00
	0.5	Rasyns	0.25	0.00
30	4.5	Rasyns	0.25	0.00
	1.0	-----	0.00	0.00
31	6.5	Lasyns	0.75	0.00
	0.5	Rasyns	0.25	0.00
32	1.5	steady	0.00	0.00
	1.0	-----	0.00	0.00
33	2.0	Lasyns	1.25	0.00
	1.0	-----	0.00	0.00
34	3.5	Rasyns	0.25	0.00
	1.0	-----	0.00	0.00
35	1.5	Lasyns	0.75	0.00
	1.0	-----	0.00	0.00
36	1.5	Lasyna	0.00	3.00
	1.0	-----	0.00	0.00
37	3.5	Lasyns	1.25	0.00
	1.0	-----	0.00	0.00
38	2.0	Rasyns	1.25	0.00
	0.5	Rasyns	0.75	0.00
39	3.0	Lasyna	0.00	3.00
	0.5	Lasyns	1.25	0.00
40	4.0	Rasyns	1.25	0.00
	0.5	Rasyns	0.25	0.00
41	5.0	Lasyna	0.00	1.00
	1.0	-----	0.00	0.00
42	3.0	steady	0.00	0.00
	1.0	-----	0.00	0.00
43	5.0	steady	0.00	0.00
	1.0	-----	0.00	0.00
44	1.5	steady	0.00	0.00
	1.0	-----	0.00	0.00
45	1.5	Rasyns	0.25	0.00
	0.5	Lasyns	0.25	0.00
46	5.0	steady	0.00	0.00
	0.5	Lasyns	0.25	0.00
47	1.5	Rasyns	0.25	0.00
	1.0	-----	0.00	0.00
48	2.0	Rasyns	0.25	0.00
	0.5	Lasyns	0.75	0.00
49	1.5	steady	0.00	0.00
	0.5	Rasyna	0.00	3.00
50	4.0	Lasyns	0.25	0.00
	1.0	-----	0.00	0.00
51	2.0	Rasyns	0.75	0.00
	1.0	-----	0.00	0.00
52	4.5	Rasyns	0.75	0.00
	0.5	Rasyns	0.25	0.00
53	4.0	Lasyns	0.75	0.00
	0.5	Lasyns	0.75	0.00

54	1.5	steady	0.00	0.00
	1.0	-----	0.00	0.00
55	2.0	Rasylms	0.25	0.00
	1.0	-----	0.00	0.00
56	1.5	Rasylms	0.75	0.00
	1.0	-----	0.00	0.00
57	2.0	Rasylms	0.75	0.00
	1.0	-----	0.00	0.00
58	2.0	Lasylms	1.25	0.00
	1.0	-----	0.00	0.00
59	3.5	Lasylms	0.25	0.00
	1.0	-----	0.00	0.00
60	2.5	Rasylms	2.25	0.00
	0.5	Lasylms	0.25	0.00
61	3.5	Rasylms	0.75	0.00
	0.5	steady	0.00	0.00
62	6.5	Lasylms	0.25	0.00
	0.5	steady	0.00	0.00
63	2.0	Lasylms	0.75	0.00
	1.0	-----	0.00	0.00
64	1.5	Lasylms	1.25	0.00
	1.0	-----	0.00	0.00
65	2.0	steady	0.00	0.00
	1.0	-----	0.00	0.00
66	3.0	Rasylms	0.25	0.00
	1.0	-----	0.00	0.00
67	2.0	steady	0.00	0.00
	0.5	Rasylms	0.00	1.00
68	3.0	Lasylms	0.00	1.00
	1.0	-----	0.00	0.00

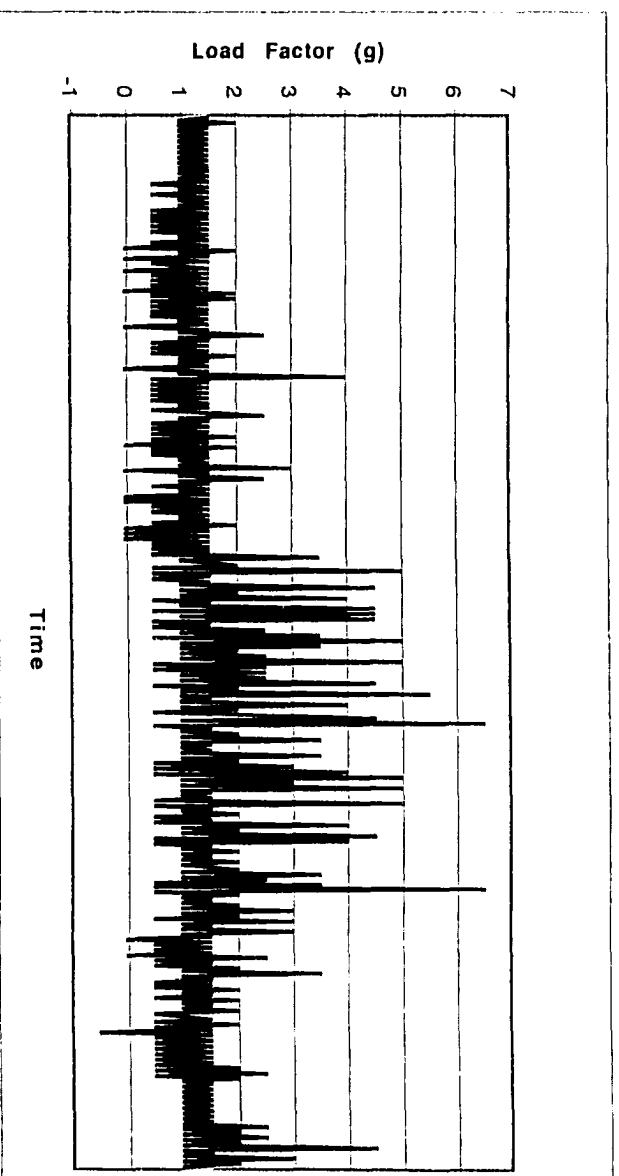


Figure 5-5 Load Factor History for the First Air-To-Air Mission I

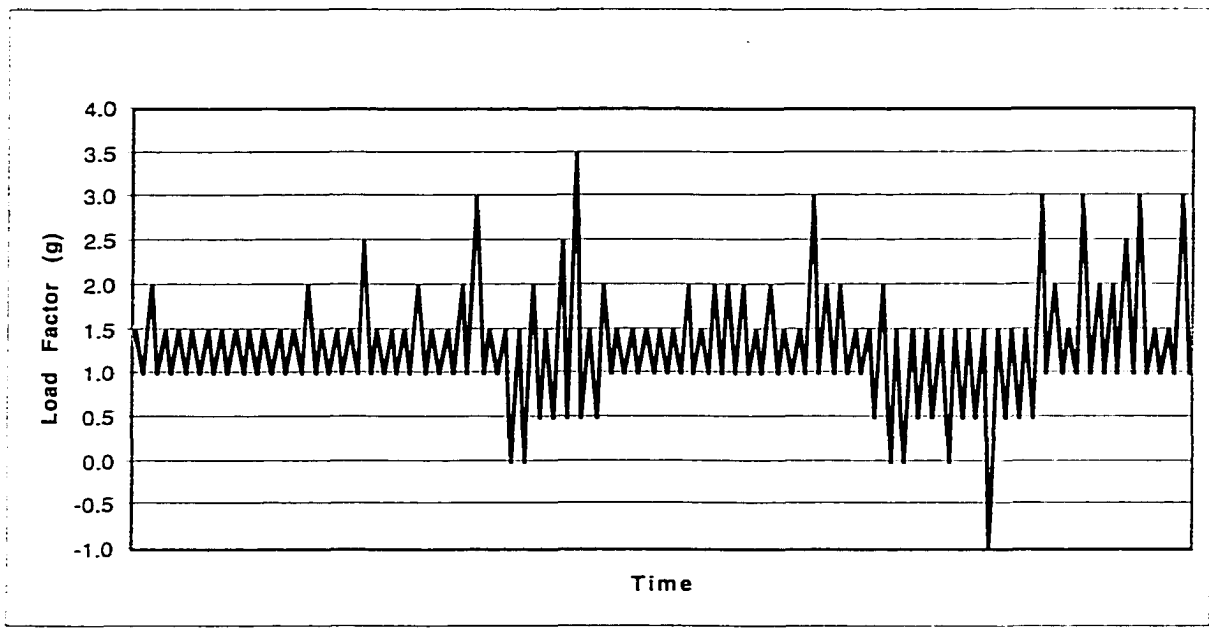


Figure 5-6 Load Factor History for the First Training Mission

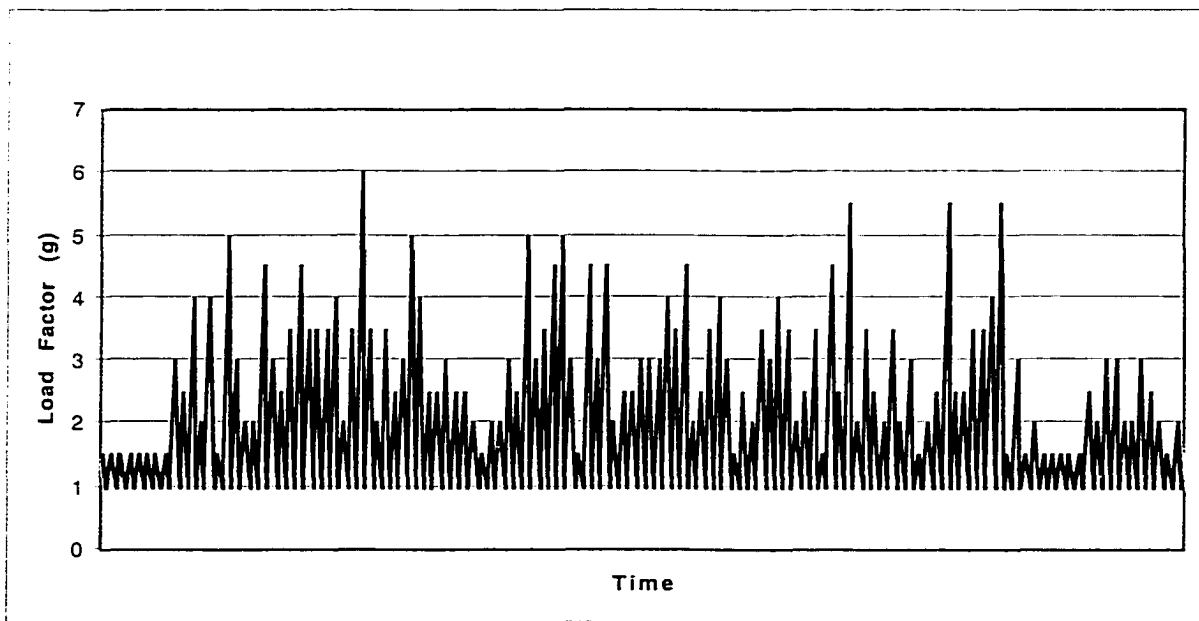


Figure 5-7 Load Factor History for the First Air-To-Ground Mission I

CHAPTER VI.

AEROELASTICITY ANALYSIS OF A FIGHTER AIRCRAFT

6.1 Introduction

The Automated Structural Optimization System (ASTROS), Version 20.1 by the McNeal-Schwendler Corporation, was used to perform aeroelastic analysis of a fighter/attack aircraft undergoing symmetric and asymmetric flight maneuvers. A bulk data deck of the aircraft finite element model was provided by the Air Force Research Laboratory AFRL/VASD, Wright-Patterson AFB. This model was based on the F-16 preliminary design model with changes made to dimensions, material properties, and skin thickness contours. A detailed description of the model and its early use can be found in the Air Force report, *An Aircraft Design Application Using ASTROS*⁴⁹.

The objective was to determine the lower wing skin stresses for a fighter aircraft under various flight conditions of altitude, airspeed, weight, normal load factor, pitch acceleration, roll rate, and roll acceleration. This information is used in Chapter 7 to convert the load factor history developed in Chapter 5 into a stress history.

6.2 Structural and Aerodynamic Models

The structural finite element model was supplied in a bulk data file, and the aerodynamic model was listed in a separate file. A flat fuselage aerodynamic model was used since preliminary design aerodynamic models typically use the simpler, flat paneling arrangement. Two serious problems were immediately encountered with this model. The finite element model and aerodynamic model, depicted in Figure 6-1, were

located in the left-hand plane (-y axis). ASTROS requires that both models be placed in the right-hand plane (+y axis). A short FORTRAN code was written to replace the y-coordinates of all grid points with the corresponding positive values. This moved the finite element and aerodynamic models to the right-hand plane. The y-coordinates of the local coordinate systems were changed accordingly. The original aerodynamic bulk data file contained a wing tip model of the AIM-9 Sidewinder air-to-air missile. Due to an I/O bug, this feature is no longer available in Version 20.1. Only a half aircraft finite element model in Figure 6-2 and an aerodynamic model in Figure 6-3 were used because of lateral symmetry about the fuselage centerline.

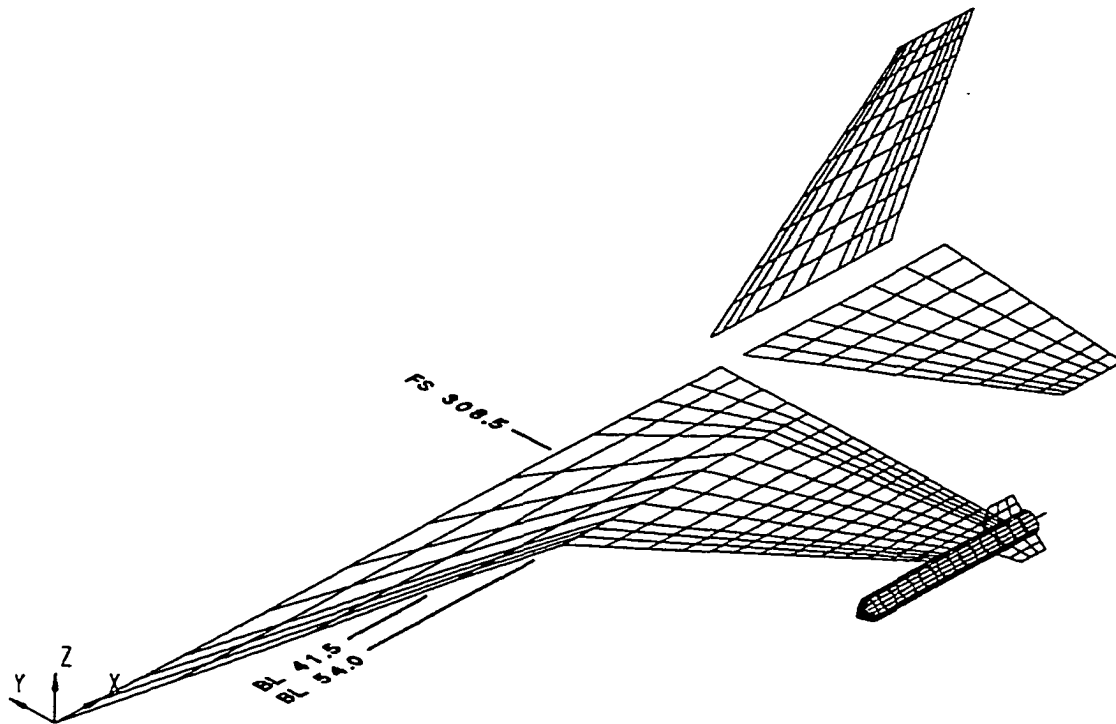


Figure 6-1 Left-Hand Side Aerodynamic Model with Sidewinder Missile

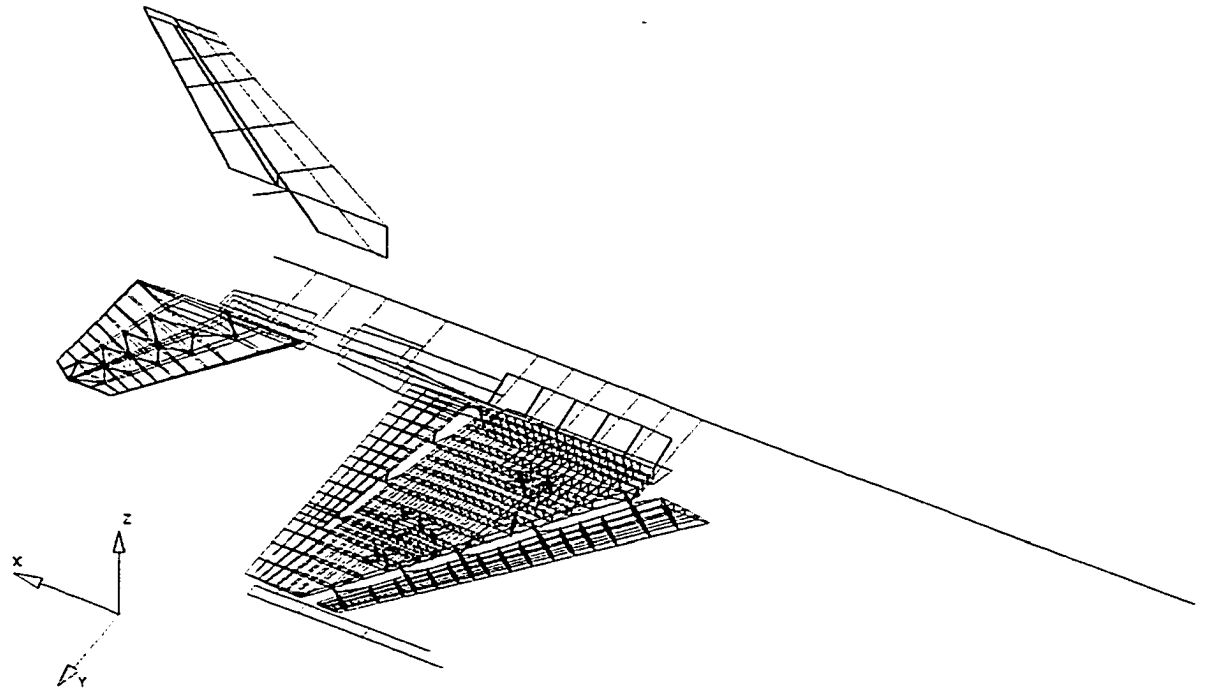


Figure 6-2 Finite Element Model of a Fighter Aircraft Structure

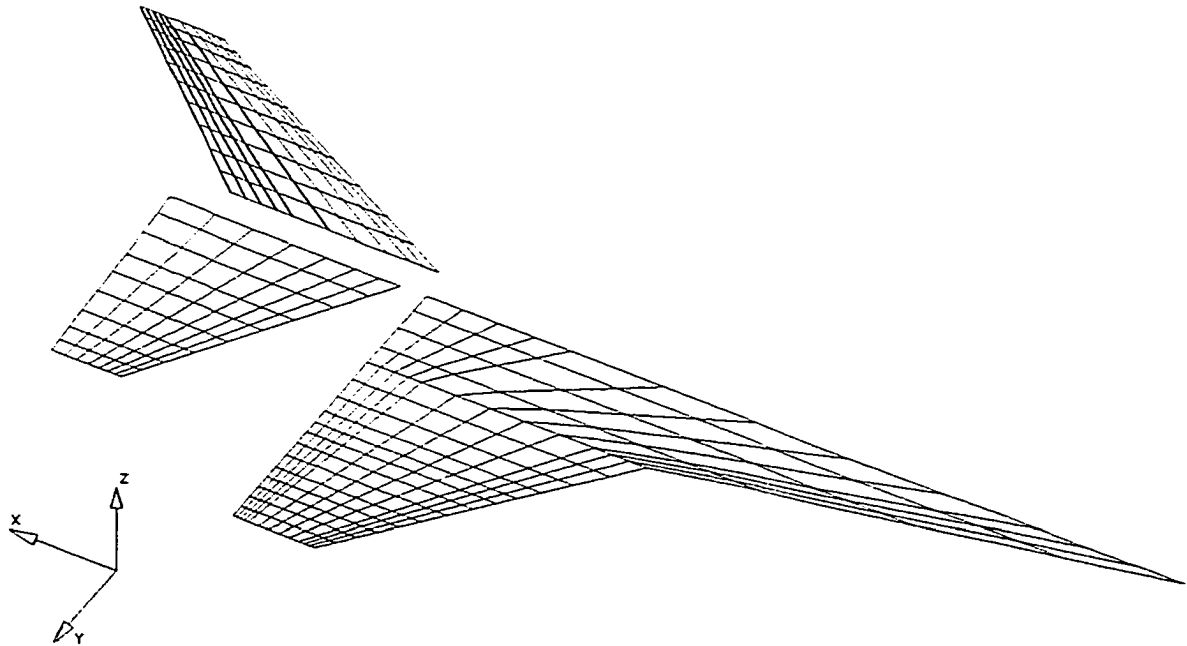


Figure 6-3 Aerodynamic Panel Model of a Fighter Aircraft

The finite element model consisted of 4,597 elements and 1,286 grid points. The aerodynamic model used 48 panels on the fuselage, 156 panels on the wing, 63 on the horizontal tail, and 100 on the fin, for a total of 367 panels. The horizontal tail was set at a negative dihedral of 6.5° defined from the fuselage centerline. Figure 6-4 shows a detailed view of the wing structure. The leading edge flap and flaperon are hinged structures and require spring elements to model the actuator stiffnesses to prevent analysis singularities.

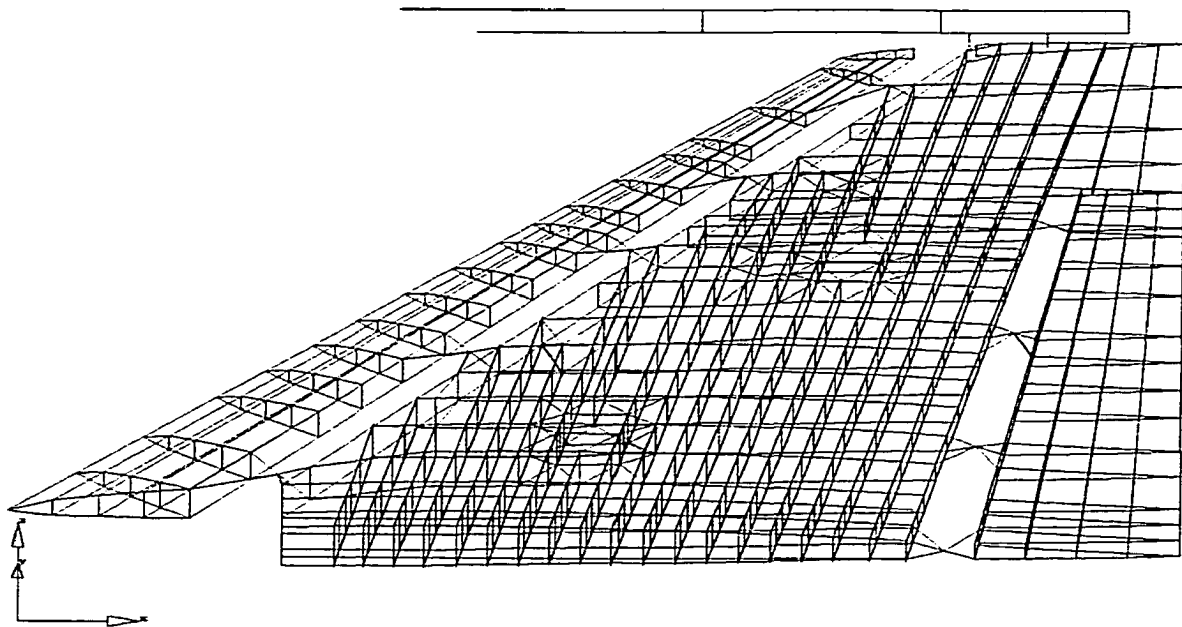


Figure 6-4 Wing Structure Finite Element Model

Details of the lower wing skin model are depicted in Figure 6-5. The wing skin element thicknesses varied from 0.17 to 0.72 inch. The loads produced by the aerodynamic model were automatically applied to the finite element model by ASTROS. Because the aerodynamic panels representing the fuselage were severely skewed, they were connected to the underlying structure via rigid load transfer. The panels representing the wing, horizontal tail, and fin in Figure 6-6 were coupled to the

underlying structure to account for flexibility effects.

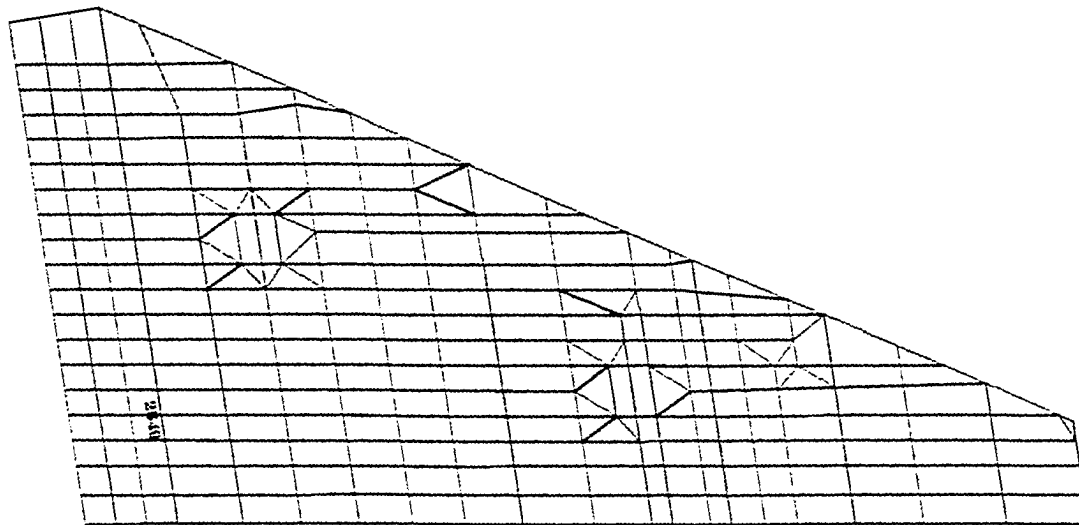


Figure 6-5 Lower Wing Skin Finite Element Model

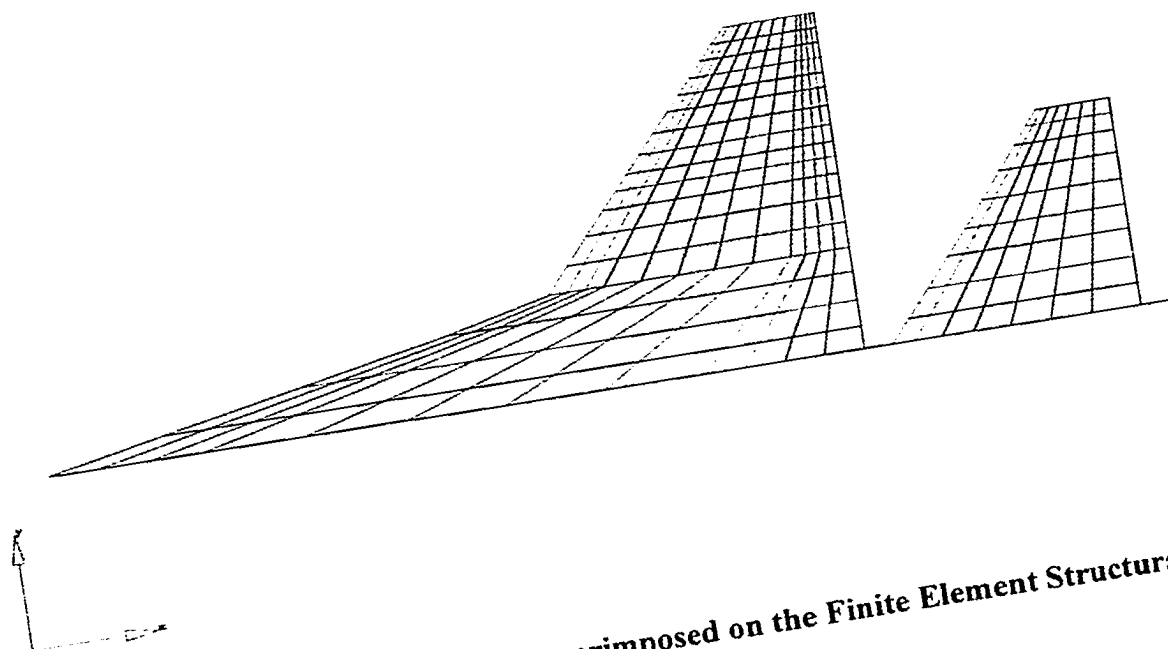


Figure 6-6 Aerodynamic Model Superimposed on the Finite Element Structural Model

6.3 Boundary Conditions

A model of one half of the aircraft structure is common and allows simulation of both symmetric and antisymmetric aircraft maneuvers. Symmetric loads, created in pull-up, push-over, or balanced turns, produce equivalent structural responses for the right and left-hand sides of the aircraft. Similarly, antisymmetric loads are created by pure roll maneuvers and, therefore, produce equal but opposite structural responses for the right and left-hand sides of the aircraft.

Boundary conditions were applied to the aircraft centerline to provide symmetric or antisymmetric behavior. The six primary degrees of freedom were defined as “1”, “2”, and “3” for the three translational degrees of freedom and “4”, “5”, and “6” for the three rotational degrees of freedom. For the symmetric boundary condition, all centerline “1246” nodal degrees of freedom were set to zero using single point constraint (SPC) bulk data cards. The “35” degrees of freedom of the node closest to the center of gravity were supported. This allowed rigid body modes, required for solving the desired trim, to be included in the steady aerodynamic solution (SAERO). For the antisymmetric boundary condition, the “4” degree of freedom was supported while all centerline “12356” nodal degrees of freedom were set to zero using SPC bulk data cards.

The load history development, discussed in the previous chapter, classified each load factor occurrence as either produced by a symmetric or asymmetric maneuver. A full aircraft model is needed to give a good response to asymmetric loads because an asymmetric boundary condition cannot be simulated with a half model. In this work, asymmetric maneuvers were simulated by the superposition of symmetric and antisymmetric load cases. Because the fuselage centerline nodal degrees of freedom

cannot be forced into asymmetric boundary conditions, the results here are somewhat inaccurate. However, only the results outboard of the wing carry-through structure were used in this research. Therefore, superposition should produce reasonable results, according to the principle of St. Venant, for asymmetric wing loading conditions.

6.4 Aeroelastic Model Verification

The aerodynamic stability derivatives were evaluated to insure proper load transfer from the aerodynamic model to the finite element model. Two flight maneuvers were analyzed with MSC-ASTROS to obtain these derivatives: a 9g symmetric pull-up and a roll with a 12.9° flaperon input. Both maneuvers were performed at Mach 0.95 and 10,000 ft. The rigid, splined, and flexible stability derivatives computed by MSC-ASTROS are listed in Table 6-1. The lift $C_{L\alpha}$ and pitching moment $C_{m\alpha}$ coefficients are produced during the symmetric maneuver simulation. The rolling moment coefficient due to roll rate $C_{l_{pb/2V}}$, the rolling moment coefficient due to yaw angle $C_{l_{\beta}}$, and the rolling moment coefficient due to flaperon angle $C_{l_{\delta\alpha}}$ are computed during the roll simulation with a 12.9° flaperon angle. An indication of proper load transfer between the aerodynamic model and the finite element model are similar values of rigid and splined stability derivatives. This did not happen with the coefficients $C_{l_{pb/2V}}$ and $C_{l_{\beta}}$. Through observation of the finite element model displacements for the roll maneuver in the post-processing program Altair Hypermesh®⁵⁰, the problem was quickly found. The fin had collapsed during the roll maneuver because of insufficient lateral stiffness in the bar elements used to model this structure. The lateral moment of inertia in the bar elements

was increased and the corresponding rigid and splined coefficients show very little differences in Table 6-2.

Table 6-1 Aerodynamic Stability Derivatives from Original Finite Element Model

Coefficients	Aeroelastic Results*		
	Mach 0.95 @ 10,000 ft		
	Rigid	Splined	Flexible
$C_{L\alpha}$.0861	.0861	.0910
$C_{m\alpha}$	-.0081	-.0082	-.0090
$C_{l_{pb/2V}}$ (rad)	-.3099	-.2890	-.3196
$C_{l\beta}$ (deg)	-.0011	.0004	.0004
$C_{l_{\delta a}}$ (deg)	.0034	.0036	.0024

* No wing tip missile

Table 6-2 Aerodynamic Stability Derivatives from Improved Finite Element Model

Coefficients	Aeroelastic Results*		
	Mach 0.95 @ 10,000 ft		
	Rigid	Splined	Flexible
$C_{L\alpha}$.0861	.0861	.0907
$C_{m\alpha}$	-.0081	-.0082	-.0090
$C_{l_{pb/2V}}$ (rad)	-.3099	-.3091	-.3240
$C_{l\beta}$ (deg)	-.0011	-.0011	.0004
$C_{l_{\delta a}}$ (deg)	.0034	.0034	.0025

* No wing tip missile

6.5 Aerodynamic Pressures

The rigid, flexible, and applied aerodynamic pressures for 3 panels from the aerodynamic model are tabulated in Table 6-3 for a 9g pull-up maneuver at Mach 0.95 and 10,000 ft. The applied pressures are the sums of the rigid and flexible pressures. The pressures in Table 6-3 represent the differences in air pressures between the upper and lower wing surfaces. The aerodynamic panel 692 is located at the leading edge wing tip

while panels 567 and 570 are centrally located in the wing.

Table 6-3 Net Aerodynamic Pressures for Select Aerodynamic Panels

Panel No.	Net Aerodynamic Pressure (psi)		
	Rigid	Flexible	Applied
567	2.00	-.384	1.617
570	.753	-.158	.595
692	40.2	11.55	51.75

6.6 Trim Results from MSC-ASTROS and ZONA ASTROS

Trim results for a symmetric 9g pull-up maneuver and an antisymmetric roll maneuver were computed for Mach 0.95 at 10,000 ft and are listed in Table 6-4. The roll maneuver was initiated with a 12.9° flaperon deflection. The structural deflection values in Table 6-4 were selected from the front spar at the wing tip. Results from the ZONA Inc. modified version of the ASTROS program, were included for comparison. The ZONA analysis used the same finite element model but used a slightly different aerodynamic model shown in Figure 6-7. ZONA ASTROS uses an in-house proprietary aerodynamic code instead of the standard USSAERO code found in MSC-ASTROS. In the ZONA model, the horizontal tail dihedral did not start at the fuselage centerline. This difference in the representation of the tail accounted for the discrepancy in the tail deflection angles between the MSC-ASTROS and ZONA ASTROS trim results. A wing deflection plot for the 9g pull-up was computed by MSC-ASTROS and is shown in Figure 6-8.

Table 6-4 Trim Results for MSC-ASTROS and ZONA ASTROS

Label	Trim Results	
	MSC	ZONA
Angle of attack (deg)	10.7	10.5
Tail deflection (deg)	-1.1	-.75
Roll rate (deg/s)	385	N/A
Deflection (in)	11.5	12.0

Figure 6-7 ZONA ASTROS Aerodynamic Panel Model

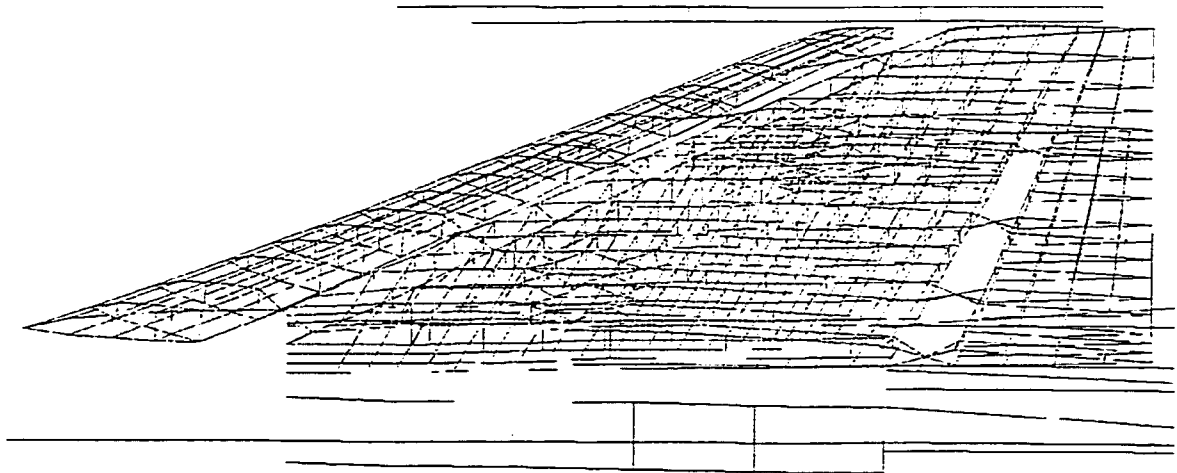


Figure 6-8 Wing Deflection for a 9g Pull-up at Mach 0.95 and 10,000 ft

6.7 Segment Stress/Load Ratio Analyses

The structural and aerodynamic models were analyzed with MSC-ASTROS for four flight maneuver types: symmetric steady state, symmetric abrupt, asymmetric steady state, and asymmetric abrupt. The structural model provided maximum (or minimum for negative n_z) principal stresses for element 2549 for the 4 flight maneuver types. Element 2549 is a QUAD4 element in the lower wing skin in Figure 6-5 and was chosen because of its proximity to the root. Wing root panels are often the source of fatigue cracking and, therefore, are the focus of a damage tolerance analysis. MSC-ASTROS provided these principal stresses for unit input values of normal load factor, pitch acceleration, roll rate, and roll acceleration for each mission segment. Only unit input values for these parameters were needed because the structural and aerodynamic analyses were linear. Multiple MSC-ASTROS analyses were performed within each of the three mission types because airspeed, altitude, and weight varied in each segment. The principal stresses from the finite element structural model were used as segment stress/load ratios. Segment stress/load ratios are used in the fatigue stress history development discussed in the next chapter. The element 2549 stress/load ratios for the air-to-air, air-to-ground, and training missions are plotted in Figures 6-9, 6-10, and 6-11 for the 4 maneuver types.

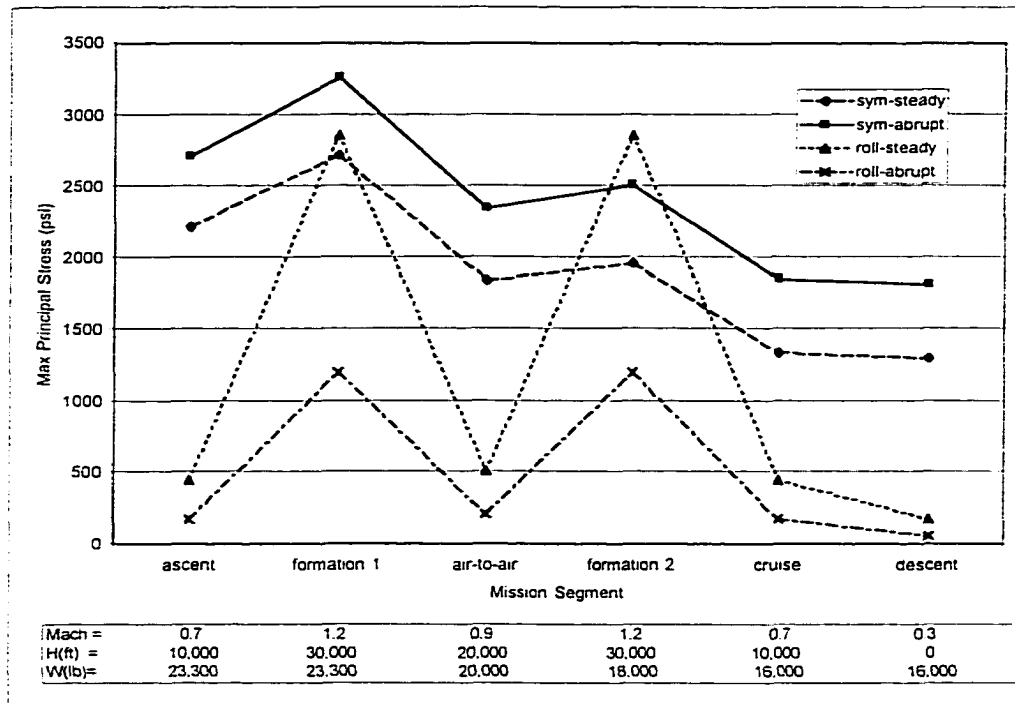


Figure 6-9 Air-to-Air Mission Stress/Load Ratios

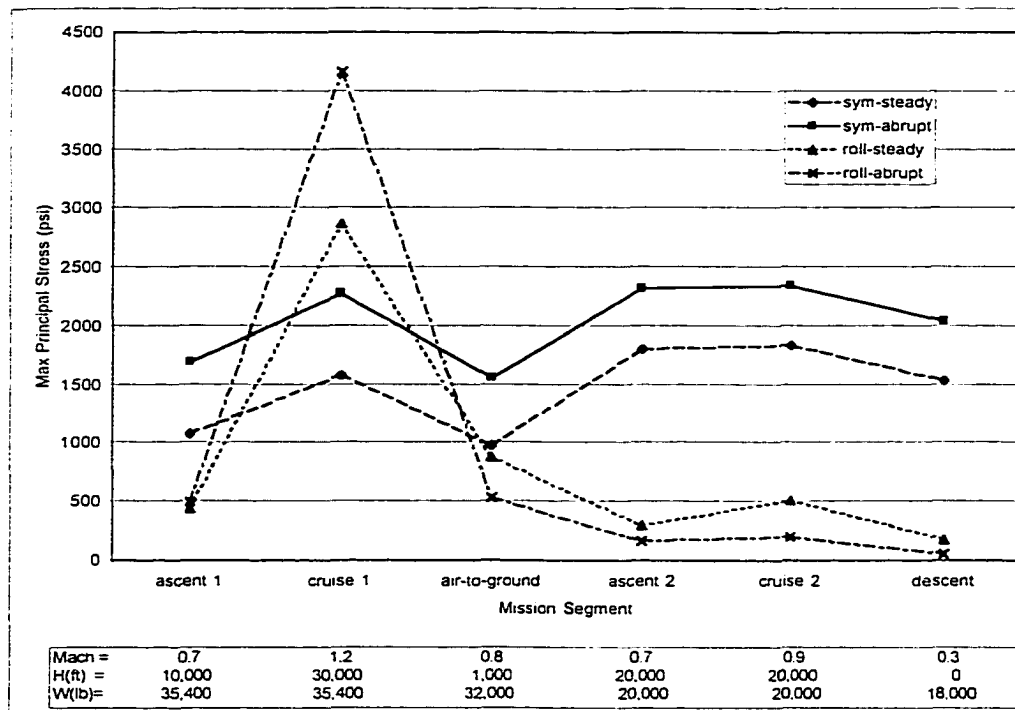


Figure 6-10 Air-to-Ground Mission Stress/Load Ratios

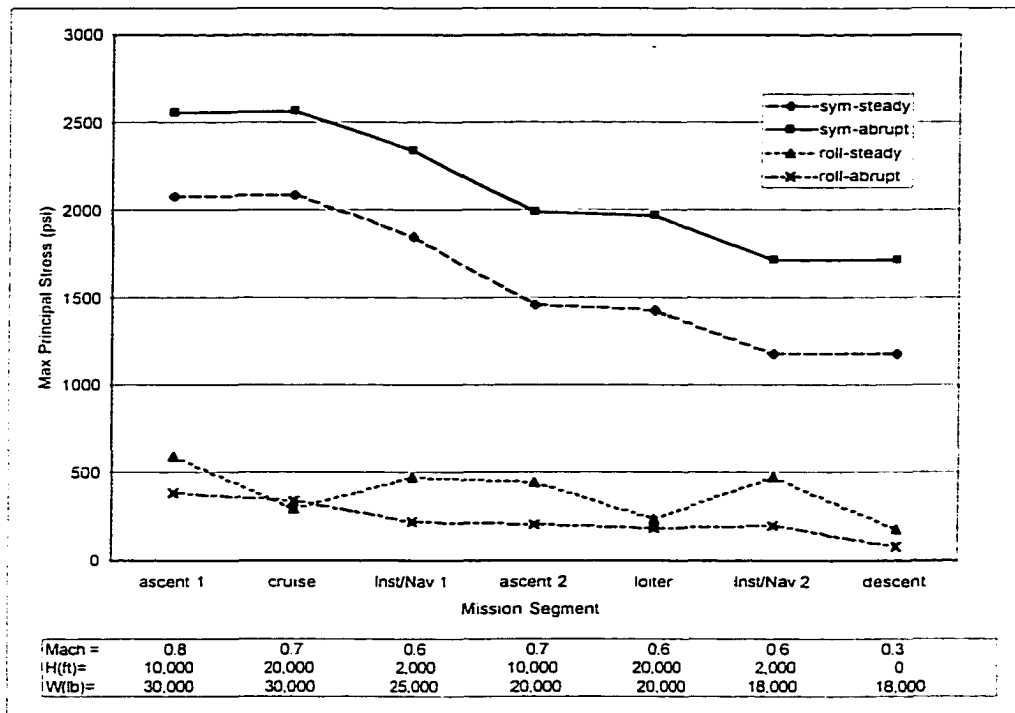


Figure 6-11 Training Mission Stress/Load Ratios

CHAPTER VII

FATIGUE STRESS HISTORY DEVELOPMENT

7.1 Introduction

A fatigue stress history was developed from the load factor history in Chapter 5 and MSC-ASTROS flight maneuver results in Chapter 6. Each occurrence in the load factor history was replaced with a stress value computed according to its maneuver type and corresponding flight parameters. Linear stress functions were developed because the stress results in Figures 6-9 through 6-11 are linear functions of load factor, pitch acceleration, roll rate, and roll acceleration. The parameters α , δ , ϵ , and η are used in these equations and vary according to segment and mission type. These parameters were supplied to the FORTRAN program “Global_local.exe”, listed in Appendix E, which automated the conversion of each load factor occurrence into stress.

7.2 Stress Functions for Symmetric Maneuvers

The aerodynamic and structural computations were linear analyses. Accordingly, symmetric maneuver stress occurrences were computed from linear equations based on either Eq. (7.1) or Eq. (7.2) for each segment within the three different mission types. The parameters α and δ were determined from the segment stress/load ratios computed from ASTROS symmetric flight maneuver analyses. Pitch acceleration \dot{q} was set at 3.0 rad/s² for symmetric abrupt maneuvers and 0.0 rad/s² for symmetric steady state maneuvers.

$$\sigma = \alpha n_z + \delta \dot{q} \quad n_z \geq 1.0 \quad (7.1)$$

$$\sigma = \alpha n_z - \delta \dot{q} \quad n_z < 1.0 \quad (7.2)$$

Table 7-1 contains the air-to-air mission maximum principal stresses from element 2549 for three values of positive normal load factor. ASTROS computed these stresses from symmetric steady state and abrupt maneuvers for the ascent segment. The following flight conditions taken from the ascent segment in Table 5-12 were used to compute the stresses: Mach = 0.7, altitude = 10,000 ft, and gross weight = 23,300 lb. The maximum principal stresses plotted in Figure 7-1 indicate a linear relationship with positive normal load factor for steady state and abrupt symmetric maneuvers.

Table 7-1 Maximum Principal Stresses for Symmetric Positive Load Factor Maneuvers in the Air-To-Air Mission: Ascent Segment

Load Factor (g)	Maximum Principal Stress (psi)	
	Symmetric Steady State	Symmetric Abrupt*
1.0	2,213.9	3,721.9
5.0	11,069.3	12,574.5
9.0	19,924.7	21,429.4

* $\dot{q} = 3.0 \text{ rad/s}^2$

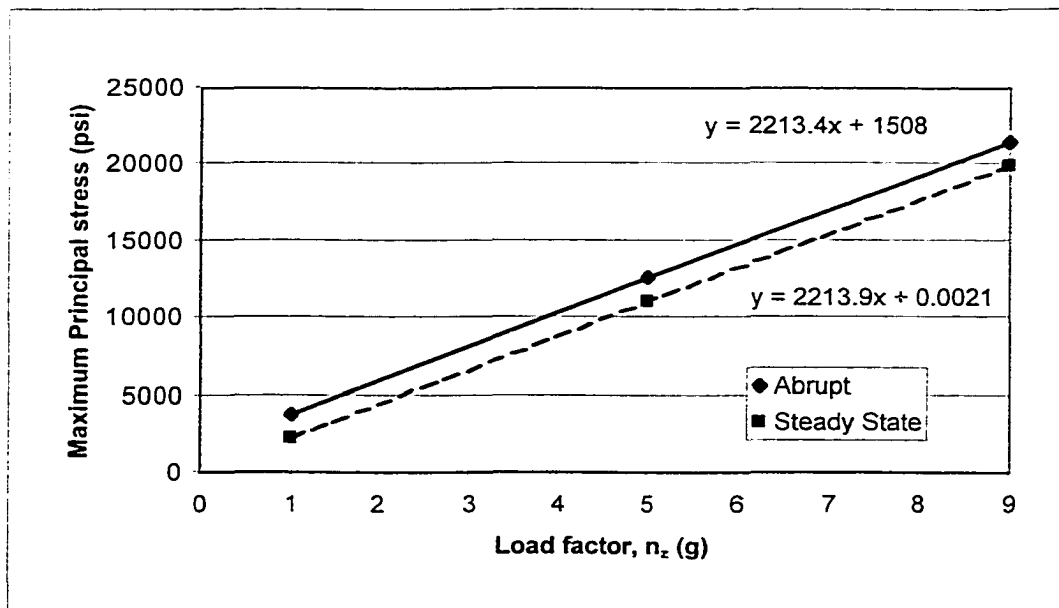


Figure 7-1 Maximum Principal Stresses for Symmetric Positive Load Factor Maneuvers in the Air-To-Air Mission: Ascent Segment

Table 7-2 contains the air-to-air mission principal stresses from element 2549 for four values of negative normal load factor. The stresses chosen for this table are either the maximum or minimum principal stresses with the largest absolute magnitude. Developing a fatigue stress history by strictly using maximum principal stresses would have ignored the effects of compressive overloads on the reduction of crack retardation. MSC-ASTROS computed these stresses from symmetric steady state and abrupt maneuvers for the ascent segment. Again, these principal stresses indicated a linear relationship with negative normal load factor for steady state and abrupt symmetric maneuvers.

Table 7-2 Principal Stresses for Symmetric Negative Load Factor Maneuvers in the Air-To-Air Mission: Ascent Segment

Load Factor (g)	Maximum or Minimum Principal Stress (psi)	
	Steady State	Abrupt*
0.5	1,106.9	-430.0
0.0	0.0	-1,513.7
-1.0	-2,213.9	-3,721.9
-5.0	-11,069.3	-12,574.5

* $\dot{q} = -3.0 \text{ rad/s}^2$

The results in Tables 7-1 and 7-2 indicate that symmetric steady state stresses in element 2549 can be represented by Eq. (7.3) for positive and negative load factors in the air-to-air mission ascent segment. The fitted linear curve of the abrupt maneuver stresses in Figure 7-1 is essentially parallel to the steady state curve and is approximated with the same slope of 2,213.9 psi in Eq. (7.4). The “y-intercept” of 1,508 psi represents the difference in steady state and abrupt stresses for a given positive load factor. From inspection of the negative load factor data (i.e., -1.0g) in Table 7-2, Eq. (7.5) is developed with the same slope as Eq. (7.4) for positive load factor maneuvers.

Subtracting the abrupt stress from the steady state stress at $-1.0g$, produces a similar “y-intercept” of $-1,508$ psi in Eq. (7.5).

$$\sigma = 2,213.9n_z \quad (7.3)$$

$$\sigma = 2,213.9n_z + 1,508 \quad n_z > 1.0 \quad (7.4)$$

$$\sigma = 2,213.9n_z - 1,508 \quad n_z < 1.0 \quad (7.5)$$

Because abrupt symmetric maneuver stresses are a linear function of pitch acceleration, Eqs. (7.4) and (7.5) are replaced with more general formulas in Eqs (7.6) and (7.7). The parameter 502.7 is obtained by prorating 1,508 to 1 rad/s^2 . This allowed symmetric steady state and abrupt stresses to be computed for any value of pitch acceleration and normal load factor. Comparing Eqs. (7.6) and (7.7) with Eqs. (7.1) and (7.2), the parameters α and δ are defined as 2,213.9 and 502.7 respectively. These parameters are unique to the air-to-air mission ascent segment. Parameters for the remaining segments are listed in Table 7-4.

$$\sigma = 2,213.9n_z + 502.7\dot{q} \quad n_z > 1.0 \quad (7.6)$$

$$\sigma = 2,213.9n_z - 502.7\dot{q} \quad n_z < 1.0 \quad (7.7)$$

7.3 Stress Functions for Asymmetric Maneuvers

ASTROS can simulate antisymmetric maneuvers (pure roll) but not the asymmetric maneuvers needed to compute asymmetric steady state and abrupt stresses in this research. In an antisymmetric maneuver analysis, ASTROS computes only the incremental loads necessary to produce pure roll. Asymmetric stresses are computed through superposition outside of ASTROS. A symmetric maneuver stress component is added to the antisymmetric roll steady state stress to produce an asymmetric steady state

maneuver stress. The antisymmetric roll steady state stress is determined from the product of the stress/load ratio ε and the roll rate p . The parameter ε is the segment stress/load ratio computed by ASTROS for an antisymmetric roll steady state maneuver with $p = 1.0$ rad/s. Roll acceleration is zero for the steady state asymmetric maneuver.

A symmetric maneuver stress component is added to the abrupt antisymmetric maneuver stress to produce an abrupt asymmetric maneuver stress. The abrupt antisymmetric maneuver stress is determined from the product of the stress/load ratio η and roll acceleration \dot{p} . The parameter η is the segment stress/load ratio computed by ASTROS for an abrupt antisymmetric maneuver with $\dot{p}=1.0$ rad/s². Roll rate is zero for the abrupt asymmetric maneuver. Asymmetric stress occurrences for steady state and abrupt maneuvers are computed with Eq. (7.8). Left steady state and abrupt rolls are represented by positive roll rates or roll accelerations, respectively. Right steady state and abrupt rolls are defined by negative roll rates or roll accelerations, respectively.

$$\sigma = \alpha n_z + \varepsilon p + \eta \dot{p} \quad (7.8)$$

Table 7-3 contains the air-to-air mission maximum principal stresses from element 2549 computed for two antisymmetric (roll) maneuvers. MSC-ASTROS computed these stresses from a steady state and an abrupt antisymmetric maneuver for the ascent segment. The same flight conditions as used in the symmetric maneuver

Table 7-3 Maximum Principal Stresses for Antisymmetric (Roll) Maneuvers in the Air-To-Air Mission: Ascent Segment

p (rad/s)	\dot{p} (rad/s ²)	Maximum Principal Stress (psi)	
		Steady State	Abrupt
4.75	0.0	2,140.0	-
0.00	19.0	-	3,265.4

analysis were used to compute these stresses: Mach = 0.7, altitude = 10,000 ft. and gross weight = 23,300 lb.

Prorating the stresses in Table 7-3 to unit values of roll rate and roll acceleration produces Eq. (7.9) for steady state and Eq. (7.10) for abrupt antisymmetric stresses. Using the superposition ideas discussed earlier, asymmetric stresses for the air-to-air mission ascent segment are computed with Eq. (7.11). Comparing Eq. (7.11) with Eq. (7.8), parameters ε and η are determined to be 450.5 and 171.9, respectively. These parameters are unique to the air-to-air mission ascent segment. Parameters for the remaining segments are listed in Table 7-4.

$$\sigma = 450.5p \quad (7.9)$$

$$\sigma = 171.9\dot{p} \quad (7.10)$$

$$\sigma = 2,213.9n_z + 450.5p + 171.9\dot{p} \quad (7.11)$$

7.4 Stress History Post-Processing

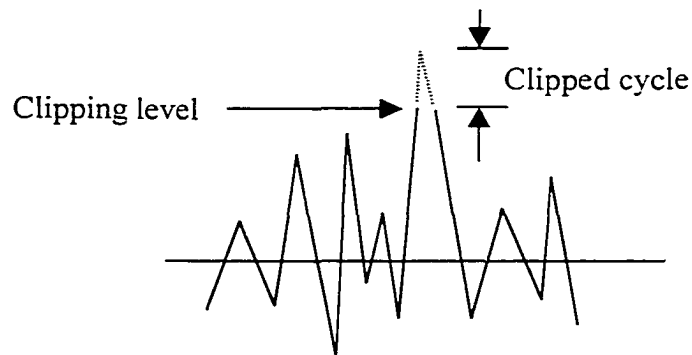
7.4.1 Clipping the Stress History

The resulting fatigue stress history was developed from element 2549 in the lower wing skin and contained a peak stress of 23,188.2 psi. This relatively high stress occurred only twice in the 500 hour block containing 436 flights. This peak stress occurred in the cruise 1 segments of an air-to-ground II mission (flight no. 267) and of an air-to-ground I mission (flight no. 277). These relatively few high stresses may cause a significant retardation effect and produce an unconservatively long fatigue life. Because some aircraft in the force may not see these high stresses, it is not realistic to include them. The USAF philosophy is to exclude high stresses that occur less frequently than

Table 7-4 Stress Function Parameters for All Mission Types and Segments

Mission Type	Segment Type	Stress Function Parameters			
		α	δ	ε	η
Air-to-Air	Ascent	2,213.9	502.7	450.5	171.9
	Formation 1	2,717.6	545.6	2,859.3	1,203.8
	Air-to-Air	1,839.9	506.0	509.3	206.5
	Formation 2	1,959.7	551.5	2,859.3	1,203.8
	Cruise	1,336.9	510.3	450.5	171.9
	Descent	1,299.4	513.4	176.0	57.7
Air-to-Ground	Ascent 1	1,085.8	613.1	450.6	500.2
	Cruise 1	1,586.3	692.3	2,864.8	4,161.8
	Air-to-Ground	984.7	584.0	880.7	533.3
	Ascent 2	1,812.1	507.7	299.2	165.9
	Cruise 2	1,839.9	506.0	509.3	206.5
	Descent	1,536.4	510.5	176.0	57.7
Training	Ascent 1	2,081.7	475.9	596.7	391.2
	Cruise	2,084.2	482.5	299.3	341.6
	Inst/nav 1	1,845.8	496.8	481.5	223.6
	Ascent 2	1,457.6	533.6	448.3	208.0
	Loiter	1,427.7	536.4	241.0	189.1
	Inst/nav 2	1,184.7	528.6	481.5	201.8
	Descent	1,179.1	536.3	177.4	84.8

10 times in 1,000 flights. Clipping is the process which reduces the magnitude of the highest stresses to the clipping stress level as shown in Figure 7-2. No cycles are omitted in clipping.

**Figure 7-2 Clipped Cycle**

In this work, the clipping stress level is selected to insure that the resulting high stresses are more numerous than 4 times in 436 flights. A FORTRAN program called “Spectrum_clipping.exe” was written to inspect the fatigue stress history for high stresses and clip these stresses to the user supplied clipping level. Table 7-5 shows the results of this inspection. The occurrences and exceedances for the three highest stress levels are tabulated. The clipping stress level of 18,500 psi was selected because it was the highest stress that occurred more than 4 times in 436 flights. Any cycle with a peak stress higher than 18,500 psi was reduced to this value.

Table 7-5 Selecting the Clipping Stress Level

Clipping Level (psi)	Occurrences	Exceedances
23,188	2	2
19,000	1	3
18,500	2	5

7.4.2 Normalizing the Stress History

Accordingly, each occurrence in the fatigue stress history was normalized by 18,500 psi. This produced a general fatigue stress history which, when multiplied through by the appropriate stress multiplication factor (SMF), can be used in a damage tolerance analysis. The stress multiplication factor is a number that AFGROW uses to multiply each peak and valley of the normalized stress history. It is a user input. Varying the stress multiplication factor will change the severity of the fatigue stress history but maintain its general shape. A user who wants to input a stress history that is not normalized would set SMF to one.

CHAPTER VIII

THE DEVELOPMENT OF DTA CONSTRAINTS

8.1 Introduction

A fatigue crack in a noninspectable location is required by USAF policy to grow for double the design life without failure. The work in Chapter 5 determined that a structure capable of 4,360 flights would be needed to meet the design life requirement of 5,000 flight hours in this example. Therefore, damage tolerance analyses were performed on the lower wing skin to determine the severest fatigue stress history that would still meet the crack growth life requirement of 8,720 flights without failure. Fatigue stress history severity was determined by entering the normalized stress history, developed earlier, into the AFGROW⁸ prediction code and iterating between the stress multiplication factor (SMF) and crack growth life calculations until 8,720 flights were achieved. Too large of an SMF would produce a stress history too severe to meet the crack growth life requirement. Too small of an SMF would produce wing skin panels that are unnecessarily heavy.

Three different crack configurations were modeled in an infinitely wide, 0.38-inch thick, lower wing panel: a through-the-thickness crack, a semi-elliptical surface crack, and a quarter-elliptical corner crack in a hole. AFGROW doesn't have stress intensity factor solutions for cracks in infinitely wide panels; setting the panel width to 10,000 inches simulated this boundary condition. A centered through-the-thickness crack in an infinitely wide panel is not a realistic configuration but does act as a baseline for future research.

This panel represented element 2549 in the lower wing skin finite element model. The wing panel material was a 2024 aluminum alloy with a yield strength of 47 ksi and a plane strain fracture toughness of $31 \text{ ksi}\sqrt{\text{in}}$. The Generalized Willenborg model with a 2.5 shut-off load ratio (SOLR) was selected to simulate crack growth retardation and acceleration effects.

The residual strength requirement (P_{xx}) was set to the limit load stress of 36.7 ksi. The limit load stress was computed by dividing the material ultimate strength of 55 ksi, found in the MSC-ASTROS input file, by a safety factor of 1.5. Specifying this residual strength requirement in the damage tolerance analysis insures that this cracked panel will always have the capability to carry limit load. This is a USAF DTA requirement. AFGROW also uses the residual strength requirement to compute the final crack length.

8.2 Through-The-Thickness Crack

A simple through-the-thickness crack with an initial half-length (a) of 0.125 inch was modeled in an infinitely wide wing panel in Figure 8-1 with AFGROW. AFGROW used the residual strength requirement to compute a final half-crack length of 0.27 inch. The results of the AFGROW iterations are presented in Table 8-1 and in Figure 8-2. A “pass” in Table 8-1 indicates the completion of a block containing 436 flights. Twenty

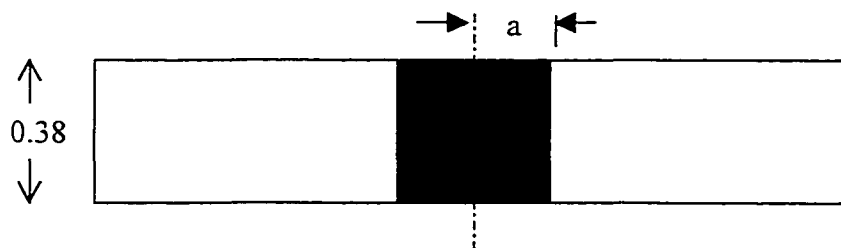


Figure 8-1 Through-the-Thickness Crack in an Infinitely Wide Panel

Table 8-1 SMF* Iterations for the Through-the-Thickness Crack

SMF (ksi)	Flights	Passes	Cycles
25.0	6,218	15	869,442
23.0	8,522	20	1,192,617
22.5	9,312	22	1,310,597
22.0	10,165	24	1,420,535

* SOLR = 2.5, Pxx = 36.7 ksi

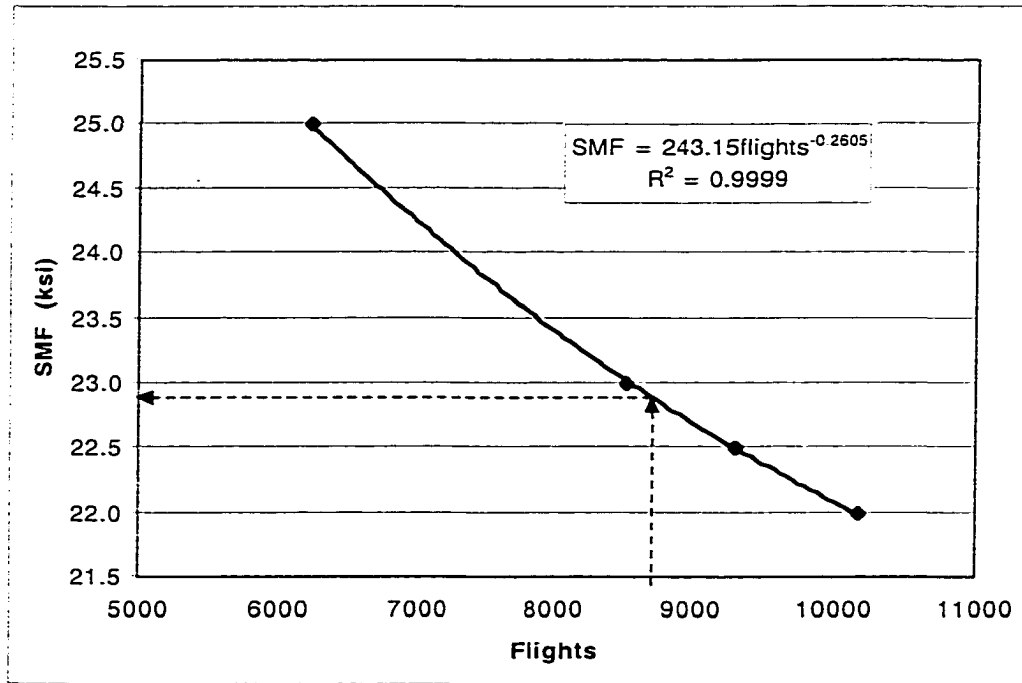


Figure 8-2 SMF Iterations for a Through-the-Thickness Crack

passes, or blocks, are needed to complete 8,720 flights. The regression analysis in Figure 8-2 indicated that these results can be modeled with Eq. (8.1).

$$SMF = 243.15 \times flights^{-0.2605} \quad (8.1)$$

Equation (8.1) produces a stress multiplication factor of 22.9 ksi for a fatigue life requirement of 8,720 flights. Supplying AFGROW with an SMF input of 22.9 ksi and executing a crack growth life analysis produced 8,747 flights for this crack configuration. This represents an error of only 0.31%. This stress multiplication factor is called the fatigue stress allowable (FSA) because it produces the severest fatigue stress history which does not cause failure for less than 8,720 flights. This FSA will be used as the

damage tolerance constraint in the design optimization of the lower wing skin for this crack configuration in Chapter 9. A plot of crack length history versus flights for the infinitely wide cracked panel is shown in Figure 8-3.

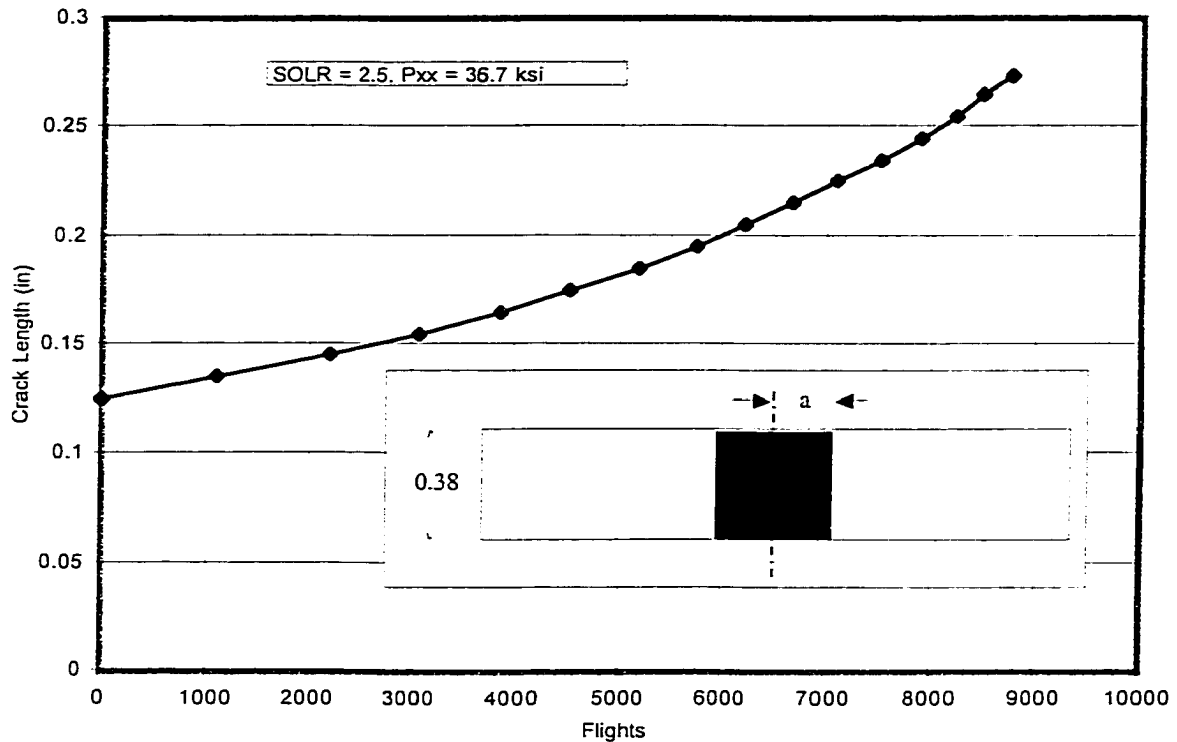


Figure 8-3 Crack Growth History for the Through-the-Thickness Crack

8.3 Semi-elliptical Surface Crack

A semi-elliptical surface crack was modeled in a 0.38 inch thick infinitely wide panel in Figure 8-4. The initial crack depth and half-crack length along the surface were both set at 0.125 inch. AFGROW used the residual strength requirement P_{xx} of 36.7 ksi to compute a 0.44-inch final crack length along the surface. The results of the AFGROW iterations are listed in Table 8-2 and presented in Figure 8-5. Again, twenty passes, or blocks, are needed to complete 8,720 flights. The regression analysis indicated that these results can be modeled with Eq. (8.2).

$$SMF = 331.15 \times flights^{-0.2589} \quad (8.2)$$

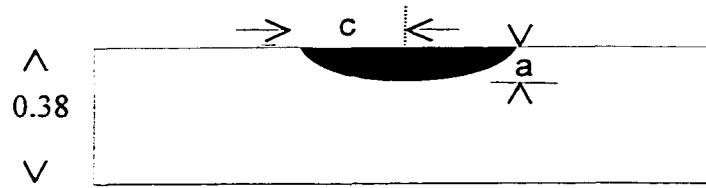


Figure 8-4 Semi-Elliptical Surface Crack in an Infinitely Wide Panel

Table 8-2 SMF* Iterations for the Semi-Elliptical Surface Crack

SMF (ksi)	Flights	Passes	Cycles
35.0	5,848	14	818,484
33.0	7,416	18	1,034,914
32.0	8,326	20	1,162,565
30.0	10,613	25	1,482,955

* SOLR = 2.5, Pxx = 36.7 ksi

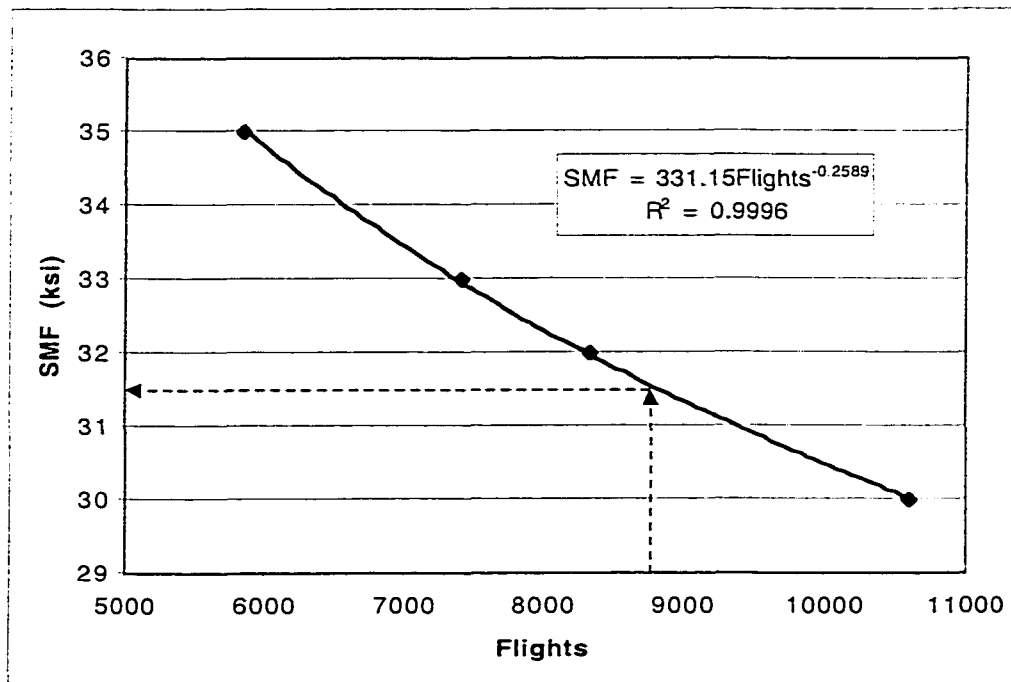


Figure 8-5 SMF Iterations for the Semi-Elliptical Surface Crack

Equation (8.2) produces a stress multiplication factor of 31.6 ksi for a fatigue life requirement of 8,720 flights. Supplying AFGROW with an SMF input of 31.6 ksi and executing a crack growth life analysis produced 8,734 flights for this crack configuration.

This represents an error of 0.16%. This stress multiplication factor is the fatigue stress allowable in this crack configuration because it produces the severest fatigue stress history which does not cause failure for less than 8,720 flights. This FSA is larger than that produced by the previous crack configuration and, therefore, was not used as a damage tolerance constraint in Chapter 9. A plot of the crack growth history for the cracked panel is shown in Figure 8-6. This plot contains the crack length history for the

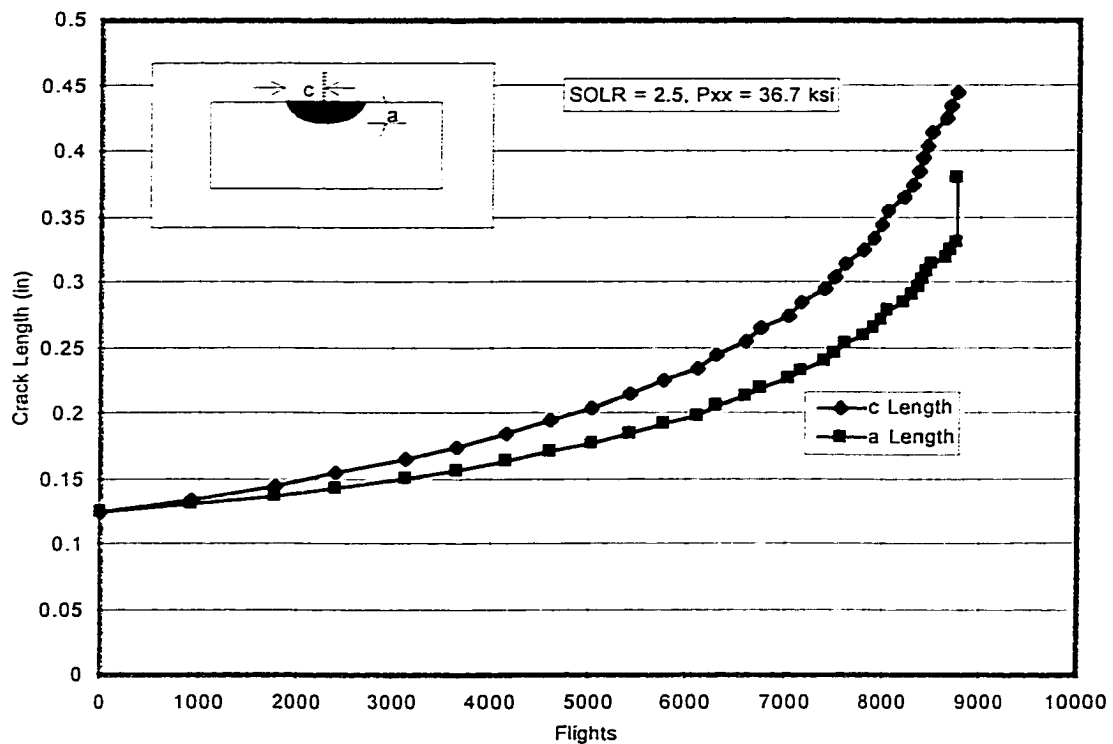


Figure 8-6 Crack Growth History for the Semi-Elliptical Surface Crack

depth (a) and surface (c) of the semi-elliptical crack. Figure 8-6 indicates that the crack grew faster along the surface than through the thickness. Once the crack depth (a) penetrated 95% of the panel thickness, AFGROW immediately modeled the crack as a through-the-thickness crack growing in the (c) direction. The vertical line at the end of crack growth curve (a) indicates this transition. The panel failed shortly after this transition took place.

8.4 Corner Crack in a Hole

A quarter-elliptical corner crack was modeled in a quarter inch diameter hole with AFGROW according to the configuration in Figure 8-7. This crack configuration is used to model the very common scenario of a fatigue crack growing from a fastener hole. Fastener holes are numerous in a wing skin panel and produce stress concentrations which promote the initiation of fatigue cracks. The hole in this AFGROW model resided in an infinitely wide panel 0.38 inch in thickness. The initial crack depth (a) and crack length (c) along the surface were both set at 0.05 inch. AFGROW used the residual strength requirement of 36.7 ksi to compute a 0.30-inch final crack length along the surface. The results of the AFGROW iterations are listed in Table 8-3 and presented in Figure 8-8. Again, twenty passes, or blocks, were needed to complete 8.720 flights. The regression analysis indicated that these results could be modeled with Eq. (8.3).

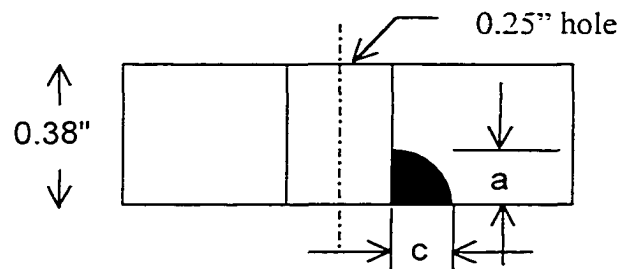


Figure 8-7 Corner Crack in a Hole in an Infinitely Wide Panel

Table 8-3 SMF* Iterations for a Corner Crack in a Hole

SMF (ksi)	Flights	Passes	Cycles
30	5,461	13	765,097
28	7,104	17	992,958
26	9,346	22	1,306,899
25	10,917	26	1,523,787

* SOLR = 2.5, P_{xx} = 36.7 ksi

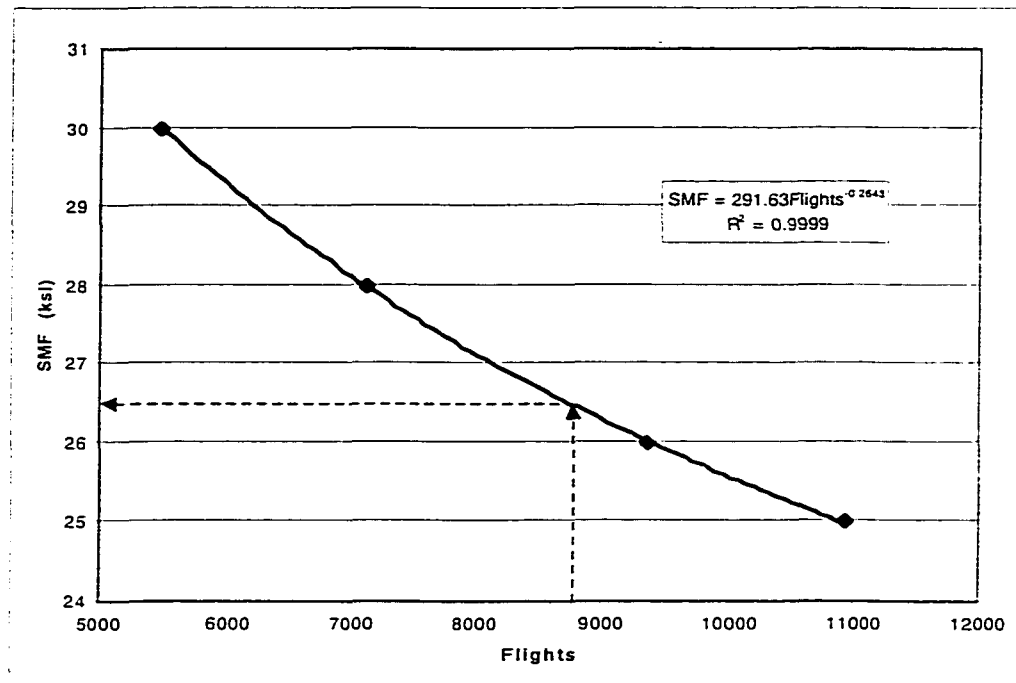


Figure 8-8 SMF Iterations for a Corner Crack in a Hole

$$SMF = 291.63 \times flights^{-0.2643} \quad (8.3)$$

Equation (8.3) produced a stress multiplication factor of 26.5 ksi for a design life requirement of 8,720 flights. Supplying AFGROW with an SMF input of 26.5 ksi and executing a crack growth life analysis produced 8,750 flights for this crack configuration. This represents an error of only 0.34%. This stress multiplication factor was the fatigue stress allowable for the corner crack hole configuration because it produced the severest fatigue stress history which does not cause failure for less than 8,720 flights. The FSA produced for this crack was larger than the through-the-thickness crack FSA and, therefore, was not used as a damage tolerance constraint in Chapter 9.

A plot of the crack growth history for the cracked panel is shown in Figure 8-9. This plot contains the crack length history for the depth (a) and surface (c) dimensions of

the quarter-elliptical corner crack growing from a hole. For this configuration, the crack depth (a) grew faster than the crack length along the surface (c). Once the crack depth (a) penetrated 95% of the panel thickness, AFGROW immediately modeled the corner crack as a through-the-thickness crack growing in the (c) direction. The vertical line at the end of the crack growth curve (a) indicates this transition. In this scenario, the panel failed (crack c obtained final length) immediately after the quarter-elliptical corner crack transitioned into a through-the-thickness crack.

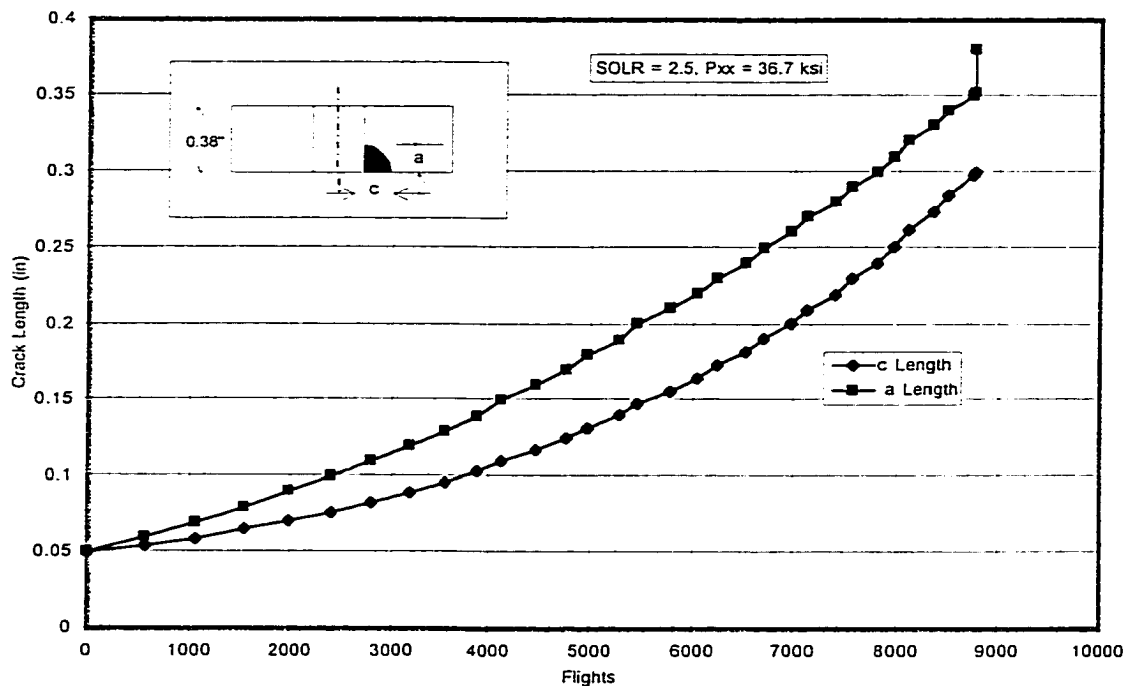


Figure 8-9 Crack Growth History for the Corner Crack in a Hole

8.5 Conclusions

Fatigue stress allowables for three crack configurations, typically found in an aircraft wing panel, were computed using the AFGROW program. Using the normalized fatigue stress history as input, AFGROW was executed to determine the appropriate

severity, through the stress multiplication factor, to insure a fatigue crack growth life that would satisfy the USAF damage tolerance policy. The results of the AFGROW iterations were fatigue stress allowables for a through-the-thickness crack, a semi-elliptical surface crack, and a quarter-elliptical corner crack in a hole. These analyses were performed with a Generalized Willenborg Retardation model, shut-off load ratio (SOLR) of 2.5, and a residual strength requirement (Pxx) of 36.7 ksi. The results of the three crack configurations are summarized in Table 8-4. The through-the-thickness crack produced the severest FSA while the semi-elliptical surface crack was relatively benign. For this reason, the through-the-thickness crack was used as the damage tolerance constraint in the design optimization of an aircraft lower wing skin as described in the next chapter.

Table 8-4 Fatigue Stress Allowable Summary for Three Crack Configurations

Crack Configuration	SOLR	Pxx (ksi)	Flights	% Error	FSA (ksi)
Through-the-thickness	2.5	36.7	8,747	0.31	22.9
Semi-elliptical surface	2.5	36.7	8,734	0.16	31.6
Corner crack in a hole	2.5	36.7	8,750	0.34	26.5

CHAPTER IX

OPTIMIZATION RESULTS

9.1 Introduction

The lower wing skin thickness of the fighter aircraft was designed with damage tolerance constraints, using the fatigue stress allowables developed in the previous chapter as maximum principal stress constraints in an MSC-ASTROS optimization. The objective was to reduce weight. Setting the fatigue stress allowable as a maximum principal stress constraint will consider the effects of mixed-mode loading on fatigue crack growth. According to Broek, fatigue cracks grow perpendicular to the maximum principal stress direction⁵¹. MSC-ASTROS does not have a maximum principal stress constraint, therefore, its function packet was employed to model the synthetic constraint function in Eq. (9.1). The constraint g_{fsa} must remain negative for the optimization to remain in the feasible design space. This is accomplished when the maximum principal stress σ_1 is less than the fatigue stress allowable σ_{fsa} .

$$g_{fsa} = \frac{\sigma_1}{\sigma_{fsa}} - 1 \quad (9.1)$$

Physically linked design variables were used in the optimizations. The maximum principal stress constraint was applied to only 17 “master” elements in the lower wing skin finite element model in Figure 9-1. A master element represented a group of elements by physically linking their thicknesses as one design variable. Each group of linked elements was free to vary independently from other groups of linked elements.

These element groups shared the same physical property card and thickness in the original finite element model. Physically linked design variables were designated with the PSHELL card physical property ID.

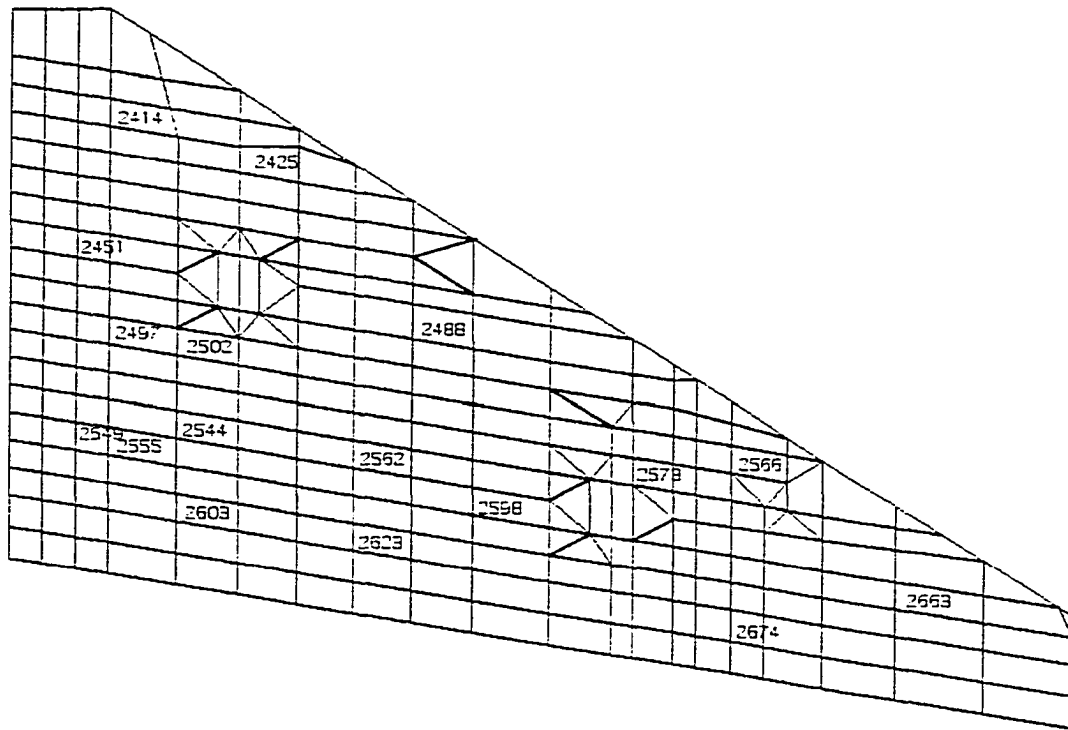


Figure 9-1 Master Element Location in the Right Lower Wing Skin

The thicknesses of the lower wing skin elements in the original finite element model are based on an F-16 design and would already have experienced some optimization at this stage in the design process. To simulate a wing structure before optimization, the thicknesses of all lower wing skin elements were initially set to 0.25 inch. The minimum and maximum thickness side constraints were set to 0.04 and 1.0 inch, respectively. The elements over the two hard point cut-outs were not designed in the optimization, and the thicknesses of these elements were set to 0.001 inch. The first

inboard row of elements was also excluded from the design set. The wing attach fittings were not modeled, and the carry-through loads were transferred to the fuselage structure through a small number of grid points on the wing skin. The resulting stress concentrations in these elements would cause them to be overdesigned if they were included. Accordingly, the first inboard row of elements was given thickness values equivalent to the production aircraft skin thickness contour.

The aerodynamic model provided loads for two symmetric and three asymmetric (roll) flight maneuvers during the optimization. The symmetric maneuvers included a 9g pull-up at Mach 0.95 at sea level and a -3g push-over at Mach 1.20 at sea level. The asymmetric maneuvers employed a 120°/sec roll rate at Mach 1.2 and 1.05 at sea level and at Mach 0.95 at 2,500 ft. These load cases are summarized in Table 9-1 along with their critical locations.

Table 9-1 ASTROS Load Cases for Optimization

Case	Critical location	Maneuver	Mach No.	Altitude
1	Max + wing root bending	9g symmetric pull up	0.95	Sea level
2	Max - wing root bending	-3g symmetric push over	1.20	Sea level
3	Max + flaperon loads	5.86g Roll, p=120°/sec	1.20	Sea level
4	Max - flaperon loads	-1g Roll, p=120°/sec	1.05	Sea level
5	Max load on hardpoints	-1g Roll, p=120°/sec	0.95	2.500

A portion of the gross weight was modeled as stores (external fuel and munitions) attached to wing hardpoints in air-to-ground missions. As discussed earlier, underwing stores provide load relief in symmetric maneuvers and, therefore, produce lower wing stresses. Low wing skin stresses allow the element thicknesses to achieve very small values during optimization. But underwing stores produce significant stresses during the asymmetric (roll) maneuvers performed in load cases 3, 4, and 5. Although MSC-

ASTROS can simultaneously apply multiple maneuver types (load cases) during optimization, it cannot automatically change the mass matrix to include underwing stores for the asymmetric maneuvers.

This issue was dealt with by executing four optimizations with two different store configurations. The first store configuration (Run 1) was consistent with an air-to-ground mission which uses 5,502.5 lb of external stores attached to underwing hard points at stations 6, 7, and 8 plus an electronic counter measure (ECM) pod attached to station 5 under the belly. The second store configuration (Run 2) simulated an air-to-air mission which uses a centerline external fuel tank at station 5 but no underwing stores. Both configurations contained a wing tip missile at station nine. After completing the first and second optimizations, the optimum thicknesses produced with the first store configuration (Run 1) were used as minimum side constraints for a third optimization with no underwing stores (Run 3). Conversely, a fourth optimization (Run 4) with underwing stores used the optimum thicknesses produced earlier with no underwing stores (Run 2) as minimum side constraints. This process insured that the final design variables were large enough to maintain structural integrity in both store configurations.

Damage tolerance requirements were employed by simultaneously applying maximum principal stress constraints for the five flight maneuvers during the MSC-ASTROS optimizations. Because the through-the-thickness crack analyzed in the previous chapter produced the severest (lowest) fatigue stress allowable, optimizations were performed only with this configuration. Finally, a design optimization was performed that included multidisciplinary constraints. Von Mises stress, aileron effectiveness, and lift effectiveness constraints were applied simultaneously during this

optimization.

9.2 Optimization with DTA Constraints

ASTROS cannot report the weight history of only the lower wing skin. Directly comparing the weight histories from the four optimizations would be difficult because the two models contained various payloads such as fuel (internal and external), external stores (bombs), pilot, and an ECM pod. The solution was to subtract all useable payloads from the reported optimization weight history. The remaining weight represented the empty structure plus permanently fixed operational equipment. This is called the operational equipment weight (OEW). The OEW histories of the four MSC-ASTROS optimizations are listed in Table 9-2 and can be compared in Figure 9-2. Optimization runs 3 and 4 started with an initial thickness of 1.0 inch to accommodate the larger minimum side constraints. This produced a larger initial gross weight than optimizations one and two. The OEW of the half-aircraft model converged in Figure 9-2 to approximately 7,987 lb.

Table 9-2 Optimization Weight Histories with DTA Constraints

Iteration No.	Optimization Operational Equipment Weight (lb)			
	Run 1 Stores	Run 2 No Stores	Run 3 No Stores	Run 4 Stores
1	8035.9	8035.7	8546.5	8546.7
2	7964.0	7997.1	8206.0	8206.2
3	7950.3	7985.7	8043.0	8050.6
4	7947.5	7982.9	7997.1	7998.7
5	7946.8	7980.6	7989.6	7987.5
6	7946.7	7979.8	7988.4	7987.0
7		7979.6	7987.8	
8		7979.4	7987.6	
9			7987.4	
10			7987.3	

Optimizations one and four converged for the same number of iterations while optimizations two and three did not. The damage tolerance constraint, enforced by the 22.9 ksi fatigue stress allowable, was never violated in the last iteration. Inspection of Figure 9-2 indicates that optimization two is a good prediction of the final design weight for optimizations three and four.

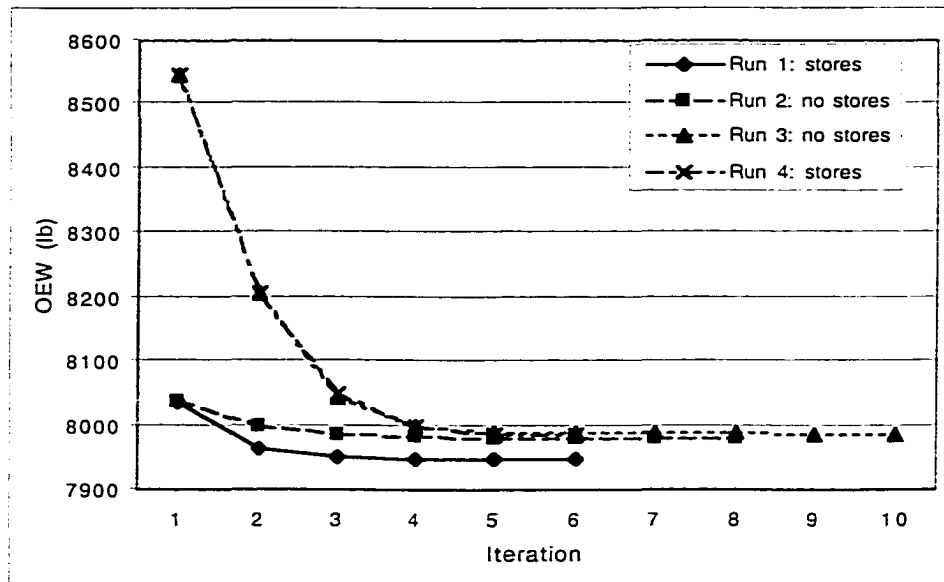


Figure 9-2 Optimization Weight Histories with DTA Constraints

The number of active constraints for each iteration is listed in Table 9-3 and Table 9-4 for optimizations one and two. Of the 58 total FSA constraints, 51 were retained as active constraints in each iteration. The number of active constraints by load case and maximum constraint values are listed in these tables to identify which maneuver was driving the optimization. In optimizations with and without stores, load case one contained the largest number of active constraints and, typically, produced the maximum constraint value. Except for a few iterations, load case one was driving the design.

The final design variables for each optimization are presented in Table 9-5, along with their corresponding master element and design variable ID's, and are plotted in

Figures 9-3 and 9-4 for comparison. Final thicknesses below 0.25 inch were typically found on wing outboard elements. Those above 0.25 inch were typically found on inboard elements.

Table 9-3 Number of Active Constraints by Load Case: Stores

Iteration	Symmetric		Asymmetric			Maximum Constraint Value
	1	2	3	4	5	
1	16*	1	6	15	13	-7.58E-2
2	17*	1	5	14	14	1.84E-3
3	17	2	4	14*	14	1.56E-2
4	17*	2	4	14	14	-5.72E-4
5	17*	1	4	14	15	5.59E-5
6	17*	1	4	14	15	1.95E-4

* Load case with maximum constraint value

Table 9-4 Number of Active Constraints by Load Case: No Stores

Iteration	Symmetric		Asymmetric			Maximum Constraint Value
	1	2	3	4	5	
1	16*	0	6	15	14	0.2766
2	17*	1	4	14	15	-0.328E-3
3	17	1	4	14*	15	2.14E-3
4	17*	1	5	14	14	0.768E-3
5	17	1	5	14*	14	2.11E-2
6	17*	1	6	13	14	8.82E-6
7	17*	1	6	13	14	1.18E-5
8	17*	1	6	13	14	3.09E-5

* Load case with maximum constraint value

Most of the design variables in Run 2 (no underwing stores) were larger than those in Run 1 (underwing stores). Symmetric maneuvers, without the benefit of load relief from underwing stores, produced high stresses in the inboard wing skin which led to higher thicknesses in those master elements. The 9g pull-up in load case 1 produced the highest maximum principal stress of 22.9 ksi. This corresponded to the fatigue stress allowable used in the MSC-ASTROS optimization for this crack configuration. The stress results of inboard element 2549 (DV 12) after optimization are presented in Table

9-6 for the 5 load cases.

Table 9-5 Final Thicknesses of the Master Elements with DTA Constraints

Variable ID	Master Element ID	Final Thicknesses (in)			
		Run 1	Run 2	Run 3	Run 4
1	2663	0.040	0.065	0.067	0.065
2	2562	0.121	0.237	0.121	0.237
3	2674	0.101	0.120	0.120	0.125
4	2566	0.234	0.116	0.234	0.208
5	2573	0.087	0.055	0.100	0.091
6	2425	0.050	0.151	0.158	0.151
7	2598	0.197	0.040	0.197	0.118
8	2414	0.123	0.317	0.313	0.317
9	2502	0.250	0.398	0.378	0.398
10	2451	0.282	0.382	0.373	0.382
11	2555	0.155	0.202	0.214	0.202
12	2549	0.184	0.288	0.294	0.288
13	2497	0.235	0.428	0.395	0.428
14	2603	0.136	0.401	0.409	0.401
15	2544	0.141	0.207	0.207	0.207
16	2623	0.103	0.058	0.103	0.076
17	2488	0.117	0.184	0.170	0.184

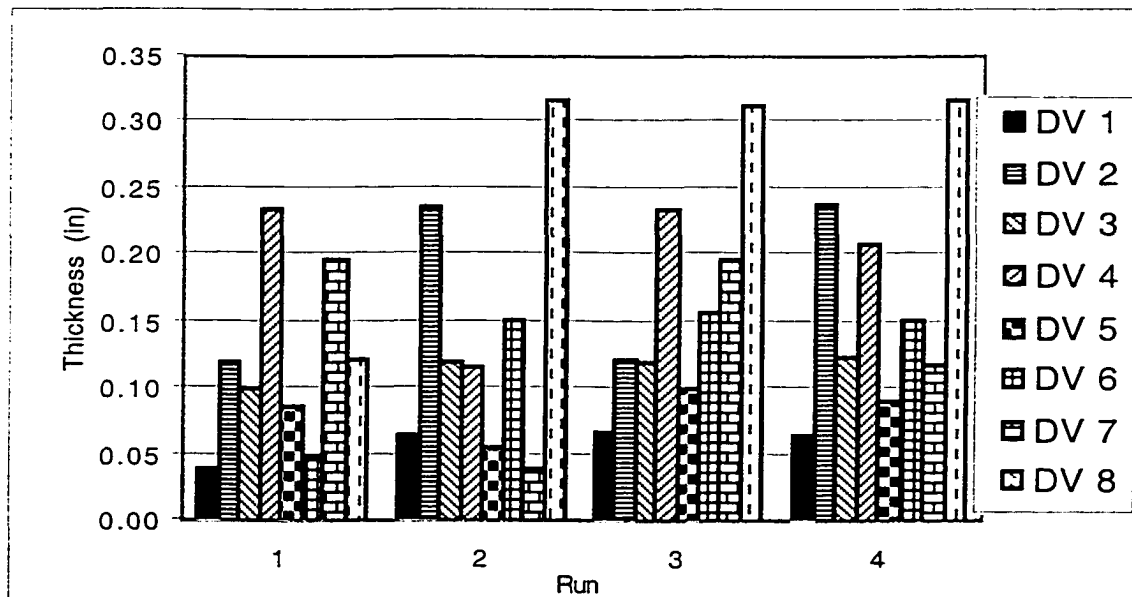


Figure 9-3 Design Variables (1-8) Versus Optimization Run

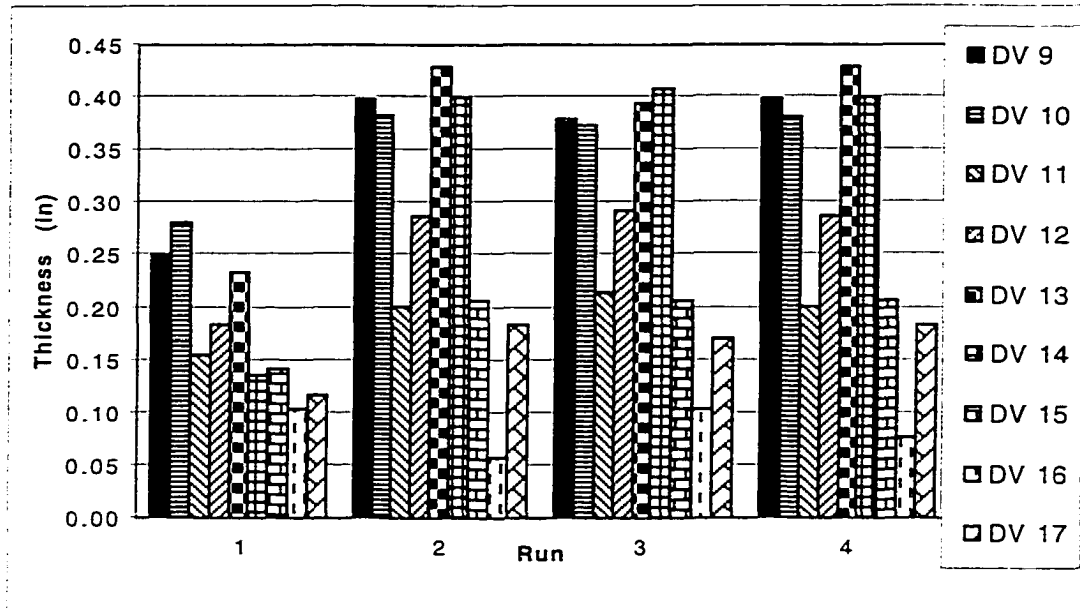


Figure 9-4 Design Variables (9-17) Versus Optimization Run

Table 9-6 Principal Stresses for Element 2549

ASTROS Load Case	Underwing Stores (Run 1)		No Underwing Stores (Run 2)	
	Maximum (psi)	Minimum (psi)	Maximum (psi)	Minimum (psi)
1	22,894.0	-4,177.1	22,900.2	-210.4
2	-948.9	-11,803.1	304.7	-9,540.7
3	1,358.2	-6,116.3	1,451.2	-4,142.5
4	9,184.4	-4,3944.4	10,250.8	-22,743.7
5	21,446.4	-10,795.7	6,487.2	-2,941.1

One may conclude that designing solely without underwing stores is sufficient, and analyses with underwing stores are unnecessary. But design variables 4, 5, 7, and 16 were larger in Run 1 (underwing stores) than in Run 2 (no underwing stores). Design variables 4, 5, and 7 were represented by master elements located near outboard hard points. Asymmetric maneuver loads, aggravated by underwing stores, produced higher stresses on these outboard master elements which led to higher optimum thicknesses. Therefore, performing only symmetric maneuver analysis without underwing stores, will underdesign hard point locations in the outboard wing skin. The solution is to optimize

with stores and, then, use the resulting optimum thicknesses as minimum side constraints for the corresponding design variables in a subsequent optimization without stores. This was the procedure used in Run 3.

The stresses for element 2598 (DV 7) after optimization are given in Table 9-7. The maximum principal stress in Run 1, load case 1, was restricted by the FSA, which limited the thickness of element 2598 from dropping below 0.197 inch. The maximum principal stresses in Run 2 were well below the FSA even with an element thickness of 0.04 inch. The stresses in Run 2 could never approach the FSA because 0.04 inch was a minimum side constraint for the design variable in this optimization.

Table 9-7 Principal Stresses for Element 2598

ASTROS Load Case	Underwing Stores (Run 1)		No Underwing Stores (Run 2)	
	Maximum (psi)	Minimum (psi)	Maximum (psi)	Minimum (psi)
1	22,894.2	-9,514.7	15,3311.2	-5,001.7
2	447.8	-8,048.3	-29.1	-5,527.9
3	1,328.2	-8,160.3	5,340.9	-7,101.5
4	9,484.2	-4,861.7	10,393.2	-22,935.2
5	5,076.1	-4,949.6	16,147.0	-7,735.5

9.5 Multidisciplinary Design Optimization

Finally, multiple constraints were simultaneously applied to the design optimization of the lower wing skin. They included damage tolerance, von Mises stress, aileron effectiveness, and lift effectiveness. The same load cases as in Table 9-1 were used. The multidisciplinary constraints had to be satisfied for all five load cases. As the through-the-thickness crack provided the worst-case scenario, the damage tolerance constraint was based on this crack configuration. The minimum, maximum, and initial

thicknesses were set to 0.04, 1.0, and 1.0 inch, respectively. The elements along the wing root and over the hard points were not designed.

Real aircraft structures experience combined loadings that produce biaxial and triaxial states of stress⁵². Considering that strength data is often determined from uniaxial testing, the question of how to predict failure of a structure under multiaxial loading needs to be addressed. The maximum distortion energy theory of failure assumes that a particular combination of stresses, which produce a von Mises stress equivalent to yield strength, will cause failure in a component. In plane stress, the von Mises stress is computed with Eq. (9.2). The tensile, compressive, and shear stress limits used in the von Mises constraint card were 55,000 psi, -55,000 psi, and 37,000 psi, respectively

$$\sigma_{vm} = \sqrt{(\sigma_x^2 + \sigma_y^2 - \sigma_x \sigma_y) + 3\tau_{xy}^2} \quad (9.2)$$

The aileron effectiveness (*AEREQ*) in Eq. (9.3) is the ratio of aileron aeroelastic efficiency to roll damping aeroelastic efficiency⁵³. Essentially, this ratio specifies the nondimensional steady state roll rate for a unit aileron deflection. It varies with wing stiffness, altitude, and Mach number.

$$AEREQ = \frac{-C_{l\delta_a}}{C_{l\dot{p}/2V}} \quad (9.3)$$

In Eq. (9.3), the $C_{l\delta_a}$ term is the rolling moment coefficient due to aileron (or flaperon for this model) angle δ_a . The $C_{l\dot{p}/2V}$ term is the rolling moment coefficient due to roll rate, \dot{p} . An aileron effectiveness of 1.0 represents a rigid wing. An aileron effectiveness approaching 0.0 indicates a very flexible wing. Negative values of aileron effectiveness are produced when the wing structure lacks sufficient rigidity to prevent roll reversal. Roll reversal is the aeroelastic phenomenon where the aircraft rolls in a

direction opposite to pilot input. Aileron effectiveness constraints are only applicable in asymmetric loading conditions. The aileron effectiveness constraints used in this research are listed in Table 9-8 along with the MSC-ASTROS load case, Mach number and altitude. These are lower bound constraints. That is, MSC-ASTROS must maintain a structural stiffness that is sufficient to produce aileron effectiveness values greater than or equal to $AEREQ$.

MSC-ASTROS would not execute with aileron effectiveness constraints applied to load cases three and four. The cause of this problem is unknown; however high dynamic pressures produced in supersonic flight may cause roll reversal, and create negative values of aileron effectiveness.

Table 9-8 Aileron Effectiveness Constraints

Load Case	Mach No.	Altitude (ft)	AEREQ
3	1.20	Sea level	-
4	1.05	Sea level	-
5	0.95	2,500	0.3

Lift effectiveness ($CLAREQ$)⁵³, represented in Eq. (9.4), is the ratio of flexible to rigid lift curve slope, $C_{l_{\alpha}}$. It also varies with wing stiffness, altitude, and Mach number. A lift effectiveness of 1.0 represents a rigid wing. Because the aerodynamic center is forward of the elastic axis for this aircraft model, the aerodynamic loading twists up the wing tip, “wash-in”, which produces additional lift. Applying an upper bound on the lift effectiveness will limit the flexibility of the wing. The lift effectiveness constraints used in this research are listed in Table 9-9 along with the MSC-ASTROS load case, Mach number, and altitude.

$$CLAREQ = \frac{(C_{l\alpha})_f}{(C_{l\alpha})_r} \quad (9.4)$$

Table 9-9 Lift Effectiveness Constraints

Load Case	Mach No.	Altitude (ft)	CLAREQ
1	0.95	10,000	1.5
2	1.20	Sea level	1.5

The OEW histories of the four MSC-ASTROS optimizations are listed in Table 9-10 and can be compared in Figure 9-5. All optimizations started with an initial thickness of the lower wing skin of 1.0 inch to accommodate the larger loads. This ensured that the first iteration started in the feasible design space. Optimizations two and three converged in the same number of iterations, while optimizations one and four took fewer iterations. The OEW of the half-aircraft model converged in Figure 9-5 to approximately 8,000 lb in the last 3 optimization runs. This OEW was higher than the optimum OEW computed with only DTA constraints. This was to be expected as multiple constraints make it difficult for an optimization to find a global minimum.

Table 9-10 Optimization History with Multidisciplinary Constraints

Iteration No.	Optimization Operational Equipment Weight (lb)			
	Run 1 Stores	Run 2 No Stores	Run 3 No Stores	Run 4 Stores
1	8546.7	8546.5	8546.5	8546.7
2	8206.2	8206.0	8206.0	8206.2
3	8043.3	8051.1	8051.1	8059.0
4	7974.5	8009.5	8011.4	8011.9
5	7968.0	8003.6	8007.8	8008.3
6	7967.5	7999.3	8007.2	8007.9
7	7967.5	7998.9	8006.9	
8		7998.7	8006.8	
9		7998.6	8006.7	
10		7998.6	8006.6	
11		7998.6	8006.6	

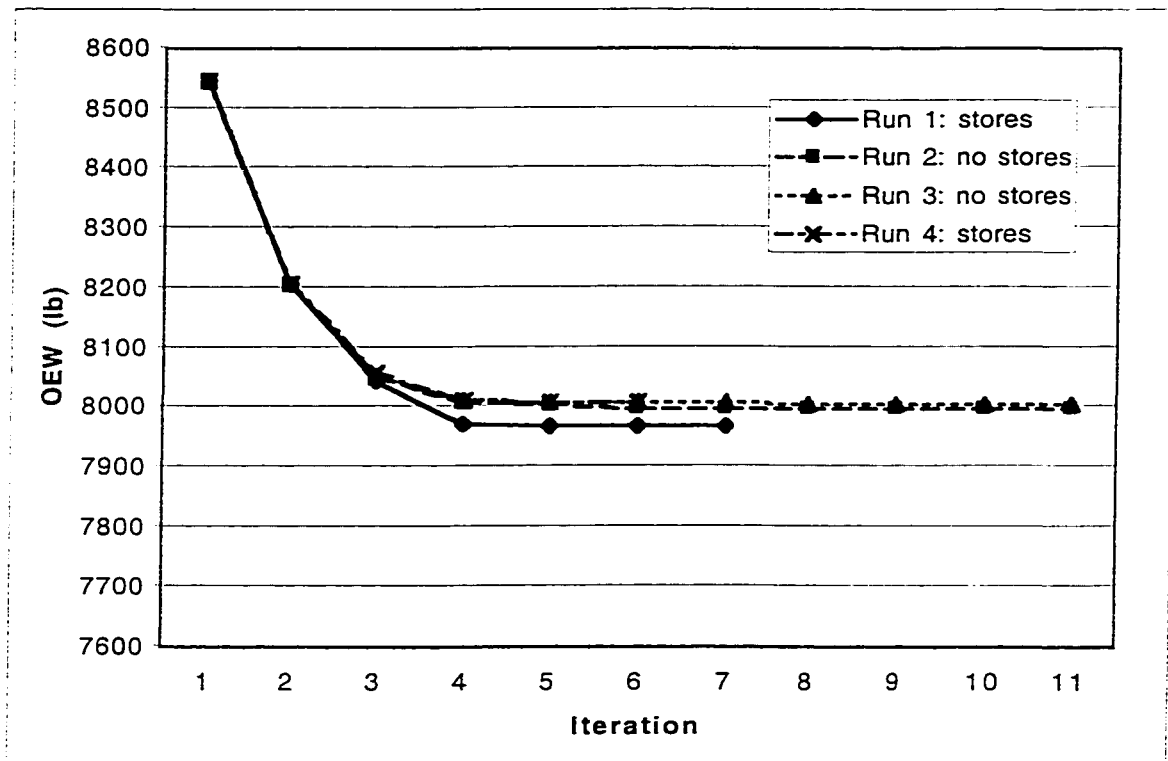


Figure 9-5 Weight History with Multidisciplinary Constraints

The maximum constraint values for each iteration and constraint type are listed in Tables 9-11 and 9-12 for optimization one with underwing stores and optimization two without underwing stores. Of the 1,428 total constraints, 51 were retained as active constraints by MSC-ASTROS in each iteration. The maximum constraint values are plotted in Figures 9-6 and 9-7 to identify which constraint type was driving the optimization. The constraint with the algebraically largest value has the greatest effect on the optimization. In optimizations with and without underwing stores, the lift and aileron effectiveness constraints drove the design in the early iterations. In both optimizations, the von Mises and DTA constraints dominated the design in subsequent iterations up to convergence. The lift effectiveness constraint changed little during these optimizations. The aileron effectiveness constraint didn't participate as much in Run two as it did in Run

one. The constraint values from Runs three and four are similar to Runs two and one. respectively.

The final thicknesses for all runs are listed in Table 9-13. The larger of the values from Runs 3 and 4 should be chosen as the final design variable.

Table 9-11 Maximum Constraint Values with Underwing Stores, Run 1

Iteration	Maximum Constraint Values			
	Lift	Aileron	von Mises	DTA
1	-0.2253	-0.3519	-0.4415	-0.7255
2	-0.2129	-0.2954	-0.1947	-0.5196
3	-0.1883	-0.1896	-0.0651	-0.0836
4	-0.1559	-0.0346	-9.598E-03	-2.043E-03
5	-0.1490	-2.472E-03	1.668E-03	2.446E-03
6	-0.1485	-1.203E-04	1.784E-04	2.921E-05
7	-0.1487	-2.849E-05	9.819E-06	1.359E-05

Table 9-12 Maximum Constraint Values without Underwing Stores, Run 2

Iteration	Maximum Constraint Values			
	Lift	Aileron	von Mises	DTA
1	-0.2622	-0.3516	-0.4548	-0.6564
2	-0.2673	-0.2950	-0.2139	-0.3261
3	-0.2676	-0.1986	-0.0588	8.812E-04
4	-0.2640	-0.1131	4.889E-03	-2.779E-03
5	-0.2619	-0.0770	5.184E-03	2.260E-02
6	-0.2607	-0.0405	7.218E-03	7.095E-03
7	-0.2606	-0.0360	5.022E-05	1.394E-04
8	-0.2605	-0.0332	-9.318E-06	6.235E-05
9	-0.2604	-0.0315	-2.443E-05	3.266E-05
10	-0.2604	-0.0302	-5.337E-05	9.775E-06
11	-0.2604	-0.0292	-3.602E-05	4.888E-06

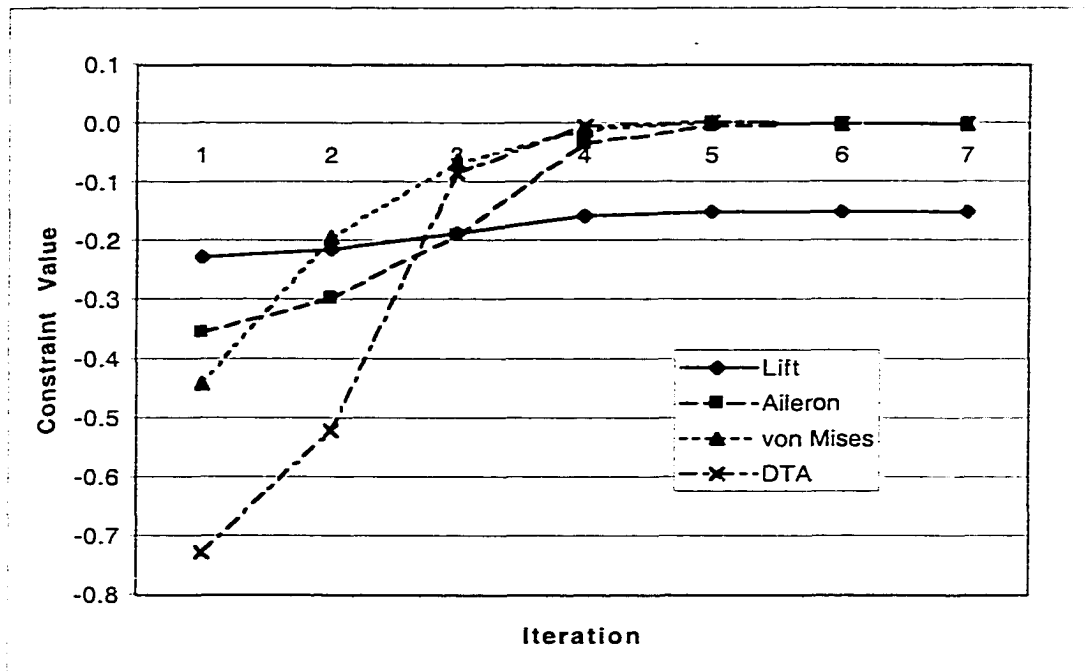


Figure 9-6 Maximum Constraint Values: Underwing Stores, Run 1

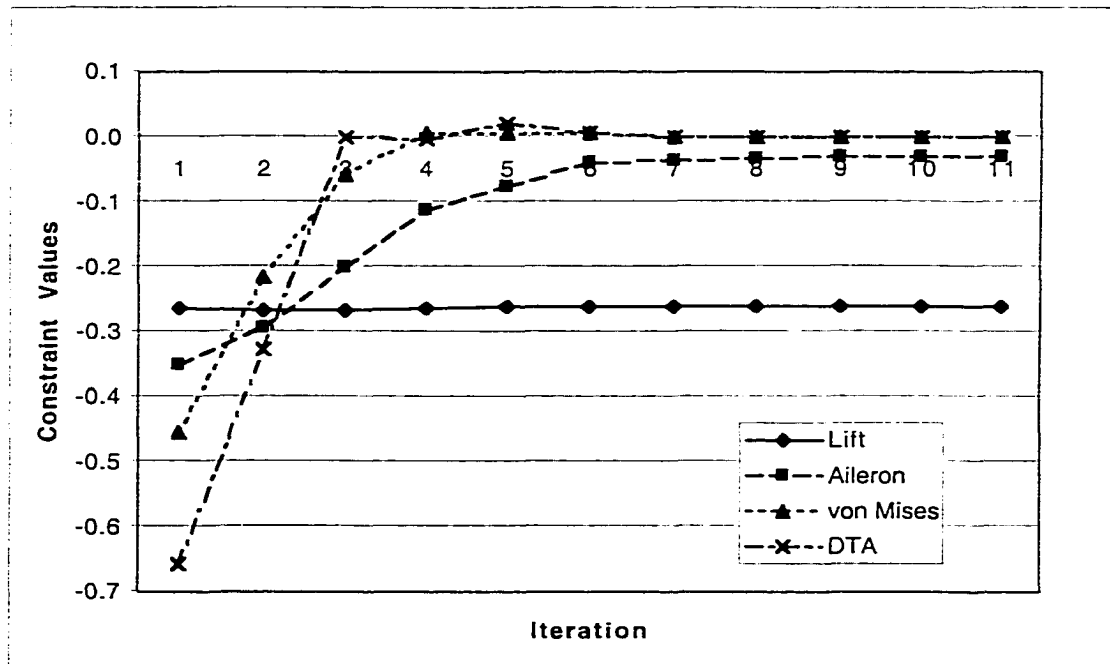


Figure 9-7 Maximum Constraint Values: No Underwing Stores, Run 2

Table 9-13 Final Design Variable Values with Multidisciplinary Constraints

Variable ID	Master Element ID	Final Thicknesses (in)			
		Run 1	Run 2	Run 3	Run 4
1	2663	0.182	0.220	0.232	0.240
2	2562	0.111	0.185	0.123	0.185
3	2674	0.108	0.123	0.125	0.143
4	2566	0.213	0.113	0.213	0.199
5	2573	0.086	0.065	0.086	0.074
6	2425	0.095	0.149	0.170	0.149
7	2598	0.157	0.040	0.157	0.105
8	2414	0.186	0.320	0.328	0.320
9	2502	0.246	0.395	0.349	0.395
10	2451	0.250	0.373	0.358	0.373
11	2555	0.122	0.140	0.144	0.140
12	2549	0.161	0.230	0.235	0.230
13	2497	0.234	0.469	0.429	0.469
14	2603	0.091	0.498	0.520	0.498
15	2544	0.114	0.164	0.168	0.164
16	2623	0.100	0.070	0.100	0.075
17	2488	0.127	0.181	0.164	0.181

9.6 Conclusions

MSC-ASTROS was used together with damage tolerance constraints to optimize cracked skin panels on the lower wing of a fighter/attack aircraft. With an aerodynamic and structural model of this aircraft, MSC-ASTROS simulated symmetric and antisymmetric maneuvers. The objective was to minimize weight without violating the design constraints.

Design optimizations with DTA requirements were performed on the lower wing skin by using the fatigue stress allowable of 22.9 ksi as a maximum principal stress constraint. This fatigue stress allowable ensured that fatigue life and residual strength requirements were met for the through-the-thickness crack configuration. Symmetric maneuver loads, produced by the 9g pull-up, created the highest stresses and essentially

dominated the design optimization of the lower wing skin. This load case contained more active constraints than other load cases and typically the maximum constraint value. Asymmetric maneuver loads should not be ignored, however, as they produce high stresses in some of the hardpoint skin elements and, therefore, controlled the design in these regions. The minimum operational equipment weight computed with damage tolerance analysis constraints was 7,987 lb.

Design optimizations were then performed on the lower wing skin with multidisciplinary constraints. Damage tolerance, von Mises stress, aileron effectiveness, and lift effectiveness constraints were applied to the structure simultaneously for all five load cases. The maximum constraint produced by each of the four constraint types was evaluated in each optimization iteration. The constraint with the algebraically largest value has the greatest effect on the optimization. Although the lift and aileron effectiveness constraints dominated early in the design optimizations, the von Mises and DTA constraints drove the designs in the later iterations in all four runs. The lift and aileron effectiveness constraints didn't contribute as much to optimization two as they did to optimization one with underwing stores. The minimum operational equipment weight computed with multidisciplinary constraints was 7,968 lb and 7,999 lb for Runs one and two, respectively and 8,007 lb and 8,008 lb for Runs three and four, respectively. Optimization of the structure with multiple constraints was more demanding than optimizing with only DTA constraints.

CHAPTER X

CONCLUSIONS AND RECOMMENDATIONS

10.1 Conclusions

Damage tolerance requirements were introduced into the global design optimization of a fighter/attack aircraft. Probabilistic models of the fatigue environment were created from regression analyses of normal load factor, roll rate, and roll acceleration exceedance data using an exponential-polynomial distribution. A flight-by-flight aircraft load history was developed from these probabilistic models. The load factor history was converted into a fatigue stress history using the results of MSC-ASTROS flight maneuver analyses. These flight maneuver results were obtained from an aerodynamic and structural model of a fighter/attack aircraft. The resulting stress history was used by AFGROW to determine the largest fatigue stress allowable to apply in a design optimization with MSC-ASTROS. This fatigue stress allowable became a damage tolerance analysis constraint which ensured that the lower wing skin could safely tolerate a fatigue crack for double the design life of the aircraft. To deal with the mixed-mode fatigue environment in the lower wing skin, the fatigue stress allowable was represented as a maximum principal stress in a pure Mode I fracture environment. With fatigue stress allowable as a maximum principal stress constraint, the lower wing skin was designed to minimum weight.

This initial research in design optimization considered only the DTA constraint. Because of limitations with MSC-ASTROS's nonstructural mass modeling capability, two optimizations were performed with underwing stores representing the air-to-ground

mission and two optimizations without underwing stores representing the air-to-air mission. It was determined that an optimization without underwing stores gives a good approximation of the final weight of an aircraft that must handle both stores configurations. The 9g pull-up load case in the configuration without underwing stores dominated the overall design of the lower wing skin. This maneuver produced the highest stresses in the lower wing skin and the largest number of active constraints. However, roll maneuvers should not be ignored as they controlled the design of the elements near outboard hard points in the underwing store configuration.

The multidisciplinary design optimization showed that both the von Mises and DTA constraints dominated the final optimum design. In both configurations, DTA and von Mises stress constraints produced the highest constraint values. In the configuration with no underwing stores, DTA constraints produced the highest constraint values and, therefore, drove the design. Thus, for an aircraft designed to the constraints used in this research, damage tolerance requirements can play an active role.

It should be emphasized that this research did not attempt to improve on the F-16 design. Its purpose was to develop a methodology or philosophy that considered fatigue failure in the preliminary design process in a multidisciplinary environment. The F-16 design process was no doubt exposed to constraints not considered here such as buckling, flutter, dynamics, store separation, manufacturability, reliability, and maintainability. The exceedance data, mission profiles, and weight configurations were based on general fighter data. These data naturally have a large impact on the fatigue performance of the structure.

10.2 Recommendations

The use of probability to produce flight-by-flight load histories is one example of non-deterministic modeling. Another example, which requires developing a probability density function of the peak stresses in the stress history, is proposed. Together with a probability density function of the residual strength, reliability interference analysis could be performed. The overlap of these two probability density functions would be a measure of reliability. This could be used to compute an associated probability of failure. The residual strength density function would be determined from the distribution of fracture toughness and crack length. The fracture toughness distribution could be found from material statistics, an assumed distribution type, and a Monte Carlo simulation. An increase in crack length would cause a corresponding increase in probability of failure. Probability of failure could be used as a design requirement or, possibly, as an optimization constraint.

The maximum principal stresses in the seventeen master elements were used here in the DTA constraint evaluations. Changing the location and number of master elements and the resulting effect on design optimization should be evaluated. Areas of high stress gradients may be significantly affected by master element location. Increasing the number of master elements would require additional constraint evaluations and, consequently, longer execution times. Selecting the optimum number of master elements with an acceptable level of accuracy and computational time may be possible.

The normalized stress history used to compute the fatigue stress allowable was developed from master element 2549. This stress history and the corresponding fatigue stress allowable from this element were used throughout the lower wing skin during the

optimization. Stress histories for other master elements were ignored in this research because of the excessive computational effort required. Nevertheless, normalized stress histories and their corresponding FSA's should be computed at the other master elements and compared with the FSA from element 2549. Automating the stress history development and FSA determination, through modification of the MSC-ASTROS source files, would make this possible.

The objective in MSC-ASTROS is to minimize structural weight by changing the thicknesses of the lower wing skin elements. This is a constrained optimization. One of the constraints used in this research was the fatigue stress allowable. But fatigue stress allowable is affected by the thickness of element 2549 in 2 ways. Changing the element thicknesses will change the load path and, subsequently, the stress history and the FSA. Thickness is also used in AFGROW for the crack growth analysis needed to find the FSA. Specifically, AFGROW uses thickness to determine the appropriate fracture toughness value, crack growth retardation, and stress intensity factors for elliptical and corner cracks. Changes in FSA should, thus, be evaluated as optimum thicknesses are obtained and used to compute new stress histories and AFGROW analyses. If these changes are significant, then the FSA should be updated and a new optimization performed.

Design trade studies should be performed to determine what parameters have a significant effect on FSA development and subsequent optimization. These trade studies would determine the sensitivity of the fatigue stress allowable to variations in these parameters. In the load history development arena, varying the exceedance data to represent changes in usage could be considered. The resulting stress histories could be

significantly affected by changing the clipping level if crack growth retardation is present. In the materials arena, da/dN data, fracture toughness, and the Willenborg retardation shut-off load ratio (SOLR) would be candidates for variation. The geometries used in the AFGROW fracture mechanics analyses would be parameters of interest. These include panel width, thickness, and whether the crack is a center crack or an eccentrically located crack. If a crack is modeled in a stiffened riveted panel, additional parameters can be evaluated to determine their effects on fatigue stress allowable. These include the ratio of stiffener stiffness to skin stiffness, rivet spacing, stiffener spacing, and rivet flexibility. All of these parameters affect the stress intensity factors that would be used in the AFGROW analyses.

10.3 Final Words

Fatigue failure can require costly in-service inspections, operational restrictions, or structural modifications. Incorporating damage tolerance requirements into the global design optimization can produce a fatigue resistant aircraft wing that will meet its design life requirement without unnecessary weight. Thus, multidisciplinary design optimization with damage tolerance requirements could reduce the overall life cycle costs of aerospace structures.

REFERENCES

- ¹ Gallagher, J. P., Giessler, F. J., and Berens, A. P., "USAF Damage Tolerant Design Handbook: Guidelines for the Analysis and Design of Damage Tolerant Aircraft Structures," AFWAL-TR-82-3073 Rev B, Wright-Patterson Air Force Base, Ohio, 1984.
- ² *Aircraft Structural Integrity Program, Airplane Requirements*, MIL-STD-1530, Aeronautical Systems Division, Wright-Patterson Air Force Base, Ohio, Dec. 1975.
- ³ *Airplane Damage Tolerance Requirements*, MIL-A-83444, Aeronautical Systems Division, Wright-Patterson Air Force Base, Ohio, Jul. 1974.
- ⁴ Broek, D., *The Practical Use of Fracture Mechanics*, Kluwer Academic, Dordrecht, Netherlands, 1989, pp. 2-17
- ⁵ Chaperon, P., Sawyer, J. P., and Jones, R., "Efficient Computational Methodology for Damage Tolerance Assessments in Conjunction with Structural Optimisation: Phase II, Interim Report", Monash University, COE-SM 97-P04, Victoria, Australia, April 1999.
- ⁶ *Axum User's Guide*, 3rd ed., Mathsoft Inc., Cambridge, Massachusetts, 1996.
- ⁷ Johnson, E.H., and Venkayya, V.B., "Automated Structural Optimization System [ASTROS], Vol. I: Theoretical Manual," AFWAL-TR-88-3028/I, Wright-Patterson Air Force Base, Ohio, Apr. 1988.
- ⁸ Harter, J. A., "AFGROW USERS GUIDE AND TECHNICAL MANUAL," AFRL-VA-WP-TR-1999-3016, Wright-Patterson Air Force Base, Ohio, Feb. 1999.
- ⁹ Anderson, T., *Fracture Mechanics: Fundamentals and Applications*, CRC Press, Boca Raton, Florida, 1991.
- ¹⁰ Tada, H., Paris, P., and Irwin, G., *The Stress Analysis of Cracks Handbook*, Paris Productions Inc., St. Louis, Missouri, 1985.
- ¹¹ Brussat, T., "Fatigue Crack Growth Analysis and Military Aircraft Structural Integrity Verification", *Structural Integrity of New and Aging Metallic Aircraft*, Short Course Program, University of California, Los Angeles, California, 1990, pp. 71-72.
- ¹² Fuchs, H. O., and Stephens, R. I., *Metal Fatigue in Engineering*, John Wiley & Sons, New York, New York, 1980.

- ¹³ E 399-90, "Standard Test Method for Plane-Strain Fracture Toughness of Metallic Materials", American Society for Testing and Materials, Philadelphia, 1990.
- ¹⁴ Gallagher, J.P., and Berens, A.P., "Damage Tolerant Design Handbook: A Compilation of Fracture and Crack Growth Data for High-Strength Alloys," WL-TR-94-4052. Wright-Patterson Air Force Base, Ohio, May 1994 (5 volumes).
- ¹⁵ Kantimathi, S., "Introduction to Damage Tolerance Analysis", Short Course Program. Fatigue Concepts, El Dorado Hills, California.
- ¹⁶ E 647, "Standard Method for Measurement of Fatigue Crack Growth Rates". American Society for Testing and Materials, Philadelphia, 1995.
- ¹⁷ Paris, P., and Erdogan, F., "A Critical Analysis of Crack Propagation Law." *Trans. ASME, J. Basic Eng.*, Vol. 85, No. 4, 1963.
- ¹⁸ Walker, E. K., "The Effect of Stress Ratio During Crack Propagation and Fatigue for 2024-T3 and 7075-T6 Aluminum," *Effects of Environment and Complex Load History on Fatigue Life*, STP 462, American Society for Testing and Materials, Philadelphia, Jan. 1970.
- ¹⁹ Forman, R. G., Kearney, V. E., and Engle, R. M., "Numerical Analysis of Crack Propagation in Cyclic-Loaded Structures," *Trans. ASME, J. Basic Eng.*, Vol. 89, No. 3, 1967, pg. 459.
- ²⁰ Bannantine, J., Comer, J., and Handrock, J., *Fundamentals of Metal Fatigue Analysis*, Prentice-Hall, Englewood Cliffs, New Jersey, 1990, pp. 196-201.
- ²¹ Stephens, R. I., Chen, D. K., and Hom, B. W., "Fatigue Crack Growth with Negative Stress Ratio Following Single Overloads in 2024-T3 and 7075-T6 Aluminum Alloys," *Fatigue Crack Growth Under Spectrum Loads*, ASTM STP 595, 1976, p. 27.
- ²² Wheeler, O. E., "Spectrum Loading and Crack Growth," *Trans. ASME, J. Basic Eng.*, Vol. 94, Mar. 1972, pp. 181-186.
- ²³ Willenborg, J., Engle, R. M., and Wood, H. A., "A Crack Growth Retardation Model Using an Effective Stress Concept," AFFDL Tech. Memo. 71-1-1FBR, Wright-Patterson Air Force Base, Ohio, Jan. 1971.
- ²⁴ Dill, H. D., and Saff, C. R., "Environment-Load Interaction Effects on Crack Growth," AFFDL-TR-78-137, Wright-Patterson Air Force Base, Ohio, Nov. 1978.

- ²⁵ Chanani, G. R., "Fundamental Investigation of Fatigue Crack Growth Retardation in Aluminum Alloys," AFML-TR-76-156, Air Force Materials Laboratory, Wright-Patterson Air Force Base, Ohio, Sept. 1976.
- ²⁶ Wei, R. P., Shih, T. T., and Fitzgerald, J. H., "Load Interaction Effects on Fatigue Crack Growth in Ti-6Al-4V Alloy," NASA CR-2239, Apr. 1973.
- ²⁷ Elber, W., "Fatigue Crack Closure Under Cyclic Tension," *Engineering Fracture Mechanics*, Vol. 2, No. 1, 1970, pp. 37-45.
- ²⁸ Hudson, C. M., "Effect of Stress Ratio on Fatigue Crack Growth in 7075-T6 and 2024-T3 Aluminum Alloy Specimens," NASA TN D-5390, Aug. 1969.
- ²⁹ Chang, J. B., and Stolpestad, J. H., "Improved Methods for Predicting Spectrum Loading Effects – Phase I Report (Vol. 1, Results and Discussions)," AFFDL-TR-79-3036, Wright-Patterson Air Force Base, Ohio, Mar. 1979.
- ³⁰ Budiansky, B., and Hutchinson, J., "Analysis of Closure in Fatigue Crack Growth," *Journal of Applied Mechanics*, Vol. 45, 1978.
- ³¹ Giessler, F., Duell, S., and Cook, R., "Handbook of Guidelines for the Development of Design Usage and Environmental Sequences for USAF Aircraft", AFWAL-TR-80-3156, Wright Patterson Air Force Base, Ohio, Feb. 1981, pp. 4.11-4.12.
- ³² Richmond, L., "Aircraft Dynamic Loads from Substandard Landing Sites," AFFDL-TR-67-145, Wright-Patterson Air Force Base, Ohio, Part V, Volume II, 1967.
- ³³ Newman, R., K. and Berens, A., P., "Analysis for the Determination of Significant Runway Roughness," AFFDL-TR-73-109, Wright-Patterson Air Force Base, Ohio, Nov. 1973.
- ³⁴ "A-10A Aircraft Fatigue Load Spectra," SR160R0003, Fairchild Republic Company, Farmingdale, New York, 18 Feb. 1975.
- ³⁵ Lomax, T., *Structural Loads Analysis for Commercial Transport Aircraft: Theory and Practice*, American Institute of Aeronautics and Astronautics, Reston, Virginia, 1996.
- ³⁶ Houbolt, J., Steiner, R., and Pratt, K. G., "Dynamic Response of Airplanes to Atmospheric Turbulence Including Flight Data on Input and Response," NASA Technical Report R-199, June 1964.

- ³⁷ Press, H., Meadows, M. T., and Hadlock, I., "A Reevaluation of Data on Atmospheric Turbulence and Airplane Gust Loads for Application in Spectral Calculations," NACA Report 1272, 1956.
- ³⁸ Eichenbaum, F., "Response of Aircraft to Three Dimensional Random Turbulence," AFFDL-TR-72-28, Air Force Flight Dynamics Laboratory, Wright-Patterson Air Force Base, Ohio, Oct. 1972.
- ³⁹ Rice, S. O., "Mathematical Analysis of Random Noise," Parts I and II, *Bell System Tech. Journal*, Volume XXII, No. 2, July 1974, pp. 282-332; Parts III and IV, Volume XXIV, No. 1, January 1945, pp. 45-156.
- ⁴⁰ Lincoln, J. W., "Development of an Aircraft Maneuver Load Spectrum Based on VGH Data," ASD-TR-80-5037, Wright-Patterson AFB, Ohio, July 1980.
- ⁴¹ Johnson, L. G., "The Median Ranks of Sample Values in Their Population with an Application to Certain Fatigue Studies", *Industrial Mathematics*, Vol. 2, 1951, pp. 1-9.
- ⁴² Abernathy, R., *The New Weibull Handbook*, Author and Publisher, 1993. pp. 2-5 - 2-9
- ⁴³ Johnson, L. G., *Theory and Technique of Variation Research*, Elsevier Publishing Company, New York, New York, 1964, pp. 1-6.
- ⁴⁴ Nelson, W., *Applied Life Data Analysis*, Wiley, New York, 1982.
- ⁴⁵ Montgomery, D. C., Runger, G. C., and Hubele, N. F., *Engineering Statistics*, John Wiley & Sons, New York, New York, 1998, pp. 322-324.
- ⁴⁶ Arrieta, A., and Striz, A., "Normal Load Factor Data Regression Analyses", *XLIX Oklahoma AIAA/ASME Symposium*, American Institute of Aeronautics and Astronautics and American Society for Mechanical Engineers, Oklahoma City, Oklahoma, February 1999.
- ⁴⁷ Rao, S. S., *Reliability-Based Design*, New York, New York, McGraw-Hill, 1992, p. 50.
- ⁴⁸ "Analysis Methods Document", *Repair Assessment Procedure and Integrated Design (RAPID)*, Version 2.0, Appendix C, Federal Aviation Administration, Atlantic City, New Jersey, July 1997.
- ⁴⁹ Love, M., Barker, D., and Bohlmann, J., "An Aircraft Design Application Using ASTROS," WL-TR-93-3037, Wright-Patterson AFB, Ohio, June 1993.

⁵⁰ *Hypermesh User's Guide*, Altair Engineering, Troy, Michigan, 2000.

⁵¹ Broek, D., *Elementary Engineering Fracture Mechanics*, Kluwar Academic Publishers, Dordrecht, Netherlands, 1991.

⁵² Curtis, H., *Fundamentals of Aircraft Structural Analysis*, Irwin, Times Mirror Higher Education Group, Chicago, Illinois, 1997, pp 150-152.

⁵³ Johnson, E.H., and Neill, D., "Automated Structural Optimization System [ASTROS], Vol. III: Applications Manual," AFWAL-TR-88-3028/III, Wright-Patterson AFB, Ohio. Dec. 1988, pp. 86-105.

Appendices

Appendix A

Load_occurrence.exe

Input File Format for Load_occurrence.exe

Enter *segname*, *seglife*, and *mission* through standard input device

ssfactor, safactor, asfactor, aafactor
 nzcode
 nz(1)
 nz(2)
 nz(3)
 etc
 nz(nzcode)
 totlneg
 ndeltan
 aneg, bneg, cneg, dneg, eneg, gneg
 totlpos
 pdeltan
 apos, bpos, cpos, dpos, epos, gpos

Definitions:

Variable	Description	Type
segname	segment name	character size 20
seglife	total segment hours per aircraft life	real
mission	number of missions in aircraft life	integer
ssfactor	symmetric steady prorated factor	real
safactor	symmetric abrupt prorated factor	real
asfactor	asymmetric steady prorated factor	real
aafactor	asymmetric abrupt prorated factor	real
nzcode	number of n_z levels	integer
nz(i)	normal load factor levels	real
totlneg	total number of negative occurrences	real
ndeltan	negative load factor range	real
xneg	negative n_z regression constants	real
totlpos	total number of positive occurrences	real
pdeltan	positive load factor range	real
xpos	positive n_z regression constants	real

air-air.inp file

.18,.02,.7,.1
25
-2.5
-2.0
-1.5
-1.0
-0.5
0.0
0.5
1.5
2.0
2.5
3.0
3.5
4.0
4.5
5.0
5.5
6.0
6.5
7.0
7.5
8.0
8.5
9.0
9.5
10.0
173727.0
0.25
0.00534403124062,3.91816576205813,2.63820833828157,1.695432607360310,0.29676358726775,0.
408139.12299
0.25
1.237865292,-0.08894300960529,-0.07687942649981,0.,0.,0.

air-ground.inp file

.075,.675,.2,.05
18
-2.0
-1.5
1.5
2.0
2.5
3.0
3.5
4.0
4.5
5.0
5.5
6.0
6.5
7.0
7.5
8.0
8.5
9.0
4.2000
0.25
7.265060305344820,1.58646127823385,0.,0.,0.,0.
224303.10411
0.25
0.778767808288,0.43694880056789,-0.18953194198649,0.,0.,0.

ascent.inp file

```
.5,0.05,.4,.05
6
1.5
2.0
2.5
3.0
3.5
4.0
0.0
0.25
0.,0.,0.,0.,0.,0.
76627.4
0.25
39.441452,-2.612233862746,-0.2620960117415,0.,0.,0.
```

cruise.inp file

```
.5,.05,.4,.05
8
1.5
2.0
2.5
3.0
3.5
4.0
4.5
5.0
0.
0.25
0.,0.,0.,0.,0.,0.
25035.676701
0.25
212896029.714465,-35.893001345452,25.4937825696542,-9.00358897296246,1.53785212950606,-
0.1027228146404010
```

descent.inp file

```
0.5,0.05,0.45
8
1.5
2.0
2.5
3.0
3.5
4.0
4.5
5.0
0.
0.25
0.,0.,0.,0.,0.,0.
44744.7726
0.25
0.468663458496,2.48323261676705,-2.12213697134575,0.573732286289668,-0.06180957563788,0.
```

formation.inp file

```
.5,.05,.4,.05
18
-2.0
-1.5
-1.0
-0.5
0.0
0.5
1.5
2.0
2.5
3.0
3.5
4.0
4.5
5.0
5.5
6.0
6.5
7.0
131428.4
0.25
0.053892750236626,5.17169022635526,-1.105431535842390,-
0.79692590644798,0.,0.
171909.2
0.25
228.317833913365,-5.53474182815898,1.06480705828766,-
0.090149073917168,0.,0.
```

instrument-navigate.inp file

```
.5,.05,.4,.05
17
-2.0
-1.5
-1.0
-0.5
0.0
0.5
1.5
2.0
2.5
3.0
3.5
4.0
4.5
5.0
5.5
6.0
6.5
36284.82712
0.25
0.074144284612993,5.44472753969549,-1.756445679257920,-1.17049521327695,0.,0.
36855.5402
0.25
376.953695842674,-6.84829465404254,2.10519138824747,-
0.366099770431446,0.02208687322489,0.
```

loiter.inp file

```
.5,.05,.4,.05
10
1.5
2.0
2.5
3.0
3.5
4.0
4.5
5.0
5.5
6.0
0.
0.25
0.,0.,0.,0.,0.,0.
68607.6243
0.25
22.312440109248,-2.82275635517908,0.31874317076790,-
0.038264389482450,0.,0.
```

Load_occurrence.exe

```
      real prob, occ, nz(25), remandr, rcycle, rmision, sumprob, ssfactor,
+safactor, seglife, asfactor, negnz(70000), posnz(70000), aneg, bneg,
+cneg, dneg, eneg, gneg, apos, bpos, cpos, dpos, epos, gpos, totlneg, totlpos,
+ndeltan, pdeltan, aafactor, posp(70000), negp(70000), prate(10),
+ptemp, truocc, paccel(8), npa(70000), ppa(70000), patemp

      integer i, k, l, start, fin, lastfin, sumocc, ssocc, saocc, Lasocc,
+Rasocc, Laaocc, Raaocc, mission, segcycl, extra, n, cyc, nzcode,
+count, pocc(10), p, pdctoc(8), pcount

      character*6 negmnv(70000), posmnv(70000), type, segname*20,
+summary*40, history*40

      common seglife

      common
aneg, bneg, cneg, dneg, eneg, gneg, apos, bpos, cpos, dpos, epos, gpos
+, totlneg, totlpos

c      Mission distribution information
c          unit 1 = segment name
c          seglife = # segment hours for A/C life
c          mission = # missions in A/C life

c      Repeated loads criteria(prorate factors)
c          ssfactor = symmetric steady, safactor = symmetric abrupt
c          asfactor = asymmetric steady, aafactor = asymmetric abrupt

c      *** input data standard device ***
write(*,*) "Enter segment file name"
      open(unit=1, file="", status="old", filetype="TEXT")

write(*,*) "Enter mission type segment name(ie. T_ascent)"
read(*,*) segname
write(*,*) "Enter segment life hours for mission type"
read(*,*) seglife
write(*,*) "Enter number of missions"
read(*,*) mission

c      *** Read maneuver factors from segment input file ***
read(1,*) ssfactor, safactor, asfactor, aafactor
      if(ssfactor + safactor + asfactor + aafactor .ne. 1.0)then
          write(*,*) "Maneuver factors don't sum to 1! Check input
file."
          stop ! if sum not equal to 1, stop execution
      endif

c      *** Create output files "_summary.out" and "_history.out" ***
summary = segname(1:len_trim(segname)) // '_summary.out'
history = segname(1:len_trim(segname)) // '_history.out'
open(unit=2, file=summary)
open(unit=3, file=history)
```

```

        read(1,*) nzcode      !number of Nz load levels
        do 2 i=1,nzcode
2          read(1,*) nz(i) !Normal Load factor levels

        read(1,*) totlneg  ! total number of negative occurrences
        read(1,*) ndeltan  ! negative load factor range
        read(1,*) aneg,bneg,cneg,dneg,eneg,gneg !negative regression
constants

        read(1,*) totlpos  ! total number of positive occurrences
        read(1,*) pdeltan  ! positive load factor range
        read(1,*) apos,bpos,cpos,dpos,epos,gpos !positive regression
constants

c      Set positive and negative load factor to 1.0 g
        do 3 i=1,70000
        posnz(i) = 1.0
        negnz(i) = 1.0
        posp(i) = 0.0
        negp(i) = 0.0
        npa(i) = 0.0
        ppa(i) = 0.0
3      negmnv(i) = '-----'

        write(2,5) ssfactor, safactor, asfactor,aafactor
        write(7,5) ssfactor, safactor, asfactor,aafactor

5      format('i',3x,'Nz',5x,'prob',13x,'occ',7x,'steady-',f4.3,2x,
+'abrupt-',f4.3,1x,'asymmetric-',f4.3,6x,'abrupt-',f4.3,/,
+62x,'Left',6x,'Right',7x,'Left',6x,'Right')

c      Initialize variables before main loop
        start = 1
        lastfin = 0
        sumocc = 0
        truocc = 0.0
        sumprob = 0.0

        do 10 i=1,nzcode
c      calculate cumulative probability at +- deltan g
        call nzprob(i,nz,occ,prob,sumprob,ndeltan,pdeltan)

c      calculate occurrences for symmetric steady/abrupt and asymmetric
steady/abrupt
        ssocc = nint(ssfactor * occ)
        saocc = nint(safactor * occ)
c      asymmetric maneuvers split between left and right
        Lasocc = nint(asfactor/2. * occ)
        Rasocc = nint(asfactor/2. * occ)
        Laaocc = nint(aafactor/2. * occ)
        Raaocc = nint(aafactor/2. * occ)
        sumocc = sumocc + ssocc + saocc + Lasocc + Rasocc + Laaocc+Raaocc

        call roll(Lasocc,pocc,prate)
        call pdot(Laaocc,pdotoc,paccel)

        do 30 k=1,6

```



```

        if(k .eq. 1)then ! index symmetric steady occurrences
            fin = ssocc + lastfin
            type = 'steady'
        endif

        if(k .eq. 2)then ! index symmetric abrupt occurrences
            fin = saocc + fin
            type = 'abrupt'
        endif

        if(k .eq. 3)then ! index asymmetric steady occurrences
            fin = Lasocc + fin
            type = 'Lasyms'
        endif

        if(k .eq. 4)then ! index asymmetric steady occurrences
            fin = Rasocc + fin
            type = 'Rasyms'
        endif

        if(k .eq. 5)then ! index asymmetric abrupt occurrences
            fin = Laaocc + fin
            type = 'Lasyma'
        endif

        if(k .eq. 6)then ! index asymmetric abrupt occurrences
            fin = Raaocc + fin
            type = 'Rasyma'
        endif
        p = 1
        ptemp = 0.0
        patemp = 0.0
        count = start + pocc(p)
        pcount = start + pdotoc(p)

        do 40 l=start,fin ! assign global index to each occurrence
c      *** Determine number of roll rate occurrences ***
            if(type .eq. 'Lasyms' .or. type .eq. 'Rasyms')then

                if (l .lt. count) then
                    ptemp = prate(p)
                else
                    p = p + 1
                    count = count + pocc(p)
                    ptemp = prate(p)
                    if(pocc(p) .eq. 0)then ! if loop counter > sum
occ's, (because of round off error)
c                        write(2,*) "pocc = 0" ! last occ will have p=0.25
rad/s
                        ptemp = .25
                    endif
                endif
            endif
        enddo

c      *** determine number of roll acceleration occurrences ***
            if(type .eq. 'Lasyma' .or. type .eq. 'Rasyma')then

```

```

c          if (i .eq. 6) then
c              write(2,*) " "
c              write(2,*) type
c              write(2,*) "start=",start, "finish=",fin
c              write(2,*) "    p=",p,"pcount=",pcount,"pdotoc=",pdotoc(p)
c              endif

              if (l .lt. pcount) then
                  patemp = paccel(p)
              else
                  p = p + 1
                  pcount = pcount + pdotoc(p)
c              write(2,*) "    new p=",p,"new pcount=",pcount
                  patemp = paccel(p)
                  if(pdotoc(p) .eq. 0)then ! if loop counter > sum
occ's, (because of round off error)
c                      write(2,*) "pdotoc = 0" ! last occ will have
pdot=1.00 rad/s2
                          patemp = 1.00
                      endif
                  endif
              endif

              if(nz(i) .lt. 1.0)then
                  negnz(l) = nz(i)
                  negmnv(l) = type
                  negp(l) = ptemp
                  npa(l) = patemp
              else
                  posnz(l) = nz(i)
                  posmnv(l) = type
                  posp(l) = ptemp
                  ppa(l) = patemp

              endif

c          if (i .eq. 6 .and. (k .eq. 5 .or. k .eq. 6)) then
c              write(2,*) "                l=",l,"pdot=",patemp
c              endif

40      continue

30      start = fin + 1
        lastfin = fin

c      *** Reinitialize counters for positive nz data ***
        if(nz(i) .eq. 0.5)then
            start = 1
            lastfin = 0
        endif

        write(2,25) i,nz(i),prob,occ,ssocc,saocc,Lasocc,Rasocc,Laaocc,
+Raaocc
        write(*,25) i,nz(i),prob,occ,ssocc,saocc,Lasocc,Rasocc,Laaocc,
+Raaocc
25      format(i2,3x,f4.1,3x,e10.4,3x,f8.1,6(3x,i8.1))

```

```

        truocc = occ + truocc ! compute the true sum of occurrences
without rounding
10      continue

        call
r(negnz,negmnv,posnz,posmnv,negp,posep,npa,ppa,sumocc,fin,cyc)

c      Select and print the cycles for each mission
      write(3,*) "segment type: ",segname
      remandr = 0.0
      start = 1
      fin = 0
      do 70 i=1,mission
        segcycl = cyc/mission

        rcycle = cyc
        rmision = mission
        remandr = rcycle/rmision - segcycl + remandr !calculate
remainder sum

        if(remandr .ge. 1.0)then
          segcycl = segcycl + 1 !if remainder sum is > 1 then add 1
occurrence
          remandr = remandr - 1.0
        endif
        fin = segcycl + fin
        write(3,*) " "
        write(3,84)"Flight",i,"No. cycles =",segcycl
        write(3,75)"cycle","load factor","maneuver
type","p(rad/s)",
+          "pdot(rad/s2)"
75      format(a5,2x,a11,2x,a13,2x,a8,1x,a12)

        n = 1
        do 80 j = start,fin
          write(3,85)n,posnz(j),posmnv(j),posep(j),ppa(j)
          write(3,86)negnz(j),negmnv(j),negp(j),npa(j)
84      format(A6,1x,I4,5x,A12,1x,I4)
85      format(i5,7x,f4.1,9x,a6,5x,f5.2,5x,f6.2)
86      format(12x,f4.1,9x,a6,5x,f5.2,5x,f6.2)
80      n = n + 1

70      start = fin + 1

      write(2,*) "segment type: ",segname
      write(*,*) "segment type: ",segname
      write(2,*) "sum probability =",sumprob
      write(*,*) "sum probability =",sumprob
      write(2,*) "total segment hours per A/C life =",seglife
      write(*,*) "total segment hours per A/C life =",seglife

      write(2,*) "# of missions with segment =",mission
      write(*,*) "# of missions with segment =",mission

      write(2,*) "sum segment occurrences per A/C life =",sumocc
      write(*,*) "sum segment occurrences per A/C life =",sumocc
      write(2,*) "true sum segment occurrences =",truocc

```

```

write(*,*) "true sum segment occurrences =",truocc

write(2,*) "sum segment cycles per A/C life =",cyc
write(*,*) "sum segment cycles per A/C life =",cyc

c   Determine the number of cycles for each segment
      segcycl = cyc/mission
      write(*,*) "number of cycles per segment =",segcycl
      write(2,*) "number of cycles per segment =",segcycl

c   Determine the number of missions with an extra cycle
      extra = cyc - segcycl*mission
      write(*,*) "number of missions with extra cycle =",extra
      write(2,*) "number of missions with extra cycle =",extra
stop
end

c   *** Load Factor Spectra Probability Analysis Subroutine ***
subroutine nzprob(i,nz,occ,prob,sumprob,ndeltan,pdeltan)

  real nz(25),sumprob,seglife,occ,total,prob,F(2),x(2),a,b,c,d,e,g,
+aneg,bneg,cneg,dneg,eneg,gneg,apos,bpos,cpos,dpos,epos,gpos,
+totlneg,totlpos,ndeltan,pdeltan

  integer i,n

  common seglife

  common aneg,bneg,cneg,dneg,eneg,gneg,apos,bpos,cpos,dpos,epos,
+gpos,totlneg,totlpos

c   Curve fitting

do 50 n = 1,2
if(nz(i) .le. 1.0) then ! Negative load spectra curve fit
  total=totlneg
  a=aneg
  b=bneg
  c=cneg
  d=dneg
  e=eneg
  g=gneg
  x(2)=nz(i) + ndeltan
  x(1)=nz(i) - ndeltan

else ! Positive load spectra curve fit
  total=totlpos
  a=apos
  b=bpos
  c=cpos
  d=dpos
  e=epos
  g=gpos
  x(2)=nz(i) + pdeltan
  x(1)=nz(i) - pdeltan
endif
c   Curve fitting equation of Probability Distribution Function
50  F(n)=a*exp(b*x(n)+c*x(n)**2+d*x(n)**3+e*x(n)**4+g*x(n)**5)

```

```

        if(nz(i) .eq. 1.5)then ! extrapolation parabolic correction
            F(1) = 1.0
        endif
        prob = abs(F(1) - F(2))    ! calculate corresponding
probability
        occ = prob * total    ! calculate total number of
occurrences

c      calculate number of segment occurrences per life
        occ = seglife * occ/1000.0
        sumprob=sumprob + prob

7      return
      end

c      *** Randomly order the segment occurrences for A/C life time
Subroutine ***
      subroutine r(negnz,negmnv,posnz,posmnv,negp,pozp,npa,ppa,sum,f,c)
        real negnz(70000),posnz(70000),jindex,negp(70000),pandex,
+         posp(70000),pindex,npa(70000),ppa(70000),npandx
        integer i,j,seed,sum,m,negl原因,f,c
        character*6 negmnv(70000),posmnv(70000),mindex

c      Compute RAN seed from system time in seconds
        include "DateTimeUtils.inc"
        record /DateTimeRec/ DateTime
        call GetTime(DateTime)
c      seconds raise to power of 3 to increase difference in seeds for
c      subsequent program executions.
        seed = DateTime.hour*3600+DateTime.minute*60 + DateTime.second**3

        neglast = sum - f          ! compute total # of negative
occurrences

c      set #negative occurrences = #positive occurrences
        if(neglast .lt. f)then
            neglast = f
            m = neglast              ! set m = # positive
occurrences
        elseif(f .lt. neglast)then
            f = neglast
            m = f                    ! set m = # positive occurrences
        endif

c      Randomly order negative occurrences
c      Range of numbers needed:  1 <= x < (m+1), excluding (m+1)
c      Range of Random generator: 0 <= x < 1
        do 10 i=1,negl原因
            j = int(RAN(seed)*m + 1)    ! j = Ran * #occurrences + 1
            jindex = negnz(j)          ! remember old nz(j)
            mindex = negmnv(j)
            pindex = negp(j)
            npandx = npa(j)

```

```

        negnz(j) = negnz(m)                ! set new nz(j) =
nz(#occurrences)
        negmnv(j) = negmnv(m)
        negp(j) = negp(m)
        npa(j) = npa(m)

        negnz(m) = jindex                  ! set new nz(#occurrences) =
old nz(j)
        negmnv(m) = mindex
        negp(m) = pindex
        npa(m) = npandx

10    m = m-1                              ! decrease # occurrences by 1

c    Randomly order positive occurrences
    m=f
    do 20 i=1,f                            ! f = total # positive occurrences
        j = int(RAN(seed)*m + 1)
        jindex = posnz(j)
        mindex = posmnv(j)
        pindex = posp(j)
        pandex = ppa(j)

        posnz(j) = posnz(m)
        posmnv(j) = posmnv(m)
        posp(j) = posp(m)
        ppa(j) = ppa(m)

        posnz(m) = jindex
        posmnv(m) = mindex
        posp(m) = pindex
        ppa(m) = pandex

20    m = m-1
    c = f                                  ! #cycles = # positive occurrences

    return
end

subroutine roll(Lasocc,pocc,prate)
real a,b,c,d,e,g,x(2),prate(10),prob,F(2)
integer i,j,Lasocc,pocc(10)

prate(1) =0.25
prate(2) =0.75
prate(3) =1.25
prate(4) =1.75
prate(5) =2.25
prate(6) =2.75
prate(7) =3.25
prate(8) =3.75
prate(9) =4.25
prate(10)=4.75

a = 1.0
b = -.4642
c = -1.04

```

```

d = .2567
e = -.02888
g = 0.0

do 10 i =1,10
x(2) = prate(i) + .25
x(1) = prate(i) - .25

do 20 j = 1,2
20   F(j)=a*exp(b*x(j)+c*x(j)**2+d*x(j)**3+e*x(j)**4+g*x(j)**5)

prob = F(1) - F(2)
pocc(i) = nint(prob*Lasocc)

c   **** if Lasocc=1 but pocc(1) is zero because of round off, set
pocc(1)=1 ****
      if(Lasocc .eq. 1 .AND. pocc(1) .eq. 0)then
          pocc(1) = 1
      endif

c   print*, "pocc", i, pocc(i)
10   continue
      return
      end

subroutine pdot(Laaocc, pdotoc, paccel)
real a,b,c,d,e,g,x(2),paccel(8),prob,F(2)
integer i,j,Laaocc,pdotoc(8)

paccel(1) =1.0
paccel(2) =3.0
paccel(3) =5.0
paccel(4) =7.0
paccel(5) =9.0
paccel(6) =11.0
paccel(7) =13.0
paccel(8) =15.0

c   *** extrapolation parabolic correction = 166,318 @ pdot = 0.0 ***
a = 129800./166318.
b = 0.0185
c = -.1555
d = .006318
e = 0.0
g = 0.0

do 10 i =1,8
x(2) = paccel(i) + 1.0
x(1) = paccel(i) - 1.0

do 20 j = 1,2
      if(x(j) .eq. 0.)then ! extrapolation parabolic correction
          F(j) = 1.0
      else
          F(j)=a*exp(b*x(j)+c*x(j)**2+d*x(j)**3+e*x(j)**4+g*x(j)**5)
      endif
20   continue

```

```

        prob = F(1) - F(2)
        pdotoc(i) = nint(prob*Laaocc)

c      **** if Laaocc=1 but pdotoc(1) is zero because of round off, set
pdotoc(1)=1 ****
        if(Laaocc .eq. 1 .AND. pdotoc(i) .eq. 0) then
            pdotoc(1) = 1
        endif

c      write(2,*) "pdotoc",pdotoc(i),"paccel=",paccel(i)
10     continue
        return
    end

```


Appendix B

Mission Segment Regression Analyses

Regression Analyses of Normal Load Factor Exceedance for Fighter Aircraft Segments

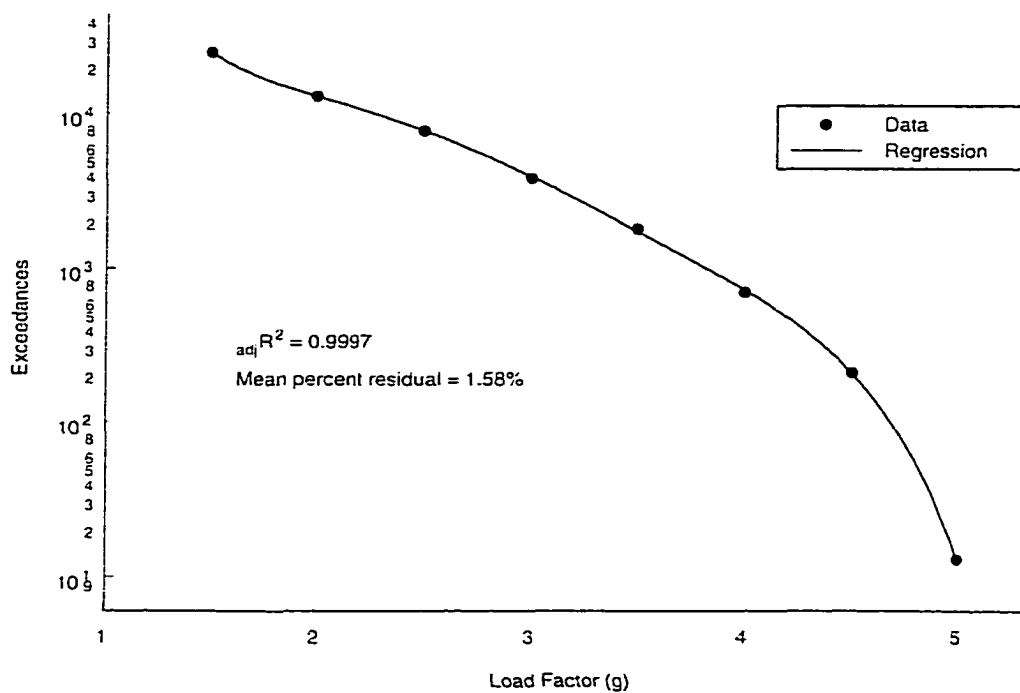


Figure B-1 Cruise Segment

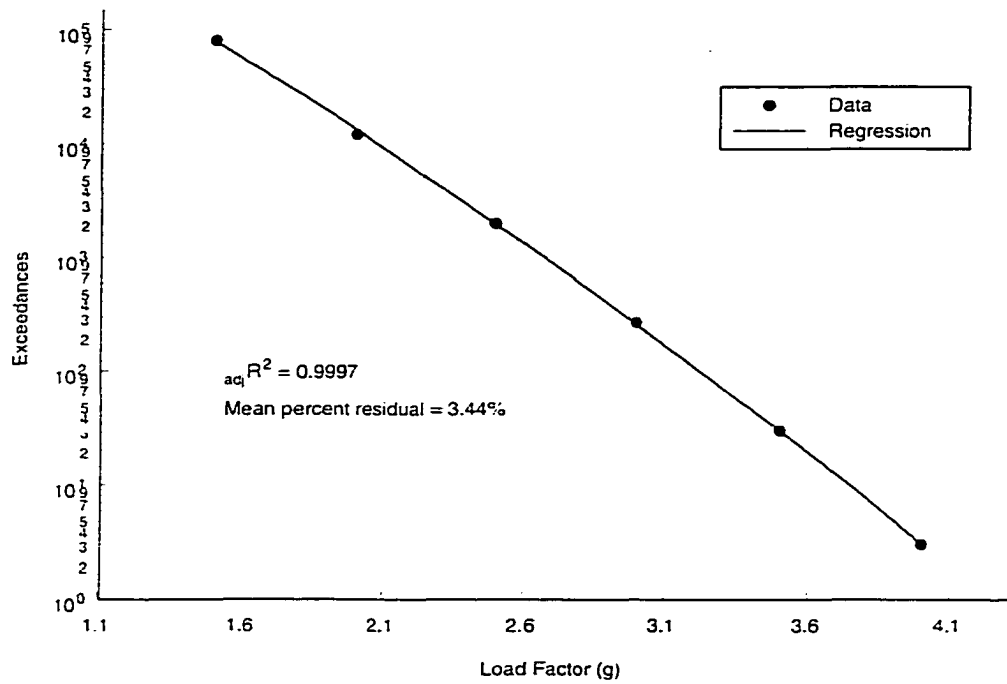


Figure B-2 Ascent Segment

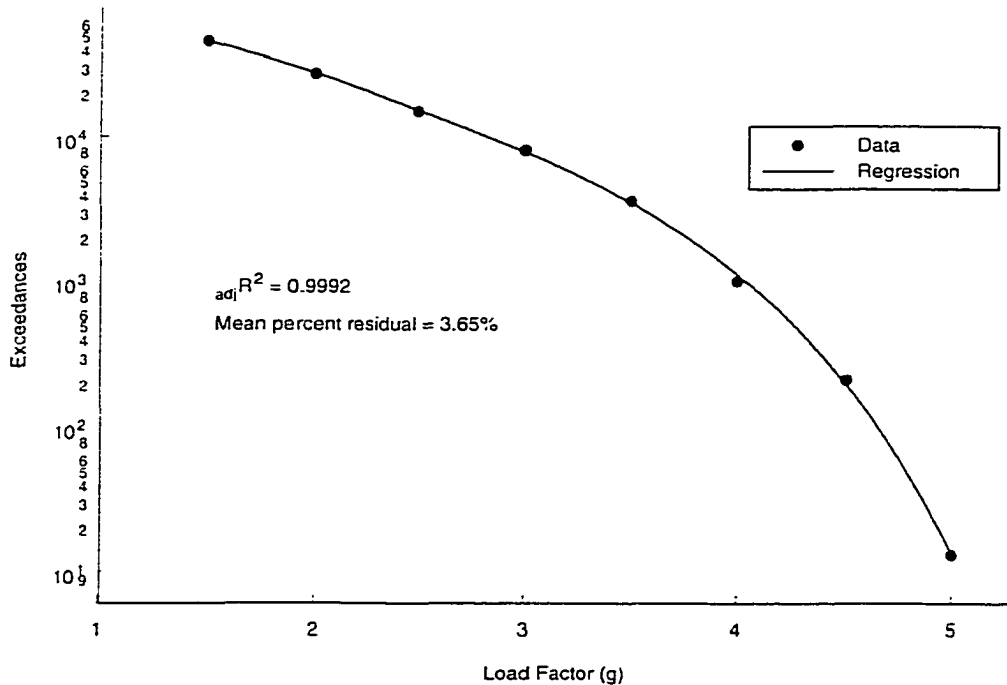


Figure B-3 Descent Segment

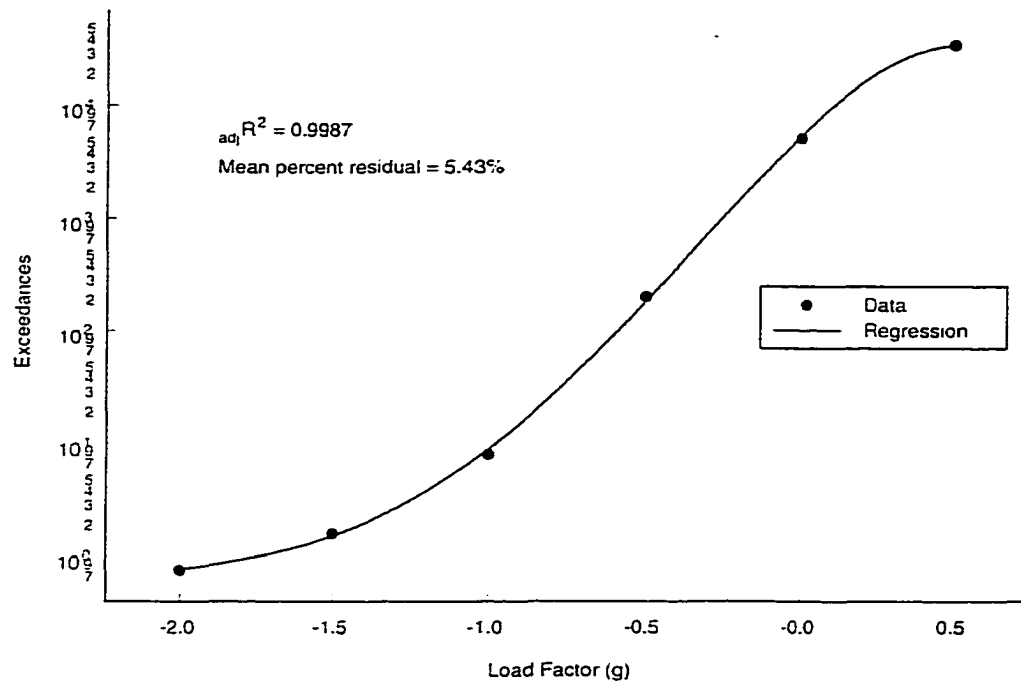


Figure B-4 Instrument & Navigation Segment: Negative Load Factors

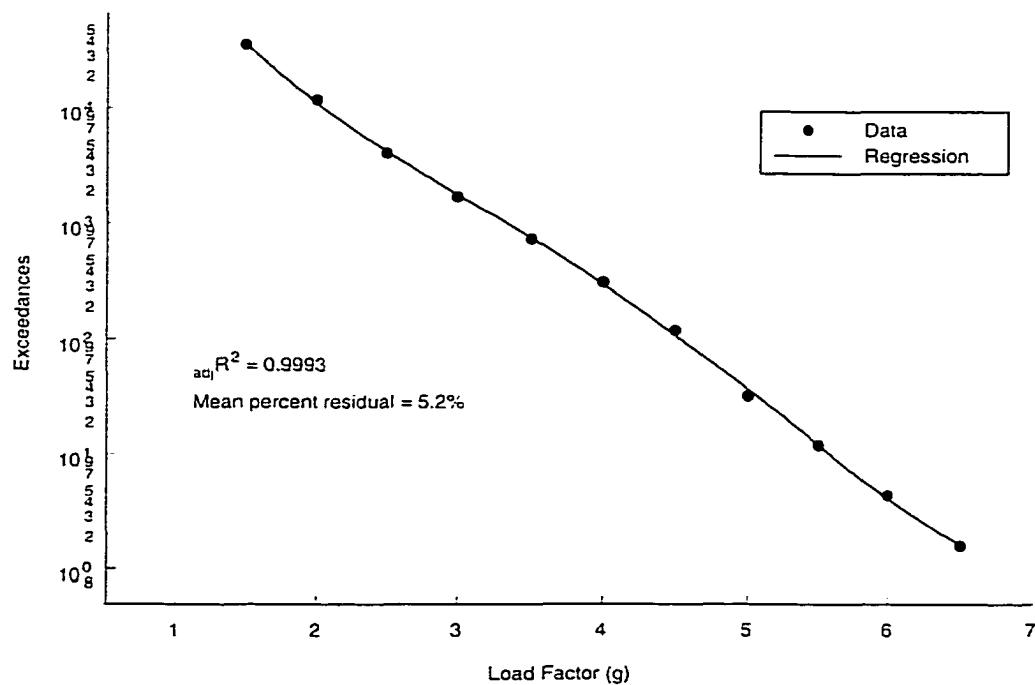


Figure B-5 Instrument & Navigation Segment: Positive Load Factors

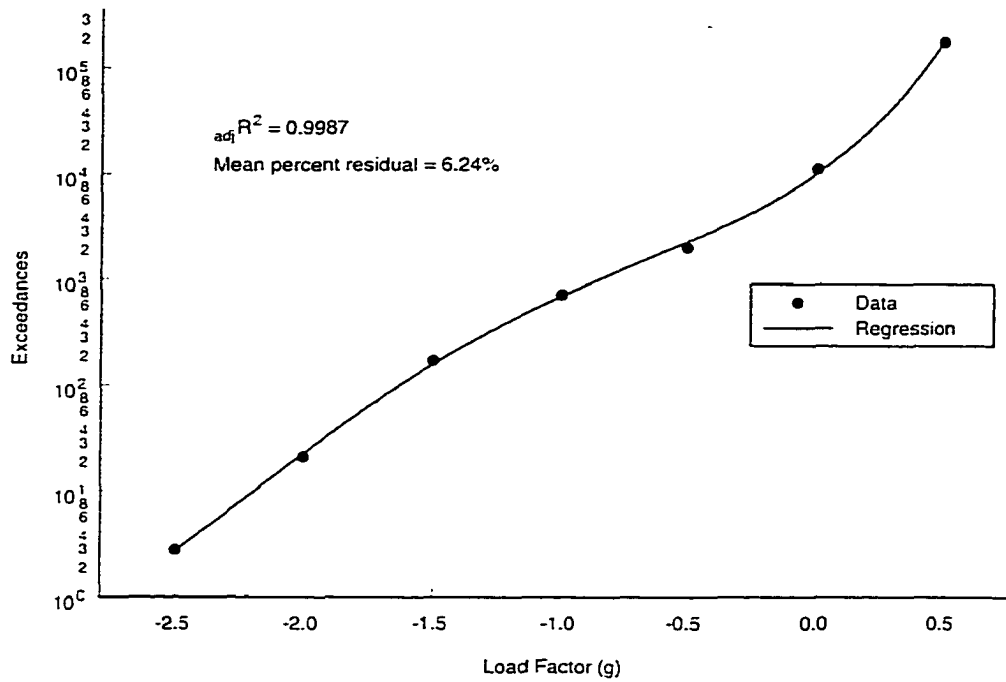


Figure B-6 Air-To-Air Segment: Negative Load Factors

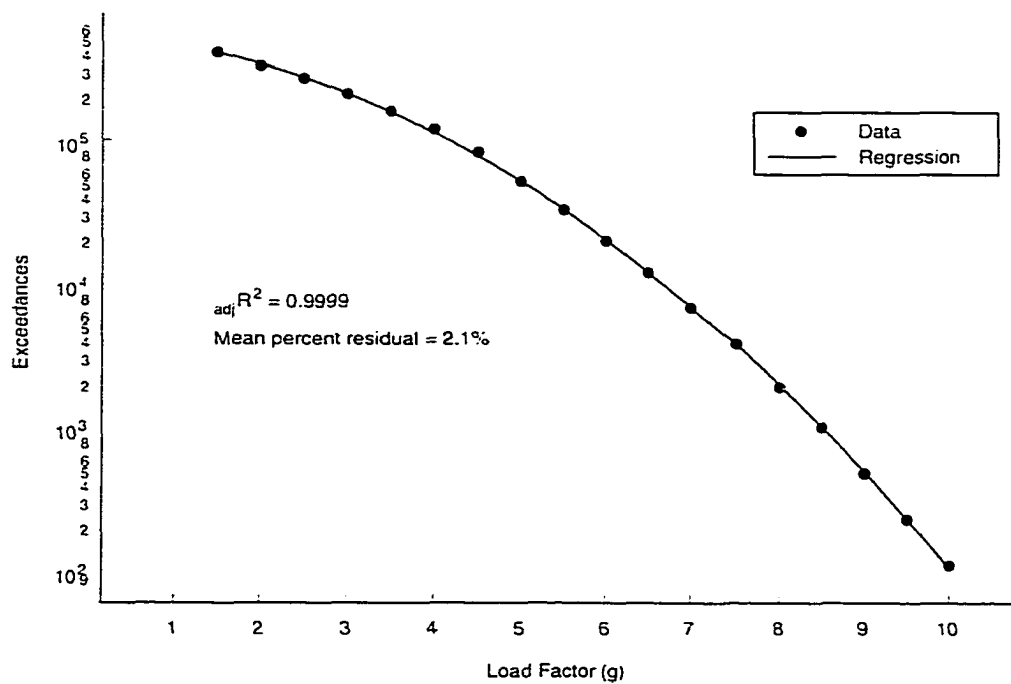


Figure B-7 Air-To-Air Segment: Positive Load Factors

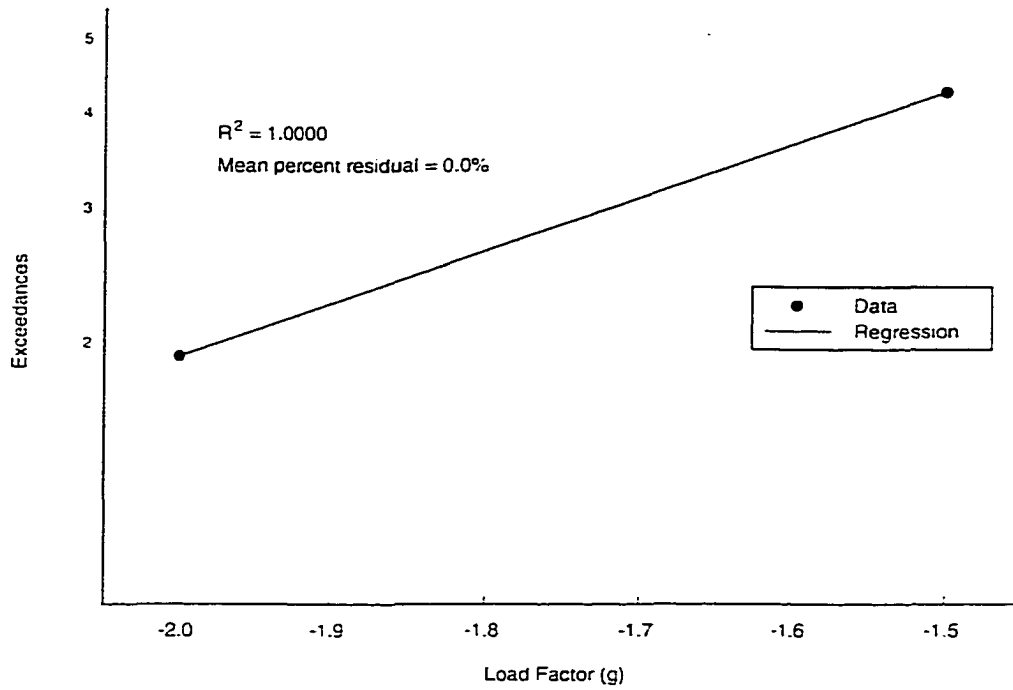


Figure B-8 Air-To-Ground Segment: Negative Load Factors

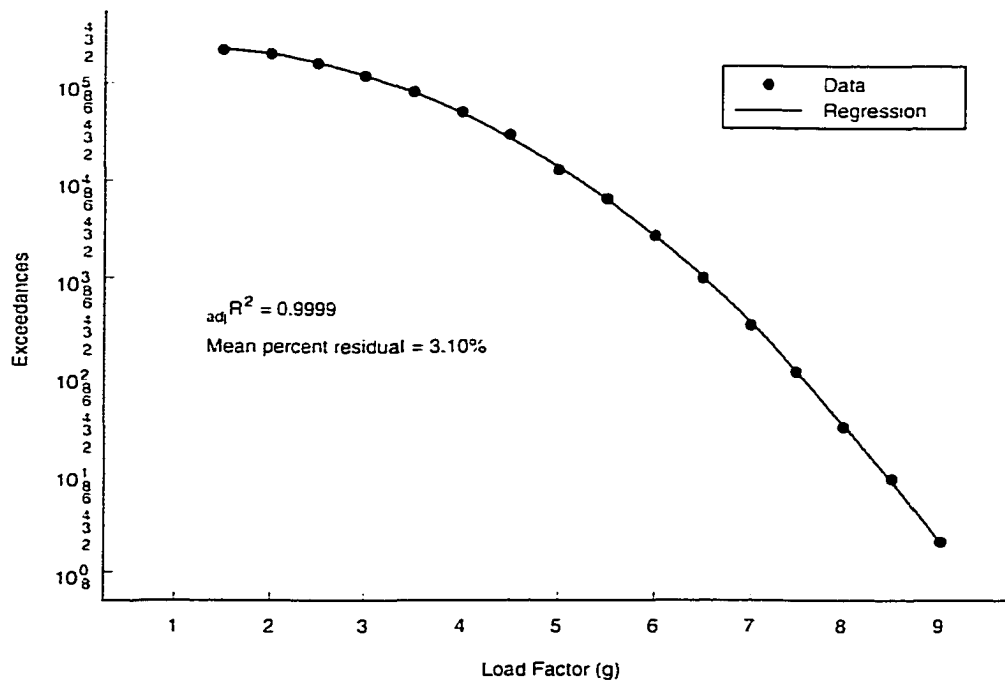


Figure B-9 Air-To-Ground Segment: Positive Load Factors

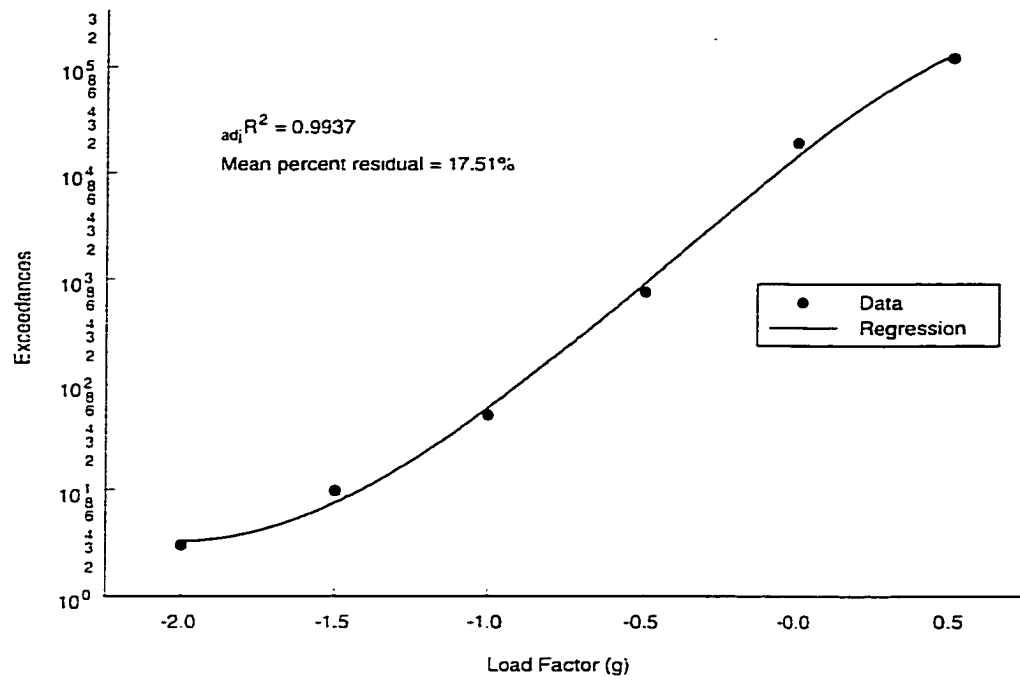


Figure B-10 Formation Segment: Negative Load Factors

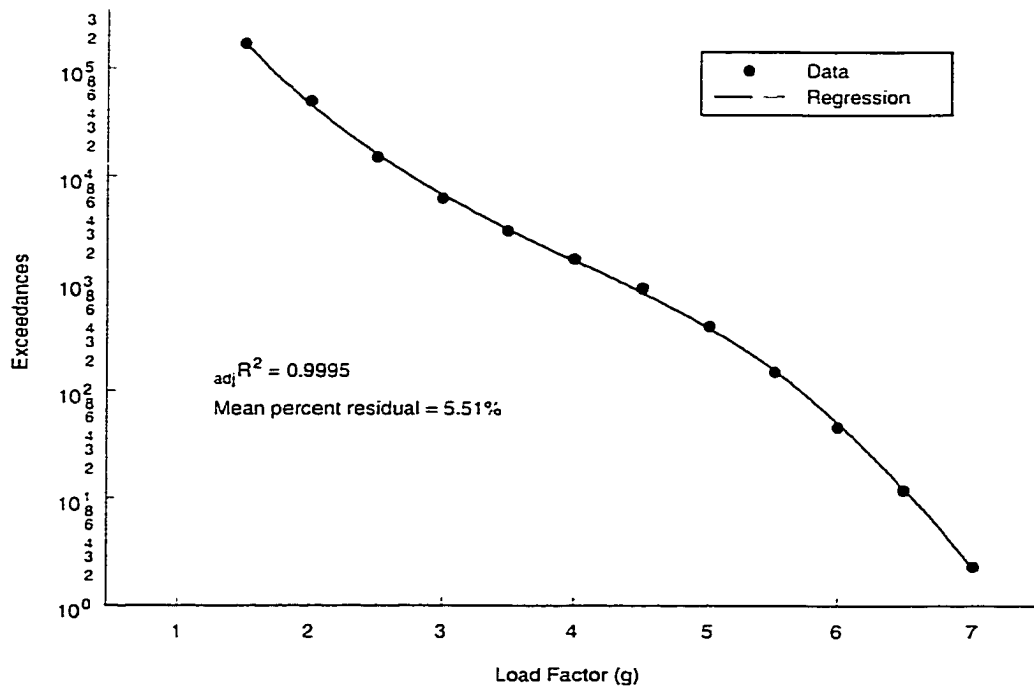


Figure B-11 Formation Segment: Positive Load Factors

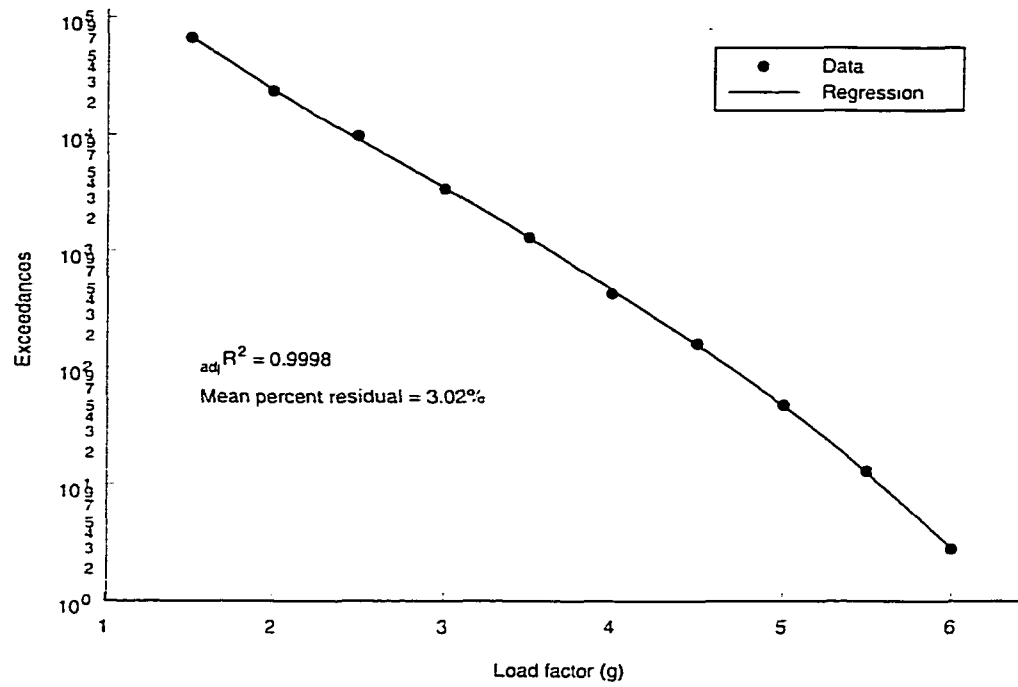


Figure B-12 Loiter Segment

Appendix C

Mission Segment Probability Analyses

Table C-1 Probability of Occurrences for Positive Load Factors: Air-To-Air Segment

n_z	Predicted	$R(n_z)$	Probability	n_z
1.25	439966.4	1.0000000		
1.50	408139.1	0.9276597	0.14768	1.5
1.75	374993.2	0.8523222		
2.00	341243.9	0.7756136	0.15326	2.0
2.25	307562.2	0.6990584		
2.50	274553.8	0.6240336	0.14733	2.5
2.75	242744.0	0.5517330		
3.00	212567.0	0.4831438	0.13270	3.0
3.25	184361.3	0.4190350		
3.50	158369.0	0.3599570	0.11278	3.5
3.75	134740.1	0.3062510		
4.00	113540.4	0.2580660	0.09087	4.0
4.25	94761.1	0.2153825		
4.50	78331.5	0.1780396	0.06962	4.5
4.75	64131.1	0.1457637		
5.00	52003.0	0.1181976	0.05084	5.0
5.25	41765.1	0.0949279		
5.50	33222.0	0.0755103	0.03544	5.5
5.75	26173.6	0.0594901		
6.00	20423.5	0.0464205	0.02361	6.0
6.25	15784.1	0.0358758		
6.50	12082.0	0.0274612	0.01506	6.5
6.75	9159.7	0.0208192		
7.00	6877.9	0.0156327	0.00919	7.0
7.25	5115.1	0.0116260		
7.50	3767.7	0.0085636	0.00538	7.5
7.75	2748.7	0.0062475		
8.00	1986.1	0.0045142	0.00302	8.0
8.25	1421.4	0.0032306		
8.50	1007.5	0.0022899	0.00162	8.5
8.75	707.3	0.0016076		
9.00	491.8	0.0011178	0.00084	9.0
9.25	338.7	0.0007698		
9.50	231.0	0.0005250	0.00042	9.5
9.75	156.1	0.0003547		
10.00	104.4	0.0002373	0.00020	10.0
10.25	69.2	0.0001573		

Table C-2 Probabilities of Occurrences for Negative Load Factors: Air-To-Air Segment

n_z	Predicted	$R(n_z)$	Probability	n_z
0.75	1882108.8	1.0000000		
0.50	173727.0	0.0923044	0.98275	0.5
0.25	32474.4	0.0172543		
0.00	10058.0	0.0053440	0.01495	0.0
-0.25	4342.2	0.0023071		
-0.50	2260.2	0.0012009	0.00164	-0.5
-0.75	1261.6	0.0006703		
-1.00	690.6	0.0003669	0.00049	-1.0
-1.25	348.5	0.0001852		
-1.50	156.8	0.0000833	0.00015	-1.5
-1.75	62.5	0.0000332		
-2.00	22.6	0.0000120	0.00003	-2.0
-2.25	7.8	0.0000041		
-2.50	2.7	0.0000015	0.00000	-2.5
-2.75	1.1	0.0000006		

Table C-3 Probabilities of Occurrences for Positive Load Factors: Air-To-Ground Segment

n_z	Predicted	$R(n_z)$	Probability	n_z
1.25	229078.4	1.0000000		
1.50	224303.1	0.9791543	0.06370	1.5
1.75	214485.2	0.9362961		
2.00	200295.1	0.8743518	0.13891	2.0
2.25	182664.5	0.7973887		
2.50	162685.6	0.7101742	0.17970	2.5
2.75	141499.5	0.6176901		
3.00	120190.8	0.5246712	0.18246	3.0
3.25	99700.9	0.4352260		
3.50	80767.6	0.3525764	0.15629	3.5
3.75	63897.9	0.2789348		
4.00	49368.2	0.2155078	0.11633	4.0
4.25	37249.3	0.1626051		
4.50	27447.4	0.1198164	0.07638	4.5
4.75	19751.2	0.0862203		
5.00	13880.3	0.0605917	0.04464	5.0
5.25	9526.0	0.0415842		
5.50	6384.7	0.0278711	0.02334	5.5
5.75	4179.0	0.0182428		
6.00	2671.3	0.0116611	0.01096	6.0
6.25	1667.6	0.0072794		
6.50	1016.6	0.0044378	0.00464	6.5
6.75	605.2	0.0026421		
7.00	351.9	0.0015362	0.00177	7.0
7.25	199.8	0.0008722		
7.50	110.8	0.0004837	0.00061	7.5
7.75	60.0	0.0002619		

Table C-4 Probabilities of Occurrences for Negative Load Factors: Air-To-Ground Segment

n_z	Predicted	$R(n_z)$	Probability	n_z
-1.25	6.2	1.000000		
-1.50	4.2	0.672593	0.54762	-1.5
-1.75	2.8	0.452381		
-2.00	1.9	0.304268	0.24773	-2.0
-2.25	1.3	0.204649		

Table C-5 Probabilities of Occurrences for Positive Load Factors: Ascent Segment

n_z	Predicted	$R(n_z)$	Probability	n_z
1.25	176303.0	1.000000		
1.50	76627.4	0.434635	0.81718	1.5
1.75	32231.5	0.182819		
2.00	13120.4	0.074420	0.15350	2.0
2.25	5168.8	0.029318		
2.50	1970.6	0.011177	0.02519	2.5
2.75	727.1	0.004124		
3.00	259.6	0.001473	0.00362	3.0
3.25	89.7	0.000509		
3.50	30.0	0.000170	0.00045	3.5
3.75	9.7	0.000055		
4.00	3.0	0.000017	0.00005	4.0
4.25	0.9	0.000005		

Table C-6 Probabilities of Occurrences for Positive Load Factors: Cruise Segment

n_z	Predicted	$R(n_z)$	Probability	n_z
1.25	49613.7	1.0000000		
1.50	25035.7	0.5046125	0.65971	1.5
1.75	16882.9	0.3402870		
2.00	12929.4	0.2606008	0.13579	2.0
2.25	10145.7	0.2044939		
2.50	7721.2	0.1556257	0.09181	2.5
2.75	5590.7	0.1126840		
3.00	3869.4	0.0779904	0.06023	3.0
3.25	2602.2	0.0524496		
3.50	1728.1	0.0348311	0.02952	3.5
3.75	1137.6	0.0229282		
4.00	727.2	0.0146564	0.01433	4.0
4.25	426.4	0.0085942		
4.50	206.4	0.0041604	0.00719	4.5
4.75	69.9	0.0014087		
5.00	13.0	0.0002628	0.00139	5.0
5.25	1.0	0.0000196		

Table C-7 Probabilities of Occurrences for Positive Load Factors: Descent Segment

n_z	Predicted	$R(n_z)$	Probability	n_z
1.25	53805.1	1.0000000		
1.50	44744.8	0.8316080	0.34040	1.5
1.75	35490.0	0.6596028		
2.00	27284.6	0.5070996	0.27780	2.0
2.25	20542.8	0.3818002		
2.50	15216.1	0.2828003	0.17599	2.5
2.75	11073.9	0.2058146		
3.00	7862.9	0.1461372	0.10587	3.0
3.25	5377.4	0.0999431		
3.50	3476.8	0.0646180	0.06140	3.5
3.75	2073.8	0.0385434		
4.00	1107.2	0.0205783	0.02906	4.0
4.25	510.4	0.0094861		
4.50	194.8	0.0036209	0.00839	4.5
4.75	58.7	0.0010912		
5.00	13.2	0.0002461	0.00105	5.0
5.25	2.1	0.0000392		

Table C-8 Probabilities of Occurrences for Positive Load Factors: Formation Segment

n_z	Predicted	$R(n_z)$	Probability	n_z
1.25	374944.4	1.0000000		
1.50	171909.2	0.4584925	0.77173	1.5
1.75	85588.2	0.2282690		
2.00	45881.8	0.1223696	0.15823	2.0
2.25	26260.8	0.0700393		
2.50	15912.8	0.0424405	0.04304	2.5
2.75	10122.5	0.0269973		
3.00	6702.8	0.0178769	0.01478	3.0
3.25	4581.3	0.0122186		
3.50	3204.8	0.0085475	0.00615	3.5
3.75	2275.3	0.0060685		
4.00	1625.7	0.0043358	0.00298	4.0
4.25	1159.0	0.0030912		
4.50	817.7	0.0021807	0.00158	4.5
4.75	566.0	0.0015094		
5.00	381.1	0.0010165	0.00085	5.0
5.25	247.6	0.0006603		
5.50	153.9	0.0004104	0.00042	5.5
5.75	90.7	0.0002419		
6.00	50.3	0.0001341	0.00017	6.0
6.25	26.0	0.0000693		
6.50	12.4	0.0000332	0.00005	6.5
6.75	5.5	0.0000145		
7.00	2.2	0.0000058	0.00001	7.0
7.25	0.8	0.0000021		
7.50	0.3	0.0000007	0.00000	7.5
7.75	0.1	0.0000002		

Table C-9 Probabilities of Occurrences for Negative Load Factors: Formation Segment

n_z	Predicted	$R(n_z)$	Probability	n_z
0.75	72571.3	1.000000		
0.50	120176.3	1.655975	0.08345	0.5
0.25	66514.9	0.916546		
0.00	18861.0	0.259897	0.86303	0.0
-0.25	3883.7	0.053516		
-0.50	761.1	0.010487	0.05115	-0.5
-0.75	172.0	0.002370		
-1.00	50.3	0.000693	0.00210	-1.0
-1.25	19.7	0.000271		
-1.50	9.9	0.000136	0.00019	-1.5
-1.75	5.6	0.000078		
-2.00	3.0	0.000041	0.00006	-2.0
-2.25	1.1	0.000015		
-2.50	0.2	0.000003	0.00002	-2.5
-2.75	0.0	0.000000		

Table C-10 Probabilities of Occurrences for Positive Load Factors: Instrument & Navigation Segment

n_z	Predicted	$R(n_z)$	Probability	n_z
1.25	76280.5	1.0000000		
1.50	36855.5	0.4831583	0.74338	1.5
1.75	19575.1	0.2566197		
2.00	11193.2	0.1467376	0.16797	2.0
2.25	6762.3	0.0886506		
2.50	4244.9	0.0556480	0.05288	2.5
2.75	2728.3	0.0357670		
3.00	1773.1	0.0232443	0.02065	3.0
3.25	1152.9	0.0151143		
3.50	743.8	0.0097506	0.00891	3.5
3.75	473.0	0.0062012		
4.00	295.3	0.0038714	0.00383	4.0
4.25	180.6	0.0023672		
4.50	108.1	0.0014174	0.00153	4.5
4.75	63.5	0.0008327		
5.00	36.8	0.0004819	0.00056	5.0
5.25	21.1	0.0002764		
5.50	12.1	0.0001584	0.00018	5.5
5.75	7.0	0.0000916		
6.00	4.1	0.0000542	0.00006	6.0
6.25	2.5	0.0000332		
6.50	1.6	0.0000214	0.00002	6.5
6.75	1.1	0.0000148		

Table C-11 Probabilities of Occurrences for Negative Load Factors: Instrument & Navigation Segment

n_z	Predicted	$R(n_z)$	Probability	n_z
0.75	19294.5	1.000000		
0.50	33656.0	1.744331	0.00548	0.5
0.25	19188.8	0.994518		
0.00	5366.0	0.278109	0.94092	0.0
-0.25	1034.1	0.053595		
-0.50	180.7	0.009363	0.05177	-0.5
-0.75	35.2	0.001827		
-1.00	8.9	0.000459	0.00167	-1.0
-1.25	3.1	0.000160		
-1.50	1.5	0.000079	0.00011	-1.5
-1.75	1.0	0.000052		
-2.00	0.8	0.000040	0.00002	-2.0
-2.25	0.6	0.000030		

Table C-12 Probabilities of Occurrences for Positive Load Factors: Loiter Segment

n_z	Predicted	$R(n_z)$	Probability	n_z
1.25	117844.3	1.0000000		
1.50	68607.6	0.5821889	0.65479	1.5
1.75	40681.1	0.3452103		
2.00	24479.9	0.2077311	0.21881	2.0
2.25	14895.9	0.1264036		
2.50	9132.9	0.0774996	0.07870	2.5
2.75	5621.8	0.0477050		
3.00	3461.8	0.0293761	0.02967	3.0
3.25	2124.9	0.0180315		
3.50	1295.5	0.0109931	0.01140	3.5
3.75	781.6	0.0066329		
4.00	465.1	0.0039466	0.00433	4.0
4.25	271.9	0.0023073		
4.50	155.6	0.0013208	0.00157	4.5
4.75	86.9	0.0007376		
5.00	47.2	0.0004004	0.00053	5.0
5.25	24.8	0.0002105		
5.50	12.6	0.0001068	0.00016	5.5
5.75	6.1	0.0000521		
6.00	2.9	0.0000244	0.00004	6.0
6.25	1.3	0.0000109		

Appendix D

Load_history.exe

Input File Format for Load_history.exe

```
subblock
mtype, sbrf
mission, start, fltotal, nsegment
segment
.
.
.
mtype, sbrf
mission, start, fltotal, nsegment
segment
.
.
.
```

Definitions:

Variable	Description	Type
subblock	number of subblocks	integer
mtype	number of mission types in subblock	integer
sbrf	number of times subblock repeats	integer
mission	mission type	character size 14
start	flight number of first subblock flight	integer
fltotal	number of consecutive flights	integer
nsegment	number of segments in mission	integer
segment	segment history file name	character size 40

block_definition.inp file

```
3
4,10
'Training',1,1,7
'T_ascent1_history.out'
'T_cruise_history.out'
'T_inst-nav1_history.out'
'T_ascent2_history.out'
'T_loiter_history.out'
'T_inst-nav2_history.out'
'T_descent_history.out'
'Air-AirI',1,9,6
'AAI_ascent_history.out'
'AAI_formation1_history.out'
'AAI_air-air_history.out'
'AAI_formation2_history.out'
'AAI_cruise_history.out'
'AAI_descent_history.out'
'Air-AirII',1,10,6
'AAII_ascent_history.out'
'AAII_formation1_history.out'
'AAII_air-air_history.out'
'AAII_formation2_history.out'
'AAII_cruise_history.out'
'AAII_descent_history.out'
'Air-AirIII',1,5,6
'AAIII_ascent_history.out'
'AAIII_formation1_history.out'
'AAIII_air-air_history.out'
'AAIII_formation2_history.out'
'AAIII_cruise_history.out'
'AAIII_descent_history.out'
3,5
'Training',11,2,7
'T_ascent1_history.out'
'T_cruise_history.out'
'T_inst-nav1_history.out'
'T_ascent2_history.out'
'T_loiter_history.out'
'T_inst-nav2_history.out'
'T_descent_history.out'
'Air-GroundI',1,10,6
'AGI_ascent1_history.out'
'AGI_cruise1_history.out'
'AGI_air-ground_history.out'
'AGI_ascent2_history.out'
'AGI_cruise2_history.out'
'AGI_descent_history.out'
'Air-GroundII',1,8,6
'AGII_ascent1_history.out'
'AGII_cruise1_history.out'
'AGII_air-ground_history.out'
'AGII_ascent2_history.out'
'AGII_cruise2_history.out'
'AGII_descent_history.out'
```

```

5,1
'Training',21,2,7
'T_ascent1_history.out'
'T_cruise_history.out'
'T_inst-nav1_history.out'
'T_ascent2_history.out'
'T_loiter_history.out'
'T_inst-nav2_history.out'
'T_descent_history.out'
'Air-AirI',91,3,6
'AAI_ascent_history.out'
'AAI_formation1_history.out'
'AAI_air-air_history.out'
'AAI_formation2_history.out'
'AAI_cruise_history.out'
'AAI_descent_history.out'
'Air-AirII',101,40,6
'AAII_ascent_history.out'
'AAII_formation1_history.out'
'AAII_air-air_history.out'
'AAII_formation2_history.out'
'AAII_cruise_history.out'
'AAII_descent_history.out'
'Air-AirIII',51,38,6
'AAIII_ascent_history.out'
'AAIII_formation1_history.out'
'AAIII_air-air_history.out'
'AAIII_formation2_history.out'
'AAIII_cruise_history.out'
'AAIII_descent_history.out'
'Training',23,3,7
'T_ascent1_history.out'
'T_cruise_history.out'
'T_inst-nav1_history.out'
'T_ascent2_history.out'
'T_loiter_history.out'
'T_inst-nav2_history.out'
'T_descent_history.out'

```

load_history.exe

```
      real nz1(100),nz2(100),prate1(100),prate2(100),pdot1(100),
+pdot2(100)
      integer i,j,k,l,m,n,subblock,mtype(5),sbrf(5),nsegment(5,10),
+flttotal(5,10),fltnum,ncycle,cycle(100),flight,start(5,10),
+finish(5,10),nlevels
      character*40 mission(5,10)*14,segment(5,10,10),title1*14,
+seaname*20,title2*6,title3*12,title4*33,maneuvr1(100)*6,
+maneuvr2(100)*6

      flight = 1
      nlevels = 0

      open(unit=1,file='block_definition.inp',status='old')
      open(unit=2,file='block_history.out')

      write(*,*) "Reading input file"
      read(1,*) subblock
      do 10 i=1,subblock
         read(1,*) mtype(i),sbrf(i)
         do 20 j=1,mttype(i)
            read(1,*) mission(i,j),start(i,j),flttotal(i,j),nsegment(i,j)
            finish(i,j)=start(i,j)-1 + flttotal(i,j)

            do 30 k=1,nsegment(i,j)
               read(1,*) segment(i,j,k)
30          continue

20          continue

10          continue

      do 40 i=1,subblock
         write(*,*) "subblock = ",i
         do 50 m=1,sbrf(i)
            do 60 j=1,mttype(i)
               do 70 l=start(i,j),finish(i,j)
                  write(2,600) "Block flight No. =",flight
                  write(2,600) "number of segment=", nsegment(i,j)

                  do 80 k=1,nsegment(i,j)
                     open(unit=3,file=segment(i,j,k),status='old') ! read-in output
file from occurrence.exe

                     read(3,100) title1,seaname

85          read(3,200) title2,fltnum,title3,ncycle

                     read(3,300) title4

      do 90 n=1,ncycle
         read(3,*) cycle(n),nz1(n),maneuvr1(n),prate1(n),pdot1(n)
90        read(3,*) nz2(n),maneuvr2(n),prate2(n),pdot2(n)
            if(fltnum .ne. 1) goto 85
            write(2,600) seaname, ncycle
            do 95 n=1,ncycle
```

```

        write(2,400) cycle(n),nz1(n),maneuvr1(n),prate1(n),pdot1(n)
95      write(2,500) nz2(n),maneuvr2(n),prate2(n),pdot2(n)
        nlevels = nlevels + ncycle
80      continue
        write(2,600) "number of levels=", nlevels
        nlevels = 0
        flight = flight + 1
70      continue
        start(i,j) = finish(i,j) + 1
        finish(i,j) = finish(i,j) + fltotal(i,j)
60      continue
50      continue
40      continue

100     format(A14,A20)
200     format(/A6,1x,I4,5x,A12,1x,I4)
300     format(A56)
400     format(I2,2X,F4.1,2X,A6,2x,f5.2,2x,f6.2)
500     format(4X,F4.1,2X,A6,2x,f5.2,2x,f6.2)
600     format(A18,I5)

        stop
        end

```

Appendix E

Global_local.exe

```
      real nz1,nz2,stress1(500),stress2(500),peakstr,qdot,a,b,c,d,smin
+,prate1,pdot1,prate2,pdot2,alpha(19),delta(19),epsilon(19),
+eta(19)
      integer flight,ncycle,cycle,nflight,nsegment,i,j,k,nlevels,
+level,blevels,l
      character*9 title1*18,title2,segname*20,maneuvr1*6,maneuvr2*6,
+title3

      common alpha,delta,epsilon,eta

      open(unit=1, file='block_history.out')
      open(unit=3, file='raw_stresses')
      open(unit=5, file='stress_parameters.inp')

      blevels = 0      ! total number of stress levels in block set to 0
      peakstr = 0.0

      write(*,*) "Enter the total number of flights"
      read(*,*) nflight

c*** Read stress function parameters from 'stress_parameters.inp' ***
c      Read parameters in the order of:
c      Training
c      Air-to-Air
c      Air-to-Ground
c      do 5 i = 1,19
c          read(5,*) alpha(i),delta(i),epsilon(i),eta(i)
c          write(*,*) alpha(i),delta(i),epsilon(i),eta(i)
5      continue

c      *** Read load factor from block_history.out file ***
c      do 10 i = 1,nflight
c          level = 1
c          read(1,600) title1,flight
c          read(1,600) title2,nsegment

c              do 20 j=1,nsegment

c                  read(1,600) segname,ncycle

c                      do 30 k=1,ncycle

c                          call stressnz(segname,a,b,c,d,qdot)

c                          read(1,500) cycle, nz1, maneuver1,prate1,pdot1
c                          read(1,550) nz2, maneuver2,prate2,pdot2

c      *** convert load factor into stress using FEA results ***
```

```

c      ***   for three maneuver types:
c      ***           101 symmetric-steady
c      ***           102 symmetric-abrupt
c      ***           103 asymmetric-steady
c      ***           104 asymmetric-abrupt
c      ***   and for each mission segment's airspeed, altitude
c      ***   and weight combination

c      *** Compute the maximum stress      ***

c      Symmetric steady and abrupt maneuvers

      if(maneuvr1 .eq. "steady")then
        qdot = 0.0
      endif
      if(nz1 .gt. 1.0)then
        stress1(level) = a*nz1 + b*qdot
      elseif(nz1 .lt. 1.0)then
        stress1(level) = a*nz1 - b*qdot
      endif

c      Asymmetric maneuvers
c      Steady State
      if(maneuvr1 .eq. "Lasysms")then
        stress1(level) = a*nz1 + c*pratel
      elseif(maneuvr1 .eq. "Rasysms")then
        stress1(level) = a*nz1 - c*pratel
c      Abrupt
      elseif(maneuvr1 .eq. "Lasyma")then
        stress1(level) = a*nz1 + d*pdot1
      elseif(maneuvr1 .eq. "Rasyma")then
        stress1(level) = a*nz1 - d*pdot1

c      lg maneuvers
      elseif(maneuvr1 .eq. "-----")then
        stress1(level) = a
      endif

c      *** Compute the minimum stress      ***
      call stressnz(segname,a,b,c,d,qdot)

c      Symmetric steady and abrupt maneuvers
      if(maneuvr2 .eq. "steady")then
        qdot = 0.0
      endif
      if(nz2 .gt. 1.0)then
        stress2(level) = a*nz2 + b*qdot
      elseif(nz2 .lt. 1.0)then
        stress2(level) = a*nz2 - b*qdot
      endif

      call stressnz(segname,a,b,c,d,qdot)

c      Asymmetric maneuvers

c      Steady State
      if(maneuvr2 .eq. "Lasysms")then

```

```

        stress2(level) = a*nz2 + c*prate2
    elseif(maneuvr2 .eq. "Rasyms") then
        stress2(level) = a*nz2 - c*prate2
c      Abrupt
    elseif(maneuvr2 .eq. "Lasyma") then
        stress2(level) = a*nz2 + d*pdot2
    elseif(maneuvr2 .eq. "Rasyma") then
        stress2(level) = a*nz2 - d*pdot2

c      lg maneuvers
        elseif(maneuvr2 .eq. "-----") then
            stress2(level) = a
        endif

        level = level + 1
        blevels = blevels + 1

30    continue

20    continue

c*** read number of levels in flight from block_history.out file ***
    read(1,600) title3, nlevels

c*** find peak stress and write cyclic stresses to temporary file
    write(3,650) flight, nlevels
    write(*,*) "flight =",flight
    do 40 level = 1,nlevels
c      check and insure stress1 is > stress2
        if(stress2(level) .gt. stress1(level)) then
            smin = stress1(level)
            stress1(level) = stress2(level)
            stress2(level) = smin
        endif
        if(stress1(level) .gt. peakstr) then
            peakstr = stress1(level)
        endif

        write(3,700) stress1(level), stress2(level)

40    continue

10    continue

    write(*,*) "peak stress =",peakstr

500    format(I2,2x,F4.1,2x,A6,2x,f5.2,2x,f6.2)
550    format(4x,F4.1,2x,A6,2x,f5.2,2x,f6.2)
600    format(A18,I5)
650    format(I4,2x,I4)
700    format(F9.2,2x,F9.2)

    close(unit=1)
    close(unit=3)

    stop

```



```

end
c      **** Mission segment stress-load ratios from ASTROS ****
subroutine stressnz(segname,a,b,c,d,qdot)
  real a,b,c,d,qdot,alpha(19),delta(19),epsilon(19),eta(19)
  integer start
  character*20 segname
  common alpha,delta,epsilon,eta

c      *** Training Mission ***
      if (segname(2:2) .eq. 'T') then
      if (segname(2:10) .eq. 'T_ascent1') then
c        write(*,*) "segment=",segname
          a = alpha(1)
          b = delta(1)
          c = epsilon(1)
          d = eta(1)
          qdot = 3.0
c        write(*,*) "a=",a
c        write(*,*) "b=",b
c        write(*,*) "c=",c
c        write(*,*) "d=",d
          endif

          if (segname(2:9) .eq. 'T_cruise') then
c            write(*,*) "segment=",segname
              a = alpha(2)
              b = delta(2)
              c = epsilon(2)
              d = eta(2)
              qdot = 3.0
            endif

            if (segname(2:12) .eq. 'T_inst-nav1') then
c              write(*,*) "segment=",segname
                a = alpha(3)
                b = delta(3)
                c = epsilon(3)
                d = eta(3)
                qdot = 3.0
              endif

              if (segname(2:10) .eq. 'T_ascent2') then
c                write(*,*) "segment=",segname
                  a = alpha(4)
                  b = delta(4)
                  c = epsilon(4)
                  d = eta(4)
                  qdot = 3.0
                endif

                if (segname(2:9) .eq. 'T_loiter') then
c                  write(*,*) "segment=",segname
                    a = alpha(5)
                    b = delta(5)
                    c = epsilon(5)
                    d = eta(5)
                    qdot = 3.0

```

```

endif

if (segname(2:12) .eq. 'T_inst-nav2') then
c   write(*,*) "segment=",segname
      a = alpha(6)
      b = delta(6)
      c = epsilon(6)
      d = eta(6)
      qdot = 3.0
endif

if (segname(2:10) .eq. 'T_descent') then
c   write(*,*) "segment=",segname
      a = alpha(7)
      b = delta(7)
      c = epsilon(7)
      d = eta(7)
      qdot = 3.0
endif
endif

c   *** Air-Air Mision ***
      if (segname(2:3) .eq. 'AA') then
        if (segname(2:5) .eq. 'AAI_') then
          start=6
        endif
        if (segname(2:6) .eq. 'AAII_') then
          start=7
        endif
        if (segname(2:6) .eq. 'AAIII') then
          start=8
        endif
      if (segname(start:start+5) .eq. 'ascent') then
c   write(*,*) "segment=",segname
        a = alpha(8)
        b = delta(8)
        c = epsilon(8)
        d = eta(8)
        qdot = 3.0
      endif
      if (segname(start:start+9) .eq. 'formation1') then
c   write(*,*) "segment=",segname
        a = alpha(9)
        b = delta(9)
        c = epsilon(9)
        d = eta(9)
        qdot = 3.0
      endif
      if (segname(start:start+6) .eq. 'air-air') then
c   write(*,*) "segment=",segname
        a = alpha(10)
        b = delta(10)
        c = epsilon(10)
        d = eta(10)
        qdot = 3.0
      endif
      if (segname(start:start+9) .eq. 'formation2') then

```

```

c      write(*,*) "segment=",segname
        a = alpha(11)
        b = delta(11)
        c = epsilon(11)
        d = eta(11)
        qdot = 3.0
      endif
      if (segname(start:start+5) .eq. 'cruise') then
c      write(*,*) "segment=",segname
        a = alpha(12)
        b = delta(12)
        c = epsilon(12)
        d = eta(12)
        qdot = 3.0
      endif
      if (segname(start:start+6) .eq. 'descent') then
c      write(*,*) "segment=",segname
        a = alpha(13)
        b = delta(13)
        c = epsilon(13)
        d = eta(13)
        qdot = 3.0
      endif
    endif

c    *** Air-Ground Mission ***
      if (segname(2:3) .eq. 'AG') then
        if (segname(2:5) .eq. 'AGI_') then
          start=6
        endif
        if (segname(2:6) .eq. 'AGII_') then
          start=7
        endif
      if (segname(start:start+6) .eq. 'ascent1') then
c      write(*,*) "segment=",segname
        a = alpha(14)
        b = delta(14)
        c = epsilon(14)
        d = eta(14)
        qdot = 3.0
      endif
      if (segname(start:start+6) .eq. 'cruise1') then
c      write(*,*) "segment=",segname
        a = alpha(15)
        b = delta(15)
        c = epsilon(15)
        d = eta(15)
        qdot = 3.0
      endif
      if (segname(start:start+9) .eq. 'air-ground') then
c      write(*,*) "segment=",segname
        a = alpha(16)
        b = delta(16)
        c = epsilon(16)
        d = eta(16)
        qdot = 3.0
      endif

```

```

        if (segname(start:start+6) .eq. 'ascent2') then
c      write(*,*) "segment=",segname
          a = alpha(17)
          b = delta(17)
          c = epsilon(17)
          d = eta(17)
          qdot = 3.0
        endif
        if (segname(start:start+6) .eq. 'cruise2') then
c      write(*,*) "segment=",segname
          a = alpha(18)
          b = delta(18)
          c = epsilon(18)
          d = eta(18)
          qdot = 3.0
        endif
        if (segname(start:start+6) .eq. 'descent') then
c      write(*,*) "segment=",segname
          a = alpha(19)
          b = delta(19)
          c = epsilon(19)
          d = eta(19)
          qdot = 3.0
        endif

      endif
    return
  end

```

Appendix F

Spectrum_clipping.exe

```
real stress1(500),stress2(500),clipstr,normal

integer flight,nflight,nlevels,level,1,counter

open(unit=2, file='clipped_stress_history.sp3')
open(unit=3, file='raw_stresses')
open(unit=4, file='clipped_stress_history01.sub')

c
counter = 0

c *** Create AFGROW spectrum information file.sp3 ***
write(2,800)

write(*,*) "Enter the total number of flights"
read(*,*) nflight
write(*,*) "Enter clipping stress"
read(*,*) clipstr
write(*,*) "Enter normalizing stress"
read(*,*) normal

c*** normalize block stress history with peak stress and write ***
c *** normalized stresses history to AFGROW spectrum file.sub ***
do 50 1 = 1,nflight
  read(3,650) flight,nlevels
  write(4,650) flight, nlevels
  do 60 level = 1,nlevels
    read(3,700) stress1(level),stress2(level)
    if (stress1(level) .gt. clipstr)then
      write(*,*) "stress=",stress1(level)
      stress1(level) = clipstr
      counter= counter + 1
    endif
    stress1(level) = stress1(level)/normal
    stress2(level) = stress2(level)/normal
    write(4,900) stress1(level),stress2(level), "1"
60  continue
50  continue

write(*,*) "normalizing stress =",normal
write(*,*) "No. of clipping events =",counter

650 format(I4,2x,I4)
700 format(F9.2,2x,F9.2)
800 format("Fighter Wing Spectrum"/"Flight"/"CYCLExCYCLE"/"1")
900 format(F10.5,2x,F10.5,2x,A1)
```

```
close(unit=2)  
close(unit=3)  
close(unit=4)
```

```
stop  
end
```